

# **For Reference**

---

**NOT TO BE TAKEN FROM THIS ROOM**

Ex LIBRIS  
UNIVERSITATIS  
ALBERTAEASIS







THE UNIVERSITY OF ALBERTA

ONE-DIMENSIONAL MODEL OF THE URBAN HEAT ISLAND

BY



CLAUDE LELIEVRE

A THESIS

SUBMITTED TO THE FACULTY OF GRADUATE STUDIES AND RESEARCH  
IN PARTIAL FULFILMENT OF THE REQUIREMENTS FOR THE DEGREE  
OF MASTER OF SCIENCE

IN

METEOROLOGY

DEPARTMENT OF GEOGRAPHY

EDMONTON, ALBERTA

FALL, 1976



## ABSTRACT

A one-dimensional numerical model of the urban heat island has been devised. It consists mainly in the interaction between a soil layer and an atmospheric layer coupled through a heat-balance equation. The heat-balance equation includes the various heat fluxes and radiation. A constant molecular diffusivity is assumed throughout the soil layer. The "second-order" modelling is used in order to close the set of atmospheric equations. The equations are transformed into finite-difference expressions. The log-linear atmospheric grid is very appropriate for a one-dimensional model because it gives a good accuracy in the low levels with a relatively small number of grid points. The initial conditions for the time-dependent model are obtained from the steady state. We assess the effect of the roughness height, of the geostrophic wind and of the soil thermal conductivity. An increase in any of these parameters decreases the amplitude of the diurnal variation of the surface temperature. Therefore, these parameters tend to produce rural areas warmer than cities. The counterbalancing effect which was not included is evaporation which reduces the rural temperature during the daytime.



## TABLE OF CONTENTS

	Page
ABSTRACT . . . . .	iv
TABLE OF CONTENTS . . . . .	v
LIST OF TABLES . . . . .	xii
LIST OF FIGURES . . . . .	xiii
CHAPTER	
I        PREVIOUS WORK . . . . .	1
1.1    Introduction . . . . .	1
1.2    Statistical Studies . . . . .	1
1.3    Unidimensional Numerical Model . . . . .	2
1.4    Two-Dimensional Models . . . . .	5
1.5    Higher-Order Closure Scheme . . . . .	8
II       DEVELOPMENT OF THE ATMOSPHERIC EQUATIONS . . . . .	10
2.1    Basic Equations . . . . .	10
2.1.1   Perfect Gas Law . . . . .	10
2.1.2   Continuity Equation . . . . .	10
2.1.3   Momentum Equation . . . . .	11
2.1.4   Energy Equation . . . . .	12
2.1.5   Water Vapor Conservation Equation . . . . .	13
2.2    Assumption of a nearly-Adiabatic Atmosphere . . . . .	14
2.2.1   Perfect Gas law . . . . .	14
2.2.2   Continuity Equation . . . . .	14
2.2.3   Momentum Equation . . . . .	15
2.2.4   Energy Equation . . . . .	15
2.2.5   Mixing-Ratio Equation . . . . .	16
2.2.6   Simplified Continuity Equation . . . . .	16



CHAPTER	Page
2.2.7 Resulting Set of Equations . . . . .	17
2.3 Ensemble Averaging . . . . .	18
2.3.1 Equations for the Mean Quantities . . . . .	18
2.3.2 Equations for the Turbulent Quantities . . . . .	19
2.4 Modelled Equations . . . . .	21
2.4.1 Energy Redistribution Term . . . . .	22
2.4.2 Pressure-Temperature Correlation Term . . . . .	27
2.4.3 Pressure-Water Vapor Correlation Term . . . . .	30
2.4.4 Dissipation Terms . . . . .	31
2.4.5 Diffusional Terms . . . . .	32
2.4.6 Pressure Diffusional Terms . . . . .	34
2.5 Modelled Equations . . . . .	36
2.5.1 Modelled Equations for the Second-Order Moments . . .	36
2.5.2 Modelled Equations for the Mean Quantities . . . . .	37
2.6 Length Scale Specification . . . . .	38
2.7 Ordering of Terms . . . . .	39
2.8 Level 3 Model . . . . .	46
2.9 The Boundary-Layer Approximation . . . . .	48
2.9.1 Equations for the Mean Quantities . . . . .	48
2.9.2 Equations for the Turbulent Quantities . . . . .	49
2.10 One-Dimensional Level 3 Equations . . . . .	51
2.10.1 Equations for the Mean Quantities . . . . .	51
2.10.2 Equations for the Turbulent Quantities . . . . .	52
2.11 Boundary Conditions . . . . .	53
2.11.1 Upper Boundary Conditions; $z \rightarrow \infty$ . . . . .	53
2.11.2 Lower Boundary Conditions: $z \rightarrow 0$ . . . . .	53



CHAPTER		Page
III	FINITE-DIFFERENCE EQUATIONS FOR THE ATMOSPHERIC VARIABLES . . . . .	58
3.1	General Remarks . . . . .	58
3.2	Log-Linear Atmospheric Grid . . . . .	60
3.3	Atmospheric Equations in Log-Linear Coordinates . .	63
3.3.1	Equations for the Mean Quantities in Log-Linear Coordinates: First Form . . . . .	65
3.3.2	Equations for the Mean Quantities in Log-Linear Coordinates: Second Form . . . . .	66
3.3.3	Equations for the Turbulent Quantities in Log-Linear Coordinates . . . . .	67
3.4	Finite-Difference Equations . . . . .	68
3.4.1	Vertical Derivatives . . . . .	69
3.4.2	Time Derivative . . . . .	71
3.4.3	Stability of the Finite-Difference Equations . . . .	71
3.4.4	Comments on the Finite-Difference Equations . . . .	74
3.5	Steady-State Model . . . . .	75
3.6	Time-Dependent Model . . . . .	76
3.7	Initialization at Each Time Step . . . . .	78
IV	SOIL LAYER . . . . .	79
4.1	Introduction . . . . .	79
4.2	Logarithmic Grid for the Soil Layer . . . . .	80
4.3	Equation for the Steady-State . . . . .	81
4.4	Time-Dependent Equation . . . . .	81
4.5	Initial Soil Temperature Profile . . . . .	82



CHAPTER		Page
V	SURFACE TEMPERATURE . . . . .	84
5.1	Net Radiation . . . . .	84
5.1.1	Outgoing Terrestrial Infrared Radiation . . . . .	85
5.1.2	Sky Infrared Radiation . . . . .	85
5.1.3	Incoming Solar Radiation . . . . .	87
5.2	Sensible Heat Flux from the Atmosphere . . . . .	89
5.3	Sensible Heat Flux from the Soil . . . . .	91
5.4	Latent Heat Flux from the Atmosphere . . . . .	91
5.5	Artificial Heat Generation . . . . .	91
5.6	Solution of the Surface Temperature Equation . . . . .	91
VI	NUMERICAL SIMULATION OF THE URBAN HEAT ISLAND . . . . .	93
6.1	Steady-State Model . . . . .	93
6.1.1	Effect of the Geostrophic Wind Speed . . . . .	93
6.1.2	Effect of Increased Roughness Height . . . . .	95
6.2	Time-Dependent Model . . . . .	97
6.2.1	Geostrophic Wind Speed . . . . .	100
6.2.2	Effect of the Roughness Height . . . . .	121
6.2.3	Effect of the Soil Conductivity . . . . .	129
6.2.4	Examination of the Other Variables . . . . .	136
6.3	Comparison of the Soil Temperatures . . . . .	144
6.4	Assessment of the Urban Heat Island Effect . . . . .	156
CONCLUSION . . . . .		158
REFERENCES . . . . .		161
APPENDIX		
A	LOG-LINEAR ATMOSPHERIC GRID . . . . .	165
A.1	Determination of IKM . . . . .	166



APPENDIX	Page
A.2 Initialization of the Other levels . . . . .	167
A.3 Accelerated Gauss-Seidel Process . . . . .	168
A.4 Detailed Analysis of OMEGA in a Specific Case . . . . .	169
A.4.1 Analysis of the Iterative Process below IKM . . . . .	169
A.4.2 Analysis of the Iterative Process Near and Above IKM .	174
A.5 Iteration Process on $\Psi$ . . . . .	175
B STEADY-STATE ATMOSPHERIC EQUATIONS . . . . .	176
B.1 Equations: First Form . . . . .	176
B.2 Mixing Length . . . . .	177
B.3 Vertical Derivative of $K_m$ . . . . .	178
B.4 Finite-Difference Equations . . . . .	179
B.4.1 Mean Wind U . . . . .	179
B.4.2 Equation for the Mean Wind V . . . . .	179
B.4.3 Equation for e . . . . .	180
B.4.4 Equation for $K_m$ . . . . .	181
B.4.5 Iteration Scheme . . . . .	181
B.5 Finite-Difference Equation for $K_t$ and $K_w$ . . . . .	183
B.6 Finite-Difference Equations: Second Form . . . . .	183
B.6.1 Equation for U . . . . .	183
B.6.2 Equation for V . . . . .	184
C TIME-DEPENDENT ATMOSPHERIC EQUATIONS . . . . .	186
C.1 Equations . . . . .	186
C.2 Notation . . . . .	186
C.3 Finite-Difference Equations: First Form . . . . .	187
C.3.1 Equation for U . . . . .	187



APPENDIX	Page
C.3.2 Equation for V . . . . .	189
C.3.3 Equation for $(H)$ . . . . .	189
C.3.4 Equation for Q . . . . .	190
C.3.5 Equation for $\epsilon$ . . . . .	191
C.3.6 Computation of $\overline{\theta^2}$ . . . . .	193
C.3.7 Computation of $\overline{q^2}$ . . . . .	194
C.3.8 Equation for $\overline{\theta q}$ . . . . .	194
C.3.9 Equation for $K_m$ . . . . .	195
C.3.10 Equation for $K_t$ . . . . .	196
C.3.11 Equation for $K_w$ . . . . .	197
C.4 Finite-Difference Equations: Second Form . . . . .	198
C.4.1 Equation for U . . . . .	198
C.4.2 Equation for V . . . . .	199
C.4.3 Equation for $(H)$ . . . . .	200
C.4.4 Equation for Q . . . . .	200
C.4.5 Other Equations . . . . .	201
C.5 Computational Problems . . . . .	202
C.5.1 Formation of Artificial Inversions: Case of no Real Inversion . . . . .	203
C.5.2 Blocking of the Height of the Daytime Inversion . .	205
C.6 Refinements to the Finite-Difference Equations . .	207
C.6.1 Double Precision . . . . .	207
C.6.2 Minimization of Round-Off Errors . . . . .	209
C.6.3 Higher-Order Approximation to the Derivatives . .	212
C.6.4 Restriction on the Temperature Profile . . . . .	212



APPENDIX		Page
D	INFRARED FLUX DUE TO WATER VAPOR . . . . .	215
D.1	Hypotheses . . . . .	215
D.2	Computation of Temperature . . . . .	216
D.3	Computation of Pressure . . . . .	216
D.4	Equation for the Infrared Flux . . . . .	217
D.5	Computation of the Infrared Flux . . . . .	218
D.5.1	For the Lower Boundary . . . . .	218
D.5.2	For the Other Levels . . . . .	218
D.5.3	Integrated Result . . . . .	219
E	SOLUTION OF THE SURFACE TEMPERATURE EQUATION . . . .	220
E.1	Solution of the Resolvent Cubic Equation . . . . .	222
E.2	Solution of the Quartic Equation . . . . .	224
F	LIST OF SYMBOLS . . . . .	225



## LIST OF TABLES

Table	Page
1. Ordering of Terms	41
2. Equations used for emissivity in the Brooks method as a function of total path length (cm)	88
3. Comparison between three steady-state simulations	94
4. Parameters for the time-dependent simulations	99
5. Comparison of the surface potential temperature between the four simulations of the urban heat island	155
6. Computed values for the grid-point heights $z(k)$ at various stages of iteration	170
7. Best OMEGA corresponding to the computed values of the grid points at various stages of iteration	171
8. Computed values of the grid-point heights $z(k)$ at various stages of iteration	172
9. Best OMEGA corresponding to the computed grid-point heights at some of the iteration steps.	172
10. Average number of elementary operations for addition and multiplication in single and double precision when we use the decimal system	208
11. Average number of elementary operations for addition and multiplication in single and double precision when we use the binary system	208
12. Restriction on $\Theta(k_0, t_0 + \Delta t)$	214



## LIST OF FIGURES

Figure	Page
1. Schematic representation of the grid used by Myrup (1969)	3
2. Schematic illustration of the horizontal variation of the depth of the internal boundary layer ( $h$ ) and of the height of the transition layer ( $h'$ )	7
3. Diagram of the horizontal variation of the depth of the internal boundary layer for a two-dimensional model in which the discontinuity in roughness height happens between two grid points	7
4. Schematic representation of the vertical distribution of the variables in the energy redistribution term. The zero value is indicated by a solid line parallel to the $z$ axis, and the dotted lines represent the behavior of the variables	25
5. Illustration of the air parcel method. The solid curve represents the mean potential temperature of the environment for an unstable situation	29
6. Normalized wind hodograph	94
7. Vertical variation of $e^2/u_*^2$	96
8. Vertical variation of $K_m/k_o u_*$	96
9. Diurnal cycle of the surface potential temperature	101
10. Warming rate at the surface	102
11. Diurnal variation of the roughness angle	103
12. Diurnal cycle of the vertical distribution of potential temperature for the case $z_o = 1$ cm, $V_g = 20$ m/sec and high soil conductivity	105
13. Diurnal cycle of the vertical distribution of potential temperature for the case $z_o = 1$ cm, $V_g = 10$ m/sec and high soil conductivity	106
14. Diurnal cycle of the vertical distribution of $\overline{w\theta}$ for the case $z_o = 1$ cm, $V_g = 20$ m/sec and high soil conductivity	108



Figure	Page
15. Diurnal cycle of the vertical distribution of $\bar{w}\Theta$ for the case $z_o = 1 \text{ cm}$ , $V_g = 10 \text{ m/sec}$ and high soil conductivity	109
16. Diurnal cycle of the vertical distribution of the coefficient of diffusivity for temperature for the case $z_o = 1 \text{ cm}$ , $V_g = 10 \text{ m/sec}$ and high soil conductivity	110
17. Diurnal cycle of the vertical distribution of the coefficient of diffusivity for temperature for the case $z_o = 1 \text{ cm}$ , $V_g = 20 \text{ m/sec}$ and high soil conductivity	111
18. Diurnal cycle of the vertical distribution of $U$ for the case $z_o = 1 \text{ cm}$ , $V_g = 10 \text{ m/sec}$ and high soil conductivity	113
19. Diurnal cycle of the vertical distribution of $U$ for the case $z_o = 1 \text{ cm}$ , $V_g = 20 \text{ m/sec}$ and high soil conductivity	114
20. Diurnal cycle of the total mean wind for the case $z_o = 1 \text{ cm}$ , $V_g = 20 \text{ m/sec}$ and high soil conductivity	115
21. Diurnal cycle of the vertical profile of $V$ for the case $z_o = 1 \text{ cm}$ , $V_g = 10 \text{ m/sec}$ and high conductivity	117
22. Diurnal variation of the vertical distribution of $V$ for the case $z_o = 1 \text{ cm}$ , $V_g = 20 \text{ m/sec}$ and high soil conductivity	118
23. Diurnal variation of the vertical profile of $e$ for the case $z_o = 1 \text{ cm}$ , $V_g = 10 \text{ m/sec}$ and high soil conductivity	119
24. Diurnal cycle of the vertical distribution of $e$ for the case $z_o = 1 \text{ cm}$ , $V_g = 20 \text{ m/sec}$ and high soil conductivity	120
25. Diurnal cycle of the atmospheric potential temperature for the case $z_o = 100 \text{ cm}$ , $V_g = 10 \text{ m/sec}$ and high soil conductivity	122
26. Diurnal cycle of the vertical profile of $\bar{w}\Theta$ for the case $z_o = 100 \text{ cm}$ , $V_g = 10 \text{ m/sec}$ and high soil conductivity	123



Figure	Page
27. Diurnal cycle of the vertical profile of $K_t$ for the case $z_o = 100 \text{ cm}$ , $V_g = 10 \text{ m/sec}$ and high soil conductivity	125
28. Diurnal cycle of the vertical profile of $\epsilon$ for the case $z_o = 100 \text{ cm}$ , $V_g = 10 \text{ m/sec}$ and high soil conductivity	126
29. Diurnal variation of the vertical profile of $U$ for the case $z_o = 100 \text{ cm}$ , $V_g = 10 \text{ m/sec}$ and high soil conductivity	127
30. Diurnal variation of the vertical profile of $V$ for the case $z_o = 100 \text{ cm}$ , $V_g = 10 \text{ m/sec}$ and high soil conductivity	128
31. Diurnal cycle of the vertical profile of the potential temperature for the case $z_o = 1 \text{ cm}$ , $V_g = 10 \text{ m/sec}$ and low conductivity in the soil	130
32. Diurnal cycle of the vertical profile of $\bar{w}\theta$ for the case $z_o = 1 \text{ cm}$ , $V_g = 10 \text{ m/sec}$ and low thermal soil conductivity	131
33. Diurnal cycle of the vertical profile of $K_t$ for the case $z_o = 1 \text{ cm}$ , $V_g = 20 \text{ m/sec}$ and high soil conductivity	132
34. Diurnal cycle of the vertical profile of $\epsilon$ for the case $z_o = 1 \text{ cm}$ , $V_g = 10 \text{ m/sec}$ and low thermal soil conductivity	133
35. Diurnal cycle of the vertical profile of $U$ for the case $z_o = 1 \text{ cm}$ , $V_g = 10 \text{ m/sec}$ and low soil conductivity	134
36. Diurnal variation of the vertical profile of $V$ for the case $z_o = 1 \text{ cm}$ , $V_g = 10 \text{ m/sec}$ and low soil conductivity	135
37. Diurnal variation of the vertical profile of $\ell$ for the case $z_o = 1 \text{ cm}$ , $V_g = 20 \text{ m/sec}$ and high soil conductivity	137
38. Diurnal variation of the vertical profile of $\bar{\theta}^2$ for the case $z_o = 1 \text{ cm}$ , $V_g = 20 \text{ m/sec}$ and high soil conductivity	139
39. Diurnal cycle of the vertical profile of $\bar{u}\theta$ for the case $z_o = 1 \text{ cm}$ , $V_g = 20 \text{ m/sec}$ and high soil conductivity	140
40. Diurnal cycle of the vertical profile of $\bar{v}\theta$ for the case $z_o = 1 \text{ cm}$ , $V_g = 20 \text{ m/sec}$ and high soil conductivity	141



Figure	Page
41. Diurnal variation of the vertical profile of $\bar{u} w$ for the case $z_o = 1 \text{ cm}$ , $V_g = 20 \text{ m/sec}$ and high soil conductivity	142
42. Diurnal cycle of the vertical profile of $\bar{v} w$ for the case $z_o = 1 \text{ cm}$ , $V_g = 20 \text{ m/sec}$ and high soil conductivity	143
43. Diurnal cycle of the vertical variation of $K_m$ for the case $z_o = 1 \text{ cm}$ , $V_g = 20 \text{ m/sec}$ and high soil conductivity	145
44. Diurnal variation of the vertical profile of $\bar{u}^2$ for the case $z_o = 1 \text{ cm}$ , $V_g = 20 \text{ m/sec}$ and high soil conductivity	146
45. Diurnal variation of the vertical profile of $\bar{v}^2$ for the case $z_o = 1 \text{ cm}$ , $V_g = 20 \text{ m/sec}$ and high soil conductivity	147
46. Diurnal variation of the vertical profile of $\bar{w}^2$ for the case $z_o = 1 \text{ cm}$ , $V_g = 20 \text{ m/sec}$ and high soil conductivity	148
47. Diurnal variation of the vertical profile of $\bar{u} v$ for the case $z_o = 1 \text{ cm}$ , $V_g = 20 \text{ m/sec}$ and high soil conductivity	149
48. Diurnal variation of the soil temperature profile for the case $z_o = 1 \text{ cm}$ , $V_g = 10 \text{ m/sec}$ and high soil conductivity	150
49. Diurnal variation of the soil temperature profile for the case $z_o = 1 \text{ cm}$ , $V_g = 10 \text{ m/sec}$ and low soil conductivity	151
50. Diurnal variation of the soil temperature profile for the case $z_o = 100 \text{ cm}$ , $V_g = 10 \text{ m/sec}$ and high soil conductivity	152
51. Diurnal variation of the soil temperature profile for the case $z_o = 1 \text{ cm}$ , $V_g = 20 \text{ m/sec}$ and high soil conductivity	153



## CHAPTER I

### PREVIOUS WORK

#### 1.1 Introduction.

The observation that the micro-climate of a city is different from the surrounding countryside has been made long ago. The most noticeable difference is observed generally in the diurnal temperature cycle with the cities usually being warmer than their outlying areas. This is why the climatic influence of the urban area has been termed the "urban heat island". The first statistical study of this effect dates back to Howard's (1833) study of London's temperature. Since then many other features have been associated with the urban effect: changes in surface roughness, in soil conductivity, in surface moisture, in albedo, in artificial heat input, in air pollution, etc. All these factors interact in a complex fashion to produce the urban heat island with which can be associated not only changes in the diurnal temperature cycle but also changes in the precipitation pattern, in fog occurrences, in wind velocities and in many other properties. Recent observations seem to indicate that the maximum temperature difference between the city and the rural area happens four to five hours after sunset and not near sunrise as could be expected. This feature was observed in Edmonton by Hage (1972), and in Vancouver and Montreal by Oke and Maxwell (1975).

#### 1.2 Statistical Studies.

Many statistical studies of the urban effect have been made:



Duckworth and Sandberg (1954), Landsberg (1956), Mitchell (1961), Roden (1966) and Bornstein (1968) are a few examples of recent ones. The general results are that the urban area is warmer on the average by up to 2-3 °C, with the maximum difference during the nighttime. In some cases the urban daytime temperature was found to be cooler than the rural one. The heat island is also generally more pronounced in the summertime with a few cities developing their maximum temperature excess during winter. This points out that the causes for the urban heat island are varied and could in some cases be minimized or enhanced by local effects due to lakes or mountains for example. The wind speed (Sundborg, 1951) and the city size (Landsberg, 1956) affect the magnitude of the temperature excess with a smaller value being associated with higher wind speeds and smaller cities.

### 1.3 Unidimensional Numerical Model.

The numerical investigation of the urban heat island is recent, e.g., Myrup (1969) was a pioneer in this domain. He used a very simple model in which the interaction between a soil layer and an atmospheric layer was studied. In Fig. 1, we have a schematic representation of Myrup's model. The soil layer contains the minimum number of levels: the bottom level is at a distance  $2d=0.5m$  from the surface and is the level at which the temperature is held constant; the temperature at the level just above the bottom is computed by equating the local change in temperature to the diffusion of temperature; the top boundary of the soil layer is the earth's surface whose temperature is computed from a heat balance equation which contains net radiation, turbulent fluxes of sensible and latent heat, and the heat flux from the soil.



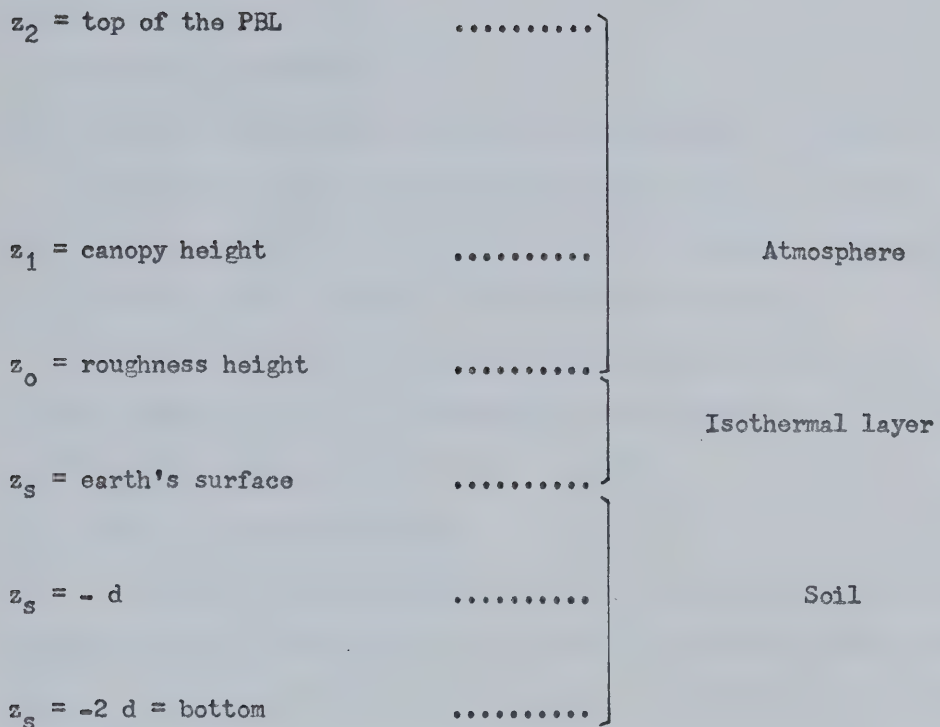


Figure 1. Schematic representation of the grid used by Myrup (1969).



The first atmospheric level is at the roughness height  $z_0$ , the next one  $z_1$  is at the canopy height, and  $z_2$  is the top of the boundary layer where the meteorological conditions are assumed to be constant. The basic assumptions are:

1. Horizontal homogeneity.
2. Turbulent diffusivities for heat and water vapor are given by the turbulent diffusivity for the near-neutral case.
3. Constant sensible and latent heat fluxes throughout the atmosphere.
4. Constant relative humidity at the roughness height.
5. Temperature, wind and mixing ratio are constant at  $z_2$ .
6. The temperature at  $z_0$  = temperature at the ground.
7. The canopy has a unique roughness height.
8. Constant infrared radiation.

The most drastic assumptions in his model are: (a) the lack of variation of the turbulent diffusivities with stability, which is totally wrong in the case of stable stratification as shown by the numerical results of Mellor and Yamada (1974), (b) the extension of the constant-flux layer up to  $z_2 = 300$  m, which is a very poor assumption in the stable stratification of the nighttime and (c) the assumption that the meteorological variables are constant at  $z_2$ , an assumption that Myrup himself found quite poor. The most obvious improvement that can be made to his model is to add more levels in order to use more realistic assumptions. His results showed the maximum excess temperature in the city during the day instead of at night as is observed. However, his model illustrated that the following parameters were important: reduction of evaporation in the city, increased roughness of the city, thermal properties of the buildings and paving materials, and wind speed. Artificial heating



did not seem to play an important role in the formation of the urban heat island.

Miller, et al. (1972) have corrected some mistakes in Myrup's model. Their model is also in one dimension and includes as a new feature an albedo model of a city which is being developed by Craig and Lowry (1972) and which takes into account radiation trapping between the walls of an ideal city. However, this refined model of the albedo will not be used in this study because it is not easily applied to a real city.

By using a more detailed soil layer and more atmospheric levels Nappo (1972) has claimed to predict that the maximum temperature difference between urban and rural areas occurs a few hours after sunset. However, his results should be viewed with caution as he used a constant-flux layer of 50 m, which according to Kuo (1968) is not capable of adequately representing the temperature variation in the thermal boundary layer. Moreover, from his graphs of the diurnal temperature cycle we get the impression that the temperature variation would be different from one day to the other.

#### 1.4 Two-Dimensional Models.

Some recent studies have extended the model to a second dimension, such that horizontal advection is possible. For example, McElroy (1972) has studied the effect of land-use strategies by alternating rough and smooth surfaces in his model, with the purpose of trying to derive benefit from the urban heat island. However, he used a constant-flux layer of 15 to 35 m, which is certainly too high for the actual overnight constant-flux layer.

Are there many advantages in going into a two-dimensional



model? Part of the answer lies in the way in which the two-dimensional model treats the discontinuity in roughness height between two adjacent horizontal grid points. In general the models assume a fixed roughness height at each grid point. Therefore, at each grid point we assume infinite homogeneity in the transverse direction and spatial homogeneity of the order of the grid-point spacing along the grid-point orientation direction. From studies of the constant-flux layer, it is clear that discontinuity in roughness heights causes the formation of an internal boundary layer as illustrated in Fig. 2. Above the internal boundary layer the turbulence is characterized by the upstream roughness height and not by the roughness height below it. The ratio of change in roughness height to fetch is approximately 1/20 on the basis of the wind profile, according to Angle (1973). In many two-dimensional models the horizontal grid-point spacing is about 500 m, and generally the change in roughness height is at most 1 m between each grid point. If we assume that the change in roughness occurs abruptly in the middle of two grid points, we get an internal boundary-layer height of 12.5 m over the second grid point as shown in Fig. 3. This means that all levels above 12.5 m are almost undisturbed yet some authors have assumed a constant-flux layer of up to 50 m, which means that they have assumed the wrong value for the lower boundary condition and that they have introduced too soon the influence of the change in roughness height at higher levels. Therefore, the two-dimensional models might not be able to represent accurately the transition from smooth rural area to rough urban area. However, the two-dimensional model has more versatility certainly because it can include vertical winds and divergence.



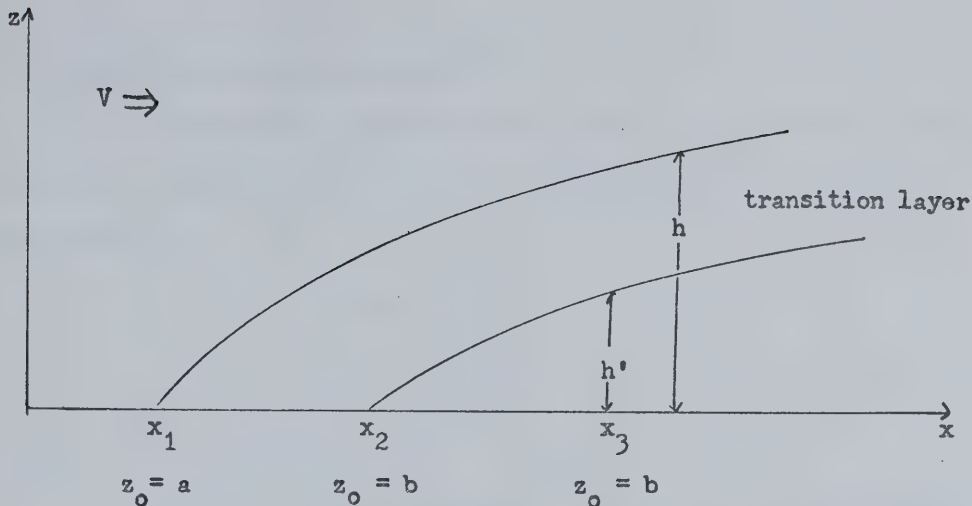


Figure 2. Schematic illustration of the horizontal variation of the depth of the internal boundary layer ( $h$ ) and of the height of the transition layer ( $h'$ ). The roughness height changes abruptly from  $a$  to  $b$  at  $x_2$ . The region above the transition layer is influenced only by  $z_o = a$ , whereas the region below the transition layer is influenced only by  $z_o = b$ . In the transition layer both  $a$  and  $b$  are influencing the flow.

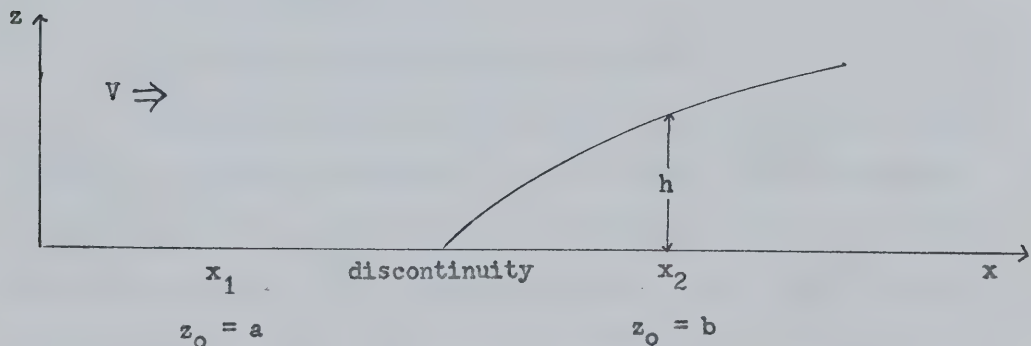


Figure 3. Diagram of the horizontal variation of the depth of the internal boundary layer for a two-dimensional model in which the discontinuity in roughness height happens between two grid points.



### 1.5 Higher-Order Closure Scheme.

All the models discussed so far have used K-theory in which the stress components are related to the gradient of the mean wind components by,

$$\overline{uw} = - K_m \frac{\partial U}{\partial z} \quad (1.1)$$

$$\overline{vw} = - K_m \frac{\partial V}{\partial z} \quad (1.2)$$

where,  $K_m$  = eddy diffusivity coefficient for momentum

$U$  and  $V$  =  $x$  and  $y$  components of the mean wind (horizontal)

$\overline{uw}$  and  $\overline{vw}$  =  $x$  and  $y$  components of the friction velocity  $u_*$

related to the stress  $\tau$  and air density  $\rho$  by:

$$u_* = (\tau / \rho)^{\frac{1}{2}} \quad (1.3)$$

Arbitrary assumptions have to be made in order to define  $K_m$ .

Close to the ground in near-neutral stability  $K_m$  has been observed empirically to behave like,

$$K_m = k_o (z + z_o) \left| \frac{\partial \vec{V}}{\partial z} \right| \quad (1.4)$$

where,  $k_o = 0.35$  = Von Karman's constant (Businger, et al., 1971)

$z_o$  = roughness height

$z$  = height above the roughness height.

K-theory has been extended outside the constant-flux layer by assuming an empirical variation of  $K_m$  with height. The near-neutral stability condition can be removed by multiplying  $K_m$  by an empirical "stability function". All of these extensions do not appear to be on a solid theoretical basis and depend rather strongly on the experimental data used to derive them. Therefore, while K-theory has the great advantage of simplicity, it can be very poor on occasion; for example



a countergradient flux has been observed during some experiments (Eskinazi and Erian, 1969) in locally-embedded regions where the stress and velocity gradients are small and this cannot be explained physically by a gradient theory like K-theory. An alternate approach in numerical modelling of the boundary-layer is the "higher-order closure" scheme, being developed, for example, by Donaldson (1973), Mellor and Yamada (1974), Meroney (1974) and many others. Mellor's and Yamada's approach seems the most promising for the study of the boundary layer. They have ordered various levels of models in terms of their simplifying assumptions, and they have imposed boundary conditions near the surface in accordance with experimental results. The weakest point of these theories is that the constants used in modelling various terms in the equations are ill-defined due to the lack of precise observations.



## CHAPTER II

### DEVELOPMENT OF THE ATMOSPHERIC EQUATIONS

#### 2.1 Basic Equations.

##### 2.1.1 Perfect Gas law.

The equation of state that will be used is the perfect gas law which is accurate enough in comparison with the uncertainties associated with many turbulent variables. However, as this model contains water vapor in variable amounts, we will use the virtual temperature concept in order to keep R, the dry atmosphere gas constant, in the equations.

$$\tilde{p} = \tilde{\rho} R \tilde{T}_v \quad (2.1)$$

where  $\sim$  indicates the instantaneous value of a variable

$\tilde{p}$  is the pressure

$\tilde{T}_v$  is the virtual temperature related to the absolute temperature  $\tilde{T}$  by,

$$\tilde{T}_v = \tilde{T} (1 + 0.6078 \tilde{q}) \quad (2.2)$$

where  $\tilde{q}$  is the mixing ratio for water vapor.

##### 2.1.2 Continuity Equation.

The continuity equation represents conservation of mass in a compressible atmosphere.

$$\frac{\partial \tilde{\rho}}{\partial t} + \frac{\partial}{\partial x_j} (\tilde{\rho} \tilde{u}_j) = 0 \quad (2.3)$$

where  $\tilde{u}_j$  is the wind component in the j direction, and

$x_j$  is the distance in the j direction.



### 2.1.3 Momentum Equation.

We will use the Navier-Stokes' equations to relate the stress  $\tilde{\tau}_{ij}$  and the rate of strain  $\tilde{\sigma}_{ij}$ . These equations require the following assumptions:

- 1) There is a linear relation between stress and rate of strain.

$$\tilde{\tau}_{ij} = -\tilde{p} \delta_{ij} + \tilde{\sigma}_{ij}$$

where  $\tilde{\sigma}_{ij} = K_{ijkl} \frac{\partial \tilde{u}_k}{\partial x_l}$

and  $K_{ijkl}$  is a fourth order tensor whose properties are defined by the next two hypotheses.

- 2) The molecular structure of the fluid is isotropic.
- 3) The divergence makes no contribution to normal stresses.
- 4) The variations in the first and second coefficients of viscosity, respectively  $\mu$  and  $\mu_*$ , are neglected.

If we add the Coriolis force and gravity the equations of motion become:

$$\tilde{\rho} \frac{\partial \tilde{u}_i}{\partial t} + \frac{\partial}{\partial x_j} (\tilde{\rho} \tilde{u}_j \tilde{u}_i) = - \frac{\partial \tilde{p}}{\partial x_i} + \frac{\partial}{\partial x_j} \tilde{\tau}_{ij} - \tilde{\rho} \tilde{g}_i - \tilde{\rho} \epsilon_{ijk} f_j \tilde{u}_k \quad (2.4)$$

where the stress equation is

$$\tilde{\tau}_{ij} = \mu \left( \frac{\partial \tilde{u}_i}{\partial x_j} + \frac{\partial \tilde{u}_j}{\partial x_i} \right) + \delta_{ij} \mu_* \frac{\partial \tilde{u}_m}{\partial x_m} \quad (2.5)$$

and where: i, j, k are indices of value 1 to 3. The repetition of an index inside a term implies summation over all the values.

$$\epsilon_{ijk} = \begin{cases} +1 & \text{if } i, j \text{ and } k \text{ are in cyclic order} \\ -1 & \text{if } i, j \text{ and } k \text{ are in non-cyclic order} \\ 0 & \text{if any of the indices are equal} \end{cases}$$

$f_j$  = Coriolis parameter



### 2.1.4 Energy Equation.

Following Godson (1958), we start with the equation for the entropy of the dry air  $\tilde{S}_a$ ,

$$d \tilde{S}_a = C_p d \ln \tilde{T} - R d \ln (\tilde{p}/\tilde{e}) \quad (2.6)$$

where  $\tilde{e}$  is the partial pressure of water vapor and

$C_p$  is the heat capacity at constant pressure of the dry air.

A similar equation is valid for  $\tilde{S}_v$ , the entropy of the water vapor:

$$d \tilde{S}_v = C_{p_v} d \ln \tilde{T} - R_w d \ln \tilde{e} \quad (2.7)$$

where  $C_{p_v}$  is the heat capacity at constant pressure of the water vapor and  $R_w$  is the gas constant for water vapor.

The following relationships are useful (Godson, 1958):

$$\xi = R/R_w$$

$$C_{p_v} = 8 C_p / (7 \xi)$$

$$\tilde{e} = \tilde{p} \tilde{q} / (q + \xi)$$

$$\tilde{p} - \tilde{e} = \xi \tilde{p} / (q + \xi)$$

We combine (2.6) and (2.7) and form the equation for  $\tilde{S}$ , the entropy of the mixture of 1 gram of dry air with  $\tilde{q}$  gram of water vapor. If we neglect some small terms involving  $(d \tilde{q})$ , we obtain

$$(1 + \tilde{q}) d \tilde{S} = (C_p + \tilde{q} C_{p_v}) d \ln \tilde{T} - (R + \tilde{q} R_w) d \ln \tilde{p} \quad (2.8)$$

We use the definition of virtual temperature and the perfect gas law, neglect some small terms including the variation of the heat capacity due to water vapor, and obtain after some manipulations

$$\tilde{\rho} \tilde{T}_v \frac{d \tilde{S}}{d t} = \tilde{\rho} C_p \frac{d \tilde{T}_v}{d t} - \frac{d \tilde{p}}{d t} \quad (2.9)$$

If we neglect radiative flux divergence, heat generated by viscous stress, and variations in the molecular heat diffusivity  $\tilde{k}$



we obtain an equation stating that the change in entropy of the dry air is due to molecular thermal diffusion,

$$\tilde{\rho}_a \tilde{T} \frac{d \tilde{S}_a}{dt} = \tilde{k} \frac{\partial}{\partial x_1} \frac{\partial}{\partial x_1} \tilde{T} \quad (2.10)$$

A similar equation holds for the change in entropy of water vapor due to molecular thermal diffusion,

$$\tilde{\rho}_v \tilde{T} \frac{d \tilde{S}_v}{dt} = \frac{\tilde{k}}{\epsilon} \frac{\partial}{\partial x_1} \frac{\partial}{\partial x_1} \tilde{T} \quad (2.11)$$

Again we compute the change in entropy for the mixture of one gram of dry air with  $\tilde{q}$  gram of water vapor,

$$\tilde{\rho} \tilde{T}_v \frac{d \tilde{S}}{dt} = \tilde{k} \left( \frac{\partial}{\partial x_1} \frac{\partial}{\partial x_1} \tilde{T}_v + \tilde{T}_v \frac{(\epsilon - 1)}{(1 + \tilde{q})^2} \left( \frac{\partial}{\partial x_1} \frac{\partial}{\partial x_1} \tilde{q} \right) \right) \quad (2.12)$$

In the last equation we have neglected two small terms of the order of  $(\Delta \tilde{q})^2$  and  $(\Delta \tilde{T} \Delta \tilde{q})$  with respect to  $\Delta \tilde{T}$  and  $\tilde{T} \Delta \tilde{q}$  for the other terms. Using the equation for water vapor conservation (2.14), we combine (2.12) with (2.9) in order to get the energy equation,

$$c_p \left( \frac{\partial \tilde{T}_v}{\partial t} + \frac{\partial}{\partial x_j} (\tilde{\rho} \tilde{u}_j \tilde{T}_v) \right) = \frac{\partial \tilde{p}}{\partial t} + \tilde{u}_j \frac{\partial \tilde{p}}{\partial x_j} + \frac{\partial}{\partial x_j} \left( \tilde{k} \frac{\partial \tilde{T}_v}{\partial x_j} \right) \quad (2.13)$$

### 2.1.5 Water Vapor Conservation Equation.

We make the hypothesis that the change in the mixing ratio following a parcel of air is due only to molecular diffusion; therefore we neglect condensation and evaporation.

$$\frac{\partial}{\partial t} (\tilde{\rho} \tilde{q}) + \frac{\partial}{\partial x_j} (\tilde{\rho} \tilde{u}_j \tilde{q}) = \frac{\partial}{\partial x_j} \left( \tilde{\mu}^\tau \frac{\partial \tilde{q}}{\partial x_j} \right) \quad (2.14)$$

In this equation we have implicitly assumed that the physical processes responsible for the diffusion of momentum are the same as those that cause molecular diffusion of temperature and of water vapor. Consequently, we can write

$$\tilde{\mu}^\tau = \tilde{k}/c_p$$



## 2.2 Assumption of a Nearly-Adiabatic Atmosphere.

If we consider the atmosphere as being in a state slightly removed from the dry adiabatic atmosphere at rest, we can express the variable  $\tilde{A}$  as being the sum of its adiabatic value  $A_o$  and a deviation  $A'$ .

$$\tilde{p} = p_o + p' \quad (2.15)$$

$$\tilde{u}_j = 0 + u'_j \quad (2.16)$$

$$\tilde{\mu} = \mu_o + \mu' \quad (2.17)$$

$$\tilde{\rho} = \rho_o + \rho' \quad (2.18)$$

$$\tilde{T}_v = T_{v_o} + T_v' \quad (2.19)$$

$$\tilde{q} = 0 + q' \quad (2.20)$$

### 2.2.1 Perfect Gas Law.

Substituting (2.15) and (2.18) in the perfect gas law (2.1), we get after separating the equation into an equation for the adiabatic state and an equation for the departures from the adiabatic state:

$$p_o = \rho_o R T_{v_o} \quad (2.21)$$

$$p' = R (\rho_o T_v' + \rho' T_{v_o} + \rho' T_v') \quad (2.22)$$

### 2.2.2 Continuity Equation.

Similarly, the continuity equation (2.3) becomes, when combined with (2.18) and (2.16):

$$\frac{\partial \rho_o}{\partial t} = 0 \quad (2.23)$$

$$\frac{\partial \rho'}{\partial t} + \frac{\partial}{\partial x_j} (\rho_o u'_j + \rho' u'_j) = 0 \quad (2.24)$$



### 2.2.3 Momentum Equation.

We now make the additional assumptions that

$$\rho' \ll \rho_0 \quad \mu' \ll \mu_0 \quad \mu_*' \ll \mu_* \quad (2.25)$$

and substitute (2.15) to (2.19) into the momentum equation (2.4) making use of (2.22) and (2.25) in order to simplify the terms.

$$\frac{\partial p_0}{\partial x_i} = -\rho_0 g_i \quad (2.26)$$

$$\rho_0 \frac{\partial u_i'}{\partial t} + \rho_0 u_j' \frac{\partial u_i'}{\partial x_j} = -\frac{\partial p'}{\partial x_i} - \rho' g_i + \frac{\partial}{\partial x_j} (\rho_0 (\frac{\partial u_i'}{\partial x_j} + \frac{\partial u_j'}{\partial x_i})) + \\ \delta_{ij} \frac{\partial}{\partial x_i} (\mu_*' \frac{\partial u_m'}{\partial x_m}) \quad (2.27)$$

### 2.2.4 Energy Equation.

We now make the substitution into the energy equation, in which the thermal diffusivity has been rewritten in terms of  $\mu$ . The following additional assumption is needed in order to simplify the equation: the heating of the fluid due to motion ( $\frac{\partial p'}{\partial t} + u_j' \frac{\partial p'}{\partial x_j} = \theta (\text{Mach})^2$ ) is neglected.

The entropy equation (2.8) is applied to the basic isentropic atmosphere and becomes,

$$\rho_0 T_{v_0} d s_0 = 0 = \rho_0 c_{p_0} d T_{v_0} - d p_0 \quad (2.28)$$

If we take the local time derivative of (2.28) and note that the entropy of the basic atmosphere is time independent, we have:

$$0 = \rho_0 c_{p_0} \frac{\partial T_{v_0}}{\partial t} - \frac{\partial p_0}{\partial t} \quad (2.29)$$

The equation for the energy of the basic atmosphere as determined by the substitution of (2.15) to (2.19) into (2.13) is,



$$c_{p_0} \frac{\partial}{\partial x_j} (\mu_o^T \frac{\partial T_{v_0}}{\partial x_j}) = - \frac{\partial p_0}{\partial t} + c_{p_0} \frac{\partial \rho_0}{\partial t} \frac{T_{v_0}}{T_{v_0}} = 0 \quad (2.30)$$

The last equality results from (2.23) and (2.29). Therefore, we are left only with the energy associated with the diabatic part of the atmosphere,

$$c_{p_0} \rho_0 \left( \frac{\partial T'_v}{\partial t} + u'_j \frac{\partial T'_v}{\partial x_j} \right) = \frac{\partial}{\partial x_j} (\mu_o^T \frac{\partial T'_v}{\partial x_j} + \mu'^T \frac{\partial T_{v_0}}{\partial x_j}) c_{p_0} \quad (2.31)$$

#### 2.2.5 Mixing-Ratio Equation.

When we introduce the adiabatic reference state into (2.14) we have,

$$\rho_0 \frac{\partial q'}{\partial t} + \rho_0 u'_j \frac{\partial q'}{\partial x_j} = \frac{\partial}{\partial x_j} (\mu_o^T \frac{\partial q'}{\partial x_j}) \quad (2.32)$$

#### 2.2.6 Simplified Continuity Equation.

From the perfect gas law equations (2.21) and (2.22), we can form the ratio of the adiabatic deviation of the pressure to the pressure of the adiabatic atmosphere,

$$\frac{p'}{p_0} = \frac{T'_v}{T_{v_0}} + \frac{\rho'}{\rho_0} + \frac{\rho' T'_v}{\rho_0 T_{v_0}} \quad (2.33)$$

As  $\rho' \ll \rho_0$  and  $T'_v \ll T_{v_0}$ , the equation reduces to,

$$\frac{p'}{p_0} = \frac{T'_v}{T_{v_0}} + \frac{\rho'}{\rho_0} \quad (2.34)$$

The changes in  $p_0$  are of the order of  $(\rho_0 u'_j)^2$  so that,

$$\frac{p'}{p_0} = \mathcal{O}\left(\frac{\rho_0 u'_j}{R T_{v_0}}\right) = \mathcal{O}(\gamma \text{ Mach}) = \frac{T'_v}{T_{v_0}} + \frac{\rho'}{\rho_0} \approx 0$$

where  $\gamma$  is the specific heat ratio of the atmosphere  $= c_{p_0}/c_{v_0}$  and  $c_{v_0}$  is the heat capacity at constant volume of the atmosphere.

$$\rho' = - \rho_0 \frac{T'_v}{T_{v_0}} / \gamma \quad (2.35)$$



Combining (2.35) and (2.24) and neglecting second-order terms, we obtain

$$\frac{\partial u'_j}{\partial x_j} = - \frac{u'_j}{\rho_o} \frac{\partial p_o}{\partial x_j} + \frac{R}{p_o} \frac{\partial}{\partial x_j} (\mu_o^T \frac{\partial T'_v}{\partial x_i} + \mu^T \frac{\partial T_{v_o}}{\partial x_j}) \quad (2.36)$$

For the atmospheric processes in the boundary layer this equation can generally be simplified to,

$$\frac{\partial u'_j}{\partial x_j} = 0 \quad (2.37)$$

### 2.2.7 Resulting Set of Equations.

If we replace  $T'_v$  by its approximate expression,

$$T'_v = T' (1 + 0.6078 q') \quad (2.38)$$

we can then easily derive the equation for  $T'$  which has the same form as the ones for  $T'_v$  and  $q'$ . Therefore, the atmospheric equations in the quasi-adiabatic atmospheric model are:

$$p_o = \rho_o R T_{v_o} \quad (2.39)$$

$$\frac{\partial p_o}{\partial x_i} = - \rho_o g_i \quad (2.40)$$

$$\rho_o \frac{\partial u'_i}{\partial t} + \rho_o u'_j \frac{\partial u'_i}{\partial x_j} = - \frac{\partial p'}{\partial x_i} + \frac{\rho_o}{T_{v_o}} g_i T'_v + \mu_o \frac{\partial}{\partial x_j} \frac{\partial}{\partial x_j} u'_i - \epsilon_{ijk} f_j u_k \quad (2.41)$$

$$\rho_o \frac{\partial T'}{\partial t} + \rho_o u'_j \frac{\partial T'}{\partial x_j} = \mu_o^T \frac{\partial}{\partial x_j} \frac{\partial}{\partial x_j} T' \quad (2.42)$$

$$\rho' \frac{\partial q'}{\partial t} + \rho_o u'_j \frac{\partial q'}{\partial x_j} = \mu_o^T \frac{\partial}{\partial x_j} \frac{\partial}{\partial x_j} q' \quad (2.43)$$

$$\rho' = - \frac{\rho_o T'_v}{T_v} \quad (2.44)$$

$$\frac{\partial u'_j}{\partial x_j} = 0 \quad (2.45)$$



### 2.3 Ensemble Averaging.

The next step is to separate each variable into a mean value and a departure from the mean. We will use the convention that a variable written in uppercase means an averaged quantity whereas if it is in lowercase it represents a fluctuating quantity.

$$u'_j = U_j + u_j \quad (2.46)$$

$$T'_j = \bar{\Theta} + \theta_j \quad (2.47)$$

$$T'_v = \bar{\Theta}_v + \theta_v \quad (2.48)$$

$$q' = Q + q \quad (2.49)$$

$$\rho' = \rho \quad (2.50)$$

$$\mu' = \mu \quad (2.51)$$

$$\nu = \mu/\rho = \text{kinematic coefficient of viscosity} \quad (2.52)$$

$$\alpha = \mu/\rho \quad (2.53)$$

#### 2.3.1 Equations for the Mean Quantities.

The equations for the mean quantities are obtained after inserting (2.46) to (2.51) into the equations of Section 2.2.7, and then taking ensemble averages of the new equations.

$$\frac{\partial U_j}{\partial x_k} = 0 \quad (2.54)$$

$$\begin{aligned} \frac{\partial U_j}{\partial t} + \frac{\partial}{\partial x_k} (U_k U_j + \bar{u}_k \bar{u}_j) + \epsilon_{ikl} f_k U_l &= - \frac{1}{\rho_0} \frac{\partial P}{\partial x_j} + \frac{g_j \bar{\Theta}_v}{T_0} \\ &+ \nu \frac{\partial^2}{\partial x_k^2} U_j \end{aligned} \quad (2.55)$$

$$\frac{\partial \bar{\Theta}}{\partial t} + \frac{\partial}{\partial x_k} (U_k \bar{\Theta} + \bar{u}_k \theta_j) = \alpha \frac{\partial^2 \bar{\Theta}}{\partial x_k^2} \quad (2.56)$$

$$\frac{\partial Q}{\partial t} + \frac{\partial}{\partial x_k} (U_k Q + \bar{u}_k q_j) = \alpha \frac{\partial^2 Q}{\partial x_k^2} \quad (2.57)$$



### 2.3.2 Equations for the Turbulent Quantities.

The equations for the turbulent quantities are derived from (2.41) to (2.45) in which the decomposition into mean and fluctuating parts has been made. From these equations are subtracted the appropriate equations for the mean quantities as given in the previous section.

$$\frac{\partial u_j}{\partial x_j} = 0 \quad (2.58)$$

$$\begin{aligned} \frac{\partial u_j}{\partial t} + \frac{\partial}{\partial x_k} (U_k u_j + u_k U_j + u_k u_j - \bar{u}_k \bar{u}_j) + \varepsilon_{ikl} f_k u_l = \\ - \frac{1}{\rho_0} \frac{\partial p}{\partial x_j} - \frac{g_i \theta_v}{T_0} + \nu \frac{\partial^2 u_j}{\partial x_k^2} \end{aligned} \quad (2.59)$$

$$\frac{\partial \theta}{\partial t} + \frac{\partial}{\partial x_k} (U_k \theta + \theta u_k + u_k \theta - \bar{u}_k \theta) = \alpha \frac{\partial^2 \theta}{\partial x_k^2} \quad (2.60)$$

$$\frac{\partial q}{\partial t} + \frac{\partial}{\partial x_k} (U_k q + Q u_k + u_k q - \bar{u}_k q) = \alpha \frac{\partial^2 q}{\partial x_k^2} \quad (2.61)$$

### 2.3.3 Equations for the Second-Order Moments.

The equations for the mean quantities involve the second-order moments for which equations will be derived from the basic set of (2.59) to (2.61). The equation for  $\bar{u}_i \bar{u}_j$  is obtained by changing the subscript  $j$  to  $i$  in equation (2.59), by multiplying the resulting equation by  $u_j$  and adding the new equation to (2.59) which has been multiplied by  $u_i$ . The final equation for  $\bar{u}_i \bar{u}_j$  is then obtained by taking the ensemble average of the last equation.

$$\begin{aligned} \frac{\partial \bar{u}_i \bar{u}_j}{\partial t} + \frac{\partial}{\partial x_k} (U_k \bar{u}_i \bar{u}_j + \bar{u}_k \bar{u}_i \bar{u}_j - \frac{\partial}{\partial x_k} \bar{u}_i \bar{u}_j) + \frac{1}{\rho_0} \frac{\partial}{\partial x_j} \bar{p} \bar{u}_i \\ + \frac{1}{\rho_0} \frac{\partial}{\partial x_1} \bar{p} \bar{u}_j + f_k (\varepsilon_{jkl} \bar{u}_l \bar{u}_i + \varepsilon_{ikl} \bar{u}_l \bar{u}_j) = - \bar{u}_k \bar{u}_i \frac{\partial \bar{u}_j}{\partial x_k} - \bar{u}_k \bar{u}_j \frac{\partial \bar{u}_i}{\partial x_k} \end{aligned}$$



$$-\frac{1}{T_o} (g_j \overline{u_i \theta_v} + g_i \overline{u_j \theta_v}) + \frac{1}{\rho_o} \overline{p(\frac{\partial u_i}{\partial x_j} + \frac{\partial u_j}{\partial x_i})} - 2\sqrt{\frac{\partial u_i}{\partial x_k} \frac{\partial u_j}{\partial x_k}} \quad (2.62)$$

Similarly the equation for  $\overline{u_j \theta}$  is obtained by multiplying (2.60) by  $u_j$  and (2.59) by  $\theta$ , adding the two resulting equations and finally taking the ensemble average. Because the equations for the other moments are found in a similar fashion, we will simply write down all the other equations without any further explanation.

$$\begin{aligned} & \frac{\partial \overline{u_j \theta}}{\partial t} + \frac{\partial}{\partial x_k} (U_k \overline{u_j \theta} + \overline{u_k u_j \theta} - \alpha \overline{u_j \frac{\partial \theta}{\partial x_k}} - \nu \overline{\theta \frac{\partial u_j}{\partial x_k}}) + \frac{1}{\rho_o} \frac{\partial \overline{p \theta}}{\partial x_j} + \epsilon_{jkl} f_k \overline{u_l \theta} \\ &= - \overline{u_j u_k \frac{\partial \theta}{\partial x_k}} - \overline{\theta u_k \frac{\partial U_j}{\partial x_k}} - \frac{1}{T_o} g_j \overline{\theta \theta_v} + \frac{1}{\rho_o} \overline{p \frac{\partial \theta}{\partial x_j}} - (\alpha + \nu) \overline{\frac{\partial u_j}{\partial x_k} \frac{\partial \theta}{\partial x_k}} \quad (2.63) \end{aligned}$$

$$\begin{aligned} & \frac{\partial \overline{u_j q}}{\partial t} + \frac{\partial}{\partial x_k} (U_k \overline{u_j q} + \overline{u_k u_i q} - \alpha \overline{u_j \frac{\partial q}{\partial x_k}} - \nu \overline{q \frac{\partial u_j}{\partial x_k}}) + \frac{1}{\rho_o} \frac{\partial \overline{p q}}{\partial x_j} + \epsilon_{jkl} f_k \overline{u_l q} \\ &= - \overline{u_j u_k \frac{\partial q}{\partial x_k}} - \overline{q u_k \frac{\partial U_j}{\partial x_k}} - \frac{g_j}{T_o} \overline{q \theta_v} + \frac{1}{\rho_o} \overline{p \frac{\partial q}{\partial x_j}} - (\alpha + \nu) \overline{\frac{\partial u_j}{\partial x_k} \frac{\partial q}{\partial x_k}} \quad (2.64) \end{aligned}$$

$$\frac{\partial \overline{\theta^2}}{\partial t} + \frac{\partial}{\partial x_k} (U_k \overline{\theta^2} + \overline{u_k \theta^2} - \alpha \overline{\frac{\partial \theta^2}{\partial x_k}}) = -2 \overline{u_k \theta} \frac{\partial \overline{\theta}}{\partial x_k} - 2\alpha \overline{\frac{\partial \theta}{\partial x_k} \frac{\partial \theta}{\partial x_k}} \quad (2.65)$$

$$\frac{\partial \overline{q^2}}{\partial t} + \frac{\partial}{\partial x_k} (U_k \overline{q^2} + \overline{u_k q^2} - \alpha \overline{\frac{\partial q^2}{\partial x_k}}) = -2 \overline{u_k q} \frac{\partial \overline{q}}{\partial x_k} - 2\alpha \overline{\frac{\partial q}{\partial x_k} \frac{\partial q}{\partial x_k}} \quad (2.66)$$

$$\frac{\partial \overline{q \theta}}{\partial t} + \frac{\partial}{\partial x_k} (U_k \overline{q \theta} + \overline{u_k q \theta} - \alpha \overline{\frac{\partial q \theta}{\partial x_k}}) = -\overline{u_k q} \frac{\partial \overline{\theta}}{\partial x_k} - \overline{u_k \theta} \frac{\partial \overline{q}}{\partial x_k} - 2\alpha \overline{\frac{\partial q}{\partial x_k} \frac{\partial \theta}{\partial x_k}} \quad (2.67)$$



## 2.4 Modelled Equations.

Equations (2.62) to (2.67) are the equations for all the second moments needed to solve the equations for the mean quantities. Unfortunately, these equations involve higher-order moments as well as covariances with pressure and many other covariances. In order to close the system we must find equations for these new covariances. One method would be to derive formally equations for these variables, but that method would introduce new covariances for which equations would be needed. This course of action does not look very promising because we would obtain an infinite set of equations always with fewer equations than variables. An alternative method consists of modelling each of the new covariances in terms of known variables for which an equation exists. We will follow Mellor and Yamada's (1974) modelling assumptions. There are some general guidelines that can be followed in that type of modelling:

- 1- The tensor properties of the term to be modelled should be preserved if possible.
- 2- The dimensions should always be respected.
- 3- The sign of each modelled term should be selected in such a way as to avoid negative scaling lengths or velocities.
- 4- We should try to use the simplest model possible which obeys guidelines 1-3 except if results indicate that a more complex model is needed.



### 2.4.1 Energy Redistribution Term.

The name "energy redistribution term" was used by Rotta (1951) when he noticed that this term partitions energy among the three energy components while not contributing to the total. Monin and Yaglom (1970) discuss Rotta's work and state that the physical justification for the modelling of this term lies in the Poisson's equation for pressure which is obtained after taking the divergence of the Navier-Stokes' equation without external forces,

$$\Delta p' = - \rho_0 \frac{\partial^2 u_i u_j}{\partial x_i \partial x_j} (\Delta x)^2 \quad (2.68)$$

If we apply Reynold's decomposition for ensemble averaging to (2.68) and subtract from it the equation for the mean pressure obtained by taking the ensemble average of (2.68), we are left with the equation for the fluctuating pressure,

$$\Delta p = - \rho_0 \frac{\partial^2 (U_i u_j + U_j u_i + u_i u_j - \bar{u}_i \bar{u}_j)}{\partial x_i \partial x_j} (\Delta x)^2 \quad (2.69)$$

This equation applies to a point element of a fluid, whereas the pressure fluctuation in our equations is representative of a vertical column and  $p$  therefore would result from integration of  $\Delta p$  over a vertical column. We will not carry out this integration here because we are interested only in the form of the terms that can be extracted by the inclusion of (2.69) in the energy redistribution term.

$$\overline{p_0 \left( \frac{\partial u_i}{\partial x_j} + \frac{\partial u_j}{\partial x_i} \right)} = \overline{\frac{\partial^2 (U_i u_j + U_j u_i + u_i u_j)}{\partial x_i \partial x_j}} - \overline{\frac{\partial^2 \bar{u}_i \bar{u}_j}{\partial x_i \partial x_j}} \left( \frac{\partial \bar{u}_i}{\partial x_j} - \frac{\partial \bar{u}_j}{\partial x_i} \right)$$

On the right-hand side of the last equation we notice the product of an averaged quantity  $\frac{\partial^2 \bar{u}_i \bar{u}_j}{\partial x_i \partial x_j}$  with  $(\frac{\partial \bar{u}_i}{\partial x_j} - \frac{\partial \bar{u}_j}{\partial x_i})$ ; therefore,



when we average this product we get terms of the form  $C'_{ijkm} \frac{\partial U_k}{\partial x_m}$ ,

where  $C'_{ijkm}$  is a fourth-order tensor yet to be determined. The other terms will involve products like  $\frac{\partial^2 U_i}{\partial x_i \partial x_j} \frac{\partial u_j}{\partial x_j}$  which are likely to give rise to terms in  $\overline{u_i u_j}$ . Therefore the energy redistribution term can be modelled by an expression like,

$$\overline{\frac{p}{\rho_0} \left( \frac{\partial u_i}{\partial x_j} + \frac{\partial u_j}{\partial x_i} \right)} = C_{ijkm} \overline{u_k u_m} + C'_{ijkm} \frac{\partial U_k}{\partial x_m} \quad (2.70)$$

Rotta (1951) then assumes that the constitutive coefficients are isotropic. That assumption has the advantage that it respects the tensor properties of the energy redistribution term and gives a relatively simple final answer.

$$C_{ijkm} = C_1 \delta_{ij} \delta_{km} + C_2 \delta_{ik} \delta_{jm} + C_3 \delta_{jk} \delta_{im} \quad (2.71)$$

$$C'_{ijkm} = C'_1 \delta_{ij} \delta_{km} + C'_2 \delta_{ik} \delta_{jm} + C'_3 \delta_{jk} \delta_{im} \quad (2.72)$$

Substituting the isotropic tensors (2.71) and (2.72) into the terms on the right-hand side of (2.70), we find

$$C_{ijkm} \overline{u_k u_m} = C_1 \delta_{ij} \overline{u_m u_m} + (C_2 + C_3) \overline{u_i u_j} \quad (2.73)$$

$$\text{and } C'_{ijkm} \frac{\partial U_k}{\partial x_m} = C'_2 \frac{\partial U_1}{\partial x_j} + C'_3 \frac{\partial U_1}{\partial x_i} \quad (2.74)$$

The equation of continuity has been used in (2.74). Due to the symmetry of the terms involving  $C'_2$  and  $C'_3$  it seems justifiable to postulate that these coefficients are equal and, therefore, that:

$$C'_{ijkm} \frac{\partial U_k}{\partial x_m} = C'_2 \left( \frac{\partial U_1}{\partial x_j} + \frac{\partial U_1}{\partial x_i} \right) \quad (2.75)$$

If we set  $i=j$  ( $i=1, 2, 3$ ) in (2.70) and add the three resulting equations we get,

$$\frac{p}{\rho_0} \left( \frac{\partial u_i}{\partial x_i} + \frac{\partial u_i}{\partial x_i} \right) = 3 C_1 e^2 + (C_2 + C_3) e^2 + 2 C'_2 \frac{\partial U_1}{\partial x_1} \quad (2.76)$$



where  $\epsilon^2 = \overline{u_i u_j}$  is proportional to the turbulent kinetic energy.

Using the continuity equation, (2.76) reduces to:

$$c_1 = -\frac{c_2 + c_3}{3} \quad (2.77)$$

Now we compare the dimensions,

$$\left[ \frac{1}{\rho_0} p \left( \frac{\partial u_i}{\partial x_j} + \frac{\partial u_j}{\partial x_i} \right) \right] = \left[ \frac{L^3}{M} \frac{M U}{T} \frac{U}{L^2} \frac{U}{L} \right] = \left[ \frac{U^2}{T} \right] = \left[ U^2 \frac{U}{L} \right] \quad (2.78)$$

$$\left[ (c_2 + c_3) \overline{u_i u_j} \right] = \left[ (c_2 + c_3) U^2 \right] \quad (2.79)$$

$$\left[ (c'_2 \left( \frac{\partial u_i}{\partial x_j} + \frac{\partial u_j}{\partial x_i} \right)) \right] = \left[ c'_2 \frac{U}{L} \right] \quad (2.80)$$

where L, M, T, and U indicate quantities with dimensions of length, mass, time and velocity, respectively. Therefore, on dimensional grounds,

$$(c_2 + c_3) = \frac{C}{3} \frac{\epsilon^2}{l_1} \quad (2.81)$$

$$c'_2 = C \frac{\epsilon^2}{l_1} \quad (2.82)$$

where  $l_1$  is a scaling length that has to be determined empirically, and C a constant that Mellor and Yamada have determined to be 0.056.

Now we have the sign to consider. The easiest way of determining the sign is to examine the variation in the vertical because the vertical gradients are normally the largest. We will first determine the sign of the energy redistribution term. Let us imagine a horizontal velocity perturbation  $u$  with a vertical profile as shown in Fig. 4 extending over the range  $2 h$  centered at  $z_c$ . From the continuity equation we would expect the vertical wind to compensate for the increase in  $u$ . Furthermore, we imagine the ideal situation in which there is no mixing of the air above and below  $z_c$  and in which half of the compensation comes from below and half from above. From Fig. 4 we can infer that



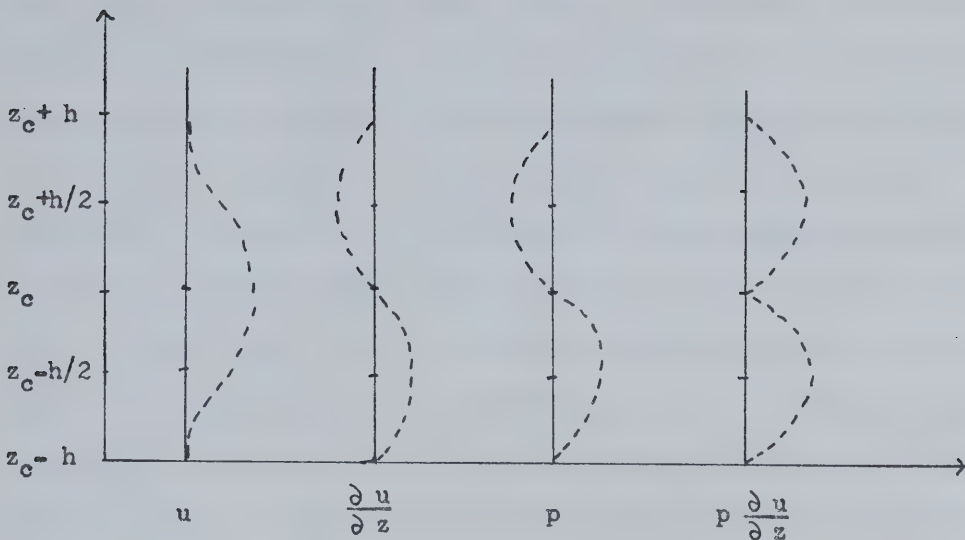


Figure 4. Shematic representation of the vertical distribution of the variables in the energy redistribution term. The zero value is indicated by a solid line parallel to the  $z$  axis, and the dotted lines represent the behavior of the variables.



air is removed around  $z_c + h$  and transported to levels near  $z_c$ . Therefore, there is a decrease in mass between  $z_c + h/2$  and  $z_c + h$  creating a negative pressure disturbance, and there is accumulation of mass below that layer down to  $z_c$  which causes the pressure disturbance to become less negative. As there is no mass transfer across  $z_c$  we expect no pressure disturbance at  $z_c$  if we neglect the dynamic effect caused by the downward vertical wind. Similar reasoning applied to the region below  $z_c$  gives upward vertical motion and a positive pressure disturbance. By comparing the  $u$  and  $p$  vertical profiles we see that the product  $p \frac{\partial u}{\partial z}$  is always positive. This idealized situation clearly shows that we expect the energy redistribution term to be positive when we consider the vertical variation of the horizontal wind.

If we use (2.82), the first two modelling terms in (2.76) become  $\frac{e}{3\ell_1} (\overline{u_i u_j} - e^2/3)$ . As we know  $e^2$  is proportional to the turbulent kinetic energy and is always positive.  $\overline{u w}$  is generally the most important covariance included in  $\overline{u_i u_j}$  and can be related to the gradient of the mean wind through a diffusivity equation,

$$-\overline{u w} = K_m \frac{\partial U}{\partial z}$$

$K_m$  is generally positive and the gradient of the mean wind is always positive in the nearly constant-flux layer. Therefore, the first two modelling terms are always negative which implies that we need a negative sign in front of them. The modelling term  $C \frac{\partial U}{\partial z}$  is always positive so that its sign agrees with the sign of the term that is being modelled. Grouping all our findings, the final result is,

$$\frac{p}{\rho_0} \left( \frac{\partial u_i}{\partial x_j} + \frac{\partial u_j}{\partial x_i} \right) = - \frac{e}{3\ell_1} (\overline{u_i u_j} - \overline{u_i} \overline{u_j} - \frac{e^2}{3}) + C e^2 \left( \frac{\partial U_i}{\partial x_j} + \frac{\partial U_j}{\partial x_i} \right) \quad (2.83)$$



This term has been modelled by many boundary-layer workers with exactly the same terms but with differences in the values of the coefficients. The coefficient C has been assigned a value of 0 by Donaldson (1973) and a value of 0.4 by Deardorff (1973). These can be compared with a value of 0.056 chosen by Mellor and Yamada. These different values show that the determination of the coefficients is not unique but depends on the experimental results used to derive these as well as on the values assigned to the coefficients of the other modelled terms. There is a closer agreement on the value of the length scale  $3\lambda_1$ . In the constant-stress layer Donaldson has chosen a value of  $0.7 z$  which compares well with the value of  $0.82z$  selected by Mellor and Yamada. Deardorff's results are not directly comparable because his model has to be applied outside the constant-stress layer. Instead of using a mixing-length approach he uses a scaling length proportional to the grid spacing which he thinks is an appropriate length for modelling sub-grid scale phenomena.

#### 2.4.2 Pressure-Temperature Correlation Term: $\overline{\frac{p}{P_o} \frac{\partial \theta}{\partial x_j}}$

This term is similar to the energy redistribution term and by similar arguments we can hope to model it by,

$$\overline{\frac{p}{P_o} \frac{\partial \theta}{\partial x_j}} = D \overline{u_j \theta} + D' \overline{\frac{\partial \Theta}{\partial x_j}} \quad (2.84)$$

We match the dimensions,

$$\left[ \overline{\frac{p}{P_o} \frac{\partial \theta}{\partial x_j}} \right] = \left[ \frac{U}{L} U \theta \right] \quad (2.85)$$

$$\left[ D \overline{u_j \theta} \right] = \left[ D U \theta \right] \quad (2.86)$$

$$\left[ D' \overline{\frac{\partial \Theta}{\partial x_j}} \right] = \left[ \frac{D'}{U} U \theta \right] \quad (2.87)$$

Mellor and Yamada have put  $D'=0$  and used  $\lambda_2$  as the appro-



priate scaling length,

$$D = \frac{e}{3\lambda_2} \quad (2.88)$$

The magnitude of the modelled term is now defined and its sign will be determined in the discussion which follows. Again we will examine only the vertical variation because the gradients of most of the atmospheric variables are almost vertical. In the case of the energy redistribution term we used the fact that the gradient of the mean horizontal wind was always positive in the lower boundary layer. However, this simple situation is changed in the case of the vertical gradient of the mean temperature. Here a positive gradient represents a stable situation whereas a negative gradient is an unstable situation. In a complete discussion we should analyse both situations, but here we will be satisfied to find the sign of the modelled term in the unstable case. Fig. 5 represents an unstable temperature profile as a function of height. We will use the method of the air parcel familiar to all meteorologists in order to get some physical insight into that term. The justification for using that method is that we are looking at small elements of the atmosphere which will conserve their identity during a short period of time. The dissipation term is very efficient for small atmospheric scales and therefore this method is valid only approximately and for very short distances. If an air parcel is lifted adiabatically and without mixing with the environment from  $z_1$  to  $z_2$  the air parcel is warmer than the environment by  $\Theta(z_1) - \Theta(z_2) = \theta_1$ . If the air parcel had been lifted from  $z_1$  to  $z_3$  the temperature difference becomes  $\Theta(z_1) - \Theta(z_3) = \theta_2 > \theta_1$ . Therefore an unstable situation is very likely to give rise to  $\frac{\partial \theta}{\partial z} > 0$ . In the atmosphere, a



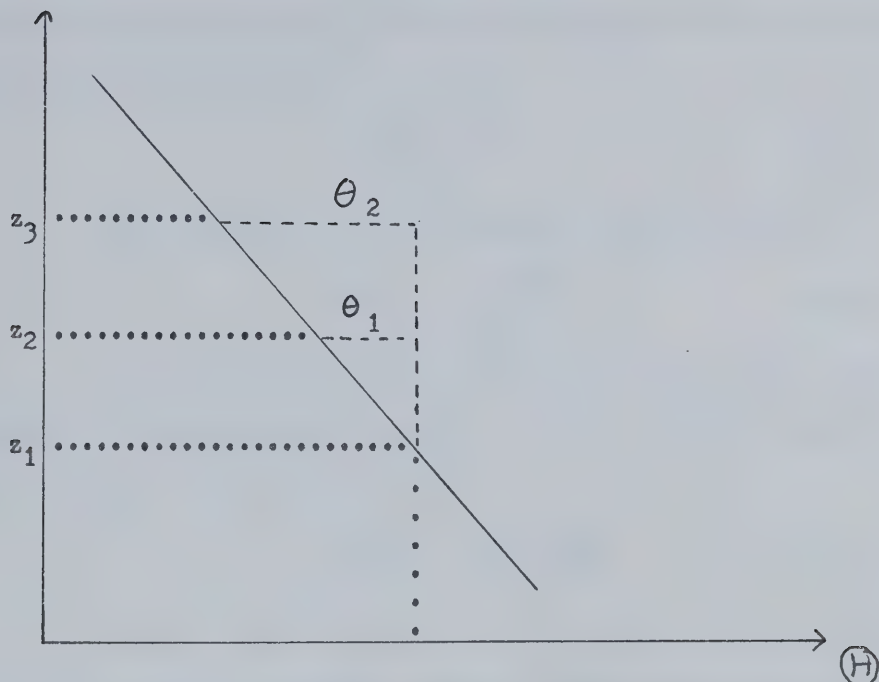


Figure 5. Illustration of the air parcel method. The solid curve represents the mean potential temperature of the environment for an unstable situation.



warmer air parcel implies a lower pressure and, therefore, this warming is associated with a negative pressure disturbance. The result in the case of an unstable lapse rate is that,

$$p \frac{\partial \theta}{\partial z} < 0 \quad (2.89)$$

The modelled term in an unstable stratification is,

$$\overline{w\theta} = - K_t \frac{\partial \theta}{\partial z} > 0 \quad (2.90)$$

$K_t$  is always positive in the lower boundary layer when the lapse rate is unstable and, therefore, we need a negative sign in front of the D term. The final result is,

$$\overline{\frac{p}{\rho_0} \frac{\partial \theta}{\partial x_j}} = - \frac{e}{3 \lambda_2} \overline{u_j \theta} \quad (2.91)$$

Donaldson (1973) has kept the same term with the scaling length  $\lambda_2 = 0.7 z$  in the lower boundary layer; this compares very well with the value of 0.82 z that Mellor and Yamada (1974) have used. Deardorff (1973) added one more term,

$$c_g = - \frac{1}{3} \delta_{ij} g \frac{\overline{\theta'^2}}{\overline{\theta^2}} \quad (2.92)$$

This term is valid only for isotropic turbulence and corresponds to a gravitational compensation effect. Deardorff (1973) admits that he does not know how rapidly this effect becomes invalid as departures from isotropy become more pronounced.

#### 2.4.3 Pressure-Water Vapor Correlation Term: $\overline{\frac{p}{\rho_0} \frac{\partial q}{\partial x_j}}$

Again we postulate that we can model this term by an expression like,



$$\overline{\frac{p}{\rho_0} \frac{\partial q}{\partial x_j}} = E \overline{u_j q} \quad (2.93)$$

The dimensions are,

$$\left[ \overline{\frac{p}{\rho_0} \frac{\partial q}{\partial x_j}} \right] = \left[ \frac{U}{L} U Q \right] \quad (2.94)$$

$$\left[ E \overline{u_j q} \right] = [E U Q] \quad (2.95)$$

Therefore,

$$E = \frac{e}{3 \lambda_3} \quad (2.96)$$

where  $\lambda_3$  is a scaling length to be determined. The sign is derived by a demonstration analogous to the one for temperature. When we consider the case of upward water vapor flux the arguments are exactly the same as in the preceding section if we replace the potential temperature by  $\theta_v = \theta + 0.6078 q$  and consider the changes in  $\theta_v$  to be caused only by the changes in  $q$ . Therefore, a negative sign is needed,

$$\overline{\frac{p}{\rho_0} \frac{\partial q}{\partial x_j}} = - \frac{e}{3 \lambda_3} \overline{u_j q} \quad (2.97)$$

#### 2.4.4 Dissipation Terms.

The dissipation terms are the ones involving the viscosity coefficient and the product of the gradient of two turbulent quantities. Following Kolmogoroff (1941) we hypothesize local small-scale isotropy. Therefore, all the dissipation terms will be modelled in terms of the simplest possible isotropic covariances.

$$2 \sqrt{\frac{\partial u_i}{\partial x_k} \frac{\partial u_j}{\partial x_k}} = F e^2 \delta_{ij} \quad (2.98)$$

The dimensions on the left side are  $[U^3/L]$ , therefore  $[F] = [U/L]$ .  $\Lambda$  will be used as the length scale for the dissipation terms, with  $e$  as the scaling velocity. The positive sign is needed if we



want destruction of covariance and not production of it. The dissipation of covariance involving any two different wind components is zero because it would require an anisotropic modelling term of the form  $\overline{u_i u_j}$ . The only isotropic covariance involving the wind is  $e^2 = \overline{u_i u_i}$  as was used in (2.98). Therefore it seems reasonable to model the dissipation term by an expression like,

$$2\sqrt{\frac{\partial u_i}{\partial x_k} \frac{\partial u_j}{\partial x_k}} = \frac{2}{3} \frac{e^2}{\Lambda_1} \delta_{ij} \quad (2.99)$$

The other terms are modelled similarly,

$$2\alpha \overline{\frac{\partial \theta}{\partial x_k} \frac{\partial \theta}{\partial x_k}} = 2 e \frac{\overline{\theta^2}}{\Lambda_2} \quad (2.100)$$

$$2\alpha \overline{\frac{\partial q}{\partial x_k} \frac{\partial q}{\partial x_k}} = 2 e \frac{\overline{q^2}}{\Lambda_3} \quad (2.101)$$

$$2\alpha \overline{\frac{\partial \theta}{\partial x_k} \frac{\partial q}{\partial x_k}} = 2 e \frac{\overline{\theta q}}{\Lambda_4} \quad (2.102)$$

The remaining two terms would require modelling terms like  $\overline{u_j \theta}$  and  $\overline{u_j q}$  which are not isotropic. For this reason they are put equal to zero.

$$\overline{\frac{\partial u_j}{\partial x_k} \frac{\partial \theta}{\partial x_k}} = \overline{\frac{\partial u_j}{\partial x_k} \frac{\partial q}{\partial x_k}} = 0 \quad (2.103)$$

#### 2.4.5 Diffusional Terms.

Most workers use a flux-gradient model for the various triple-moments terms. This implies a turbulent redistribution that leads to smoothing and hence the terms are often called "diffusional". The formula proposed by Mellor and Yamada (1974) is,

$$\overline{u_k u_i u_j} = G \left( \frac{\partial \overline{u_i u_j}}{\partial x_k} + \frac{\partial \overline{u_i u_k}}{\partial x_j} + \frac{\partial \overline{u_j u_k}}{\partial x_i} \right) \quad (2.104)$$



That formula appears appropriate and we determine that  $[G] = [L U]$  from a consideration of the dimensions. We choose  $\lambda$  as the scaling length for the diffusional terms, keep  $e$  as the scaling velocity, and give a negative sign to the expression in order to be consistent with the gradient form in which it is written. We have finally,

$$\overline{u_k u_1 u_j} = -e \lambda_1 \left( \frac{\partial \overline{u_i u_j}}{\partial x_k} + \frac{\partial \overline{u_i u_k}}{\partial x_j} + \frac{\partial \overline{u_j u_k}}{\partial x_i} \right) \quad (2.105)$$

More complex expressions have been derived from a more physical basis. For example, Hanjalic and Launder (1972) have modelled the pressure correlation terms by terms similar to the ones derived in sections (2.4.1) to (2.4.3) and then have derived the equations for the third moments. They have applied the quasi-normal assumption to the fourth moments and have neglected the remaining terms. The final result is a term like,

$$\overline{u_k u_1 u_j} = G' \left( \overline{u_k u_1} \frac{\partial \overline{u_i u_j}}{\partial x_1} + \overline{u_1 u_1} \frac{\partial \overline{u_j u_k}}{\partial x_1} + \overline{u_j u_k} \frac{\partial \overline{u_i u_k}}{\partial x_1} \right) \quad (2.106)$$

Wyngaard (1973) has shown that the assumption of free convection predicted that both  $\overline{w^3}$  and  $\partial \overline{w^2} / \partial z$  were positive. These predictions are partly supported by the results of the Kansas experiment. Therefore an expression like,

$$\overline{w^3} = G \left( \frac{\partial \overline{w^2}}{\partial z} \right) \quad (2.107)$$

would require a positive value for  $G$  and not a negative value as in our model. Therefore, the modelling of the triple correlation terms will prove to be very poor in all cases where free convection dominates. However, we are modelling forced convection and Wyngaard's finding might not apply there.



Using the same assumptions the remaining triple covariance terms are modelled similarly,

$$\overline{u_k \theta^2} = - e \lambda_2 \left( \frac{\partial \overline{\theta^2}}{\partial x_k} \right) \quad (2.108)$$

$$\overline{u_k u_j \theta} = - e \lambda_3 \left( \frac{\partial \overline{u_k \theta}}{\partial x_j} + \frac{\partial \overline{u_j \theta}}{\partial x_k} \right) \quad (2.109)$$

$$\overline{u_k u_j q} = - e \lambda_4 \left( \frac{\partial \overline{u_k q}}{\partial x_j} + \frac{\partial \overline{u_j q}}{\partial x_k} \right) \quad (2.110)$$

$$\overline{u_k q^2} = - e \lambda_5 \frac{\partial \overline{q^2}}{\partial x_k} \quad (2.111)$$

$$\overline{u_k q \theta} = - e \lambda_6 \frac{\partial \overline{\theta q}}{\partial x_k} \quad (2.112)$$

Again we expect these expressions to be valid in forced convection as is the case in the surface layer with relatively strong winds. In order to model correctly these terms in the free-convection limit we would need supplementary terms probably involving buoyancy.

#### 2.4.6 Pressure Diffusional Terms.

Hanjalic and Launder (1972) have found experimentally that these terms were small. Therefore, we shall neglect these terms,

$$\overline{p u_i} = \overline{p \theta} = \overline{p q} = 0 \quad (2.113)$$

Some authors have proposed models for these terms. For example, Donaldson (1973) has used a model in which the terms are nonproductive as in,

$$\overline{p \theta} = - \rho_o e \Lambda' \frac{\partial}{\partial x_1} \overline{u_1 \theta}$$



where  $\Lambda'$  is a scaling length. However, Donaldson (1973) reports that Taulbee (1973) had to use a small negative value for  $\Lambda'$  in order to obtain better agreement between computations and experimental results. This means that it is better probably to neglect the pressure diffusion-al terms until we have sufficient experimental results to suggest a physical basis for the modelling of these terms.



## 2.5 Modelled Equations.

### 2.5.1 Modelled Equations for the Second-Order Moments.

We insert all the modelling terms into the second-order moment equations (2.62) to (2.67) and neglect the molecular diffusive terms as well as those involving the Coriolis force which are a few orders of magnitude smaller than the other terms. The modelled equations for the second-order moments are:

$$\frac{D \overline{u_i u_j}}{Dt} - \frac{\partial}{\partial x_k} \left[ e \lambda_1 \left( \frac{\partial \overline{u_i u_k}}{\partial x_j} + \frac{\partial \overline{u_i u_j}}{\partial x_k} + \frac{\partial \overline{u_j u_k}}{\partial x_i} \right) \right] = - \overline{u_k u_i} \frac{\partial U_j}{\partial x_k} - \overline{u_k u_j} \frac{\partial U_i}{\partial x_k} - \frac{1}{T_o} (g_j \overline{u_i \theta_v} + g_i \overline{u_j \theta_v}) - \frac{e}{3 \ell_1} (\overline{u_i u_j} - \delta_{ij} \frac{e^2}{3}) + c_1 e^2 \times \left( \frac{\partial U_i}{\partial x_j} + \frac{\partial U_j}{\partial x_i} \right) - \frac{2}{3} \frac{e^2}{\Lambda_1} \delta_{ij} \quad (2.114)$$

$$\frac{D \overline{u_j \theta}}{Dt} - \frac{\partial}{\partial x_k} \left[ e \lambda_3 \left( \frac{\partial \overline{u_k \theta}}{\partial x_j} + \frac{\partial \overline{u_j \theta}}{\partial x_k} \right) \right] = - \overline{u_j u_k} \frac{\partial \overline{\theta}}{\partial x_k} - \overline{u_k \theta} \frac{\partial U_j}{\partial x_k} - \frac{1}{T_o} g_j \overline{\theta \theta_v} - \frac{e}{3 \ell_2} \overline{u_j \theta} \quad (2.115)$$

$$\frac{D \overline{u_j q}}{Dt} - \frac{\partial}{\partial x_k} \left[ e \lambda_4 \left( \frac{\partial \overline{u_k q}}{\partial x_j} + \frac{\partial \overline{u_j q}}{\partial x_k} \right) \right] = - \overline{u_j u_k} \frac{\partial Q}{\partial x_k} - \overline{u_k q} \frac{\partial U_j}{\partial x_k} - \frac{g_j}{T_o} \overline{q \theta_v} - \frac{e}{3 \ell_3} \overline{u_j q} \quad (2.116)$$

$$\frac{D \overline{\theta^2}}{Dt} - \frac{\partial}{\partial x_k} \left[ e \lambda_2 \left( \frac{\partial \overline{\theta^2}}{\partial x_k} \right) \right] = - 2 \overline{u_k \theta} \frac{\partial \overline{\theta}}{\partial x_k} - 2 e \overline{\theta^2} / \Lambda_2 \quad (2.117)$$

$$\frac{D \overline{q^2}}{Dt} - \frac{\partial}{\partial x_k} \left( e \lambda_5 \frac{\partial \overline{q^2}}{\partial x_k} \right) = - 2 \overline{u_k q} \frac{\partial Q}{\partial x_k} - 2 e \overline{q^2} / \Lambda_3 \quad (2.118)$$

$$\frac{D \overline{q \theta}}{Dt} - \frac{\partial}{\partial x_k} \left( e \lambda_6 \frac{\partial \overline{q \theta}}{\partial x_k} \right) = - \overline{u_k \theta} \frac{\partial Q}{\partial x_k} - \overline{u_k q} \frac{\partial \overline{\theta}}{\partial x_k} - 2 e \overline{q \theta} / \Lambda_4 \quad (2.119)$$



The Lagrangian derivative is defined as,

$$\frac{D}{Dt} = \frac{\partial}{\partial t} + U_k \frac{\partial}{\partial x_k}$$

### 2.5.2 Modelled Equations for the Mean Quantities.

The equations for the mean quantities are not directly affected by the modelling and, therefore, we will use equations (2.54) to (2.57) in which we neglect the small molecular diffusion terms and replace the Eulerian time derivative by the Lagrangian one.

$$\frac{\partial U_j}{\partial x_j} = 0 \quad (2.120)$$

$$\frac{D U_j}{Dt} + \frac{\partial}{\partial x_k} (\overline{u_k u_j}) + \varepsilon_{ikl} f_k U_l = - \frac{1}{\rho_0} \frac{\partial P}{\partial x_j} + \frac{g_j \overline{H}_v}{T_0} \quad (2.121)$$

$$\frac{D \overline{H}}{Dt} + \frac{\partial}{\partial x_k} (\overline{u_k \theta}) = 0 \quad (2.122)$$

$$\frac{D Q}{Dt} + \frac{\partial}{\partial x_k} (\overline{u_k q}) = 0 \quad (2.123)$$



## 2.6 Length Scale Specification.

Up until now the scaling lengths used in modelling  $\lambda_1, \lambda_2, \Lambda_1$  and the constant  $C_1$  have not been specified. If we accept the results obtained by Mellor and Yamada (1974) we get the following relationships,

$$\lambda_1 = \lambda_2 = \lambda_3 = 0.78 \quad (2.124)$$

$$\lambda_1 = \lambda_2 = \lambda_3 = \lambda_4 = \lambda_5 = \lambda_6 = 0.23 \quad (2.125)$$

$$\Lambda_1 = 15.0 \quad (2.126)$$

$$\Lambda_2 = \Lambda_3 = \Lambda_4 = 8.0 \quad (2.127)$$

We have assumed that water vapor behaves like temperature with respect to turbulent properties, so that their respective length scales are identical.  $\lambda$  is the fundamental length to be determined. We will use Blackadar's (1962) formula,

$$\lambda = \frac{k_o(z+z_o)}{1 + \frac{k_o(z+z_o)}{\lambda_o}} \quad (2.128)$$

$\lambda_o$  is a constant which fixes the size of the largest eddies and whose value depends on the stability of the atmosphere. That formula holds for the two known asymptotes of the length scale: close to the ground it behaves like  $\lambda = k_o(z+z_o)$ , and much above  $z_o$  it reaches its maximum value  $\lambda_o$ . We must specify  $\lambda_o$  and to do so, we adopt the arbitrary formulation of Mellor and Yamada (1974) which is,

$$\lambda_o = 0.1 \frac{\int_{z_o}^{\infty} z e^{-dz}}{\int_{z_o}^{\infty} e^{-dz}} \quad (2.129)$$

Equation (2.129) gives a reasonable number of the order of 30 m in the case of neutral stability.  $\lambda_o$  increases with stability and decreases with instability. Finally,  $C_1$  is given the value 0.056 following Mellor and Yamada (1974).



## 2.7 Ordering of Terms.

Mellor and Yamada (1974) have described a method of ordering terms which works quite well. The method consists in separating the isotropic part from the anisotropic part in all of the equations. That task is simple as only equation (2.114) consists of a mixture of the two. Equations (2.115) to (2.116) contain only anisotropic terms and equations (2.117)-(2.119) contain only isotropic terms. Going back to equation (2.114) we note that the isotropic part is the energy equation obtained by the addition of the three equations in which  $i=j$ , for  $i=1,2,3$ . Therefore, the equation for the isotropic part is,

$$\frac{D e^2}{Dt} - \frac{\partial}{\partial x_k} \left[ e \lambda_1 \left( \frac{\partial e^2}{\partial x_k} + 2 \frac{\partial \overline{u_i u_k}}{\partial x_i} \right) \right] = - 2 \overline{u_k u_i} \frac{\partial U_i}{\partial x_k} - 2 \frac{g_i}{T_o} \overline{u_i \theta_v} - \frac{2 e^3}{\Lambda_1} \quad (2.130)$$

The anisotropic part is found by subtracting  $\delta_{ij}/3$  times equation (2.130) from (2.114).

$$\begin{aligned} & \frac{D}{Dt} \left( \overline{u_i u_j} - \frac{\delta_{ij}}{3} \overline{u_k^2} \right) - \frac{\partial}{\partial x_k} \left\{ e \lambda_1 \left[ \frac{\partial \overline{u_i u_j}}{\partial x_k} + \frac{\partial \overline{u_i u_k}}{\partial x_j} + \frac{\partial \overline{u_j u_k}}{\partial x_i} \right. \right. \\ & \left. \left. - \frac{\delta_{ij}}{3} \left( \frac{\partial \overline{u_l^2}}{\partial x_k} + 2 \frac{\partial \overline{u_l u_k}}{\partial x_l} \right) \right] \right\} = - \overline{u_k u_i} \frac{\partial U_j}{\partial x_k} - \overline{u_k u_j} \frac{\partial U_i}{\partial x_k} \\ & + \frac{2}{3} \delta_{ij} \overline{u_k u_l} \frac{\partial U_l}{\partial x_k} - \frac{1}{T_o} (g_j \overline{u_i \theta_v} + g_i \overline{u_j \theta_v} - \frac{2}{3} \delta_{ij} g_l \overline{u_l \theta_v}) \\ & - \frac{e}{3 \lambda_1} \left( \overline{u_i u_j} - \frac{\delta_{ij}}{3} e^2 \right) + c_1 e^2 \left( \frac{\partial U_i}{\partial x_j} + \frac{\partial U_j}{\partial x_i} \right) \end{aligned} \quad (2.131)$$

We define nondimensional departures from isotropy  $a_{ij}$ ,  $b_i$  and  $c_1$  so that,

$$\overline{u_i u_j} = \left( \frac{\delta_{ij}}{3} + a_{ij} \right) \quad (2.132)$$



$$a_{ii} = 0 \quad (2.133)$$

$$\overline{u_1 \theta} = b_1 \circ \varphi \quad (2.134)$$

$$\overline{u_1 q} = c_1 \circ \psi \quad (2.135)$$

where,

$$\varphi^2 = \overline{\theta^2} \quad (2.136)$$

$$\psi^2 = \overline{q^2} \quad (2.137)$$

We estimate the order of magnitude by letting,

$$\lambda = \mathcal{O}(\lambda_i) \quad (2.138)$$

$$\Lambda = \mathcal{O}(\Lambda_i) \quad (2.139)$$

$$a^2 = \mathcal{O}(a_{ij}^2) \quad (2.140)$$

$$v_x^2 = \mathcal{O}\left(\frac{\partial U_1}{\partial x_j}\right)^2 \quad (2.141)$$

$$\Theta_x^2 = \mathcal{O}\left(\frac{\partial H}{\partial x_1}\right)^2 \quad (2.142)$$

$$Q_x^2 = \mathcal{O}\left(\frac{\partial Q}{\partial x_1}\right)^2 \quad (2.143)$$

$$b^2 = \mathcal{O}(b_1^2) \quad (2.144)$$

$$c^2 = \mathcal{O}(c_1^2) \quad (2.145)$$

$$g^2 = \mathcal{O}(g_1^2) \quad (2.146)$$

The purpose of that exercise is to involve the ratio  $\lambda/\Lambda$  in the equations. From neutral experimental data Mellor and Yamada have shown that this ratio is generally of the order of 0.05 to 0.10. This gives an objective method for ordering the terms by neglecting the terms which are smaller by a factor of the order of  $\lambda/\Lambda$ . Table 1 is the result of such ordering; the first lines in each block are the equations for the second-order moments in which (2.132) to (2.135) have been used; the second lines in each block are the order of magnitude of each



Table 1. Ordering of Terms. This table is similar to table 1 in Mellor and Yamada (1974) page 1794.

- The first lines in each block are the equations for the second-order moments in which the departures from isotropy  $a$ ,  $b$  and  $c$  are used.
  - The second lines are the order of magnitude of each of the terms.
  - The third lines are the order of magnitude of the dominant terms.

$$1) \frac{D e^2}{D t} - \frac{\partial}{\partial x_k} \left\{ \theta \lambda_1 \frac{5}{3} \frac{\partial e^2}{\partial x_k} [1 + \theta(a)] \right\} = -2a_{ki} e^2 \frac{\partial U_i}{\partial x_k} - 2\theta g_i \left( \frac{b_i \varphi}{T_o} + 0.61 c_i \psi \right) - \frac{2e^3}{\lambda_1} \quad (2.147)$$

$$2) \frac{U_e^2}{L} \quad \frac{U_e^2}{L} \quad a_e^2 U_x \quad g_e \left( \frac{b_e \psi}{T_0} + 0.61c_e \psi \right) \quad \frac{e^3}{\Lambda}$$

$$3) \quad \frac{e^3}{\Lambda} \quad \frac{e^3}{\Lambda} \quad \frac{e^3}{\Lambda}$$

$$1) \frac{D(e^2 a_{ij})}{D t} - \frac{\partial}{\partial x_k} \left\{ \frac{e \lambda_1}{3} \left[ \left( \delta_{ik} \frac{\partial e^2}{\partial x_j} + \delta_{jk} \frac{\partial e^2}{\partial x_i} - \frac{2}{3} \delta_{ij} \frac{\partial e^2}{\partial x_k} \right) [1 + \mathcal{O}(a)] + a_{ij} \frac{\partial e^2}{\partial x_k} \right] \right\} =$$

$$2) \frac{a U e^2}{L} \quad \frac{U e^2}{L}$$

$$1) - e^2 \left[ \left( \frac{\delta_{ki}}{3} + a_{ki} \right) \frac{\partial U_j}{\partial x_k} + \left( \frac{\delta_{kj}}{3} + a_{kj} \right) \frac{\partial U_i}{\partial x_k} - \frac{2}{3} \delta_{ij} a_{kl} \frac{\partial U_l}{\partial x_k} - c_1 \left( \frac{\partial U_i}{\partial x_j} + \frac{\partial U_j}{\partial x_i} \right) \right]$$

$$2) \quad e^2 U_x [1 + \theta(a)]$$

$$3) \quad \frac{e^3}{a} \Delta [1 + O(a)]$$

$$1) -e(g_j b_j + g_i b_i) \frac{\varphi}{T_0} + 0.61 \Psi(g_j c_j + g_i c_i) - \frac{2}{3} \delta_{ij} e g_1 (b_1 \varphi + c_1 \Psi) - \frac{e^3 a_{ij}}{3 f_1}$$

$$2) \quad \text{e.g. } \left( \frac{b\varphi}{T_0} + 0.61 c\psi \right)$$

$$3) \quad \frac{e^3}{\Delta}$$



Second part of table 1.

$$1) \frac{D\overline{\theta^2}}{Dt} - \frac{\partial}{\partial x_k} \left( e \lambda_2 \frac{\partial \overline{\theta^2}}{\partial x_k} \right) = -2e\varphi b_k \frac{\partial \overline{\theta}}{\partial x_k} - 2\frac{e}{\Lambda_2} \overline{\theta^2} \quad (2.149)$$

$$2) \frac{U\overline{\varphi^2}}{L} \quad \frac{U\overline{\varphi^2}}{L} \quad e\varphi b \overline{\theta_x} = \frac{e\overline{\varphi^2}}{\Lambda}$$

$$3) \quad \frac{e\overline{\varphi^2}}{\Lambda} \quad \frac{e\overline{\varphi^2}}{\Lambda}$$


---

$$1) \frac{D\overline{q^2}}{Dt} - \frac{\partial}{\partial x_k} \left( e \lambda_5 \frac{\partial \overline{q^2}}{\partial x_k} \right) = -2e c_k \psi \frac{\partial \overline{q}}{\partial x_k} - 2\frac{e}{\Lambda_3} \overline{q^2} \quad (2.150)$$

$$2) \frac{U\overline{\psi^2}}{L} \quad \frac{U\overline{\psi^2}}{L} \quad e\psi b \overline{\theta_x} = \frac{e\overline{\psi^2}}{\Lambda}$$

$$3) \quad \frac{e\overline{\psi^2}}{\Lambda} \quad \frac{e\overline{\psi^2}}{\Lambda}$$


---

$$1) \frac{D}{Dt} (b_j e \varphi) - \frac{\partial}{\partial x_k} \left[ e \lambda_3 \left( \frac{\partial b_j e \varphi}{\partial x_k} + \frac{\partial b_k e \varphi}{\partial x_j} \right) \right] = -e^2 \left( \frac{\delta_{ik}}{3} + a_{jk} \right) \frac{\partial \overline{\theta}}{\partial x_k}$$

$$2) \frac{b U e \varphi}{L} \quad \frac{b U e \varphi}{L} \quad e^2 \overline{\theta_x} [1 + \mathcal{O}(a)]$$

$$3) \quad \frac{e^2 [1 + \mathcal{O}(a)]}{b \Lambda}$$

$$1) -e\varphi b_k \frac{\partial U_i}{\partial x_k} - g_j \left( \frac{\overline{\theta^2}}{T_0} + 0.61 \overline{\theta q} \right) - \frac{e^2 \varphi b_i}{3\ell_2} \quad (2.151)$$

$$2) e\varphi b U_x \quad g \left( \frac{\overline{\theta^2}}{T_0} + 0.61 \varphi \psi \right) \quad \frac{e^2 \varphi b}{\ell}$$

$$3) \frac{e^2 \varphi}{\Lambda} \quad \frac{e^2 \varphi}{\Lambda} \left( \frac{1}{c} + \frac{1}{b} \right) \quad \frac{e^2 \varphi}{b \Lambda}$$



Third part of table 1.

$$1) \frac{D}{Dt}(c_j e\psi) - \frac{\partial}{\partial x_k} [e\lambda_4(\frac{\partial c_j e\psi}{\partial x_k} + \frac{\partial c_k e\psi}{\partial x_j})] = -e^2(\frac{f_{jk}}{3} + a_{jk}) \frac{\partial Q}{\partial x_k}$$

$$2) \frac{c U e \psi}{L} \quad \frac{c U e \psi}{L} \quad e^2 Q_x (1 + \theta(a))$$

$$3) \quad \frac{e^2 (1 + \theta(a))}{c \Lambda}$$

$$1) -e c_k \psi \frac{\partial U_j}{\partial x_k} - g_j e (\frac{q \theta}{T_o} + 0.61 \bar{q}^2) - \frac{c_j e^2 \psi}{3 \ell_3} \quad (2.152)$$

$$2) e c \psi U_x \quad g e (0.61 \psi^2 + \frac{q \psi}{T_o}) \quad \frac{c e^2 \psi}{\ell}$$

$$3) \frac{e^2 \psi}{\Lambda} \quad \frac{e^2 \psi}{\Lambda} (\frac{1}{b} + \frac{1}{c}) \quad \frac{e^2 \psi}{c \Lambda}$$


---

$$1) \frac{D \bar{q} \theta}{Dt} - \frac{\partial}{\partial x_k} (e \lambda_6 \frac{\partial \bar{q} \theta}{\partial x_k}) = -c_k e \psi \frac{\partial \bar{H}}{\partial x_k} - b_k e \varphi \frac{\partial Q}{\partial x_k} - 2 \frac{e}{\Lambda_4} \bar{q} \theta \quad (2.153)$$

$$2) \frac{U \varphi \psi}{L} \quad \frac{U \varphi \psi}{L} \quad e c \psi \Theta_x \quad e b \varphi Q_x \quad \frac{e \varphi \psi}{\Lambda}$$

$$3) \quad \frac{e \varphi \psi}{\Lambda} \quad \frac{e \varphi \psi}{\Lambda} \quad \frac{e \varphi \psi}{\Lambda}$$



term as given by equations (2.136) to (2.146); finally the third lines in each block are the order of magnitude of the dominant terms in each equation; these lines are obtained when we make use of the relationships between the various terms, which will be derived in the following discussion.

As a first step, we will discuss the simple case of neutral flow by neglecting buoyancy which is done by giving a value of zero to  $g$ . We assume that the production and dissipation terms are dominant in all of the equations (2.147) to (2.153). The production terms are the ones involving the gradient of the mean quantities, whereas the dissipation terms are the ones containing  $\epsilon$  times the second-order moment considered. We apply this assumption to (2.147) and (2.148),

$$\alpha \epsilon^2 U_x = \frac{\epsilon^3}{\Lambda} \quad (2.154)$$

$$\epsilon^2 U_x = \alpha \epsilon^3 / \Lambda \quad (2.155)$$

We combine the last two expressions to get,

$$\alpha^2 = \Lambda / \epsilon \quad (2.156)$$

$$U_x = \Lambda / (\alpha \epsilon) \quad (2.157)$$

The domination of the production and dissipation terms implies that the right-hand sides of (2.149) and (2.150) are the most important terms, therefore

$$\epsilon \phi b \Theta_x = \epsilon \phi^2 / \Lambda \quad (2.158)$$

$$\epsilon \psi c Q_x = \epsilon \psi^2 / \Lambda \quad (2.159)$$

Using this assumption in the other equations we have,

$$\epsilon^2 \Theta_x = \epsilon^2 \phi b / \Lambda \quad (2.159)$$

$$\epsilon^2 Q_x = \epsilon^2 \psi c / \Lambda \quad (2.160)$$

The last four equations yield the following,



$$b^2 = \lambda / \Lambda \quad (2.161)$$

$$c^2 = \lambda / \Lambda \quad (2.162)$$

$$\Theta_x = \varphi / (b \Lambda) \quad (2.163)$$

$$Q_x = \psi / (c \Lambda) \quad (2.164)$$

Obviously we have  $a=b=c$ . If we allow buoyant energy production to be of the same order of magnitude as the dominant parameters, we get,

$$\frac{g \varphi}{T_0} = \frac{e^2}{b \Lambda} \quad (2.165)$$

$$0.61 g = \frac{e^2}{c \Lambda} \quad (2.166)$$

The ordering of the terms has not been completed yet because the diffusion and advection terms involve a wind scale  $U$  and a length  $L$  which are undefined. Mellor and Yamada (1974) have made a 4-level classification. The level 4 model is the most complex and keeps all the terms. The other levels are obtained by assigning a value to the relative order of magnitude of the diffusion and advection terms. For example level 1 is the simplest model in which the diffusion and advection terms are neglected as well as other terms of order  $a=(\lambda/\Lambda)^{\frac{1}{2}}$ . In the next section we will discuss in detail how level 3 is obtained.



## 2.8 Level 3 Model.

We consider the equation for the kinetic turbulent energy  $e^2$  and look at the dominant component of the diffusion term which is the vertical component. We assume that the vertical derivative is of the order of  $1/\Lambda$  so that the diffusion term becomes,

$$\frac{\partial}{\partial z} (e \lambda \frac{\partial e^2}{\partial z}) = O(\frac{1}{\Lambda} \frac{\lambda}{\Lambda} e^3) = O(\frac{a^2 e^3}{\Lambda}) \quad (2.167)$$

where the last equality comes from  $\lambda/\Lambda = O(a^2)$  which seems to be justified from experimental data and numerical boundary-layer modelling (Mellor and Herring; 1968, 1973). Level 2 keeps (2.167) intact. However, this relationship is quite uncertain and it is possible that the diffusion terms without being dominant, are more important than (2.167) implies. Therefore, in level 3 we replace  $a^2$  by  $a$  in (2.167) and get for the order of magnitude of the diffusion term,

$$\frac{U}{L} e^2 = a \frac{e^3}{\Lambda} \quad (2.168)$$

Accordingly, the ratio  $U/L$  is defined and can be used in (2.147) to (2.153) to get the final estimate of the order of magnitude of each of the terms. Next, we multiply every ordering term in (2.148) by  $a$ , in (2.151) by  $b$  and in (2.152) by  $c$  and neglect all the terms of  $O(a^2)$ ,  $O(b^2)$  and  $O(c^2)$ . The final result is,

$$\frac{D e^2}{Dt} - \frac{\partial}{\partial x_k} (e \lambda_1 \frac{5}{3} \frac{\partial e^2}{\partial x_k}) = -2 \overline{u_k u_i} \frac{\partial U_i}{\partial x_k} - 2 \frac{g_k}{T_o} \overline{u_k \theta_v} - 2 \frac{e^3}{\Lambda_1} \quad (2.169)$$

$$\begin{aligned} \overline{u_i u_j} &= \frac{\delta_{ij}}{3} e^2 - \frac{3}{e} \frac{\ell_1}{\lambda_1} [(\overline{u_k u_i} - c_1 e^2 \delta_{ki}) \frac{\partial U_i}{\partial x_k} + (\overline{u_k u_j} - c_1 e^2 \delta_{kj}) \frac{\partial U_i}{\partial x_k}] \\ &- \frac{2}{3} \delta_{ij} \overline{u_k u_l} \frac{\partial U_l}{\partial x_k} - 3 \frac{\ell_1}{e T_o} (g_j \overline{u_i \theta_v} + g_i \overline{u_j \theta_v} - \frac{2}{3} \delta_{ij} g_1 \overline{u_1 \theta_v}) \\ &+ 3 \frac{\ell_1}{e} \frac{\partial}{\partial x_k} \left[ \frac{e \lambda_1}{3} \left( \delta_{ik} \frac{\partial e^2}{\partial x_j} + \delta_{jk} \frac{\partial e^2}{\partial x_i} - \frac{2}{3} \delta_{ij} \frac{\partial e^2}{\partial x_k} \right) \right] \end{aligned} \quad (2.170)$$



$$\frac{D \overline{\theta^2}}{Dt} - \frac{\partial}{\partial x_k} \left( e \lambda_2 \frac{\partial \overline{\theta^2}}{\partial x_k} \right) = -2 \overline{u_k \theta} \frac{\partial \overline{\theta}}{\partial x_k} - 2 \frac{e}{\lambda_2} \overline{\theta^2} \quad (2.171)$$

$$\frac{D \overline{q^2}}{Dt} - \frac{\partial}{\partial x_k} \left( e \lambda_5 \frac{\partial \overline{q^2}}{\partial x_k} \right) = -2 \overline{u_k q} \frac{\partial \overline{q}}{\partial x_k} - 2 \frac{e}{\lambda_3} \overline{q^2} \quad (2.172)$$

$$\frac{D \overline{q \theta}}{Dt} - \frac{\partial}{\partial x_k} \left( e \lambda_6 \frac{\partial \overline{q \theta}}{\partial x_k} \right) = -\overline{u_k q} \frac{\partial \overline{\theta}}{\partial x_k} - \overline{u_k \theta} \frac{\partial \overline{q}}{\partial x_k} - 2 \frac{e}{\lambda_4} \overline{q \theta} \quad (2.173)$$

$$\overline{u_j \theta} = -3 \frac{\ell_2}{e} \left( \overline{u_j u_k} \frac{\partial \overline{\theta}}{\partial x_k} + \overline{u_k \theta} \frac{\partial \overline{U_j}}{\partial x_k} + \frac{g_j}{T_o} \overline{\theta \theta_v} \right) \quad (2.174)$$

$$\overline{u_j q} = -3 \frac{\ell_3}{e} \left( \overline{u_j u_k} \frac{\partial \overline{q}}{\partial x_k} + \overline{u_k q} \frac{\partial \overline{U_j}}{\partial x_k} + \frac{g_j}{T_o} \overline{q \theta_v} \right) \quad (2.175)$$



## 2.9 The Boundary-Layer Approximation.

We will restrict ourselves to the boundary layer in which the two following approximations can be made.

- 1) The vertical gradients are very much larger than the horizontal gradients,

$$\frac{\partial}{\partial x} \ll \frac{\partial}{\partial z} \quad \frac{\partial}{\partial y} \ll \frac{\partial}{\partial z} \quad (2.176)$$

That implies that the horizontal gradients will be neglected with respect to the vertical gradient except in the continuity equation and in the terms involving the horizontal gradient of the mean pressure.

- 2) The hydrostatic approximation will be used.

### 2.9.1 Equations for the Mean Quantities.

We use the standard coordinate system  $(x, y, z)$  in which  $z$  is the vertical coordinate and  $x$  and  $y$  are the horizontal ones.  $U$  and  $V$  are the mean horizontal velocities and  $W$  is the mean vertical velocity. The equations for the mean properties become,

$$\frac{\partial U}{\partial x} + \frac{\partial V}{\partial y} + \frac{\partial W}{\partial z} = 0 \quad (2.177)$$

$$\frac{D U}{D t} + \frac{\partial}{\partial z} (\bar{u} w) = - \frac{1}{\rho_0} \frac{\partial P}{\partial x} + f v \quad (2.178)$$

$$\frac{D V}{D t} + \frac{\partial}{\partial z} (\bar{v} w) = - \frac{1}{\rho_0} \frac{\partial P}{\partial y} - f u \quad (2.179)$$

$$\frac{D(\bar{\theta})}{D t} + \frac{\partial}{\partial z} (\bar{w} \theta) = 0 \quad (2.180)$$

$$\frac{D Q}{D t} + \frac{\partial}{\partial z} (\bar{w} q) = 0 \quad (2.181)$$

$$\frac{\partial P}{\partial z} = \frac{g \theta_v}{T_0} \quad (2.182)$$



### 2.9.2 Equations for the Turbulent Quantities.

We define the diffusion operator as,

$$\mathcal{D}_\alpha(\cdot) = \frac{\partial}{\partial z} \left[ e \lambda_\alpha \frac{\partial}{\partial z} (\cdot) \right] \quad (2.183)$$

and the production components as,

$$P_{ij} = - \overline{w u_i} \frac{\partial U_j}{\partial z} \quad (2.184)$$

The equations for the turbulent quantities can be written in the boundary layer as,

$$\frac{D(e^2/2)}{Dt} - \frac{5}{3} \mathcal{D}_1 \left( \frac{e^2}{2} \right) = P_{xx} + P_{yy} + \frac{g}{T_0} \overline{w \theta_v} - \frac{e^3}{\Lambda_1} \quad (2.185)$$

$$\frac{D(\overline{\theta^2}/2)}{Dt} - \mathcal{D}_2 \left( \frac{\overline{\theta^2}}{2} \right) = - \overline{w \theta} \frac{\partial \overline{\theta}}{\partial z} - \frac{e \overline{\theta^2}}{\Lambda_2} \quad (2.186)$$

$$\frac{D(\overline{q^2}/2)}{Dt} - \mathcal{D}_5 \left( \frac{\overline{q^2}}{2} \right) = - \overline{w q} \frac{\partial Q}{\partial z} - \frac{e \overline{q^2}}{\Lambda_3} \quad (2.187)$$

$$\frac{D \overline{q \theta}}{Dt} - \mathcal{D}_6 \left( \overline{q \theta} \right) = - \overline{w q} \frac{\partial \overline{\theta}}{\partial z} - \overline{w \theta} \frac{\partial Q}{\partial z} - 2 \frac{e \overline{q \theta}}{\Lambda_4} \quad (2.188)$$

$$\overline{u^2} = \frac{e^2}{3} + \frac{\lambda_1}{e} (4P_{xx} - 2P_{yy} - 2 \frac{g}{T_0} \overline{w \theta_v}) - \frac{\lambda_1}{e} \mathcal{D}_1 \left( \frac{2}{3} e^2 \right) \quad (2.189)$$

$$\overline{v^2} = \frac{e^2}{3} + \frac{\lambda_1}{e} (-2P_{xx} + 4P_{yy} - 2 \frac{g}{T_0} \overline{w \theta_v}) - \frac{\lambda_1}{e} \mathcal{D}_1 \left( \frac{2}{3} e^2 \right) \quad (2.190)$$

$$\overline{w^2} = \frac{e^2}{3} + \frac{\lambda_1}{e} (-2P_{xx} - 2P_{yy} + 4 \frac{g}{T_0} \overline{w \theta_v}) + \frac{\lambda_1}{e} \mathcal{D}_1 \left( \frac{4}{3} e^2 \right) \quad (2.191)$$

$$- \overline{u v} = \frac{3 \lambda_1}{e} (-P_{yx} - P_{xy}) \quad (2.192)$$

$$- \overline{u w} = \frac{3 \lambda_1}{e} \left[ (w^2 - C_1 e^2) \frac{\partial U}{\partial z} - \frac{g}{T_0} \overline{u \theta_v} \right] \quad (2.193)$$

$$- \overline{v w} = \frac{3 \lambda_1}{e} \left[ (w^2 - C_1 e^2) \frac{\partial V}{\partial z} - \frac{g}{T_0} \overline{v \theta_v} \right] \quad (2.194)$$

$$- \overline{u \theta} = \frac{3 \lambda_2}{e} \left( \overline{u w} \frac{\partial \overline{\theta}}{\partial z} + \overline{w \theta} \frac{\partial \overline{U}}{\partial z} \right) \quad (2.195)$$

$$- \overline{v \theta} = \frac{3 \lambda_2}{e} \left( \overline{v w} \frac{\partial \overline{\theta}}{\partial z} + \overline{w \theta} \frac{\partial \overline{V}}{\partial z} \right) \quad (2.196)$$



$$-\overline{w\theta} = \frac{3l_2}{e} \left( \overline{w^2} \frac{\partial \Theta}{\partial z} - \frac{g}{T_0} \overline{\theta \theta_v} \right) \quad (2.197)$$

$$-\overline{uq} = \frac{3l_3}{e} \left( \overline{uw} \frac{\partial Q}{\partial z} + \overline{wq} \frac{\partial U}{\partial z} \right) \quad (2.198)$$

$$-\overline{vq} = \frac{3l_3}{e} \left( \overline{vw} \frac{\partial Q}{\partial z} + \overline{wq} \frac{\partial V}{\partial z} \right) \quad (2.199)$$

$$-\overline{wq} = \frac{3l_3}{e} \left( \overline{w^2} \frac{\partial Q}{\partial z} - \frac{g}{T_0} \overline{q \theta_v} \right) \quad (2.200)$$

We now have a closed system of 22 equations in 22 unknowns. This set of equations can be reduced to a smaller one by elimination of some of the variables. We will also use the turbulent eddy diffusivities as defined by,

$$-\overline{uw} = K_m \frac{\partial U}{\partial z} \quad (2.201)$$

$$-\overline{vw} = K_m \frac{\partial V}{\partial z} \quad (2.202)$$

$$-\overline{w\theta} = K_t \frac{\partial \Theta}{\partial z} \quad (2.203)$$

$$-\overline{wq} = K_w \frac{\partial Q}{\partial z} \quad (2.204)$$

In the case of level 3 the eddy diffusivity for momentum has the same value in the x and y directions; this can be proven easily by finding the same expression for  $K_m$  from equation (2.192) and from equation (2.194). The division of (2.201) by (2.202) gives,

$$\frac{\overline{uw}}{\overline{vw}} = \frac{\frac{\partial U}{\partial z}}{\frac{\partial V}{\partial z}} \quad (2.205)$$

We define

$$\left| \frac{\partial V}{\partial z} \right|^2 = \left( \frac{\partial U}{\partial z} \right)^2 + \left( \frac{\partial V}{\partial z} \right)^2 \quad (2.206)$$

In order to reduce the number of equations, we eliminate some variables, use the eddy diffusivities and equations (2.205)-(2.206).



## 2.10 One-Dimensional Level 3 Equations.

The equations for the unidimensional case are obtained by assuming horizontal homogeneity which implies that there is no horizontal advection. In this case the vertically-integrated continuity equation yields,

$$W = \text{constant} \quad (2.207)$$

In fact, because the boundary conditions require that the mean vertical wind vanishes at the ground and at the top of the boundary layer, the constant  $W = 0$ . Therefore, the Lagrangian time derivative becomes equal to the local time derivative,

$$\frac{D}{Dt} = \frac{\partial}{\partial t} + U \frac{\partial}{\partial x} + V \frac{\partial}{\partial y} + W \frac{\partial}{\partial z} = \frac{\partial}{\partial t} \quad (2.208)$$

In order to simplify things further we will assume that the geostrophic wind remains constant throughout the period of time considered; this allows us to replace the horizontal pressure gradient by the geostrophic wind. Therefore, it is not necessary to compute the mean pressure in a one-dimensional model. We now write down all the atmospheric equations that we need.

### 2.10.1 Equations for the Mean Quantities.

$$\frac{\partial U}{\partial t} - \frac{\partial}{\partial z} \left( K_m \frac{\partial U}{\partial z} \right) = f (V - V_g) \quad (2.209)$$

$$\frac{\partial V}{\partial t} - \frac{\partial}{\partial z} \left( K_m \frac{\partial V}{\partial z} \right) = f (U_g - U) \quad (2.210)$$

$$\frac{\partial \Theta}{\partial t} - \frac{\partial}{\partial z} \left( K_t \frac{\partial \Theta}{\partial z} \right) = 0 \quad (2.211)$$

$$\frac{\partial Q}{\partial t} - \frac{\partial}{\partial z} \left( K_w \frac{\partial Q}{\partial z} \right) = 0 \quad (2.212)$$



### 2.10.2 Equations for the Turbulent Quantities.

$$\frac{\partial \bar{e}^2}{\partial t} - \frac{1.15}{3} \frac{\partial}{\partial z} (\epsilon l \frac{\partial \bar{e}^2}{\partial z}) = 2(K_m \left| \frac{\partial \vec{V}}{\partial z} \right|^2 + \frac{g}{T_0} \bar{w}\bar{\theta} + 0.61g \bar{w}\bar{q} - \frac{\epsilon^3}{B_1 l}) \quad (2.213)$$

$$\frac{\partial \bar{\theta}^2}{\partial t} - 0.23 \frac{\partial}{\partial z} (\epsilon l \frac{\partial \bar{\theta}^2}{\partial z}) = 2(K_t \left( \frac{\partial \bar{\theta}}{\partial z} \right)^2 - \frac{\epsilon \bar{\theta}^2}{B_2 l}) \quad (2.214)$$

$$\frac{\partial \bar{q}^2}{\partial t} - 0.23 \frac{\partial}{\partial z} (\epsilon l \frac{\partial \bar{q}^2}{\partial z}) = 2(K_w \left( \frac{\partial \bar{q}}{\partial z} \right)^2 - \frac{\epsilon \bar{q}^2}{B_3 l}) \quad (2.215)$$

$$\frac{\partial \bar{q}\bar{\theta}}{\partial t} - 0.23 \frac{\partial}{\partial z} (\epsilon l \frac{\partial \bar{q}\bar{\theta}}{\partial z}) = (K_m + K_t) \frac{\partial \bar{q}}{\partial z} \frac{\partial \bar{\theta}}{\partial z} - \frac{2\epsilon \bar{q}\bar{\theta}}{B_4 l} \quad (2.216)$$

$$K_m = \frac{\lambda_1 \left\{ (1-3C_1) \epsilon^3 + 4 \lambda_1 D_1 (\epsilon^2) + 3g \left[ \frac{1}{T_0} (4 \lambda_1 + 3 \lambda_2) \bar{w}\bar{\theta} + 0.61 (4 \lambda_1 + 3 \lambda_3) \bar{w}\bar{q} \right] \right\}}{\epsilon^2 + 6 \lambda_1^2 \left| \frac{\partial \vec{V}}{\partial z} \right|^2 + 9g \lambda_1 \left( \frac{\lambda_2}{T_0} \frac{\partial \bar{\theta}}{\partial z} + 0.61 \lambda_3 \frac{\partial \bar{q}}{\partial z} \right)} \quad (2.217)$$

$$K_t = \frac{\lambda_2 \left[ \epsilon^3 + 4 \lambda_1 D_1 (\epsilon^2) - 6 \lambda_1 K_m \left| \frac{\partial \vec{V}}{\partial z} \right|^2 - 12 \times 0.61 \lambda_1 g K_w \frac{\partial \bar{q}}{\partial z} - \frac{3\epsilon g \left( \frac{\bar{\theta}^2}{T_0} + 0.61 \bar{q}\bar{\theta} \right)}{\partial \bar{\theta} / \partial z} \right]}{\epsilon^2 + 12 \frac{g}{T_0} \lambda_1 \lambda_2 \frac{\partial \bar{\theta}}{\partial z}} \quad (2.218)$$

$$K_w = \frac{\lambda_3 \left[ \epsilon^3 + 4 \lambda_1 D_1 (\epsilon^2) - 6 \lambda_1 K_m \left| \frac{\partial \vec{V}}{\partial z} \right|^2 - 12 \lambda_1 \frac{g}{T_0} K_t \frac{\partial \bar{\theta}}{\partial z} - \frac{3\epsilon g \left( \frac{\bar{q}\bar{\theta}}{T_0} + 0.61 \bar{q}^2 \right)}{\partial \bar{q} / \partial z} \right]}{\epsilon^2 + 12 \times 0.61 g \lambda_1 \lambda_3 \frac{\partial \bar{q}}{\partial z}} \quad (2.219)$$

The number of variables in the one-dimensional problem has been reduced to 12. We have 11 equations from (2.209) to (2.219) and the equation for  $\lambda$  is given by (2.128), which gives us a closed set of equations.



## 2.11 Boundary Conditions.

In a one-dimensional model there are only two boundaries: the top at which the meteorological variables reach their synoptic values and the bottom which is fixed near the surface of the earth.

### 2.11.1 Upper Boundary Conditions: $z \rightarrow \infty$ .

- 1) All of the turbulent quantities including the coefficients of eddy diffusivity vanish at the top of the boundary layer.
- 2) All of the mean quantities except pressure are kept fixed at the top of the boundary layer. The mean wind reaches there its geostrophic value. We need pressure only in the computations of the atmospheric infrared radiation which do not require a great precision in the computation of pressure so that it is sufficient to determine the pressure from the hydrostatic equation. The pressure will be kept fixed at the ground which implies that the upper pressure will vary with any variation in the mean virtual temperature of the layer.

$$U(z_{\text{top}}) = U_g \quad (2.220)$$

$$V(z_{\text{top}}) = V_g \quad (2.221)$$

$$\Theta(z_{\text{top}}) = \text{synoptic value} \quad (2.222)$$

$$Q(z_{\text{top}}) = \text{synoptic value} \quad (2.223)$$

$$P(z_{\text{top}}) = \text{value determined by the hydrostatic equation} \quad (2.224)$$

$$\text{Turbulent quantities } (z_{\text{top}}) = 0 \quad (2.225)$$

### 2.11.2 Lower Boundary Conditions: $z \rightarrow 0$ .

The basic assumption is that turbulent diffusion is dominant in the surface layer so that the equations for the mean quantities simplify to,

$$\frac{\partial}{\partial z} (\bar{u} \bar{w}) = 0 \quad \bar{u} \bar{w} = \text{constant} = - u_*^2 \cos \alpha \quad (2.226)$$



$$\frac{\partial}{\partial z} (\overline{v w}) = 0 \quad \overline{v w} = \text{constant} = - u_*^2 \sin \alpha \quad (2.227)$$

$$\frac{\partial}{\partial z} (\overline{w \theta}) = 0 \quad \overline{w \theta} = \text{constant} = - H \quad (2.228)$$

$$\frac{\partial}{\partial z} (\overline{w q}) = 0 \quad \overline{w q} = \text{constant} = - E \quad (2.229)$$

where  $\alpha$  is the roughness angle made by the friction velocity  $u_*$  with respect to the  $x$ -axis.  $H$  is the heat flux and  $E$  is the flux of water vapor. Therefore, the formation of a region of constant stress and constant heat and water vapor fluxes close to the ground is a direct consequence of our assumption that the dominant process is diffusion. The next thing to consider is the behavior of  $K_m$ , the eddy diffusivity for momentum, in the surface layer. Its dimensions are [cm<sup>2</sup>/ sec] = speed  $\times$  length. The scaling length becomes  $\ell = k_o (z + z_o)$  in the lower boundary layer and the appropriate scaling velocity is  $u_*$ . Therefore, it is appropriate to expect that,

$$K_m(z \rightarrow z_o) = u_* \ell = k_o u_* (z + z_o) \quad (2.230)$$

Using the definition of  $K_m$ , we can write,

$$\frac{\partial U}{\partial z} = - \frac{\overline{u w}}{K_m} = \frac{u_* \cos \alpha}{k_o (z + z_o)} \quad (2.231)$$

We integrate the last expression and obtain,

$$U = \frac{u_* \cos \alpha}{k_o} \ln \left( \frac{z + z_o}{z_o} \right) \quad (2.232)$$

$V$  can be derived similarly,

$$V = \frac{u_* \sin \alpha}{k_o} \ln \left( \frac{z + z_o}{z_o} \right) \quad (2.233)$$

If we use the definition of  $K_t$  we obtain,

$$\frac{\partial \Theta}{\partial z} = - \frac{\overline{w \theta}}{K_t} = \frac{H \Pr_t}{u_* k_o (z + z_o)} \quad (2.234)$$



The last expression was obtained by relating  $K_t$  to  $K_m$  with the help of the turbulent Prandtl number which is simply the ratio of  $K_m$  over  $K_t$ . The Prandtl number has to be evaluated from the equations in the constant-flux layer. We must be very careful in doing so as the following discussion will prove. The equations for  $K_m$  and  $K_t$  are (2.217) and (2.218). In the constant-flux layer we can neglect buoyancy and the diffusion terms containing  $\bar{D}_1$ , so that the limiting value of the ratio of  $K_m$  over  $K_t$  is,

$$\frac{K_m}{K_t} = \frac{A_1}{A_2} \frac{\ell (1-3C_1) e^3}{\ell e^3} = (1-3C_1) = 0.832 \quad (2.235)$$

However, when we use the level 4 model of Mellor and Yamada (1974) we get a slightly different result. We start from their equations (37c), (38b) and (40c) in which buoyancy and diffusion terms have been neglected as well as any time derivative.

$$0 = - \frac{e}{\lambda_1} \left( \bar{w^2} - \frac{e^2}{3} \right) - 2 \frac{e^3}{\Lambda_1} \quad (2.236)$$

$$0 = - \left( \bar{w^2} - C_1 e^2 \right) \frac{\partial U}{\partial z} - \frac{e \bar{u w}}{3 \Lambda_1} \quad (2.237)$$

$$0 = - \bar{w^2} \frac{\partial \bar{H}}{\partial z} - \frac{e \bar{w \theta}}{3 \lambda_2} \quad (2.238)$$

We isolate the desired covariances,

$$\bar{w^2} = \frac{e^2}{3} - 2 \frac{\lambda_1}{\Lambda_1} e^2 \quad (2.239)$$

$$\bar{u w} = - \frac{3 \lambda_1}{e} \left( \bar{w^2} - C_1 e^2 \right) \frac{\partial U}{\partial z} \quad (2.240)$$

$$\bar{w \theta} = - \frac{3 \lambda_2}{e} \bar{w^2} \frac{\partial \bar{H}}{\partial z} \quad (2.241)$$

The last two equations give the value of the coefficients of diffusivity,



$$K_m = \frac{3\ell_1}{e} \left( \frac{\overline{w^2}}{e^2} - C_1 e^2 \right) \quad (2.242)$$

$$K_t = \frac{3\ell_2}{e} \overline{w^2} \quad (2.243)$$

Their ratio becomes, after using the expression for  $\overline{w^2}$

$$\frac{K_m}{K_t} = \frac{\ell_1 \left( \frac{e^2}{3} - 2 \frac{\ell_1}{A_1} e^2 - C_1 e^2 \right)}{\ell_2 \left( \frac{e^2}{3} - 2 \frac{\ell_1}{A_1} e^2 \right)} = \frac{A_1 \left( \frac{1}{3} - C_1 - 2 \frac{A_1}{B_1} \right)}{A_2 \left( \frac{1}{3} - 2 \frac{A_1}{B_1} \right)} = 0.756 \quad (2.244)$$

The difference between the two expressions is caused by the rearrangement of terms which occurred when we separated the isotropic part from the anisotropic one. In level 3, the dissipation term in  $A_1$  is not explicit but is contained in the terms in  $e^2$ . Therefore, the most straightforward way of obtaining  $P_{rt}$  is to go back to the equations of level 4.

If we integrate (2.234) we obtain,

$$\textcircled{H} - \textcircled{H}(z_0) = \frac{H P_{rt}}{u_* k_0} \ln \left( \frac{z+z_0}{z_0} \right) \quad (2.245)$$

Due to the fact that the scaling lengths for water vapor were chosen equal to those for temperature, the ratio  $K_m/K_w$  is equal to the Prandtl number. We integrate the equation for the gradient of  $Q$  obtained from the definition of  $K_w$  and get,

$$Q - Q(z_0) = \frac{E P_{rt}}{u_* k_0} \ln \left( \frac{z+z_0}{z_0} \right) \quad (2.246)$$

After having multiplied (2.185) to (2.183) by  $\ell$ , we note that the diffusion terms in  $D$  and the buoyant terms contain  $\ell$  which goes to zero as  $z$  goes to zero. In the constant-flux layer these terms are neglected as well as the small time-derivative terms. The final lower boundary values are:



$$e^3(z_o) = B_1 u_*^3 \quad (2.247)$$

$$\overline{\theta^2}(z_o) = \frac{H^2 B_2}{u_*^2 B_1^{v_3}} P_{rt} \quad (2.248)$$

$$\overline{q^2}(z_o) = \frac{E^2 B_3}{u_*^2 B_1^{v_3}} P_{rt} \quad (2.249)$$

$$\overline{q\theta}(z_o) = \frac{E H B_4}{u_*^2 B_1^{v_3}} P_{rt} \quad (2.250)$$

$$\overline{u^2}(z_o) = e^2(z_o) \left( \frac{1}{3} + \frac{A_1}{B_1} (4 \cos^2 \alpha - 2 \sin^2 \alpha) \right) \quad (2.251)$$

$$\overline{v^2}(z_o) = e^2(z_o) \left( \frac{1}{3} + \frac{A_1}{B_1} (4 \sin^2 \alpha - 2 \cos^2 \alpha) \right) \quad (2.252)$$

$$\overline{w^2}(z_o) = e^2(z_o) \left( \frac{1}{3} - 2 \frac{A_1}{B_1} \right) \quad (2.253)$$

$$\overline{u v}(z_o) = 6 \sin \alpha \cos \alpha e^2(z_o) \frac{A_1}{B_1} \quad (2.254)$$

$$\overline{u \theta}(z_o) = \frac{3 A_2}{B_1^{v_3}} H (P_{rt} + 1) \cos \alpha \quad (2.255)$$

$$\overline{v \theta}(z_o) = \frac{3 A_2}{B_1^{v_3}} H (P_{rt} + 1) \sin \alpha \quad (2.256)$$

$$\overline{u q}(z_o) = \frac{3 A_3}{B_1^{v_3}} E (P_{rt} + 1) \cos \alpha \quad (2.257)$$

$$\overline{v q}(z_o) = \frac{3 A_3}{B_1^{v_3}} E (P_{rt} + 1) \sin \alpha \quad (2.258)$$

$$K_m(z \rightarrow z_o) = k_o (z_o + z) u_* \quad (2.259)$$

$$K_t(z \rightarrow z_o) = k_o (z_o + z) \frac{u_*}{P_{rt}} \quad (2.260)$$

$$K_w(z \rightarrow z_o) = k_o (z_o + z) \frac{u_*}{P_{rt}} \quad (2.261)$$



## CHAPTER III

### FINITE-DIFFERENCE EQUATIONS FOR THE ATMOSPHERIC VARIABLES

#### 3.1 General Remarks.

There are two main methods for solving numerically the atmospheric equations: the spectral method and the finite-difference method. Each method has advantages and disadvantages. These are discussed very briefly below.

The spectral method involves the decomposition of the variables into a finite number of spectral components. This can be accomplished, for example, by a Fourier time series,

$$u_j(\vec{x}, t) = \sum_{k=1}^{k=k_0} v_j(k, t) \exp(i k \cdot \vec{x}) \quad (3.1)$$

where  $u_j(\vec{x}, t)$  is the variable in the space-time domain and,  
 $v_j(k, t)$  is the spectral component in the wavenumber-time domain,

$k_0$  is the highest wavenumber that is retained. It is a measure of the resolution of the spectral representation.

The atmospheric equations are transformed into wavenumber space which gives us an equation for each of the spectral components. The first problem arises when we wish to have a vertical resolution of less than one meter in the lower boundary layer. We would need to compute over a thousand spectral components which is an enormous task when the atmospheric equations being used are complex. One way of getting around that problem would be to divide the boundary layer into a 10-to 50-meters thick surface layer and into an upper layer extending up



to the top of the boundary layer. The spectral equations could then be solved separately in these two regions, which would increase the vertical resolution to the desired value in the surface layer without having to compute more than 10 to 100 spectral components. The linkage between these two layers could present some problems related to the fact that we are not solving the spectral equations for the same wavenumbers in both layers.

The finite-difference method has been used for a long time and numerous schemes have been devised ranging from simple ones to sophisticated ones. Basically the method requires replacement of the derivatives by finite differences. We will use centred finite differences. For example, the vertical derivative at the grid point  $k$  of a function  $A$  is approximated by the difference between the value of the function  $A$  at one grid point above  $k$  and its value at one grid point below, divided by the distance ( $2\Delta z$ ) separating the two grid points,

$$\frac{\partial A}{\partial z} \Big|_k = \frac{\Delta A}{\Delta z} \Big|_k = \frac{A(k+1) - A(k-1)}{2\Delta z} \quad (3.2)$$

All of the finite-difference formulae are referred to a grid. We can choose the grid as we please. We know that some of the atmospheric variables, for example, the mean wind and the mean temperature, vary rapidly in the surface layer and more slowly above that. Therefore, we need much more resolution near the ground than at great heights. The ideal solution would require logarithmically-spaced grid points in the surface layer and linearly-spaced grid points in the upper boundary layer. This type of grid would have the advantages of giving good resolution near the ground and of involving relatively few grid points. This can be achieved in a continuous



manner by the log-linear transformation of coordinates with properly chosen parameters. There are some drawbacks related to the usage of finite-difference methods of which non-linear instability, aliasing and errors due to space truncation are major ones.

The finite-difference method was preferred for its simplicity, its potential for increased resolution near the ground, and its smaller computing-time requirement.

### 3.2 Log-Linear Atmospheric Grid.

The best way of designing a log-linear grid is to transform the linear coordinates ( $z$ ) into log-linear coordinates ( $\gamma$ ). This has the advantage of simplifying the finite-difference expressions which would be complex and position-dependent in a non-linear grid. In the transformed  $\gamma$ -coordinates the spacing is linear. An appropriate transformation for meteorological processes in the surface layer is,

$$\gamma = AC \left( \frac{1}{k_o} \ln \left( \frac{z + z'_o}{z'_o} \right) + \frac{z}{z'_o} \right) \quad (3.3)$$

where,  $AC$  = an arbitrary constant that depends on the number of grid points and the height of the uppermost grid point,

$z'_o$  = a constant chosen as closely as possible to the average value of  $\ell_o$ , the maximum size of the eddies,

$z'_o$  = a constant chosen equal to the roughness height  $z_o$  whenever possible,

$k_o$  = Von Karman's constant.

We will now demonstrate that we have the best grid possible in the surface layer if  $z'_o = \ell_o$  and  $z'_o = z_o$ . If we take the derivative



of  $\gamma$  with respect to  $z$ , we obtain:

$$\frac{\partial \gamma}{\partial z} = AC \left( \frac{1}{k_o(z+z_o')} + \frac{1}{l_o'} \right) \quad (3.4)$$

The mixing length can be expressed as,

$$l = \frac{1}{\frac{1}{k_o(z+z_o)} + \frac{1}{l_o}} \quad (3.5)$$

Therefore, in the ideal case we have:

$$\frac{\partial \gamma}{\partial z} = \frac{AC}{l} \quad (3.6)$$

and expressions like,

$$l \frac{\partial B}{\partial z} = l \frac{\partial B}{\partial \gamma} \frac{\partial \gamma}{\partial z} = AC \frac{\Delta B}{\Delta \gamma} \quad (3.7)$$

are encountered frequently and evaluated exactly by the finite-difference method in  $\gamma$ -coordinates. Additional proof comes from consideration of the wind profile in the surface layer:

$$\frac{\partial U}{\partial z} = \frac{u_* \cos \alpha}{k_o(z+z_o)} \quad (3.8)$$

In  $\gamma$ -coordinates (3.8) can be rewritten as,

$$\frac{\partial U}{\partial \gamma} = \frac{u_* \cos \alpha}{AC} \left( 1 + \frac{k_o(z+z_o)}{l_o} \right)^{-1} \quad (3.9)$$

As long as  $(z+z_o) \ll l_o$ ,  $U$  will vary almost linearly in  $\gamma$ -coordinates from one grid point to the other. Therefore, the finite-difference approximation to (3.9) will be very accurate. Similar arguments are valid also for  $V$ ,  $\Theta$  and  $Q$ .

The largest errors would be caused by  $z_o' \neq z_o$ , in which case (3.9) becomes,

$$\frac{\partial U}{\partial \gamma} = \frac{u_* \cos \alpha}{AC} \frac{(z+z_o')}{(z+z_o)} \left[ 1 + \frac{k_o(z+z_o)}{l_o} \right] \quad (3.10)$$

In the case where  $z_o'$  is much different from  $z_o$ , (3.10) is



highly non-linear for small values of  $z$ .

The influence of a difference between  $\ell_o$  and  $\ell'_o$  is considerably smaller in the surface layer than the difference between  $z_o$  and  $z'_o$ . In this case we have,

$$\left( \frac{\partial U}{\partial Y} \right)' = \frac{u_* \cos \alpha}{AC} \left( 1 + \frac{k_o(z+z_o)}{\ell'_o} \right)^{-1} \quad (3.11)$$

The ratio of (3.11) to (3.9) is,

$$\frac{\left( \frac{\partial U}{\partial Y} \right)'}{\left( \frac{\partial U}{\partial Y} \right)} = 1 + \frac{k_o(z+z_o)}{\ell_o \ell'_o} (\ell'_o - \ell_o) \quad (3.12)$$

For example, given  $z_o = 1$  cm,  $\ell'_o = 27$  m, and  $k_o = 0.35$ , then a maximum value for  $\ell_o$  is about 8000cm, in which case (3.12) becomes  $1 + 0.00008588(z+z_o)$ . The error is less than 1 % for  $z < 1$  m, and it is less than 10 % for  $z < 10$  m. Therefore, the influence of a difference between  $\ell'_o$  and  $\ell_o$  is more important above 10 m but in this region (3.8) begins to break down. Therefore, we expect that the log-linear coordinates will give excellent finite-difference approximations to the atmospheric equations in the surface layer without requiring too many grid points.



### 3.3 Atmospheric Equations in Log-Linear Coordinates.

We will transform all of our equations into the log-linear coordinates.

$$\gamma = AC \left( \frac{1}{k_o} \ln \left( \frac{z+z_o}{z_o} \right) + \frac{z}{l'_o} \right)$$

In the transformed coordinates  $\gamma = 0$  at  $z = 0$ , which corresponds to the roughness height  $z_o$ .  $AC$  is a constant which is defined by the specification of the number of grid points and the height of the top of the boundary layer. If we call the last grid point  $\gamma_{\max}$  and the height of the top of the boundary layer  $z_{\text{top}}$ , we get,

$$AC = \gamma_{\max} \left( \frac{1}{k_o} \ln \left( \frac{z_{\max}+z_o}{z_o} \right) + \frac{z_{\max}}{l'_o} \right)^{-1} \quad (3.13)$$

The next step is to determine the intermediate values of  $z$  by an iterative method based on the behavior of the log-linear transformation at small and large values of  $z$ . Close to the ground the coordinates are predominantly logarithmic. Therefore, as a first approximation we neglect the linear term,

$$z = z_o (\exp(k_o \gamma / AC) - 1) \quad (3.14)$$

The next guesses involve the complete formula,

$$z = z_o \left\{ \exp \left[ k_o (\gamma / AC - z / l'_o) - 1 \right] \right\} \quad (3.15)$$

The iteration is completed whenever the difference between two successive guesses is smaller than a predetermined value. Near the top of the boundary layer the coordinates become almost linear. As a first approximation we assume that the grid points are linearly spaced,

$$z = z_{\text{top}} \gamma / \gamma_{\max} \quad (3.16)$$

The successive guesses are given by the complete formula,

$$z = l'_o \left\{ \gamma / AC - \frac{1}{k_o} \left[ \ln \left( \frac{z+z_o}{z_o} \right) \right] \right\} \quad (3.17)$$



The iteration is continued until the difference between two successive iterations becomes smaller than a predefined value. The complete numerical scheme is more complex if we want a rapid solution at all grid points and especially at those intermediate grid points where the influence of the logarithmic and linear terms is about equal. In Appendix A we describe the complete numerical treatment of the derivation of the log-linear grid.

The first derivative of  $\psi$  with respect to  $z$  has been obtained in (3.4) and the second derivative of  $\psi$  with respect to  $z$  is,

$$\frac{\partial^2 \psi}{\partial z^2} = - \frac{AC}{k_o(z+z_o)} z \quad (3.18)$$

The second derivative does not involve  $\psi'_o$  which means that the second derivative is evaluated as exactly as possible as long as  $z'_o = z_o$ . The two derivatives are computed by inserting the value of  $z$  corresponding to each grid point.

Now we will transform the equations from the  $z$ -coordinates to the  $\psi$ -coordinates. In order to generalize the transformation we will use the variables A and B as representations of the atmospheric variables. Any variable which is not differentiated will keep its identity unchanged at the grid point  $\psi_i$  corresponding to the height  $z_i$ ,

$$A(z_i) = A(\psi_i) \quad (3.19)$$

The first derivative in  $z$ -coordinates is transformed into  $\psi$ -coordinates with the help of the chain rule of differentiation,

$$\frac{\partial A}{\partial z} = \frac{\partial A}{\partial \psi} \frac{\partial \psi}{\partial z} \quad (3.20)$$

We must be careful when we transform the second derivative in  $z$ -coordinates into  $\psi$ -coordinates. The correct way of doing the



transformation is,

$$\frac{\partial^2 A}{\partial z^2} = \frac{\partial}{\partial z} \left( \frac{\partial A}{\partial z} \right) = \frac{\partial}{\partial z} \left( \frac{\partial A}{\partial y} \frac{\partial y}{\partial z} \right) \quad (3.21)$$

The chain rule of differentiation is valid only for the first derivative and has been applied to the inside term of (3.21).

Now we differentiate both terms with respect to  $z$ ,

$$\frac{\partial^2 A}{\partial z^2} = \frac{\partial^2 A}{\partial z \partial y} \frac{\partial y}{\partial z} + \frac{\partial A}{\partial y} \frac{\partial^2 y}{\partial z^2} \quad (3.22)$$

After a few manipulations the final result is,

$$\frac{\partial^2 A}{\partial z^2} = \frac{\partial^2 A}{\partial y^2} \left( \frac{\partial y}{\partial z} \right)^2 + \frac{\partial A}{\partial y} \frac{\partial^2 y}{\partial z^2} \quad (3.23)$$

Now we can estimate the diffusion terms,

$$\frac{\partial}{\partial z} \left( A \frac{\partial B}{\partial z} \right) = \frac{\partial A}{\partial z} \frac{\partial B}{\partial z} + A \frac{\partial^2 B}{\partial z^2} \quad (3.24)$$

If we use (3.20) and (3.23) we obtain,

$$\frac{\partial}{\partial z} \left( A \frac{\partial B}{\partial z} \right) = \frac{\partial B}{\partial y} \left( \frac{\partial A}{\partial y} \left( \frac{\partial y}{\partial z} \right)^2 + A \frac{\partial^2 y}{\partial z^2} \right) + \frac{\partial^2 B}{\partial y^2} A \left( \frac{\partial y}{\partial z} \right)^2 \quad (3.25)$$

We can now proceed with the transformation of coordinates.

### 3.3.1 Equations for the Mean Quantities in Log-Linear Coordinates:

#### First Form.

We will transform the set of equations for the mean quantities (2.209) to (2.212) in  $y$ -coordinates.

$$\frac{\partial U}{\partial t} - \frac{\partial^2 U}{\partial y^2} K_m \left( \frac{\partial y}{\partial z} \right)^2 - \frac{\partial U}{\partial y} \left( \frac{\partial K_m}{\partial y} \left( \frac{\partial y}{\partial z} \right)^2 + K_m \frac{\partial^2 y}{\partial z^2} \right) = f(V - V_g) \quad (3.26)$$

$$\frac{\partial V}{\partial t} - \frac{\partial^2 V}{\partial y^2} K_m \left( \frac{\partial y}{\partial z} \right)^2 - \frac{\partial V}{\partial y} \left( \frac{\partial K_m}{\partial y} \left( \frac{\partial y}{\partial z} \right)^2 + K_m \frac{\partial^2 y}{\partial z^2} \right) = f(U_g - U) \quad (3.27)$$

$$\frac{\partial \Theta}{\partial t} - \frac{\partial^2 \Theta}{\partial y^2} K_t \left( \frac{\partial y}{\partial z} \right)^2 - \frac{\partial \Theta}{\partial y} \left( \frac{\partial K_t}{\partial y} \left( \frac{\partial y}{\partial z} \right)^2 + K_t \frac{\partial^2 y}{\partial z^2} \right) = 0 \quad (3.28)$$

$$\frac{\partial Q}{\partial t} - \frac{\partial^2 Q}{\partial y^2} K_w \left( \frac{\partial y}{\partial z} \right)^2 - \frac{\partial Q}{\partial y} \left( \frac{\partial K_w}{\partial y} \left( \frac{\partial y}{\partial z} \right)^2 + K_w \frac{\partial^2 y}{\partial z^2} \right) = 0 \quad (3.29)$$



### 3.3.2 Equations for the Mean Quantities in Log-Linear Coordinates:

#### Second Form.

Equations (3.26) to (3.28) have been used successfully by Estoque (1973) in his numerical model of the boundary layer. However, he has used an arbitrary formulation for  $K_t$  which is less critically dependent on the sign of the temperature gradient than the formulation obtained from second-order modelling. Some of the problems encountered with the utilization of (3.28) are: formation of many artificial inversions and the blocking of the daytime inversion height at a grid point near the ground. These problems can be overcome only by very arbitrary assumptions. These problems are discussed in detail in Appendix C.

There is another way of writing the diffusion term in  $\psi$ -coordinates,

$$\frac{\partial}{\partial z} (K_t \frac{\partial \psi}{\partial z}) = \left[ \frac{\partial}{\partial \psi} (K_t \frac{\partial \psi}{\partial \eta} \frac{\partial \eta}{\partial z}) \right] \frac{\partial \eta}{\partial z}$$

This formulation uses the vertical variation of the heat flux which insures a consistent vertical profile of not only the temperature but also of the heat flux. We can use the same type of formulation for U, V and Q and obtain a new set of equations for the mean quantities.

$$\frac{\partial U}{\partial t} - \left[ \frac{\partial}{\partial \psi} (K_m \frac{\partial U}{\partial \psi} \frac{\partial \psi}{\partial z}) \right] \frac{\partial \psi}{\partial z} = f(V - V_g) \quad (3.26')$$

$$\frac{\partial V}{\partial t} - \left[ \frac{\partial}{\partial \psi} (K_m \frac{\partial V}{\partial \psi} \frac{\partial \psi}{\partial z}) \right] \frac{\partial \psi}{\partial z} = f(U_g - U) \quad (3.27')$$

$$\frac{\partial H}{\partial t} - \left[ \frac{\partial}{\partial \psi} (K_t \frac{\partial H}{\partial \psi} \frac{\partial \psi}{\partial z}) \right] \frac{\partial \psi}{\partial z} = 0 \quad (3.28')$$

$$\frac{\partial Q}{\partial t} - \left[ \frac{\partial}{\partial \psi} (K_w \frac{\partial Q}{\partial \psi} \frac{\partial \psi}{\partial z}) \right] \frac{\partial \psi}{\partial z} = 0 \quad (3.29')$$



### 3.3.3 Equations for the Turbulent Quantities in Log-Linear Coordinates.

We will now transform (2.213) to (2.219) into  $\psi$ -coordinates.

We define the diffusion operator  $\mathcal{D}(\cdot)$  as,

$$\mathcal{D}(\cdot) = (\epsilon l \frac{\partial}{\partial z}) \frac{\partial^2}{\partial \psi^2} + \left( \frac{\partial \epsilon l}{\partial \psi} \left( \frac{\partial \psi}{\partial z} \right)^2 + \epsilon l \frac{\partial^2 \psi}{\partial z^2} \right) \frac{\partial}{\partial \psi} \quad (3.30)$$

The equations for the turbulent quantities are:

$$\frac{\partial \epsilon^2}{\partial t} - \frac{1.15}{3} \mathcal{D}(\epsilon^2) = 2 \left[ K_m \left| \frac{\partial \vec{v}}{\partial \psi} \right|^2 \left( \frac{\partial \psi}{\partial z} \right)^2 - g \left( \frac{K_t}{T_0} \frac{\partial \Theta}{\partial \psi} + 0.61 K_w \frac{\partial Q}{\partial \psi} \right) \frac{\partial \psi}{\partial z} - \frac{\epsilon^3}{B_1 l} \right] \quad (3.31)$$

$$\frac{\partial \overline{\theta^2}}{\partial t} - 0.23 \mathcal{D}(\overline{\theta^2}) = 2 \left[ K_t \left( \frac{\partial \Theta}{\partial \psi} \right)^2 \left( \frac{\partial \psi}{\partial z} \right)^2 - \frac{\epsilon \overline{\theta^2}}{B_2 l} \right] \quad (3.32)$$

$$\frac{\partial \overline{q^2}}{\partial t} - 0.23 \mathcal{D}(\overline{q^2}) = 2 \left[ K_w \left( \frac{\partial Q}{\partial \psi} \right)^2 \left( \frac{\partial \psi}{\partial z} \right)^2 - \frac{\epsilon \overline{q^2}}{B_3 l} \right] \quad (3.33)$$

$$\frac{\partial \overline{q\theta}}{\partial t} - 0.23 \mathcal{D}(\overline{q\theta}) = (K_w + K_t) \left( \frac{\partial \Theta}{\partial \psi} \frac{\partial Q}{\partial \psi} \right) \left( \frac{\partial \psi}{\partial z} \right)^2 - \frac{2 \epsilon \overline{q\theta}}{B_4 l} \quad (3.34)$$

$$K_m = \frac{A_1 l \left[ (1-3C_1) \epsilon^3 + 4x0.23 A_1 l \mathcal{D}(\epsilon^2) - 21 A_1 l g \left( \frac{K_t}{T_0} \frac{\partial \Theta}{\partial \psi} + 0.61 K_w \frac{\partial Q}{\partial \psi} \right) \frac{\partial \epsilon}{\partial z} \right]}{\epsilon^2 + 6A_1^2 l^2 \left| \frac{\partial \vec{v}}{\partial \psi} \right|^2 \left( \frac{\partial \psi}{\partial z} \right)^2 + 9A_1^2 l^2 g \left( \frac{1}{T_0} \frac{\partial \Theta}{\partial \psi} + 0.61 \frac{\partial Q}{\partial \psi} \right) \frac{\partial \psi}{\partial z}} \quad (3.35)$$

$$K_t = [A_1 l (\epsilon^3 + 4x0.23 A_1 l \mathcal{D}(\epsilon^2) - 6A_1 l K_m \left| \frac{\partial \vec{v}}{\partial \psi} \right|^2 \left( \frac{\partial \psi}{\partial z} \right)^2 - 12x0.61 A_1 l g K_w \frac{\partial Q}{\partial \psi} \frac{\partial \psi}{\partial z} - 3 \epsilon g (\overline{\theta^2}/T_0 + 0.61 \overline{q\theta}) / (\frac{\partial \Theta}{\partial \psi} \frac{\partial Q}{\partial z})] \div (\epsilon^2 + 12A_1^2 l^2 g \frac{\partial \Theta}{\partial z} \frac{\partial Q}{\partial z} / T_0) \quad (3.36)$$

$$K_w = [A_1 l (\epsilon^3 + 4x0.23 A_1 l \mathcal{D}(\epsilon^2) - 6A_1 l K_m \left| \frac{\partial \vec{v}}{\partial \psi} \right|^2 \left( \frac{\partial \psi}{\partial z} \right)^2 - 12A_1 l \frac{g}{T_0} K_t \frac{\partial \Theta}{\partial \psi} \frac{\partial \psi}{\partial z} - 3 \epsilon g (\overline{q\theta}/T_0 + 0.61 \overline{q^2}) / (\frac{\partial Q}{\partial \psi} \frac{\partial \psi}{\partial z})] \div (\epsilon^2 + 12A_1^2 l^2 0.61 g \frac{\partial Q}{\partial \psi} \frac{\partial \psi}{\partial z}) \quad (3.37)$$



### 3.4 Finite-Difference Equations.

A Taylor's series expansion around the grid point  $k_0$  at the time  $t_0$  is used to derive the finite-difference equations:

$$f(x_0 + m \Delta x) = f(x_0) + m \Delta x \left. \frac{\partial f}{\partial x} \right|_{x_0} + \dots + \left( \frac{m \Delta x}{n!} \right)^n \left. \frac{\partial^n f}{\partial x^n} \right|_{x_0} + \dots \quad (3.38)$$

where,  $x_0$  can represent  $t_0$  or  $k_0$ ,

$\Delta x$  is the increment  $\Delta t$  or  $\Delta k$ ,

$m$  is the number of increments (positive or negative),

$n$  is any positive integer.

There are many types of finite-difference approximations to the derivatives. For example the forward-Euler finite-difference approximation to the first time derivative uses (3.38) with  $m = 1$ ,

$$\left. \frac{\partial f}{\partial t} \right|_{t_0} = \frac{f(t_0 + \Delta t) - f(t_0)}{\Delta t} \quad (3.39)$$

The truncation error is estimated from the first neglected term in the Taylor's series,

$$T_{\text{runc}}^t = \frac{(\Delta t)}{2!} \left. \frac{\partial^2 f}{\partial t^2} \right|_{t_0} \quad (3.40)$$

The centered finite difference is another important type of finite difference. In this case we use (3.38) for  $m=1$  and  $m=-1$  and subtract the two series from one another to get,

$$\left. \frac{\partial f}{\partial t} \right|_{t_0} = \frac{f(t_0 + \Delta t) - f(t_0 - \Delta t)}{2 \Delta t} \quad (3.41)$$

In this case the truncation error becomes,

$$T_{\text{runc}}^t = \frac{(\Delta t)^2}{3!} \left. \frac{\partial^3 f}{\partial t^3} \right|_{t_0} \quad (3.42)$$

which is expected to be smaller than (3.40) because it involves a higher derivative term.



### 3.4.1 Vertical Derivatives.

We will use centered finite-difference approximations for all of the vertical derivatives, mainly because we expect that the truncation errors associated with centered finite-difference schemes are smaller than those associated with non-centered schemes. If we make use of the fact that  $\Delta \gamma = \Delta k = 1$ , the simplest centered finite-difference approximation to the first  $\gamma$ -derivative becomes,

$$\left. \frac{\partial f}{\partial \gamma} \right|_{k_0} = \frac{f(k_0+1) - f(k_0-1)}{2} \quad (3.43)$$

whose truncation error is,

$$T_{\text{runc}}^k = -\frac{1}{6} \left. \frac{\partial^3 f}{\partial \gamma^3} \right|_{k_0} \quad (3.44)$$

Therefore, (3.43) will be in error whenever the third derivative is important. We have already shown that the mean atmospheric variables vary almost linearly in  $\gamma$ -coordinates in the lower boundary layer. Therefore, the third derivative is small in this region and (3.43) is an excellent approximation to the first derivative. However, at some height above  $z_0$  we expect large non-linear variations in the atmospheric variables. In this case the third derivative becomes relatively large and causes serious truncation errors. One way of reducing this effect is to use more grid points which is very costly in terms of computing time. An alternative approach is to use a higher-order approximation to the derivative in the region where the non-linear variations are expected to be important. This is done by adding the finite-difference expression for the truncation error (3.44) to the finite-difference expression for the first derivative (3.43). When this is done we obtain,



$$\left. \frac{\partial f}{\partial y} \right|_{k_0} = \frac{-f(k_0+2) + 8[f(k_0+1) - f(k_0-1)] + f(k_0-2)}{12} \quad (3.45)$$

and the truncation error becomes,

$$T_{\text{runc}}^k = \frac{1}{30} \frac{\partial^5 f}{\partial y^5} \quad (3.46)$$

The atmospheric variables vary relatively smoothly in the boundary layer and the fifth derivative can be expected to be fairly small. This can be checked by evaluating the fifth derivative by a finite-difference expression.

In order to find the second derivative we form Taylor's series for  $m=1$  and for  $m=-1$ , add the two series together and obtain,

$$\left. \frac{\partial^2 f}{\partial y^2} \right|_{k_0} = f(k_0+1) - 2f(k_0) + f(k_0-1) \quad (3.47)$$

The truncation error is,

$$T_{\text{runc}}^k = -\frac{1}{4!} \frac{\partial^4 f}{\partial y^4} \quad (3.48)$$

The truncation error of (3.47) seems to be fairly small because it depends on the fourth derivative. However, in the case of a strong nocturnal inversion (3.47) may have a relatively large truncation error at a few grid points. If this is needed we can use the following improved approximation to the second derivative,

$$\left. \frac{\partial^2 f}{\partial y^2} \right|_{k_0} = \frac{-f(k_0+2) + 16f(k_0+1) - 30f(k_0) + 16f(k_0-1) - f(k_0-2)}{12} \quad (3.49)$$

whose truncation error is,

$$T_{\text{runc}}^k = -\frac{1}{90} \frac{\partial^6 f}{\partial y^6} \quad (3.50)$$



### 3.4.2 Time Derivative.

Suppose that we must solve,

$$\frac{\partial f}{\partial t} = A(f, t) \quad (3.51)$$

We estimate this expression at the time  $t_0 + \frac{1}{2} \Delta t$ . The right-hand side of (3.51) can be estimated at the time  $t_0 + \frac{1}{2} \Delta t$  as the average between the value of  $A$  at  $t_0$  and its value at  $t_0 + \Delta t$ ,

$$A(f, t_0 + \frac{1}{2} \Delta t) = \frac{1}{2}[A(f, t_0) + A(f, t_0 + \Delta t)] \quad (3.52)$$

and the left-hand side becomes,

$$\left. \frac{\partial f}{\partial t} \right|_{t_0 + \frac{1}{2} \Delta t} = \frac{f(t_0 + \Delta t) - f(t_0)}{\Delta t} \quad (3.53)$$

Equation (3.53) is similar to (3.39) but they are taken to be valid at different times. The truncation error becomes,

$$T_{\text{runc}}^t = -\frac{(\Delta t)^2}{24} \left. \frac{\partial^3 f}{\partial t^3} \right|_{t_0 + \frac{1}{2} \Delta t} \quad (3.54)$$

This method is implicit because it involves the function  $A$  at the time step  $t_0 + \Delta t$  which is not known a priori but must be obtained by some iteration technique.

### 3.4.3 Stability of the Finite-Difference Equations.

Many of the equations in the model are of the form,

$$\frac{\partial f}{\partial t} = A(1) \frac{\partial^2 f}{\partial y^2} + A(2) \frac{\partial f}{\partial y} + A(3) f \quad (3.55)$$

where  $A(1)$ ,  $A(2)$  and  $A(3)$  are functions of  $f$ ,  $t$ ,  $y$  and of other atmospheric variables. The equations are, therefore, non linear which renders very difficult a complete analysis of stability. We will assume that the coefficients are constant in order to simplify the analysis of the stability of the finite-difference equations.



We rewrite (3.55) using the finite-difference approximations as given by (3.53), (3.52), (3.47) and (3.43).

$$\frac{f(k_o, t_o + \Delta t) - f(k_o, t_o)}{(\Delta t/2)} = A(1)[f(k_o+1, t_o) - 2f(k_o, t_o) + f(k_o-1, t_o)] + A(2)[f(k_o+1, t_o) - f(k_o-1, t_o) + f(k_o+1, t_o + \Delta t) - f(k_o-1, t_o + \Delta t)]/2 + A(3)[f(k_o, t_o) + f(k_o, t_o + \Delta t)] \quad (3.56)$$

We suppose that the exact solution of the finite-difference equations is one of the Fourier modes,

$$f(k_o+m, t_o+n \Delta t) = D \exp\{i[(k_o+m)l - (t_o+n \Delta t)\sigma]\} \quad (3.57)$$

where,  $D$  = amplitude,

$l$  = wavenumber,

$\sigma$  = frequency.

Substituting (3.57) in (3.56) and simplifying,

$$\frac{e^{i\sigma\Delta t}-1}{(\Delta t/2)} = (e^{i\sigma\Delta t+1})A(1)(e^{il}+e^{-il}-2) + A(2)(e^{il}-e^{-il}) + A(3)/2 \quad (3.58)$$

We replace the exponentials by the appropriate sine and cosine terms and obtain, after sorting out real and imaginary parts,

$$\cos \sigma \Delta t - 1 = \Delta t [\cos(\sigma \Delta t) A(1)(\cos l - 1) + A(3)/2] - A(2) [\sin \sigma \Delta t \sin l] \quad (3.59)$$

$$\sin \sigma \Delta t = \Delta t [\sin(\sigma \Delta t) A(1)(\cos l - 1) + A(3)/2] + A(2) \cos \sigma \Delta t \sin l \quad (3.60)$$

We square (3.60) and obtain, after a few manipulations,

$$\sin^2 \sigma \Delta t = \frac{1}{1 + \left\{ \frac{1 - \Delta t [A(1)(\cos l - 1) + A(3)/2]}{t A(2) \sin l} \right\}^2}$$

Therefore, the following is true for any real  $l$ ,

$$\sin^2 \sigma \Delta t \leq 1 \quad (3.62)$$



This implies that  $\sigma$  is always real and that the computations are unconditionally stable.

#### 3.4.4 Comments on the Finite-Difference Equations.

We need initial conditions in order to use the time-dependent model. If we were devising an operational model we would need initial conditions that correspond closely to physical reality and we would have to rely on measured atmospheric variables. In our case we do not have any experimental data for initialization of all variables. We are interested in a numerical simulation which would represent a possible urban heat island but not an actual one. Therefore, it seems justifiable to use the steady-state equations in order to derive the initial conditions. However, if we use the steady-state equations for all atmospheric variables, we are led to an undesirable result. The steady-state equation for  $\Theta$  is,

$$\frac{\partial}{\partial z} \left( K_t \frac{\partial \Theta}{\partial z} \right) = 0 \quad (3.63)$$

which implies that,

$$K_t \frac{\partial \Theta}{\partial z} = \text{constant} \quad (3.64)$$

Therefore, the assumption of steady state implies that the constant-flux layer extends up to the top of the boundary layer, which is physically unrealistic because we do not expect the formation of a constant-flux layer deeper than about 100 m. Moreover, (3.64) implies that,

$$\frac{\partial \Theta}{\partial z} = \frac{\text{constant}}{K_t} \quad (3.65)$$



This would cause the temperature gradient to increase near the top of the boundary layer where  $K_t$  decreases to a very small value. One way of getting around that problem is to assign a thickness to the constant-flux layer and to keep the temperature profile fixed above that layer. This has the disadvantage of being rather arbitrary. An alternative is to assume an isentropic atmosphere, because we expect that the atmosphere will be nearly isentropic at the time of maximum temperature.

The equation for  $Q$  is similar to the equation for  $(\dot{H})$ . Therefore, we suppose a constant mixing ratio initially. Evaporation depends on the temperature of the air and it is very likely that the maximum value of  $Q$  occurs at the time of maximum temperature if the water supply is not limited. Therefore, it seems reasonable to expect that the latent heat flux and the sensible heat flux will behave similarly.

The above discussion is valid certainly for the lower boundary layer where the changes in the surface properties are rapidly felt at all levels. However, above 100 m there is a time lag involved so that at the time when the heat flux vanishes at the surface (near the time of maximum temperature), the heat flux might still be important above the surface layer. This points out that the initial conditions can be fairly poor above the surface layer and that the model should be run for a few days of real time before we are certain that the model is independent of the initial conditions.

The equations for the steady state are considerably simplified by our assumptions and only  $U$ ,  $V$ ,  $K_m$ ,  $\epsilon$  and  $\lambda$  need to be computed. The transformation of all the equations into finite-difference form is a fairly lengthy exercise which adds no physical insight to the pro-



blem. For this reason the transformations are presented in detail in Appendix B for the steady-state equations, and in Appendix C for the time-dependent equations.

### 3.5 Steady-State Model.

We will use the Gauss-Seidel iteration scheme. Let  $F_{\text{comp}}$ ,  $F_{\text{past}}$ , and  $F_{\text{new}}$ , be the value of  $F$  calculated from the equations, the last value of  $F$  in the iteration scheme, and the new value of  $F$  in the iteration scheme, respectively. We call the difference,

$$\text{DIFF} = F_{\text{comp}} - F_{\text{past}} \quad (3.66)$$

and let the new value be,

$$F_{\text{new}} = F_{\text{past}} + \text{OMEGA DIFF} \quad (3.67)$$

where OMEGA is the acceleration factor which can vary from 0 to 2,

OMEGA = 0 we keep the last value:  $F_{\text{new}} = F_{\text{past}}$

OMEGA = 1 we keep the calculated value  $F_{\text{new}} = F_{\text{past}}$

OMEGA > 1 acceleration

OMEGA < 1 deceleration.

The iteration needs some initial values in order to start the computations. It is preferable to use the best possible estimate of initial conditions. For example, we can suppose a linear variation of U and V from  $z_0$  to 1000 m, where they would reach their geostrophic values. Above 1000 m U and V can be assumed initially to have their respective geostrophic values. We can assume a constant initial value of about  $50000 \text{ cm}^2/\text{sec}$  for  $K_m$  in the lowest 1000 m and a linear decrease from that value to its top boundary condition above 1000 m. We can assume a value of around 3000 cm for  $\lambda_0$  and compute  $\lambda$  from its



equation. We initialize  $\epsilon$  by assuming a linear decrease from a maximum of the order of 80 cm/sec at the roughness height to its minimum top boundary value.

In the lower boundary layer and up to about 1000 m an OMEGA of 1 to 1.2 is satisfactory. When we use (3.26) and (3.27), we find that OMEGA must be reduced in the upper boundary layer if we want convergence of the iterations.  $K_m$  is determined partly by the vertical gradient of the wind and the wind is determined partly by the vertical gradient of  $K_m$ . Near the top of the boundary layer the wind varies very slowly with height so that great accuracy is needed in the wind in order to estimate properly  $K_m$ . For the first few iterations we can expect large errors in the vertical derivative of the wind and these errors can cause  $K_m$  to be estimated incorrectly by up to one order of magnitude. This in turn increases the error in the wind, and the cycle is repeated over and over and causes rapid divergence. Therefore, in order to get convergence we have to use a small OMEGA near the top of the boundary layer. However, when we use (3.26') and (3.27') these difficulties do not arise because these equations compute the stress directly and, therefore, will give reasonable values for the vertical gradient of the wind even if  $K_m$  is badly initialized.

### 3.6 Time-Dependent Model.

We use an implicit scheme which we have shown to be unconditionally stable for linear equations. A time step of 10 minutes was used successfully and is a fair compromise between resolution and computing time. It would not have been possible to use explicit me-



thods which must obey criteria limiting the time step because the vertical spacing in the lower boundary layer is very small and would have required extremely small time steps. The Dufort-Frankel (1953) scheme was tried unsuccessfully because it showed instability by producing waves of large amplitude and of period  $2\Delta t$ . These waves could not be eliminated even after using a time filter which removed waves of period  $2\Delta t$  exactly. This instability was rather small when a time step of 1 second was used, but such a time step required too much computing time.

The variables at the time  $t_0 + \Delta t$  were evaluated by an iterative scheme which used the accelerated Gauss-Seidel method. The equations were relatively well behaved in the surface layer where an OMEGA slightly greater than 1 could be used generally. However, during the nighttime inversion  $K_t$  decreases rapidly in the region between 5 m and 100 m. This causes some problems in the iteration scheme similar to the ones encountered in the solution of the steady-state equations near the top of the boundary layer. Therefore, an OMEGA of about 0.7 has given good results whereas an OMEGA greater than 0.8 has often caused divergence of the solution. Near the top of the boundary layer the variables converged more rapidly in the time-dependent model than in the steady-state case because of the domination of the time-derivative term which tended to stabilize the iteration procedure. The best value for OMEGA has to be found by trial and error.



### 3.7 Initialization at Each Time Step.

In order to reduce computing time it is desirable to use the best possible initial values for all the variables. This can be done by extrapolating from the values of the variables at the past time steps. If we stored only two time steps we must use linear extrapolation which could be inadequate in some cases of rapid changes as happens near sunrise, for example. A quadratic extrapolation would certainly give much better results at the expense of an increase of 50% in the storage requirements. We now derive a formula for the extrapolation. The variable A can be expressed in terms of a second degree polynomial like,

$$A = a t^2 + b t + c \quad (3.68)$$

We compute A at  $t = 0, 1$  and  $2$ ,

$$A(0) = c \quad (3.69)$$

$$A(1) = a + b + c \quad (3.70)$$

$$A(2) = 4 a + 2 b + c \quad (3.71)$$

After elimination we find that,

$$a = \frac{A(2) - 2 A(1) + A(0)}{2} \quad (3.71)$$

$$b = \frac{4 A(1) - 3 A(0) - A(2)}{2} \quad (3.72)$$

The extrapolated value at  $t = 3$  becomes,

$$A(3) = 9 a + 3 b + c \quad (3.73)$$

We use the values of a, b and c in (3.73),

$$A(3) = A(0) + 3 [A(2)-A(1)] \quad (3.74)$$

Formula (3.74) is used to get the extrapolated value of all of the variables.



## CHAPTER IV

### SOIL LAYER

#### 4.1 Introduction.

The soil layer is modelled relatively simply. The basic equation is,

$$\frac{D T_s}{D t} = \frac{\partial}{\partial z_s} (K_s \frac{\partial T_s}{\partial z_s}) \quad (4.1)$$

where,  $T_s$  = soil temperature,

$K_s$  = soil thermal diffusivity,

$z_s$  = vertical coordinate into the soil.

Equation (4.1) simply implies that the changes in soil temperature are caused by the thermal diffusion between adjacent layers of soil. The basic assumptions are,

- 1) The soil composition is vertically homogeneous so that  $K_s$  is constant for the soil layer. However this assumption can be removed easily in the case of a more complex soil layer, as  $K_s$  can be varied in any manner without basic alteration of the model. For example, we can superpose layers of soil with different thermal diffusivities, or we can vary  $K_s$  with the help of any function representative of the vertical variation of  $K_s$  in a given soil layer.
- 2) The horizontal thermal advection is negligible. This implies that the mean thermal gradient is vertical and that the soil layer is fairly homogeneous in the horizontal at all levels.
- 3) The lower boundary is fixed at 1 m below the surface of the



earth where the temperature is assumed to be constant at all times over the period of one day.

#### 4.2 Logarithmic Grid for the Soil Layer.

We expect that we will find the steepest temperature gradient in the top few centimeters of the soil layer and the weakest gradient near the lower boundary. It is therefore appropriate to devise a grid which gives more resolution close to the earth's surface than at 1 m below it. A logarithmic grid has been devised for the soil layer and makes use of the following transformation of coordinates,

$$\xi = A' \ln (1+z_s) \quad (4.2)$$

where,  $\xi$  = logarithmic coordinate,

$A'$  = a constant determined from the choice of the number of grid points and the depth of the soil layer.

We have chosen a grid with 10 points. The transformation of coordinates is completely defined if we require that,

$$\xi = 0 \text{ at } z_s = 0 \text{ cm}$$

$$\xi = 9 \text{ at } z_s = 100 \text{ cm}$$

In this case we have,

$$A' = 1.95$$

$$z_s = 0.000000 \text{ cm at } \xi = 0$$

$$z_s = 0.669945 \text{ cm at } \xi = 1$$

$$z_s = 1.788719 \text{ cm at } \xi = 2$$

$$z_s = 3.657010 \text{ cm at } \xi = 3$$

$$z_s = 6.776953 \text{ cm at } \xi = 4$$

$$z_s = 11.98709 \text{ cm at } \xi = 5$$

$$z_s = 20.68774 \text{ cm at } \xi = 6$$



$$z_s = 35.21734 \text{ cm at } \xi = 7$$

$$z_s = 59.48100 \text{ cm at } \xi = 8$$

$$z_s = 100.0000 \text{ cm at } \xi = 9$$

The first and second derivatives of  $\xi$  with respect to  $z_s$  can be evaluated exactly,

$$\frac{\partial \xi}{\partial z_s} = \frac{A^*}{1+z_s} \quad (4.3)$$

$$\frac{\partial^2 \xi}{\partial z_s^2} = -\frac{A^*}{(1+z_s)^2} \quad (4.4)$$

Equation (4.1) is transformed into  $\xi$ -coordinates and becomes,

$$\frac{\partial T_s}{\partial t} = K_s \left[ \frac{\partial T_s}{\partial \xi} \frac{\partial^2 \xi}{\partial z_s^2} + \frac{\partial^2 T_s}{\partial \xi^2} \left( \frac{\partial \xi}{\partial z_s} \right)^2 \right] \quad (4.5)$$

#### 4.3 Equation for the Steady State.

The equation for the steady state is obtained by setting the time derivative to zero, in which case (4.1) reduces to,

$$K_s \frac{\partial^2 T_s}{\partial z_s^2} = 0 \quad (4.6)$$

This implies that,

$$\frac{\partial T_s}{\partial z_s} = \text{constant} = C \quad (4.7)$$

Under steady-state conditions we will obtain a linear variation in the soil temperature.

#### 4.4 Time-Dependent Equation.

We will use an implicit finite-difference approximation to the time-dependent equation so that the computations will be absolutely stable. The implicit scheme is the same as the one for the atmospheric equations in which the time derivative is evaluated at the time



$t_o + \frac{1}{2} \Delta t$ . We transform (4.5) into a finite-difference equation and make use of the fact that  $\Delta \xi = \Delta k = 1$  to get,

$$T_s(k_o, t_o + \Delta t)[1 + \Delta t K_s DDZ2(k_o)] = T_s(k_o, t_o) + \frac{\Delta t}{2} K_s \left\{ [T_s(k_o+1, t_o) + T_s(k_o+1, t_o + \Delta t) - T_s(k_o-1, t_o) - T_s(k_o-1, t_o + \Delta t)] DDZ2(k_o) + [T_s(k_o+1, t_o) + T_s(k_o+1, t_o + \Delta t) - 2T_s(k_o, t_o) - 2T_s(k_o, t_o + \Delta t) + T_s(k_o-1, t_o) + T_s(k_o-1, t_o + \Delta t)] DDZ2(k_o) \right\} \quad (4.8)$$

where,

$$DDZ2(k_o) = \left( \frac{\partial \xi^2}{\partial z_s^2} \right) \Big|_{k_o}$$

$$DDZ2(k_o) = \frac{1}{2} \left( \frac{\partial^2 \xi^2}{\partial z_s^2} \right) \Big|_{k_o}$$

#### 4.5 Initial Soil Temperature Profile.

The urban heat island model is started at the time of maximum temperature because the atmospheric heat flux is approximately zero near the ground at that time. However, it is probable that the soil heat flux reaches its maximum value near the time of maximum surface temperature so that a special initialization is needed for the soil temperature profile. This can be done by integrating the soil equation for a few days of real time, letting the surface temperature vary according to a diurnal cycle as given by a cyclic function like a sine. At the end of a few days of real time the soil temperature profile should have adjusted to a value fairly close to the one it should have over a diurnal cycle. The soil temperature profile computed at the time of maximum temperature will be used as the initial soil temperature profile in the urban heat island model. However, the exact amplitude of the diurnal temperature wave is not generally known a priori so that the derived temperature profile must be put into a form which would



be useable for any temperature difference between the surface and the lower boundary. This is done by computing ZS( $k$ ) which gives a weight to DIFF, the temperature difference between the surface and the lower boundary, at each grid point.

$$\text{DIFF} = T_s(0) - T_s(9) \quad (4.9)$$

And ZS( $k$ ) is defined by,

$$ZS(k) = [T_s(k) - T_s(9)] / \text{DIFF} \quad (4.10)$$

Therefore, in the complete program for the steady state, we will not compute the temperature profile but assume it to be of the form,

$$T_s(k) = T_s(9) + ZS(k) \times [T_s(0) - T_s(9)] \quad (4.11)$$

Equation (4.11) should give better initial conditions than (4.7) which assumes a linear variation of temperature in the soil.



## CHAPTER V

### SURFACE TEMPERATURE

The temperature at the earth's surface is determined by a heat-balance equation which includes long-wave and short-wave radiation, heat flux from the ground, latent and sensible heat fluxes from the atmosphere and artificial heat input generated by a city.

$$R_n = - (\rho C_p H + \rho_s c_s S + \rho L E) + A \quad (5.1)$$

where,  $R_n$  = net radiation at the earth's surface,

$\rho$  = atmospheric air density,

$\rho_s$  = density of the soil,

$C_p$  = heat capacity at constant pressure of the atmosphere,

$c_s$  = heat capacity of the soil,

$L$  = latent heat of vaporization,

$H$  = sensible heat flux from the atmosphere,

$E$  = latent heat flux from the atmosphere,

$S$  = sensible heat flux from the soil,

$A$  = artificial heat.

#### 5.1 Net Radiation.

The radiation balance at the earth's surface is,

$$R_n = I_a + R\downarrow - R\uparrow \quad (5.2)$$

where,  $I_a$  = net solar radiation,

$R\downarrow$  = infrared sky radiation,

$R\uparrow$  = terrestrial outgoing infrared radiation



### 5.1.1 Outgoing Terrestrial Infrared Radiation.

We will assume that the earth's surface radiates like a gray body,

$$R \uparrow = \epsilon_1 \sigma T^4 \quad (5.3)$$

where,  $\epsilon_1$  = emissivity of the earth's surface

$\sigma$  = Stefan-Boltzmann constant

T = temperature of the earth's surface

### 5.1.2 Sky Infrared Radiation.

Most of the sky infrared radiation is emitted by water vapor and carbon dioxide. The exact radiation transfer equations become extremely complex when we divide the spectrum into many frequency bands in order to model the selective absorptivity and emissivity of  $H_2O$  and  $CO_2$ . In order to keep the model simple it is necessary to average the infrared radiation over all of the spectrum. The climatological models which use only the observed temperature and humidity at the observing weather station are too simplistic. A compromise between accuracy and reasonable computing time is the Brooks (1950) model as described by Atwater (1966). Brooks has presented values of the emissivity  $\epsilon$  and of  $\frac{d\epsilon}{dw}$ , the slope of the emissivity curve for water vapor with respect to the path length w. Haltiner and Martin (1957) have modelled the infrared radiation due to the atmospheric carbon dioxide in terms of the infrared emission of the earth's surface,

$$R \downarrow (CO_2) = 0.18 \epsilon_1 \sigma T^4 \quad (5.4)$$

We will derive the radiative transfer equation for water



vapor. Our starting point is Schwarzschild's equation for monochromatic radiation,

$$dI_{\nu} = - \rho k_{\nu} [I_{\nu} - B_{\nu}(T)] ds \quad (5.5)$$

where,  $I_{\nu}$  = intensity of radiation at frequency  $\nu$ ,

$k_{\nu}$  = absorption coefficient of water vapor in a thin layer  $ds$ ,

$B_{\nu}$  = blackbody radiance as given by Planck's law,

Now we relate  $ds$  to the absorber path length  $du$ ,

$$ds = \sec \psi du \quad (5.6)$$

where  $\psi$  = zenith angle.

We include the integral over the zenith angle in  $du$  and obtain for the downward radiation,

$$dI_{\nu} = k_{\nu} [I_{\nu} - B_{\nu}(T)] du \quad (5.7)$$

We integrate (5.7) over frequency and path length,

$$F_{\nu}^{\downarrow}(u=0) = \int_0^{\infty} dv \int_0^{u_t} B \frac{\partial T(u, u')}{\partial u} du' \quad (5.8)$$

where  $u_t$  = total path length.

The Brooks model transforms (5.8) into a finite-difference equation,

$$F_w(0) = \sum_{j=1}^n \overline{(\sigma T^4)}_j \left( \frac{\partial \xi}{\partial u} \right) \Delta u \quad (5.9)$$

where  $\Delta u$  is the path length in a given layer as given by

$$\Delta u = \left( \frac{P}{1000} \right)^a 1000 q \frac{\Delta p}{g} \quad (5.10)$$

where,  $a$  = constant between  $\frac{1}{2}$  and 1,

$g$  = gravity,

$p$  = pressure in millibars,

$q$  = mixing ratio for water vapor.



Elliot and Stevens (1961) have derived equations for the emissivity from the data of Brooks (1950), and Hales et al. (1963) have presented an equation for short path lengths. In Table 2 we summarize these equations. The constant  $a$  which appears in (5.10) has to be determined from radiation experiments. Atwater (1967) points out that a value of  $\frac{1}{2}$  or 1 is used generally. In our model we will choose the simplest formulation ( $a=1$ ) because the actual formulation for the infrared radiation is not a crucial factor in understanding the urban heat island when the radiative flux divergence is neglected.

In Appendix D we describe in detail how the computation of the infrared is done. In that computation we have made the assumption that the surface pressure is constant over the period of one day. This is justified because the actual value of the pressure is not used in the computation of the mean wind but only in the computation of the infrared flux. However, this is not a serious restriction because we can allow the surface pressure to vary according to the synoptic conditions if these are known.

### 5.1.3 Incoming Solar Radiation.

The solar radiation received at the earth's surface is,

$$I_a = R_o (1-a) \cos(Z) (T_r)^{\sec Z} \quad (5.11)$$

where,  $R_o$  = solar constant,

$a$  = albedo of the earth's surface,

$T_r$  = transmissivity of the cloudless atmosphere,

$Z$  = zenith solar angle determined by,

$$\cos Z = \sin(\varphi) \sin(\delta) - \cos(\varphi) \cos(\delta) \cos(2\pi/\lambda t) \quad (5.12)$$



TABLE 2. Equations used for emissivity in the Brooks method, as a function of total path length (cm). This table is a reproduction of Atwater's (1967) Table 2, p 827.

$\epsilon = 0.1579 \log(1 + 4275 w)$	$0 < w < 10^{-4}$
$\epsilon = 0.0396 \ln w + 0.389$	$10^{-4} < w < 10^{-3}$
$\epsilon = 0.0565 \ln w + 0.506$	$10^{-3} < w < 10^{-2}$
$\epsilon = 0.0653 \ln w + 0.546$	$10^{-2} < w < 10^{-1}$
$\epsilon = 0.0778 \ln w + 0.575$	$10^{-1} < w$

The first entry is from Hales et al. (1963) and the last four entries are from Elliot and Stevens (1961).



where,  $\varphi$  = latitude,

$\delta$  = solar declination which depends on the time of year and varies from  $23^\circ$  (summer) to  $-23^\circ$  (winter)

$\Omega$  = earth's angular velocity.

## 5.2 Sensible Heat Flux from the Atmosphere.

The atmospheric heat flux is,

$$H = \lim_{z \rightarrow z_0} (K_t \frac{\partial H}{\partial z}) \quad (5.13)$$

This theory is valid only above the roughness height whereas the heat-balance equation is applied at the interface between the atmosphere and the soil. Therefore, we need an equation relating the temperature at  $z_0$  to the temperature at the ground level. There are many possible equations depending mainly on the nature of the roughness elements. The most common assumption is to assume an isothermal layer from the earth's surface up to  $z_0$ . This has the advantage of simplicity and is a justifiable assumption in the case of small roughness elements. However, in the case of large roughness elements like a forest or a city such an assumption is certainly not realistic for that layer of air. In the case of a thick forest we can expect that the maximum temperature will be reached at about the level of the average height of the trees. In that case the effective surface where the radiation balance should be used would not be at the ground but at the height where the vegetation absorbs most of the incoming solar radiation. Therefore, we can expect that the modelling of the layer between the roughness height and the earth's surface will depend mainly on the physical situation to be modelled.



Consider an extreme case in which the assumption of constant heat flux would be valid down to the ground. This could be the case for a relatively rigid, tall and sparse grass through which the air could circulate easily and which has a relatively high roughness height. In this case we can apply (5.13) in the layer below  $z_o$ . We average (5.13) over the layer between  $z_o$  and the ground and obtain,

$$H = \overline{K_t} \frac{\partial \Theta}{\partial z} \quad (5.14)$$

In a finite-difference form this is expressed as,

$$\Theta(z_o) = \Theta(z=0) + z_o \frac{H}{\overline{K_t}} \quad (5.15)$$

The coefficient of eddy diffusivity for temperature  $K_t$  varies linearly near the roughness height so that a good average for  $K_t$  over the layer is,

$$\overline{K_t} = \frac{1}{2} [K_t(z_o) + K_t(0)] = (K_t)_{\text{mol}} + \frac{k_o z_o}{2 P_{rt}} \quad (5.16)$$

where,  $(K_t)_{\text{mol}}$  = molecular diffusivity =  $0.18 \text{ cm}^2/\text{sec}$ .

In general we can neglect the molecular diffusivity with respect to the turbulent diffusivity, in which case (5.15) can be rewritten as,

$$\Theta(z_o) = \Theta(z=0) + \frac{P_{rt}}{k_o} H \quad (5.17)$$

We can generalize (5.17).  $H$  is computed near the roughness height and is an interesting variable to keep in the formula as well as the ground temperature and therefore the following can be used,

$$\Theta(z_o) = \Theta(z=0) + B H \quad (5.18)$$

Some special cases of this formula are,



$B = 0$  implies an isothermal layer between  $z_0$  and the ground.

$B = \frac{2 P_{rt}}{k_0}$  implies a constant heat-flux layer between  $z_0$  and the ground.

$B < 0$  implies that the temperature gradient in the layer between  $z_0$  and the ground has a different value from the temperature gradient in the layer above  $z_0$ . This could be the case, for example, for a dense forest.

### 5.3 Sensible Heat Flux from the Soil.

The sensible heat flux from the soil is simply,

$$S = \lim_{z \rightarrow 0} (K_s \frac{\partial T_s}{\partial z_s}) \quad (5.19)$$

### 5.4 Latent Heat Flux from the Atmosphere.

The latent heat flux from the atmosphere is,

$$E = \lim_{z \rightarrow z_0} (K_w \frac{\partial Q}{\partial z}) \quad (5.20)$$

### 5.5 Artificial Heat Generation.

Artificial heat generation is likely to be more important during the winter months than during the summer months. In fact, during the summertime we would expect that the man-generated heat would be insignificant when compared to the high solar energy input. All of the numerical simulations will be done for summertime situations in which artificial heat is neglected completely.

### 5.6 Solution of the Surface Temperature Equation.

We now have a mathematical expression for each of the terms in (5.1) and the unknown variable is surface temperature. The next



step is to write down these expressions in finite-difference form. The resulting fourth-degree equation is then solved exactly yielding directly the surface temperature. The numerical solution is described in detail in Appendix E.



## CHAPTER VI

### NUMERICAL SIMULATION OF THE URBAN HEAT ISLAND

#### 6.1 Steady-State Model.

The steady-state model is used mainly to provide initial conditions for the time-dependent model. Therefore, we do not require a great accuracy in the numerical results because that does not affect greatly the time-dependent model. This implies that we must be careful in our interpretation of small differences between two steady-state simulations. Three situations were simulated:

- a) small roughness height (1cm) and moderate geostrophic wind (10 m/sec).
- b) Small roughness height (1 cm) and strong geostrophic wind (20 m/sec).
- c) Large roughness height (100 cm) and moderate geostrophic wind (10 m/sec).

From these three cases we should be able to assess the effects of the geostrophic wind speed and of the roughness height.

#### 6.1.1 Effect of the Geostrophic Wind Speed.

Fig. 6 represents the wind hodographs for the three cases. The hodographs for moderate and strong geostrophic winds are virtually on the same normalized curve. The main difference is the height at which the relationship between  $U$  and  $V$  is realized. Table 3 shows more clearly the effect of the increased wind speed. We define arbitrarily the constant-stress layer as the layer close to the ground in which the stress does not vary by more than 20%. The constant-stress layer doubles approximately with a geostrophic wind twice as strong to reach a thickness



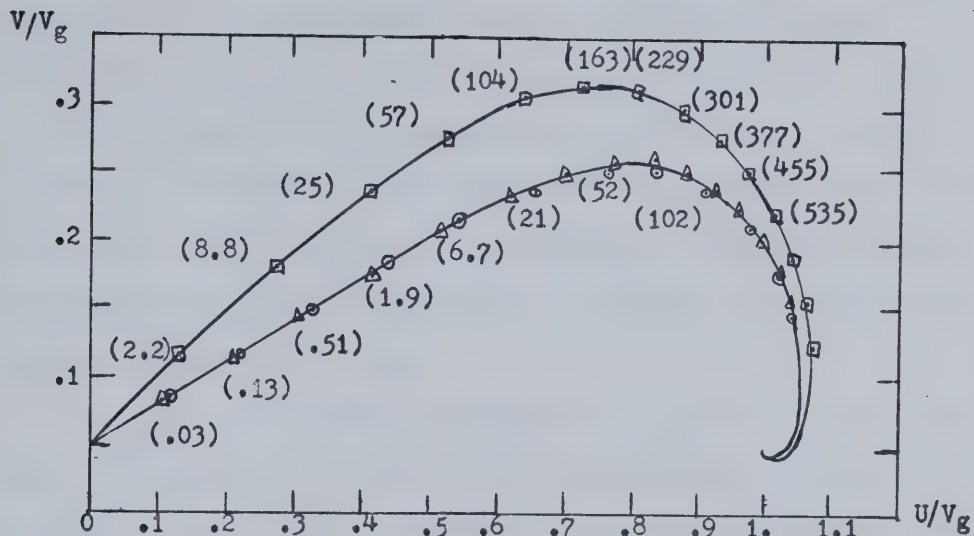


Figure 6. Normalized wind hodograph. The various symbols are:

- for the case  $V_g = 10 \text{ m/sec}$ ,  $z_0 = 1 \text{ cm}$ ,
- △ for the case  $V_g = 20 \text{ m/sec}$ ,  $z_0 = 1 \text{ cm}$  and,
- for the case  $V_g = 10 \text{ m/sec}$ ,  $z_0 = 100 \text{ cm}$ .

The number inside the parentheses is the height in meters.

Table 3. Comparison between three steady-state simulations.

case parameter	#1	#2	#3
$z_0$	1 cm	1 cm	100 cm
$V_g$	10 m/sec	20 m/sec	10 m/sec
$\alpha$	$17.34^\circ$	$17.53^\circ$	$26.14^\circ$
max $U/V_g$	1.0477	1.0504	1.0630
max $V/V_g$	0.205	0.210	0.264
$u_{\frac{1}{2}}$	30.19 m/sec	56.76 m/sec	45.26 m/sec
Top of c.-s. layer	120 m	240 m	180 m



of 240 m. The roughness angle  $\alpha$  is comparable in both cases. Greater accuracy in the numerical results would have been needed in order to assess with certainty the effect of the increased geostrophic wind on  $\alpha$ . From Estoque's (1973) numerical model we would have expected a decrease of  $1^\circ$  in  $\alpha$  due to the doubling of the geostrophic wind and not an increase of  $0.2^\circ$  as obtained in our numerical simulation. The maximum normalized values for both U and V are larger by about 1% for the case of strong geostrophic wind.

In Fig. 7 we compare the behavior of  $e^2/u_*^2$  for all the situations. We observe that the turbulent energy is nearly constant in the constant stress-layer as indicated by the lower straight line, but decreases rather rapidly above that layer for the case of moderate geostrophic wind and much more slowly for the case of strong geostrophic wind. Fig. 8 gives the vertical profile of  $K_m/k_0 u_*$ . The lower boundary value is  $z_0$ . In the constant-stress layer we have a linear relationship between  $K_m$  and  $z$  as indicated by the lower straight line in the nearly log-log graph. The vertical axis in Figs. 7 and 8 is the  $\epsilon$ -coordinate expressed in terms of ordinary heights: therefore, it is logarithmic in the lowest part and nearly linear in the upper part. Both Figs. 7 and 8 indicate that the turbulence will be greatly increased above the constant-flux layer in the case of strong geostrophic wind. This causes a substantial increase in the boundary-layer depth which exceeds 1900 m for the strong wind case as compared to 1300 m for the moderate wind case.

#### 6.1.2 Effect of Increased Roughness Height.

In Fig. 6 we observe that the rougher terrain causes an



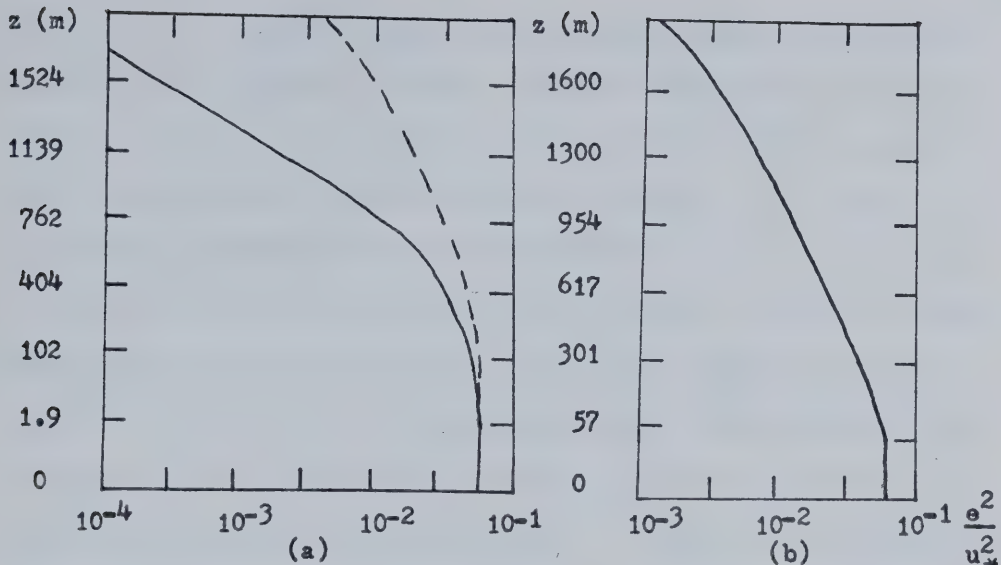


Figure 7. Vertical variation of  $e^2/u_*^2$ : a) over  $z_0=1 \text{ cm}$ . Solid line:  $V_g=10 \text{ m/sec}$ . Dotted line:  $V_g=20 \text{ m/sec}$ . b) Over  $z_0=100 \text{ cm}$ .

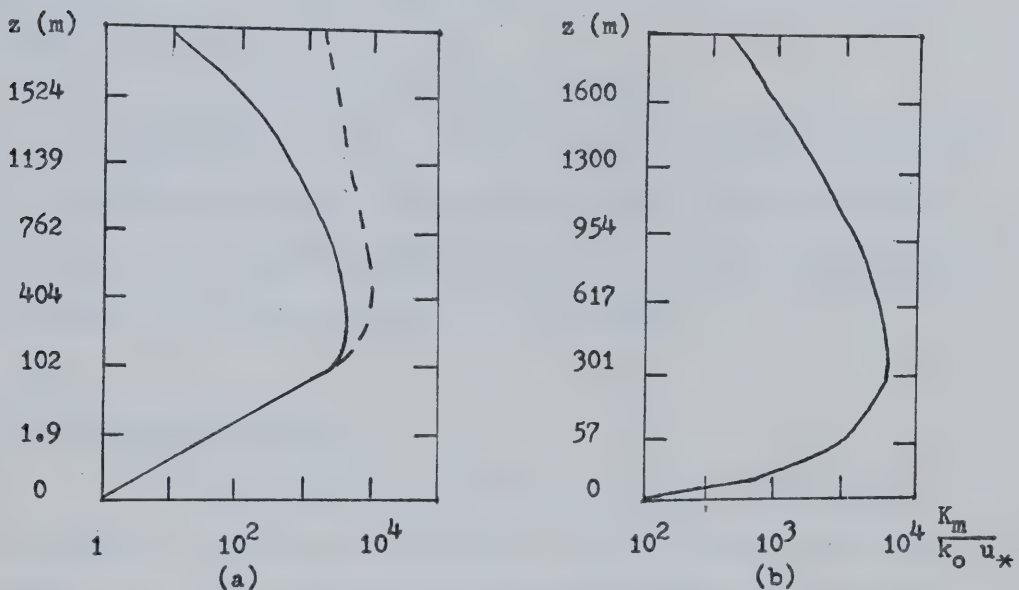


Figure 8. Vertical variation of  $K_m/k_o u_x$ : a) Over  $z_0=1 \text{ cm}$ . Dotted line for  $V_g=20 \text{ m/sec}$  and solid line for  $V_g=10 \text{ m/sec}$ . b) Over  $z_0=100 \text{ cm}$ .



increase in the roughness angle as expected from theoretical considerations. The increase of  $8.5^\circ$  for a change in roughness height of 2 orders of magnitude agrees very well with Estoque's (1973) Fig. 6.4. From Table 3 we can see that the maximum values for U and V are, respectively, 1.5% and 30% larger over rougher terrain. The top of the constant-stress layer is increased by about 50% by a change in roughness height of two orders of magnitude. The friction velocity  $u_*$  is also increased by 50%. This is an interesting result because Table 3 seems to indicate a linear relationship between  $u_*$  and the top of the constant-stress layer under neutral conditions. However, such a relationship would need to be investigated over a wider range of roughness heights and of geostrophic wind speeds. From the knowledge of  $u_*$  we could estimate the height of the constant-stress layer by a formula like:

$$\text{Top of c.-s. layer} = 400 u_*$$

From Figs. 7 and 8 we deduce that both  $\epsilon^2$  and  $K_m$  are increased by an increase in  $z_o$ . Again, the increase in the turbulence is greater above the constant-stress layer than below it. This increases the depth of the boundary layer by at least 50%.

## 6.2 Time-Dependent Model.

The time-dependent model was run with the second form of the equations for the mean quantities. The model ran smoothly with OMEGA = 0.7. We have supposed that convergence was reached whenever the differences between two successive iterative values for the diffusivity coefficients were all smaller than  $10 \text{ cm}^2/\text{sec}$ . In the constant-stress layer, this generally insures an accuracy of 0.1 m/sec in



the mean winds and of  $0.001^{\circ}\text{C}$  in  $\text{H}$ ). Above the constant-stress layer the accuracy is generally greater because the variables are varying more slowly with respect to time. The model is started at the time of maximum temperature which occurs near 2 PM. The parameters common to all simulations are:

$$\delta = 23^{\circ} \text{ (summer solstice)}$$

$$\phi = 53^{\circ} \text{ (Edmonton's latitude)}$$

$$T_r = 0.85$$

$$\xi_1 = 0.82$$

$$\text{albedo} = 0.25$$

$$P(z_o) = 940 \text{ mb (altitude near 2200 feet)}$$

$$Q = 0.006 \text{ g/g}$$

Four simulations were made:

- a) Moderate wind, small roughness height and high soil conductivity.
- b) Strong wind, small roughness height and high soil conductivity.
- c) Moderate wind, large roughness height and high soil conductivity.
- d) Moderate wind, small roughness height and low soil conductivity.

Table 4 lists the differences in the external parameters for the four cases under study. From these four simulations we should be able to assess the effect of the geostrophic wind speed, the effect of the roughness height and the effect of the soil conductivity. Using simulation a) as a reference, we will compare  $U$ ,  $V$ ,  $\text{H}$ ,  $K_t$  and  $\overline{w\theta}$  for the three other cases. Then, we will examine the diurnal cycle of the other turbulent quantities using model b). Model b) is chosen in this case because its diurnal cycle is smoother than the others due to the increased turbulence caused by the stronger geostrophic wind.



Table 4. Parameters for the time-dependent simulations.

parameter \ model #	1	2	3	4
$z_0$ [cm]	1	1	100	1
$v_g$ [m/sec]	10	20	10	10
$\rho_s$ [g/cm <sup>3</sup> ]	2.6	2.6	2.6	1.8
$k_s$ [cm <sup>2</sup> /sec]	0.021	0.021	0.021	0.0053
$c_s$ [ergs/(g- °C)]	$1.25 \times 10^7$	$1.25 \times 10^7$	$1.25 \times 10^7$	$8.3 \times 10^6$
$\rho_s k_s c_s$ [ergs/(cm-sec- °C)]	$4.53 \times 10^5$	$4.53 \times 10^5$	$4.53 \times 10^5$	$1.19 \times 10^5$



### 6.2.1 Geostrophic Wind Speed.

Fig. 9 shows the diurnal variation of the surface temperature. The increased geostrophic wind reduces the amplitude of the diurnal cycle: the minimum temperature is increased by  $2.92^{\circ}\text{C}$  and the second-day maximum temperature is decreased by  $1.71^{\circ}\text{C}$ . There is no detectable time lag between the two temperature cycles and they both reach their minimum near 4.30 AM and their maximum near 2.30 PM. The surface cooling rate illustrated in Fig. 10 also shows the moderating effect of the stronger wind. Stronger winds increase the mixing which allows a deeper layer to cool down or warm up, thus decreasing the amplitude of the diurnal temperature cycle. We see in Fig. 11 that the amplitude of the diurnal variation of the roughness angle is also reduced by the stronger wind. The shape of both curves is similar. We observe a rapid decrease in  $\alpha$  during the first 6 hours after the time of maximum temperature. However, the surface cooling rate has reached its maximum intensity near 6 PM and is decreasing rapidly between 6 PM and 8 PM. This reduces the growth rate of  $\alpha$  which reaches a secondary maximum near 7 to 8 PM.  $\alpha$  decreases after the decrease in the cooling rate because the level of maximum cooling rate shifts higher, destabilizing slightly the layer close to the ground. However, after a while a deep layer above the ground becomes so stable as to permit a continuous increase in  $\alpha$ , which is observed between 11 PM and 6 AM. After 8 AM  $\alpha$  exhibits a tendency to decrease. However, we observe a large oscillation with minimum near 9 AM and maximum near 11 AM. This is similar to the overnight maximum in  $\alpha$ . The maximum warming rate occurs near 9 AM. Due to enhanced turbulence under unstable conditions, the slight decrease in the warming rate after 9 AM is



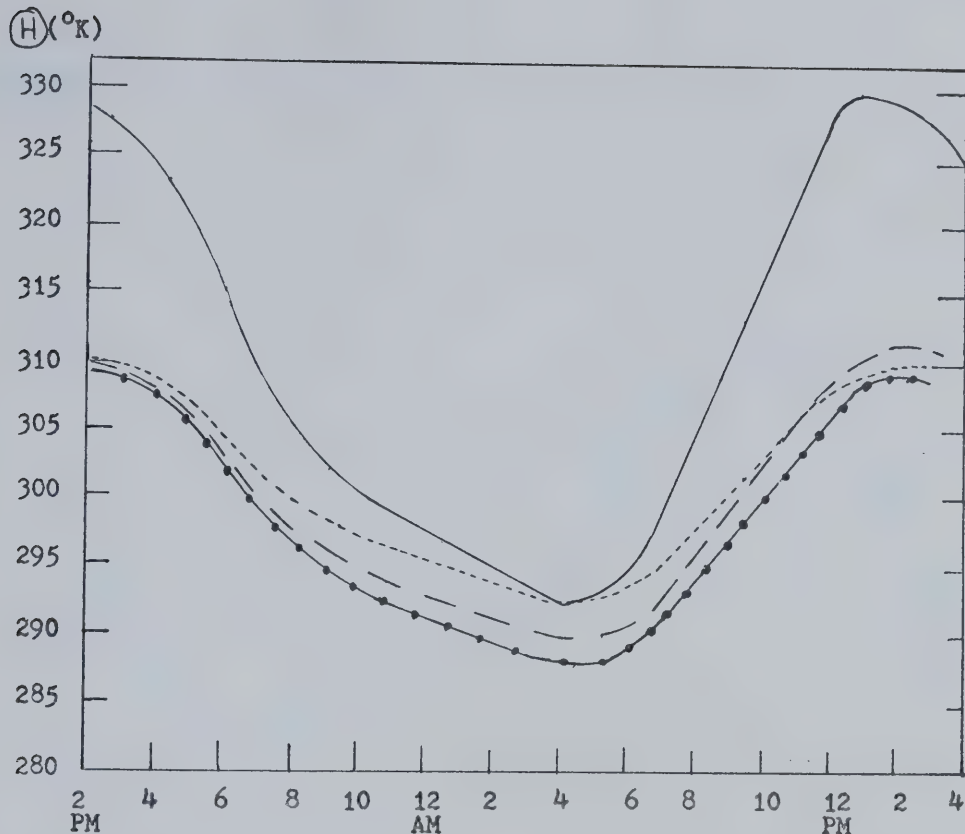


Figure 9. Diurnal cycle of the surface potential temperature. The different curves represent the following:

- $z_0 = 1 \text{ cm}$ ,  $V_g = 10 \text{ m/sec}$ , soil thermal conductivity = low.
- $z_0 = 100 \text{ cm}$ ,  $V_g = 10 \text{ m/sec}$ , soil thermal conductivity = high.
- - -  $z_0 = 1 \text{ cm}$ ,  $V_g = 10 \text{ m/sec}$ , soil thermal conductivity = high.
- · -  $z_0 = 1 \text{ cm}$ ,  $V_g = 20 \text{ m/sec}$ , soil thermal conductivity = high.

The hour in this and the subsequent graphs is expressed in solar time related to the mountain standard time by:  $LST = MST - 0.6$ .

Sunrise occurs at  $3\frac{40}{60}$  AM LST and sunset at  $8\frac{20}{60}$  PM LST.



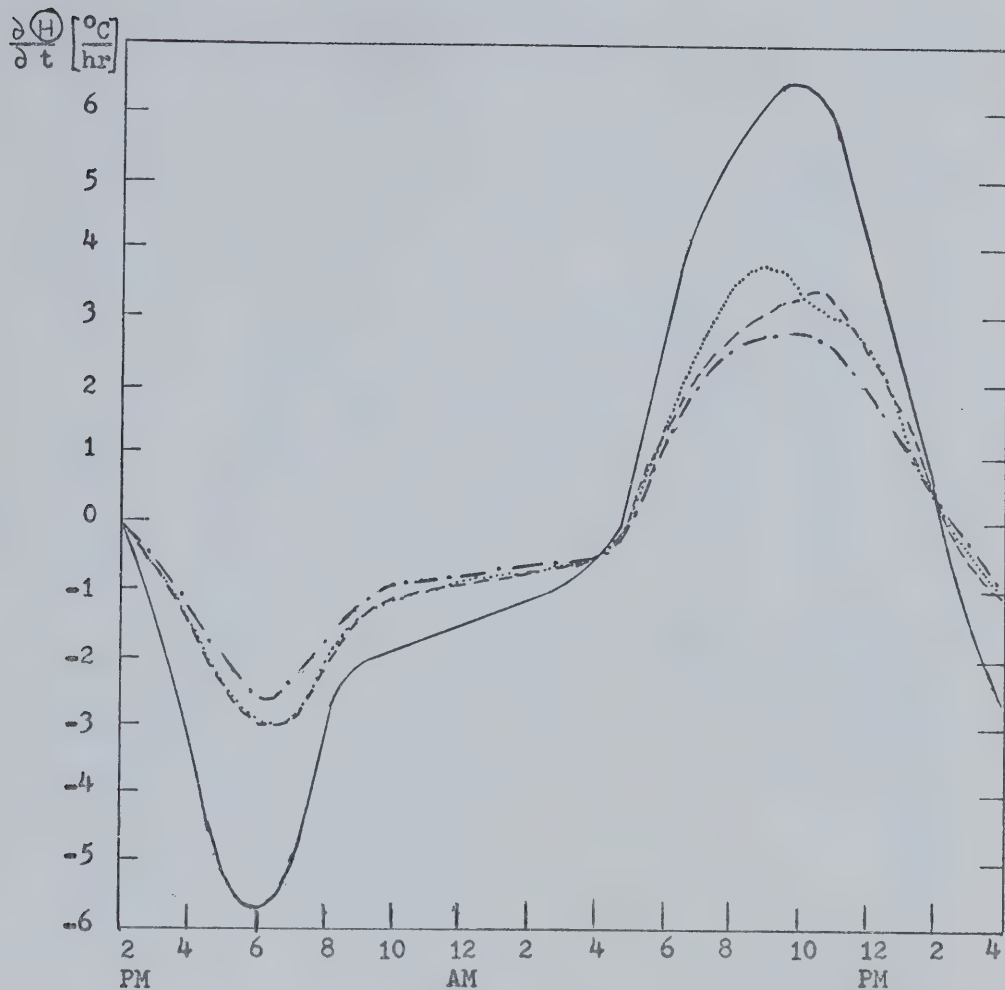


Figure 10. Warming rate at the surface. The four curves represent:

- $z_o = 1 \text{ cm}$ ,  $V_g = 10 \text{ m/sec}$ , soil thermal conductivity = low.
- .....  $z_o = 100 \text{ cm}$ ,  $V_g = 10 \text{ m/sec}$ , soil thermal conductivity = high.
- $z_o = 1 \text{ cm}$ ,  $V_g = 10 \text{ m/sec}$ , soil thermal conductivity = high.
- - -  $z_o = 1 \text{ cm}$ ,  $V_g = 20 \text{ m/sec}$ , soil thermal conductivity = high.



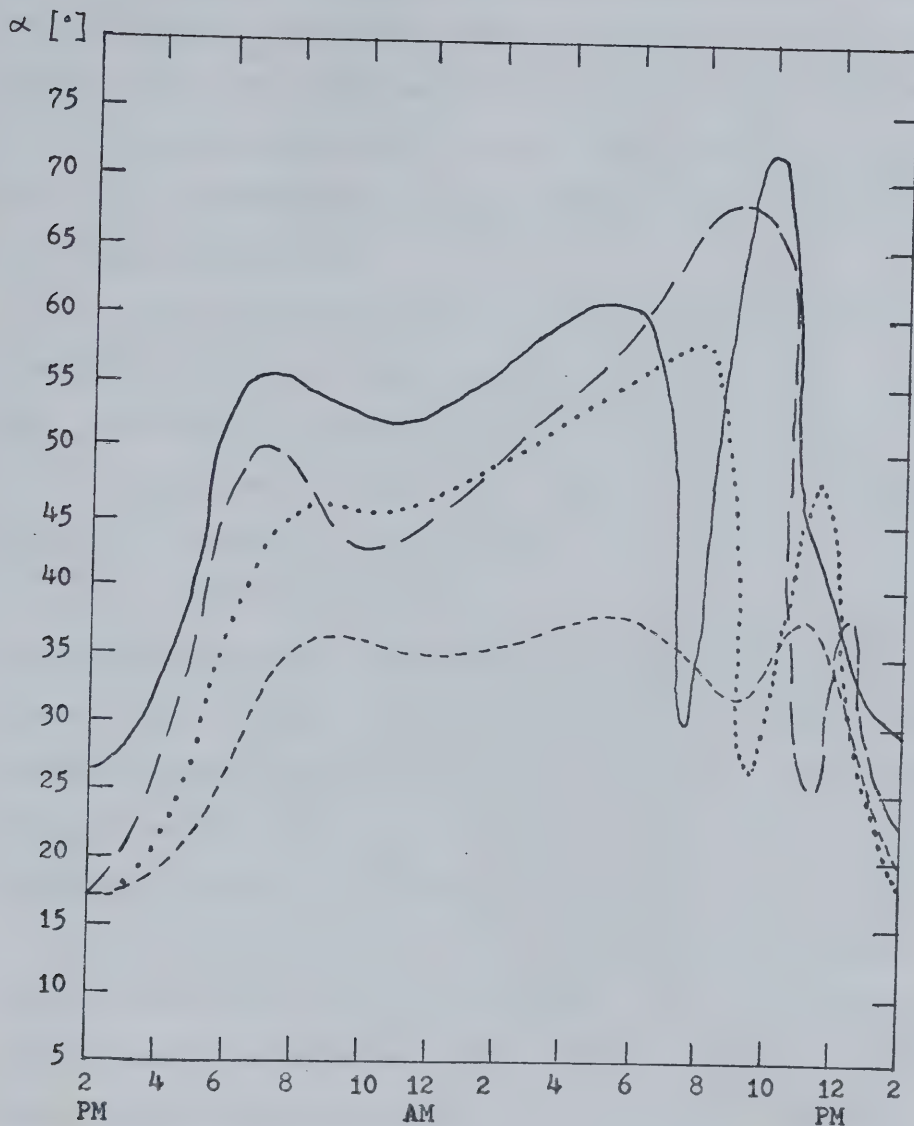


Figure 11. Diurnal variation of the roughness angle. The various curves are:

- $z_o = 1 \text{ cm}, V_g = 10 \text{ m/sec}$ , soil thermal conductivity = low.
- $z_o = 100 \text{ cm}, V_g = 10 \text{ m/sec}$ , soil thermal conductivity = high.
- $z_o = 1 \text{ cm}, V_g = 10 \text{ m/sec}$ , soil thermal conductivity = high.
- $z_o = 1 \text{ cm}, V_g = 20 \text{ m/sec}$ , soil thermal conductivity = high.



almost immediately reflected in  $\alpha$  which increases suddenly. The oscillation is certainly amplified by the finite grid because the inversion height is not lifted continuously but by discrete steps. Therefore, even if there are some physical reasons for the oscillation in  $\alpha$  near 10 AM, the amplitude of the phenomenon is certainly much smaller than indicated in Fig. 11.

Figs. 12 and 13 represent the diurnal cycle of the vertical distribution of  $\Theta$  for strong and moderate geostrophic winds, respectively. With moderate geostrophic winds the nocturnal cooling is only  $0.03^{\circ}\text{C}$  at 240 m and  $0.1^{\circ}\text{C}$  at 166 m. However, with strong geostrophic winds the overnight cooling at 166 m, 240 m and 670 m is, respectively,  $12.3^{\circ}\text{C}$ ,  $6^{\circ}\text{C}$  and  $0.1^{\circ}\text{C}$ . This is a reflection of the increased turbulence and deeper mixing layer. One interesting feature of the model is that it predicts a delay between the time at which the surface temperature starts increasing after sunrise and the time at which the atmosphere becomes unstable in the lowest levels. Near sunrise the atmospheric heat flux is positive and it will take some time before it changes sign. The increase in surface temperature destabilizes the lower layer which increases the turbulence and the coefficient of eddy diffusivity and therefore permits a slower decrease in the heat flux. That delay is about one hour for the moderate wind case but reaches two hours in the case of strong winds. The surface temperature warms up by  $0.7^{\circ}\text{C}$  in the moderate-wind case and by  $2.4^{\circ}\text{C}$  in the strong-wind case before the lower atmosphere becomes unstable. The Kansas experiments have shown an average delay of one hour between sunrise and the appearance of an unstable lapse rate at 6 m (Wyngaard; 1973). This agrees very well with our results if we



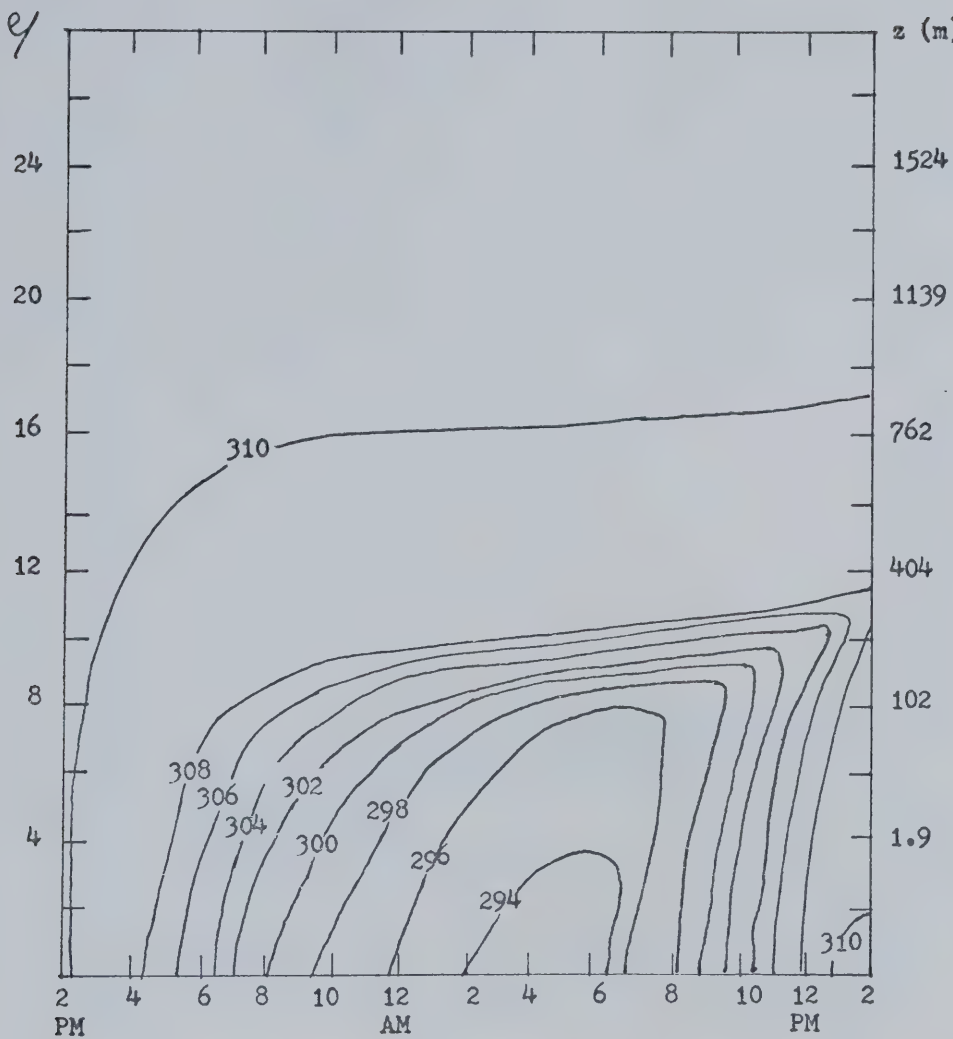


Figure 12. Diurnal cycle of the vertical distribution of potential temperature for the case  $z_0 = 1$  cm,  $V_g = 20$  m/sec and high soil conductivity. The units are [ $^{\circ}$ K].



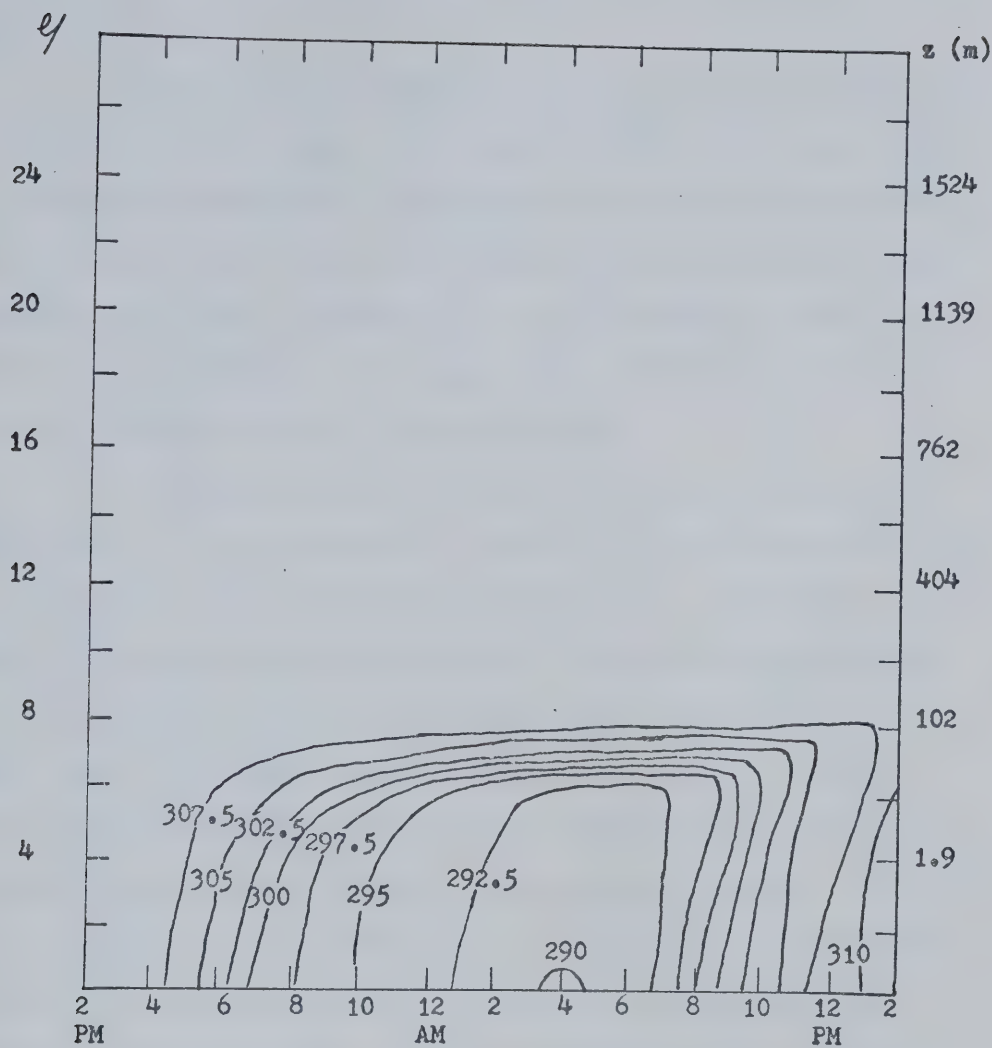


Figure 13. Diurnal cycle of the vertical distribution of potential temperature for the case  $z_0 = 1$  cm,  $V_g = 10$  m/sec and high soil conductivity. The units are [ $^{\circ}$ K].



suppose that the average geostrophic wind during these experiments was less than 10 m/sec.

The heat flux is represented in Figs. 14 and 15 for the cases of high and moderate winds. We observe that  $\bar{w\theta}$  is more than doubled by doubling the geostrophic wind speed. The phase difference already noted in the surface value of  $\bar{w\theta}$  between the two simulations is also apparent up to 50 m. We observe also that the inversion height is lifted more rapidly with the stronger winds after the instability has been established in the lower grid points.

By comparing Fig. 16 with Fig. 17 we can say that the maximum value for  $K_t$  is increased by a factor of 2 to 4 and that the height at which that maximum occurs is shifted upwards by about 50 m. Therefore,  $\bar{w\theta}$  is larger with stronger winds, even if the temperature gradients are smaller, because of the much larger values for  $K_t$  in that case. The general shape of both curves for  $K_t$  is similar: very high values during near neutral and unstable situations and very small values everywhere overnight during stable situations. We observe also a marked difference between the first day and the second day due to the fact that the upper levels have remained stable during the 24-hour cycle which caused a decrease in  $K_t$  above 500 m. The model has a tendency to produce negative values for  $K_t$  under very stable conditions. We reset  $K_t$  automatically to a very small number of the order of  $10^{-2} \text{ cm}^2/\text{sec}$  whenever that happens. We need that restriction in order to insure the stability of the finite-difference scheme. Otherwise we would get the formation of many artificial inversions which could easily prevent the convergence of the model. This problem is more serious in the moderate wind case as 5 to 6 levels



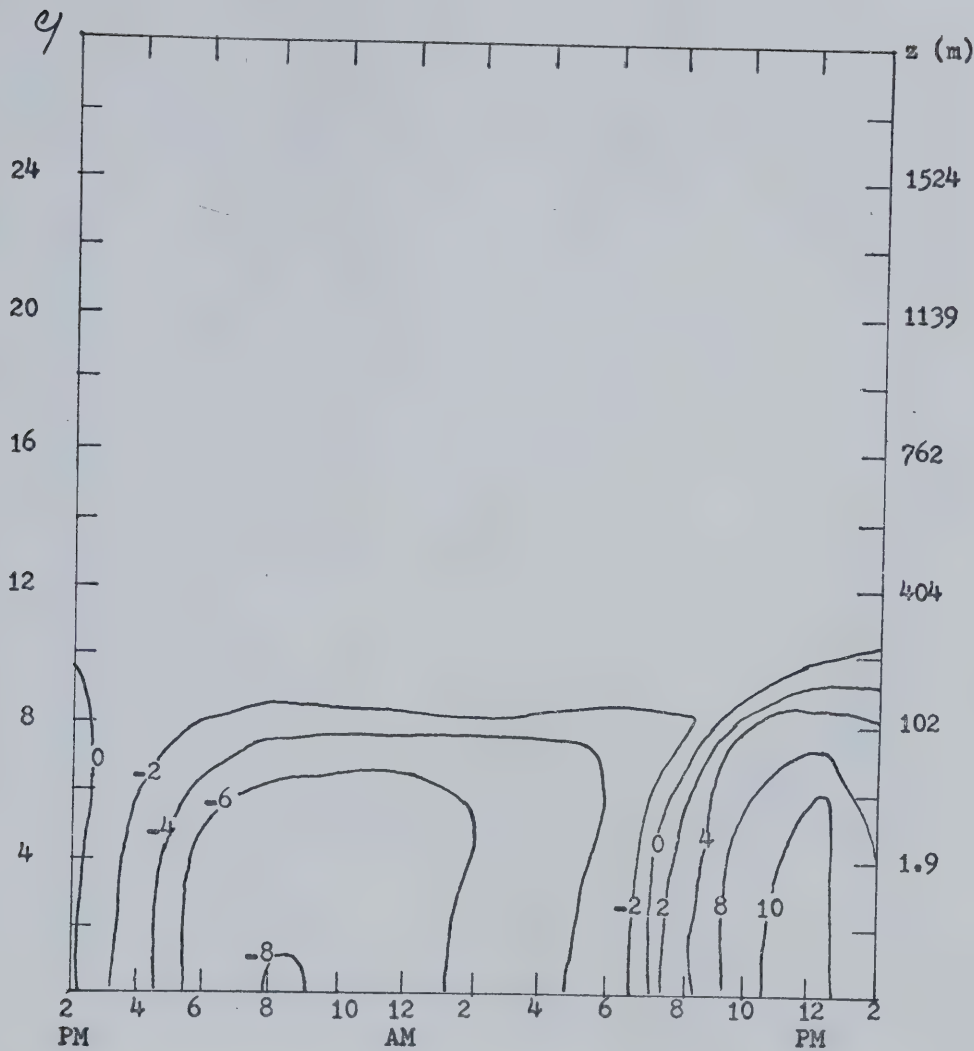


Figure 14. Diurnal cycle of the vertical distribution of  $\overline{w\theta}$  for the case  $z_0 = 1$  cm,  $V_g = 20$  m/sec and high soil conductivity. The units are [ $\text{cm} \ ^\circ\text{C sec}^{-1}$ ].



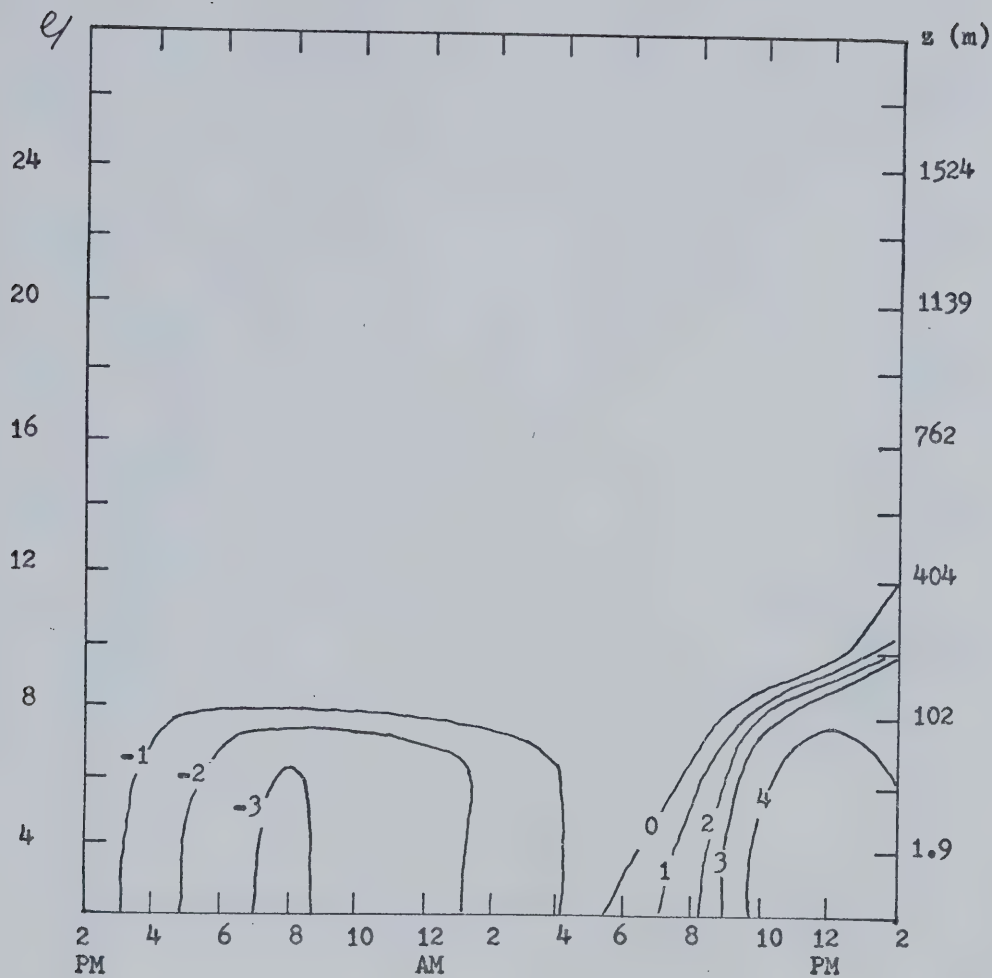


Figure 15. Diurnal cycle of the vertical distribution of  $\bar{w}\theta$  for the case  $z_0 = 1$  cm,  $V_g = 10$  m/sec and high soil conductivity. The units are  $[\text{cm } ^\circ\text{C sec}^{-1}]$ .



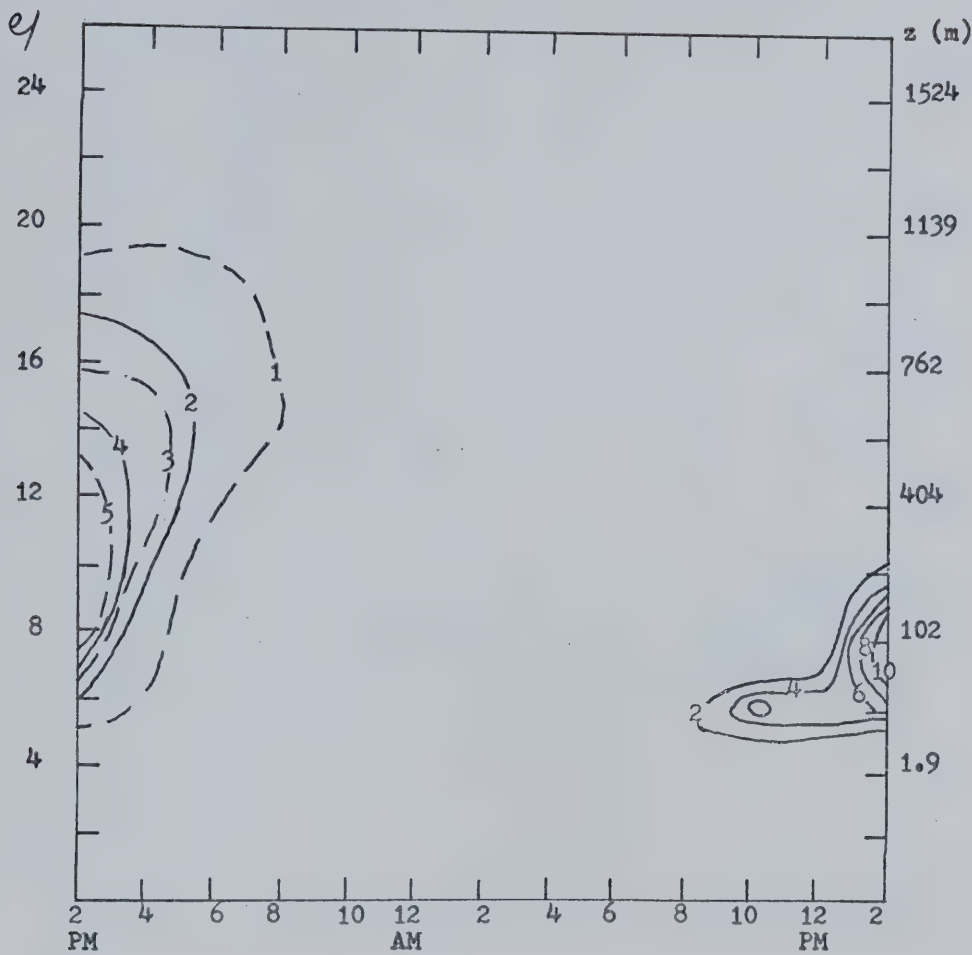


Figure 16. Diurnal cycle of the vertical distribution of the coefficient of diffusivity for temperature for the case  $z_0 = 1$  cm,  $V_g = 10$  m/sec and high soil conductivity. The units are [ $10^4$  cm $^2$ /sec].



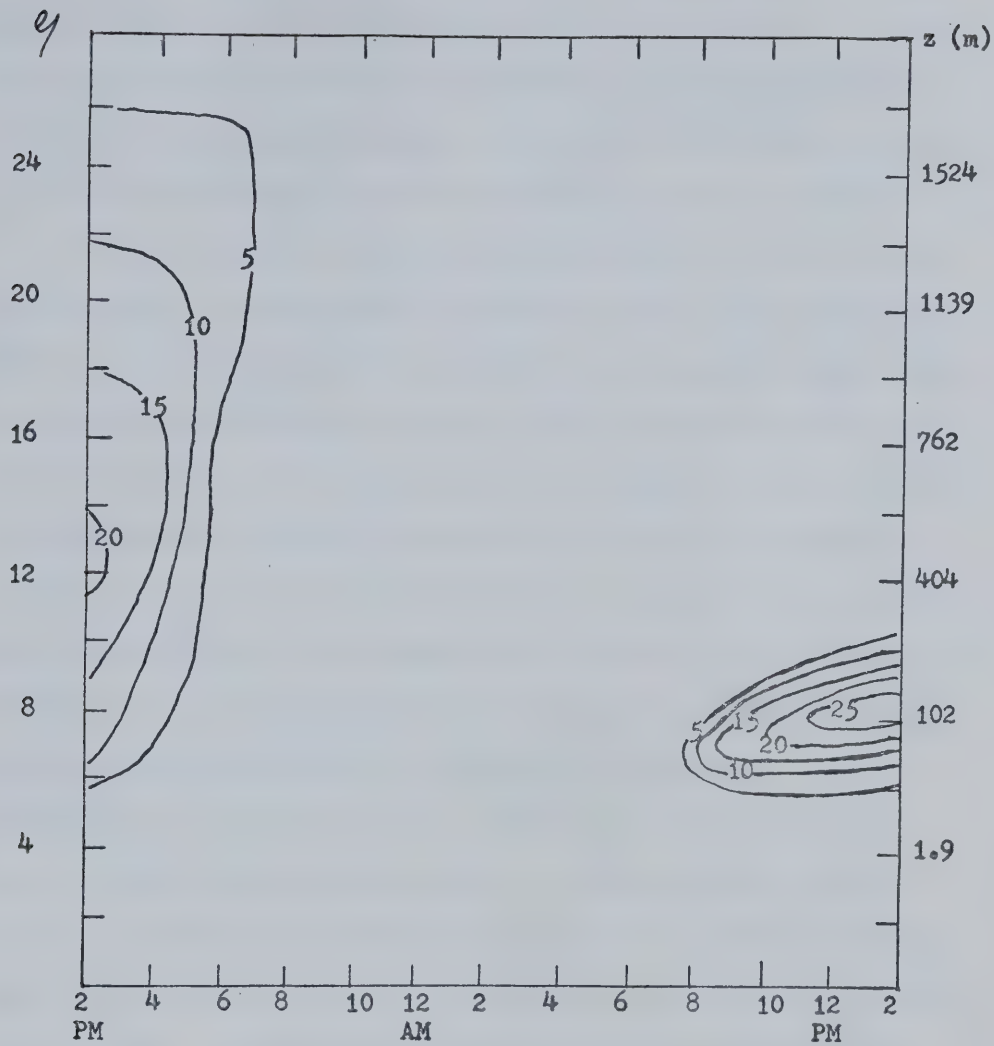


Figure 17. Diurnal cycle of the vertical distribution of the coefficient of diffusivity for temperature for the case  $z_0 = 1$  cm,  $V_g = 20$  m/sec and high soil conductivity. The units are  $[10^4 \text{ cm}^2/\text{sec}]$ .



are computed with negative values by early morning. With strong geostrophic winds only one or two levels exhibit that tendency. We feel that allowing negative values for  $K_t$  would not change significantly the results while compromising the convergence of the iterative process. This is the justification for not allowing  $K_t$  to become negative.

Figs. 18 and 19 show the diurnal variation of  $U$  for moderate and strong winds. Both graphs are similar in shape. The maximum wind gradient is near the ground under unstable or near-neutral lapse rates. The wind gradient decreases overnight in both the upper boundary layer and the lower part of the surface layer. The region of large overnight wind gradient is concentrated between 20 m and 50 m for the moderate wind case and between 20 m and 166 m for the strong-wind case. Between about 100 m and 300 m,  $U$  has maxima near 12 PM and 12 AM and minima near 5 AM and 5 PM. The overnight maximum is caused by an inertial oscillation which takes place some time after the initial cooling when the friction force decreases above 50 m within a short period of time, from a relatively large daytime value to an extremely small value. There is a tendency for the wind to "overshoot" its geostrophic value which is caused by the non-zero time derivative term in the equations of motion. Fig. 20 illustrates the diurnal cycle of the total wind speed at different heights for the case of strong geostrophic winds. Near the ground the first minimum occurs near 8 PM, just after the time of maximum cooling rate. The decreasing cooling rate after 6 PM permits a small recovery in the surface wind speed which reaches a secondary maximum near 12 AM. The stabilization of the cooling rate after 10 PM causes a further decrease in the surface wind until sunrise. After sunrise, the surface wind increases to reach its maximum near the time



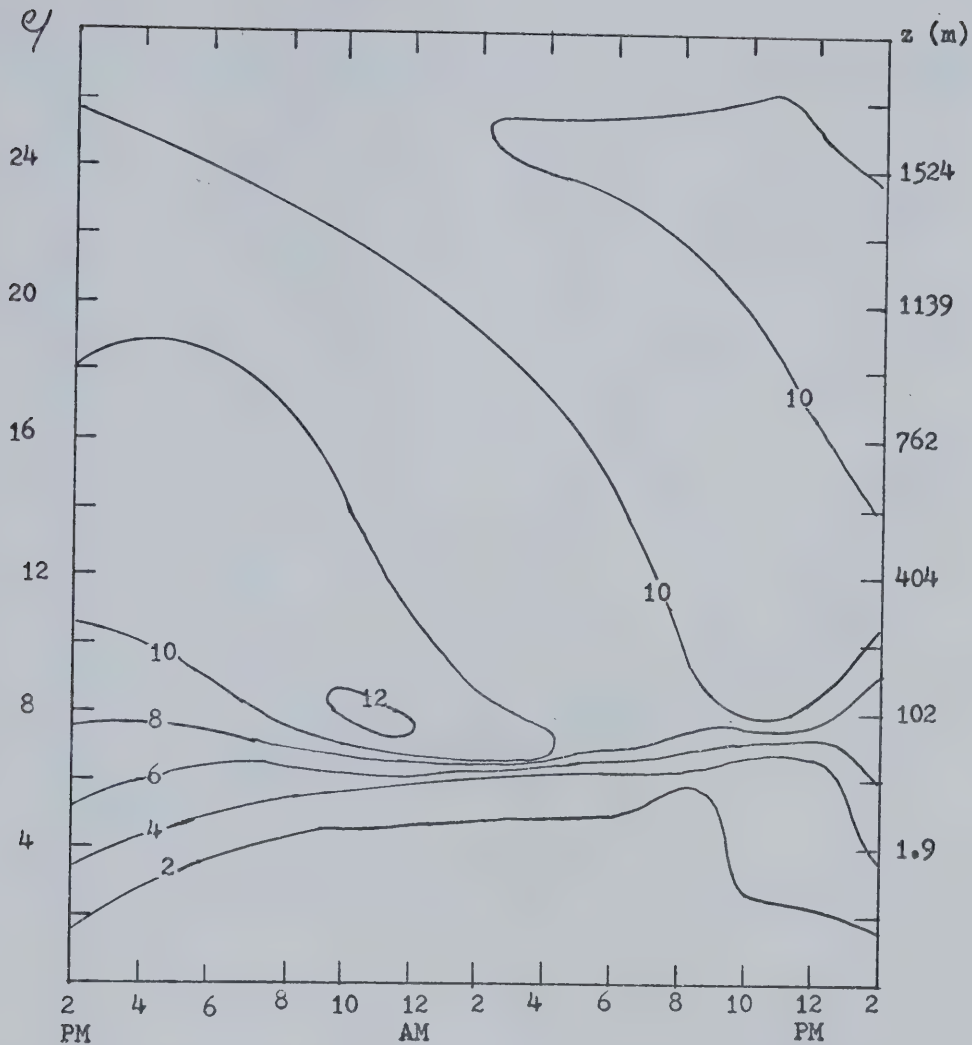


Figure 18. Diurnal cycle of the vertical distribution of  $U$  for the case of  $z_0 = 1$  cm,  $V_g = 10$  m/sec and high soil conductivity. The units are [m/sec].



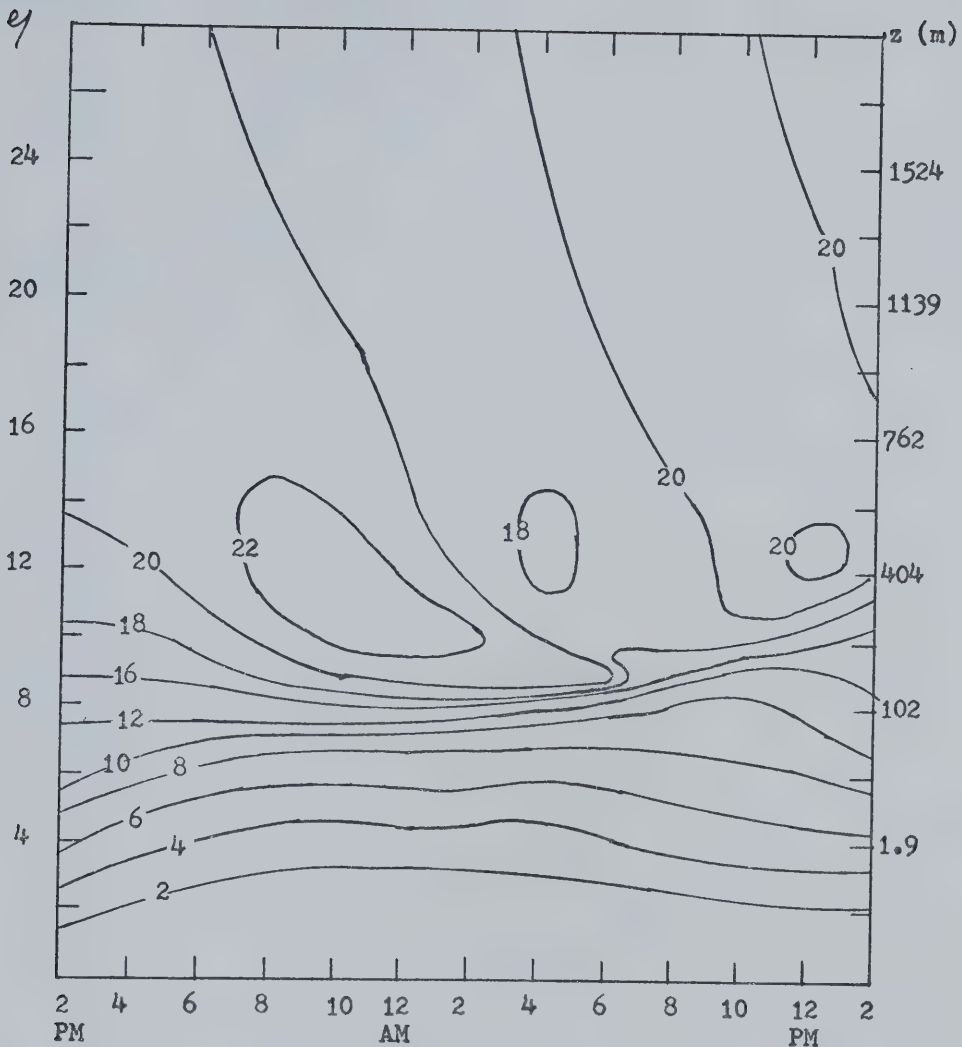


Figure 19. Diurnal cycle of the vertical distribution of  $U$  for the case  $z_0 = 1$  cm,  $V_g = 20$  m/sec and high soil conductivity. The units are [m/sec].



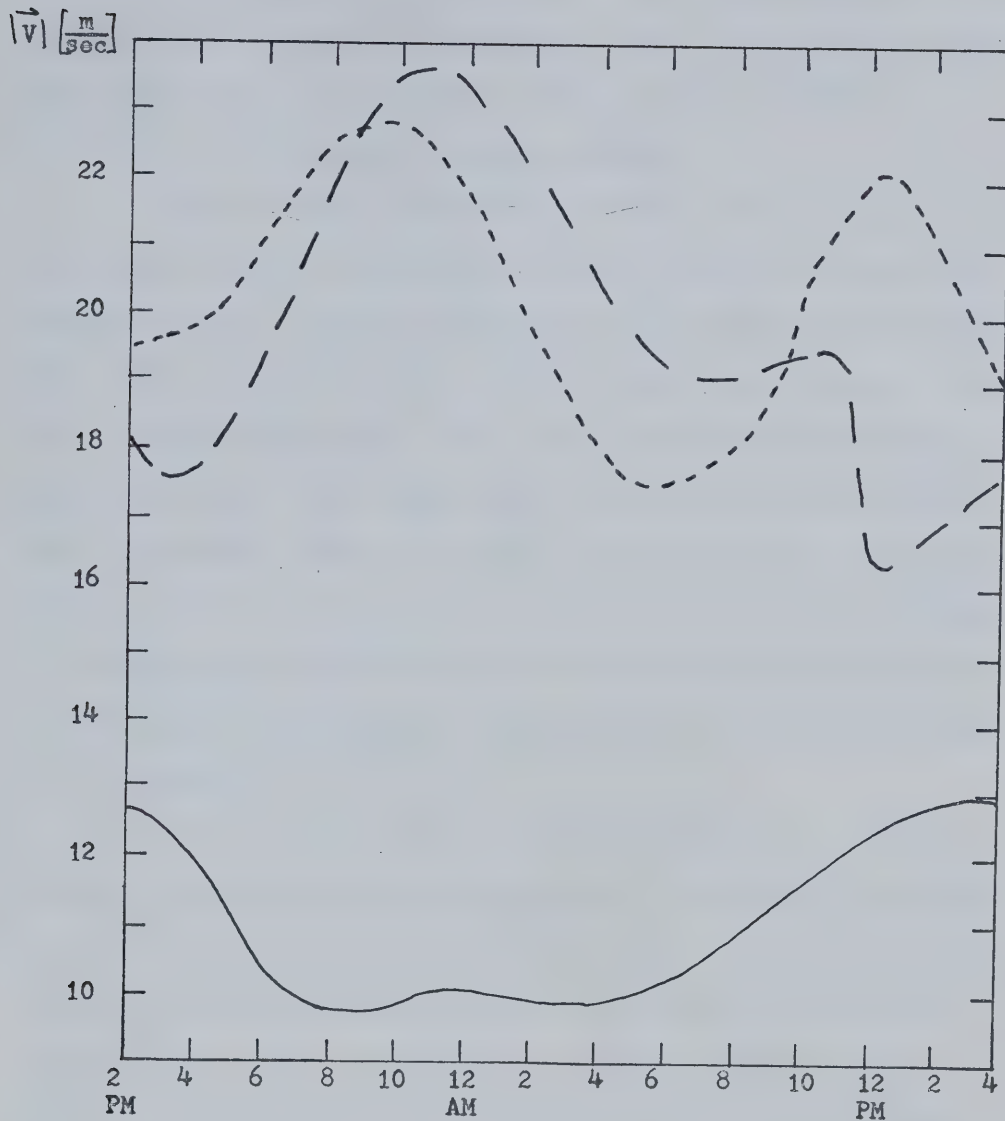


Figure 20. Diurnal cycle of the total mean wind for the case  $z_0 = 1$  cm,  $V_g = 20$  m/sec and high soil conductivity. The various curves represent the following heights:

- $\gamma = 6, z = 21$  m
- $\gamma = 10, z = 240$  m
- - -  $\gamma = 12, z = 404$  m.



of maximum temperature. With strong winds the maximum amplitude of the double-maximum-wind cycle is reached near 404 m. The overnight maximum near 12 AM is due to the inertial oscillation and the maximum near 12 PM is due to the influence of surface heating.

Figs. 21 and 22 represent the diurnal cycle of  $V$ . In the surface layer,  $V$  increases generally overnight causing an increase in the roughness angle.  $V$  reaches a secondary maximum near 8 PM in the vicinity of 40 m for moderate winds and of 80 m for strong winds.  $V$  shows also a daytime maximum near 11 AM. The region of overnight maximum gradient for  $V$  is slightly higher than the region of maximum gradient for  $U$ . Above that region,  $V$  undergoes a double cycle with maxima near 4 PM and 10 AM and negative minima near 2 AM and 2 PM. The influence of the higher wind speed is to spread out the velocity gradient over a larger region and to shift the position of the maximum winds higher in the atmosphere.

Figs. 23 and 24 represent the diurnal cycle of  $\epsilon$ . We have a rough estimate of the constant-stress layer by looking at the layer in which  $\epsilon$  does not vary by more than 20%. For the moderate-wind case, the height of the constant-stress layer is near 120 m under neutral conditions and could be as high as 400 m during unstable situations. It seems more difficult to define a constant-stress layer overnight because the stress reaches its maximum value above the ground, near 7 m. In any case, it seems that the lowest overnight constant-stress layer was around 20 m, and happened just after sunrise. The strong wind case is similar with the turbulent energy in the surface layer being twice as large during daytime and  $2\frac{1}{2}$  times during nighttime. The height of the constant-stress layer varies from its value of 240 m



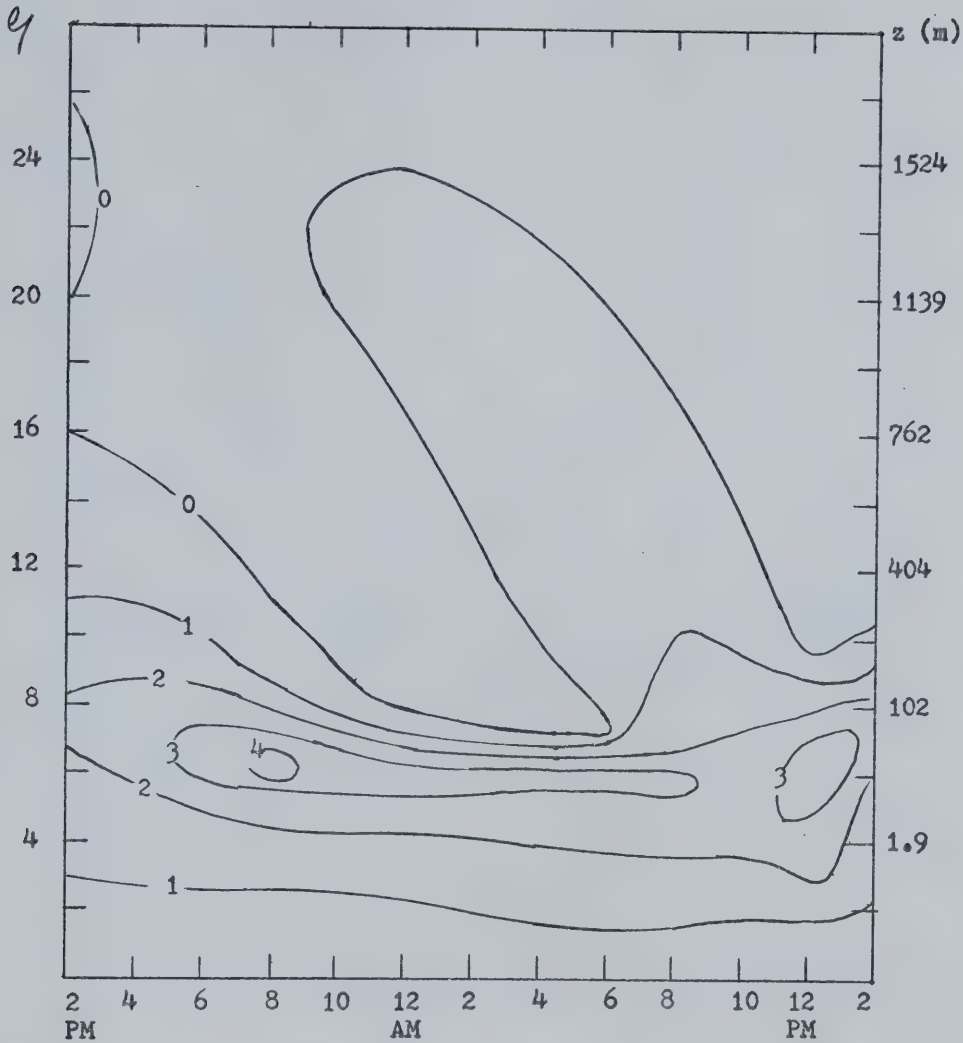


Figure 21. Diurnal cycle of the vertical profile of  $V$  for the case  $z_0 = 1$  cm,  $V_g = 10$  m/sec and high conductivity. The units are [m/sec].



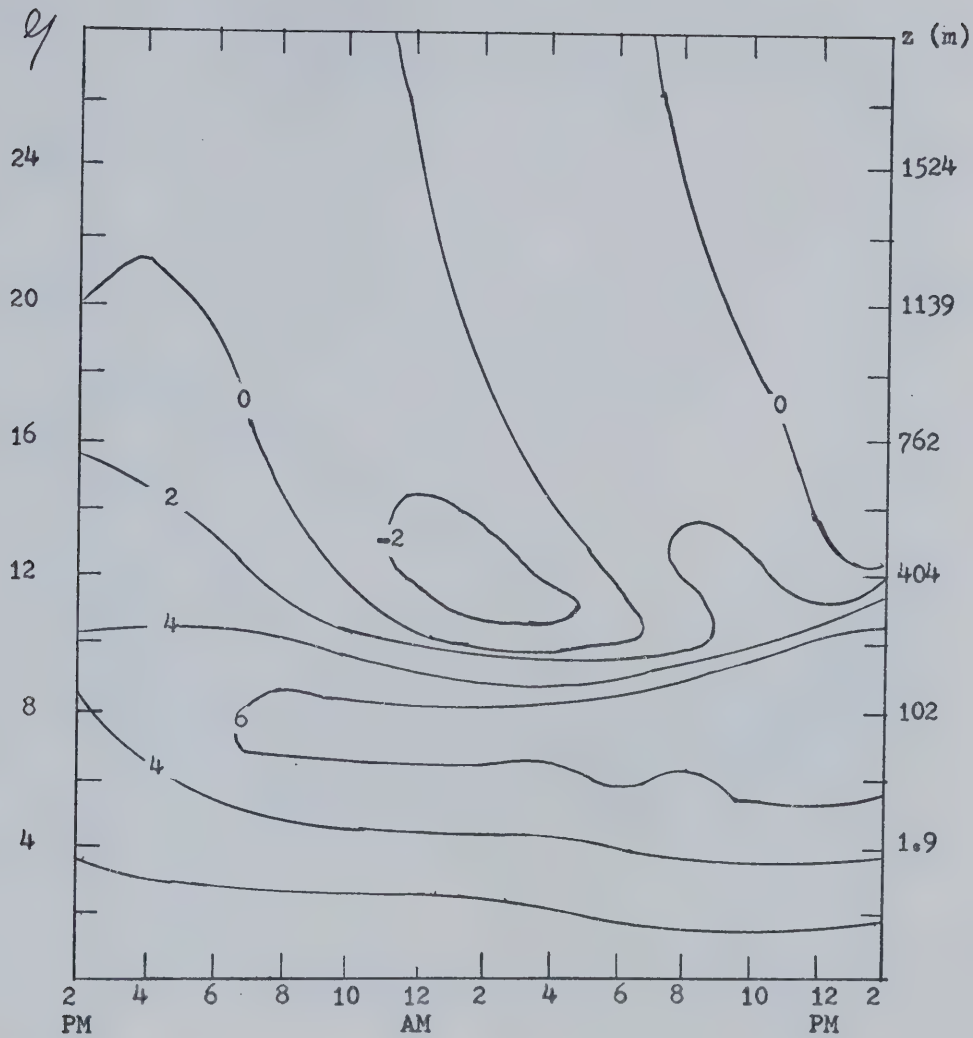


Figure 22. Diurnal variation of the vertical distribution of  $V$  for the case  $z_0 = 1$  cm,  $V_g = 20$  m/sec and high soil conductivity. The units are [m/sec].



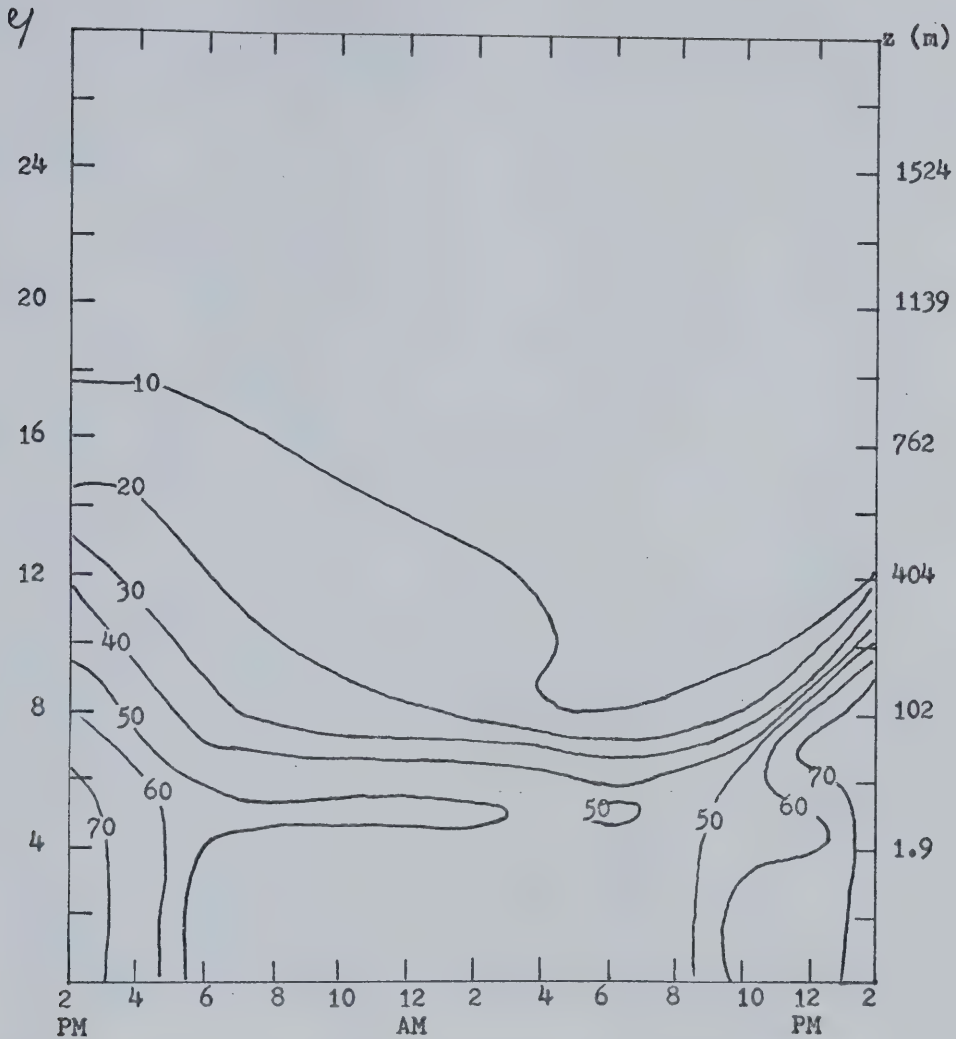


Figure 23. Diurnal variation of the vertical profile of  $e$  for the case  $z_0 = 1$  cm,  $V_g = 10$  m/sec and high soil conductivity. The units are [ $\text{cm}^2/\text{sec}^2$ ].



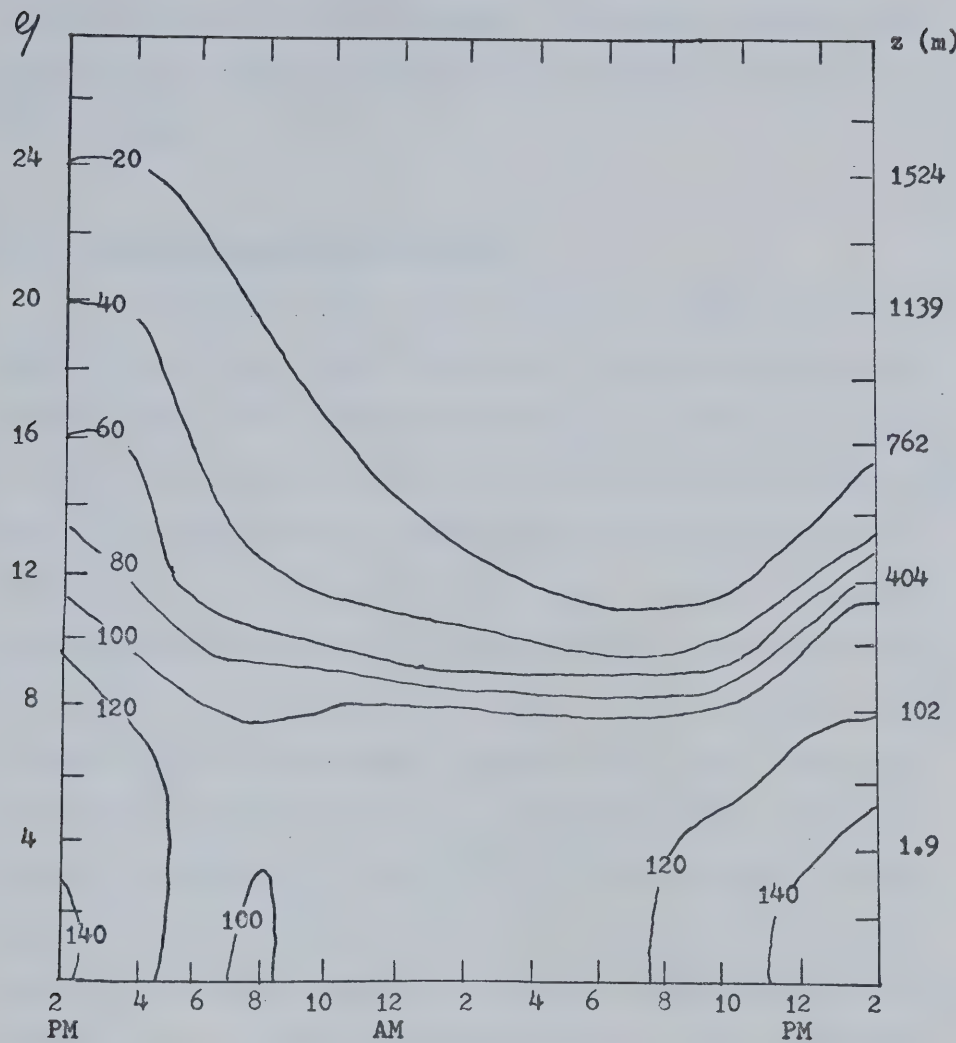


Figure 24. Diurnal cycle of the vertical distribution of  $\epsilon$  for the case  $z_0 = 1$  cm,  $V_g = 20$  m/sec and high soil conductivity. The units are  $[cm^2/sec^2]$ .



under neutral conditions to above 320 m under unstable lapse rate and goes down to 120 m overnight. The maximum daytime value of the constant-stress layer depth depends strongly on the depth of the unstable layer.

#### 6.2.2 Effect of the Roughness Height.

We go back to Fig. 9 and note that the temperatures over rough terrain always remain lower than the temperatures over smooth terrain. The initial temperature difference is 1.4 °C, it increases to 1.8 °C by sunrise and to 2.7 °C by the time of maximum temperature. The greater cooling over the rough terrain during the nighttime is contrary to theoretical expectations because we expect that with the enhanced turbulence over the rough terrain, a deeper layer will cool down, thus increasing relatively the surface temperature. Fig. 10 shows that the cooling rates over smooth and rough terrain are almost identical until 6 AM. A more detailed analysis of the data reveals that between 2 PM and 8 PM, the air over the rough terrain cools down more slowly in agreement with the theory. However, this situation is reversed between 8 PM and 4 AM. When we compare Fig. 25 with Fig. 13, we observe that the temperature gradient in both cases accumulates between 20 and 100 m. For  $z_0 = 1$  cm, the temperature difference near sunrise between 20 m and 50 m is 10.6 °C, and between 50 m and 100 m is 7 °C. Similarly, for  $z_0 = 100$  cm, the difference is 6.5 °C between 20 m and 50 m, and 9.7 °C between 50 m and 100 m. Therefore, a deeper layer is cooling over the rough terrain as indicated by the spreading out of the temperature gradient. Now, we compare the heat fluxes in the atmosphere as represented in Figs. 15 and 26. In the



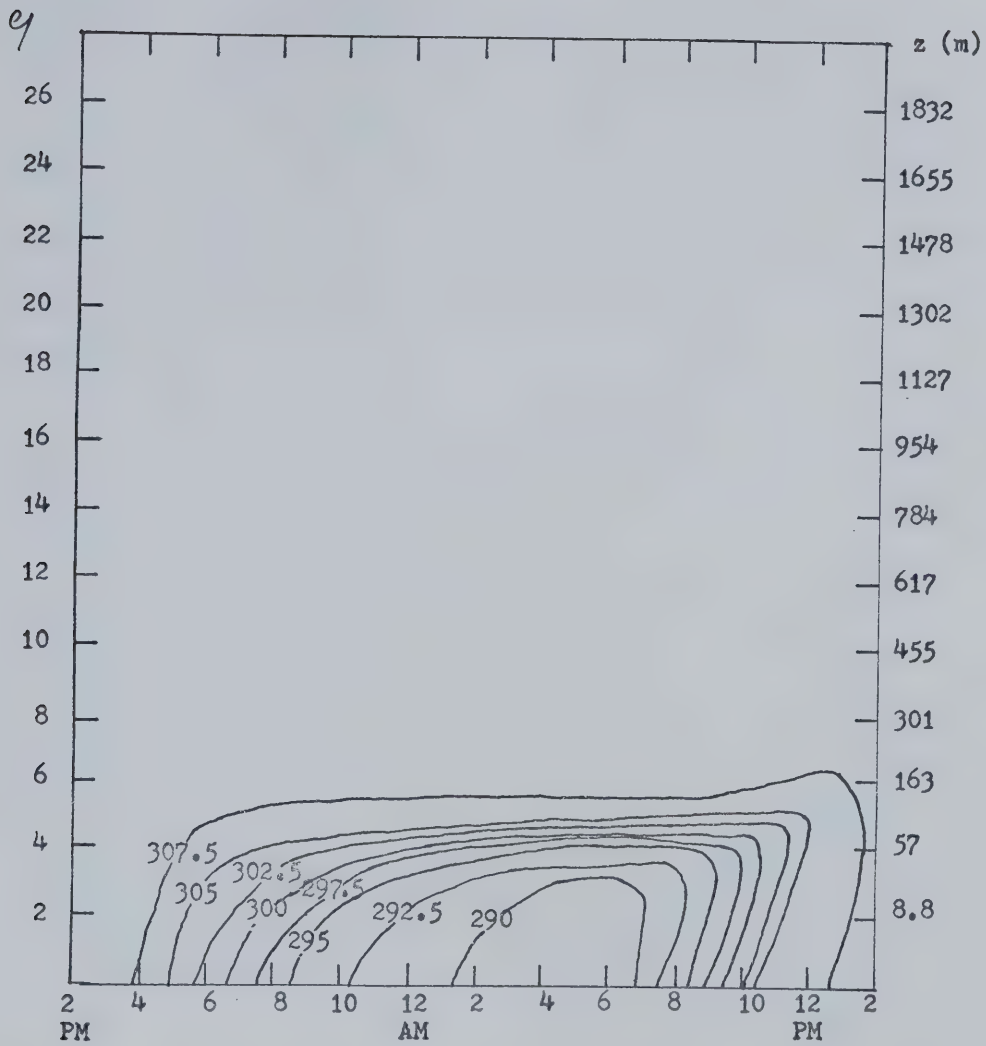


Figure 25. Diurnal cycle of the atmospheric potential temperature for the case  $z_0 = 100$  cm,  $V_g = 10$  m/sec and high soil conductivity. The units are [ $^{\circ}$ K].



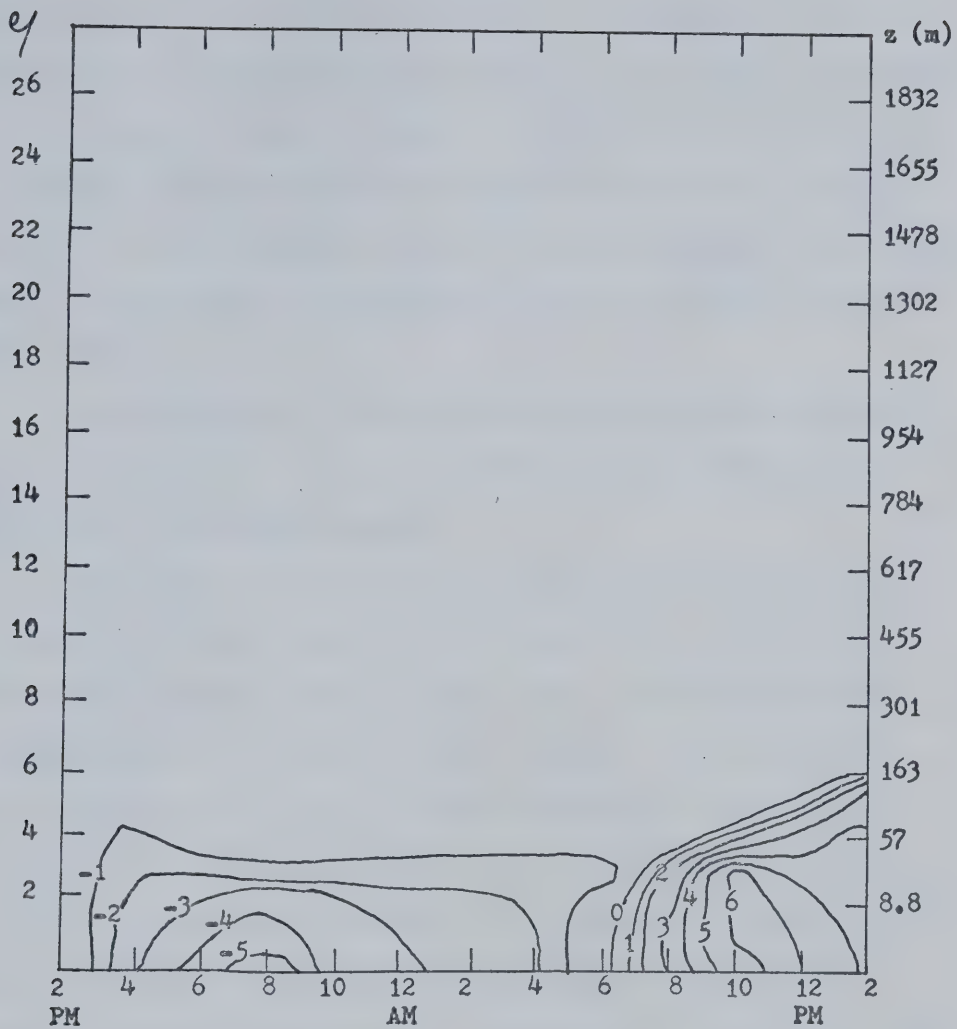


Figure 26. Diurnal cycle of the vertical profile of  $\bar{w}\theta$  for the case  $z_0 = 100$  cm,  $V_g = 10$  m/sec and high soil conductivity. The units are [cm- $^{\circ}$ C/sec].



lower boundary layer, the heat flux is about twice as large over rough terrain between 4 PM and 8 PM. After 8 PM, the difference between the two heat fluxes diminishes to become negligible by sunrise. The influence of the larger roughness height is reflected in the fact that the heat flux has a larger value over a deeper layer over rough terrain than over the smooth terrain. There is also more diffusion over rougher terrain as demonstrated by the higher values of  $K_t$  in Fig. 27 as compared to Fig. 16.

Comparing Figs. 28 and 23, we note that the turbulent energy in the surface layer is increased by 50% over rough terrain during daytime, and only by 25% overnight.

Figs. 29 and 18 show that the diurnal cycle of  $U$  is similar over smooth and rough terrains. The overnight wind gradient which was concentrated between 20 m and 50 m over smooth terrain is now spread between 20 m and 100 m over the rougher terrain. The double-wind-maxima feature above 100 m is also very evident over rough terrain. The diurnal cycle of  $V$  over rough terrain is very similar to the one over smooth terrain as demonstrated by the comparison of Fig. 30 with Fig. 21. The rough terrain induces more turbulence which causes a spreading of the wind gradient and a shifting of the maximum wind speed higher. The only other major difference is in the roughness angle which is illustrated in Fig. 11. The roughness angle is generally 10 to 15 degrees greater over the rougher terrain. The oscillation in  $\alpha$  after sunrise has a larger amplitude over the rough terrain and reaches  $40^\circ$ .

Therefore, the rougher terrain creates more turbulence at all times even if the difference in turbulent energy and heat flux



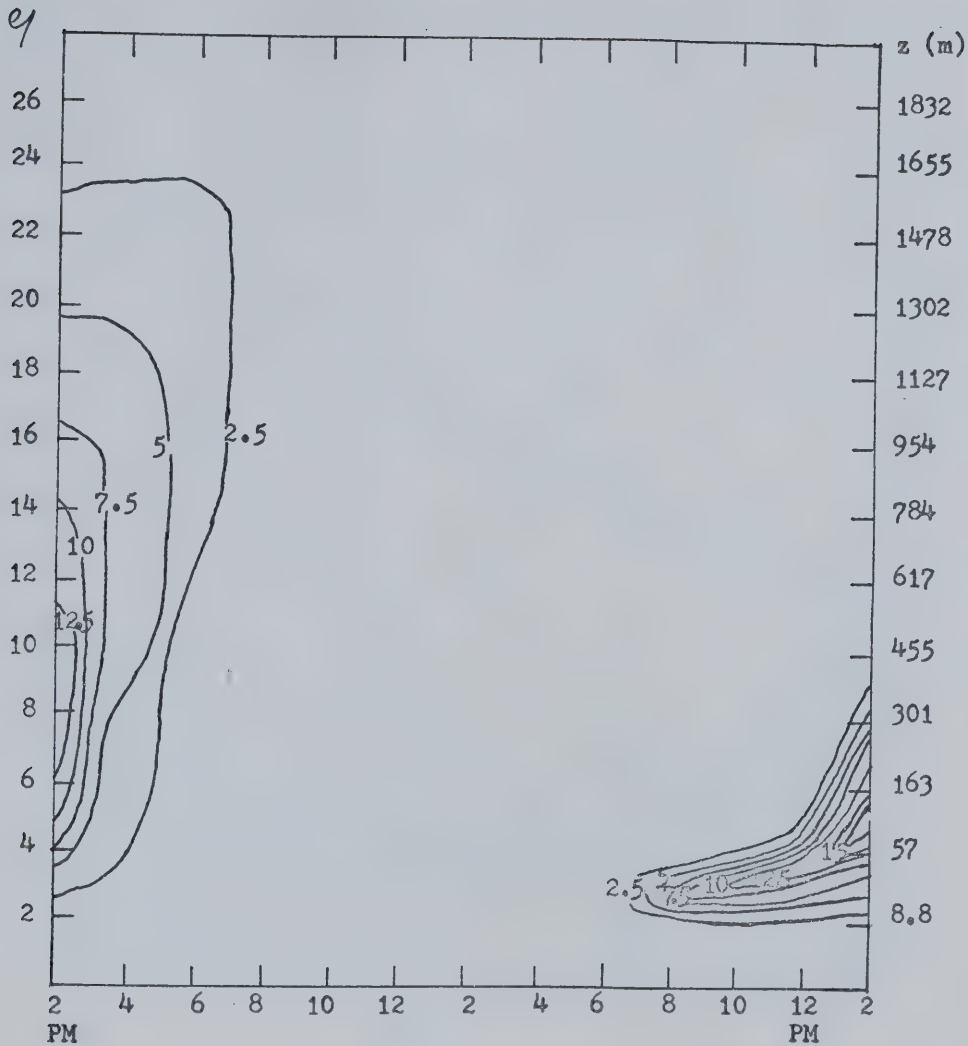


Figure 27. Diurnal cycle of the vertical profile of  $K_t$  for the case  $z_0 = 100$  cm,  $V_g = 10$  m/sec and high soil conductivity. The units are  $[10^4 \text{ cm}^2/\text{sec}]$ .



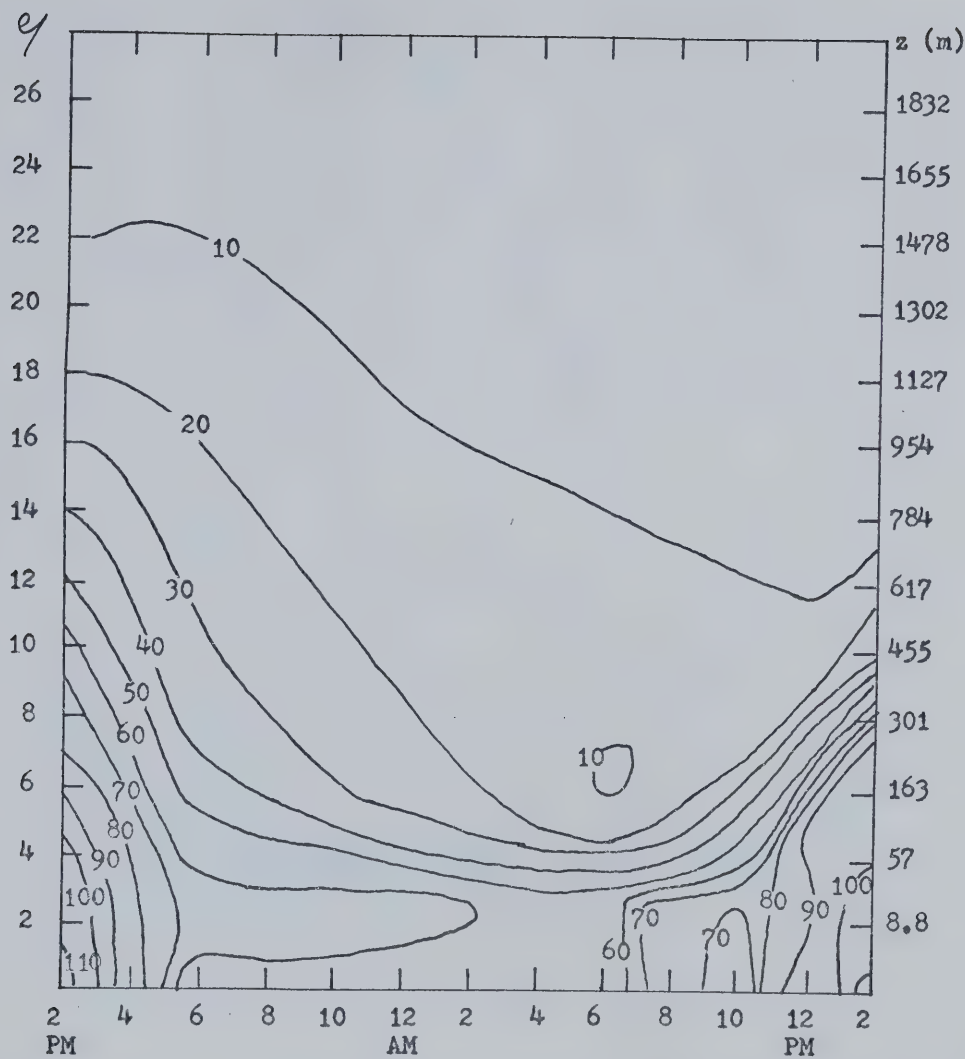


Figure 28. Diurnal cycle of the vertical profile of  $e$  for the case  $z_0 = 100$  cm,  $V_g = 10$  m/sec and high soil conductivity. The units are  $[\text{cm}^2/\text{sec}^2]$ .



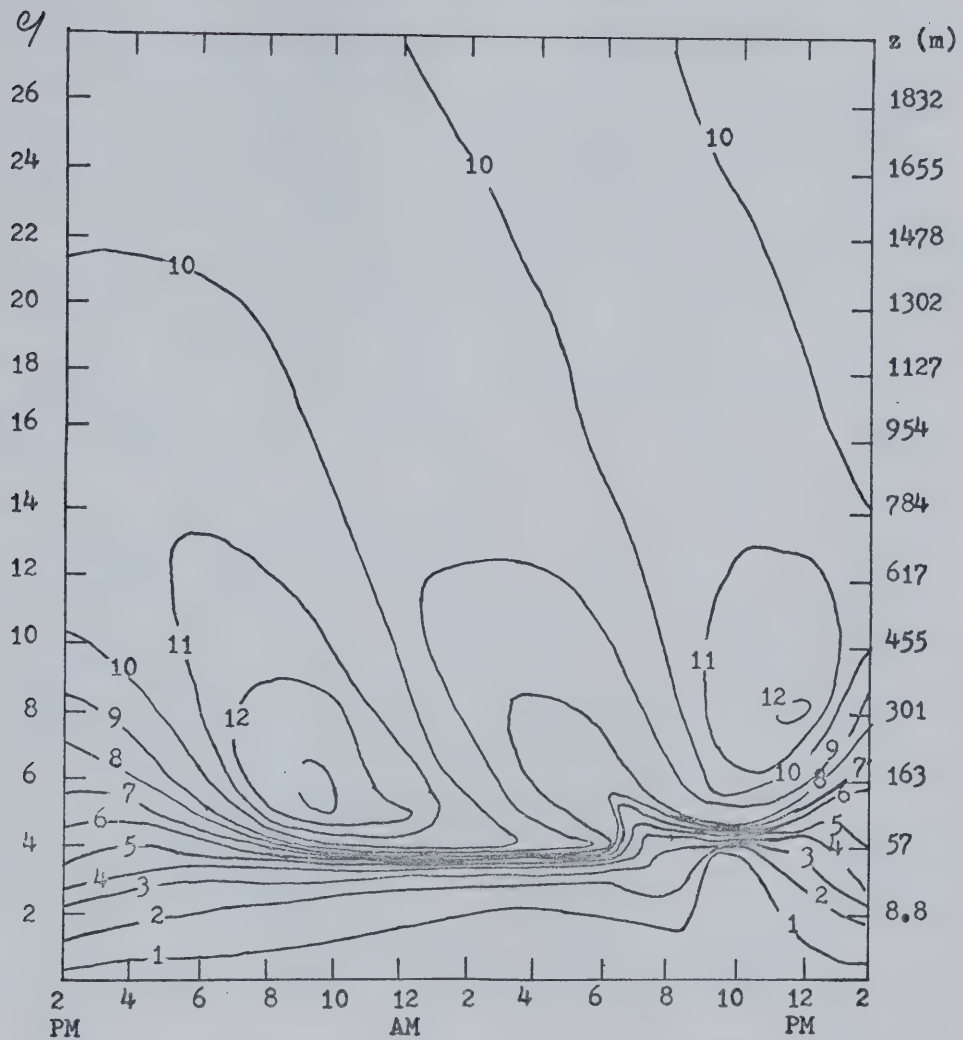


Figure 29. Diurnal variation of the vertical profile of  $U$  for the case  $z_0 = 100$  cm,  $V_g = 10$  m/sec and high soil conductivity. The units are [m/sec].



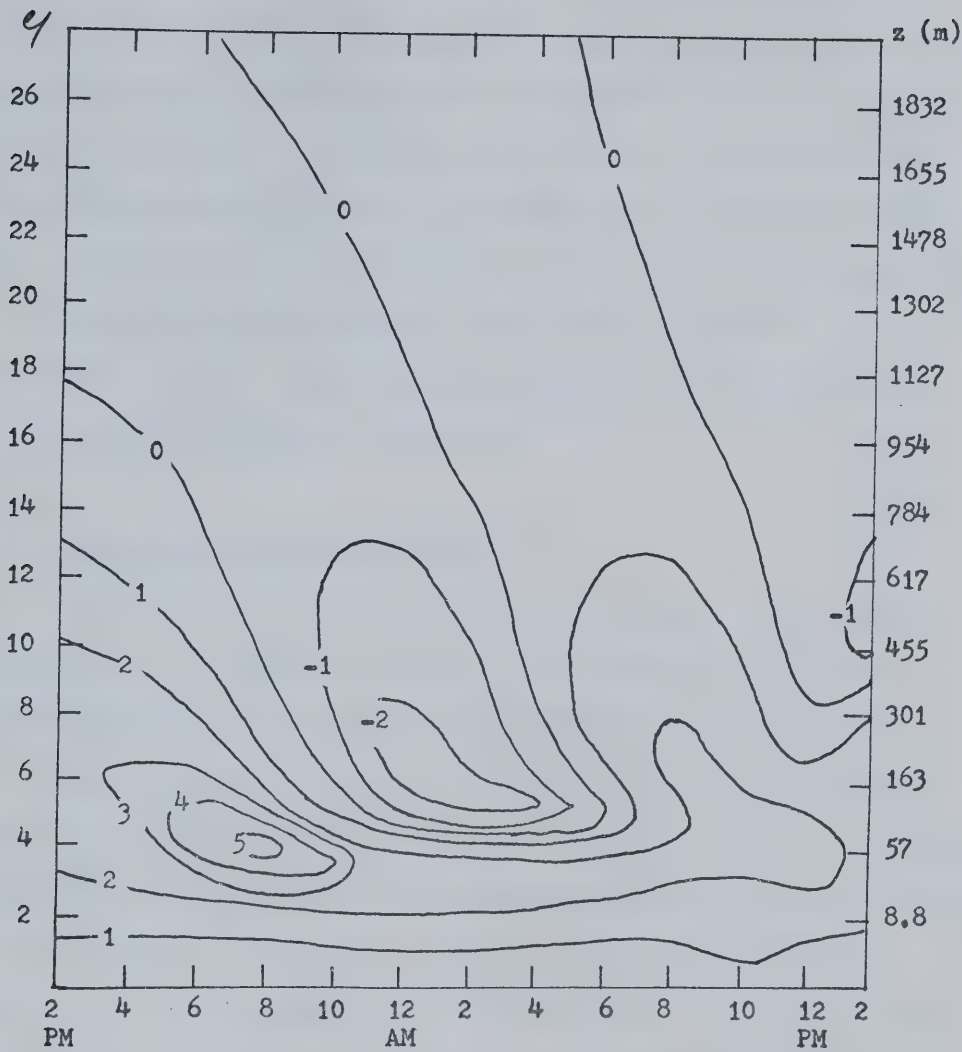


Figure 30. Diurnal variation of the vertical profile of  $V$  for the case  $z_0 = 100 \text{ cm}$ ,  $V_g = 10 \text{ m/sec}$  and high soil conductivity. The units are [m/sec].



is reduced overnight due to the stability. The greater cooling over the rougher terrain between 8 AM and 4 PM remains unexplained. A plausible explanation would be that the two simulations have not converged sufficiently to their true values at each time step, creating an artificial difference between the two simulations which has persisted overnight. Therefore, it seems necessary to require more accuracy than  $10 \text{ cm}^2/\text{sec}$  overnight because the maximum value of  $K_t$  is reduced by an order of magnitude overnight which reduces considerably the relative accuracy with which we solve the equations.

#### 6.2.3 Effect of the Soil Conductivity.

Fig. 9 shows that the effect of decreasing the soil thermal conductivity is to amplify the diurnal temperature wave at the surface of the earth. The maximum surface temperature is increased by  $18.5^\circ\text{C}$  and the minimum by  $2.8^\circ\text{C}$ . As indicated in Fig. 10, the warming rate is twice as large over the poorly-conductive soil. The graphs of  $\bar{H}$  and  $\bar{w\theta}$  over the poorly-conductive soil are Figs. 31 and 32. These are very similar to Figs. 13 and 15 which represent the same variables over a good conductive soil. The only major difference is in the intensity of the cooling which is more pronounced over a soil with low thermal conductivity. Fig. 33 reveals the influence of the amplification of the diurnal temperature wave on the atmospheric diffusivity. Over a poorly conductive soil,  $K_t$  is larger under unstable conditions and smaller under stable conditions.

The behavior of  $e$  over a soil with low conductivity is represented in Fig. 34 and is basically the same as over a soil with high conductivity as represented in Fig. 23. Due to strong cooling, the



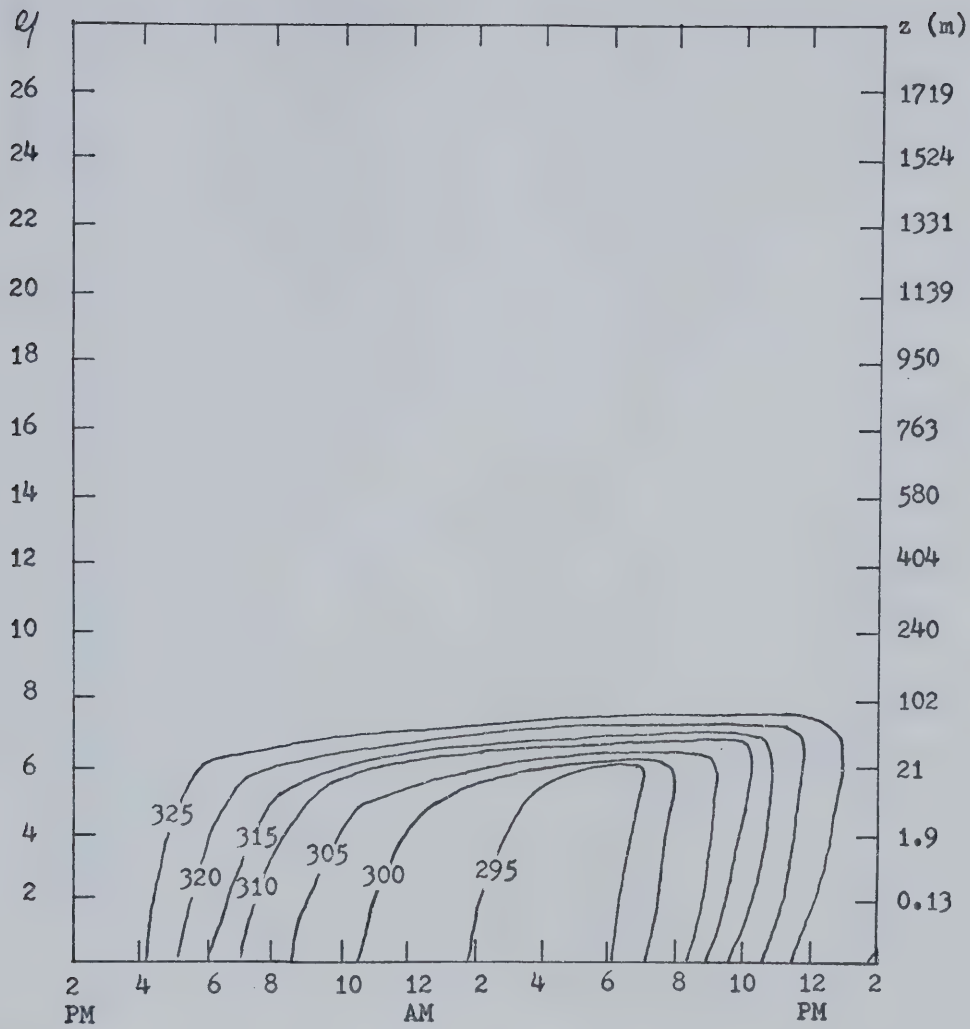


Figure 31. Diurnal cycle of the vertical profile of the potential temperature for the case  $z_0 = 1$  cm,  $V_g = 10$  m/sec and low conductivity in the soil. The units are [ $^{\circ}$ K].



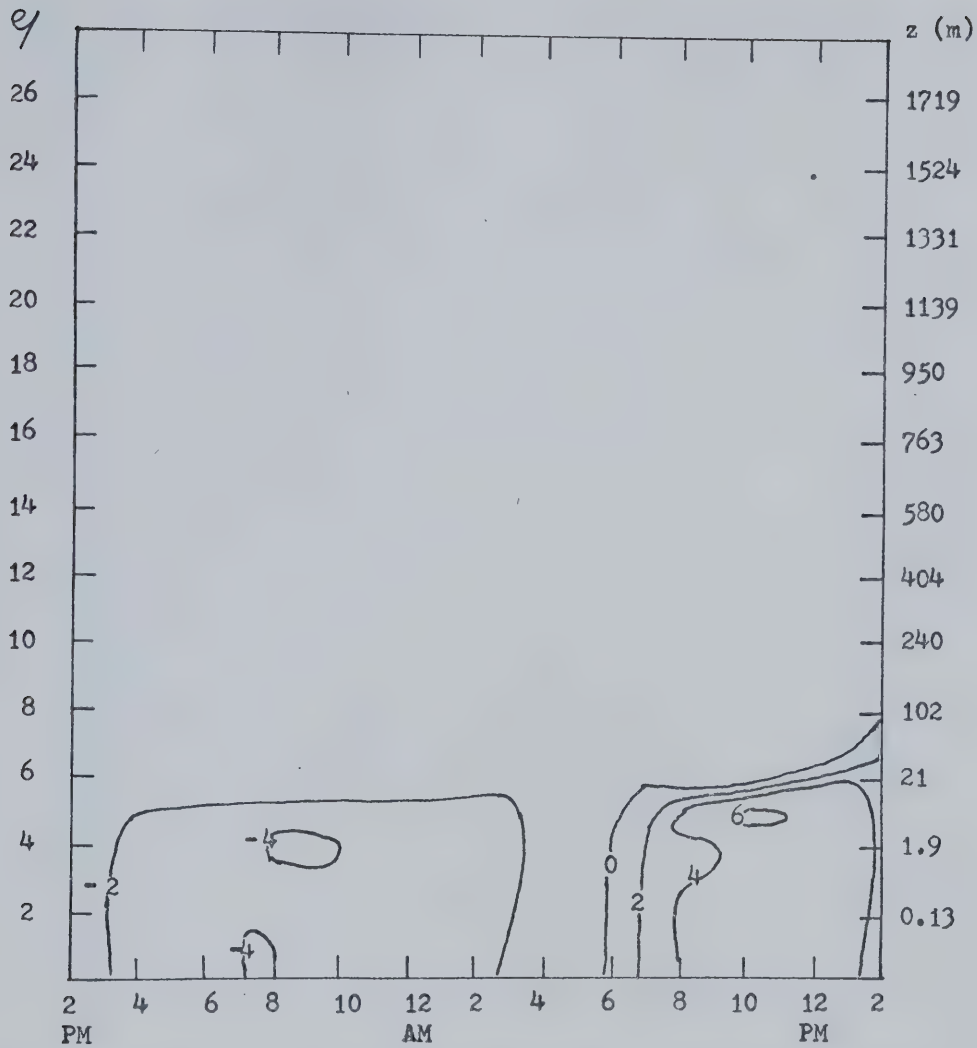


Figure 32. Diurnal cycle of the vertical profile of  $\bar{w}\theta$  for the case  $z_0 = 1 \text{ cm}$ ,  $V_g = 10 \text{ m/sec}$  and low thermal soil conductivity. The units are  $[\text{cm}^{-1}\text{C/sec}]$ .



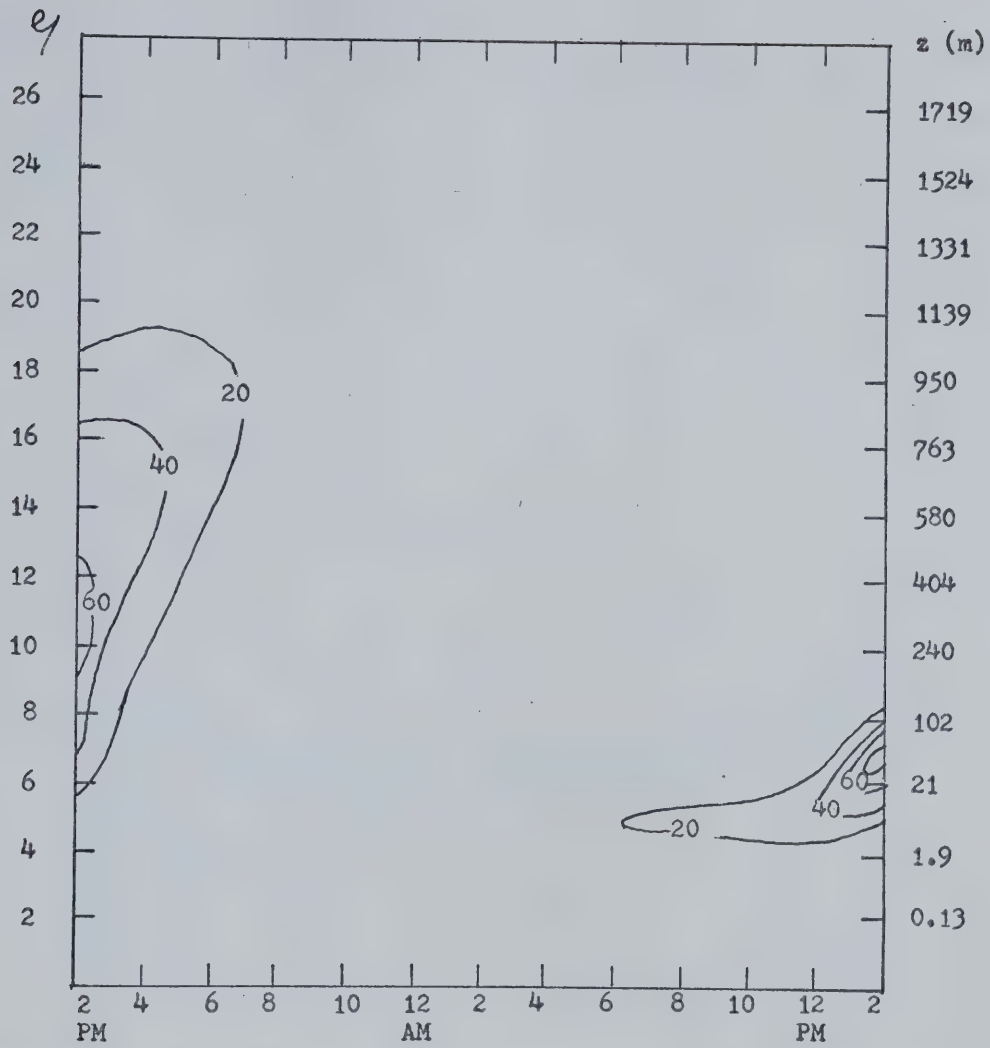


Figure 33. Diurnal cycle of the vertical profile of  $K_t$  for the case  $z_0 = 1 \text{ cm}$ ,  $V_g = 20 \text{ m/sec}$  and high soil conductivity. The units are  $[\text{cm}^2/\text{sec}]$ .



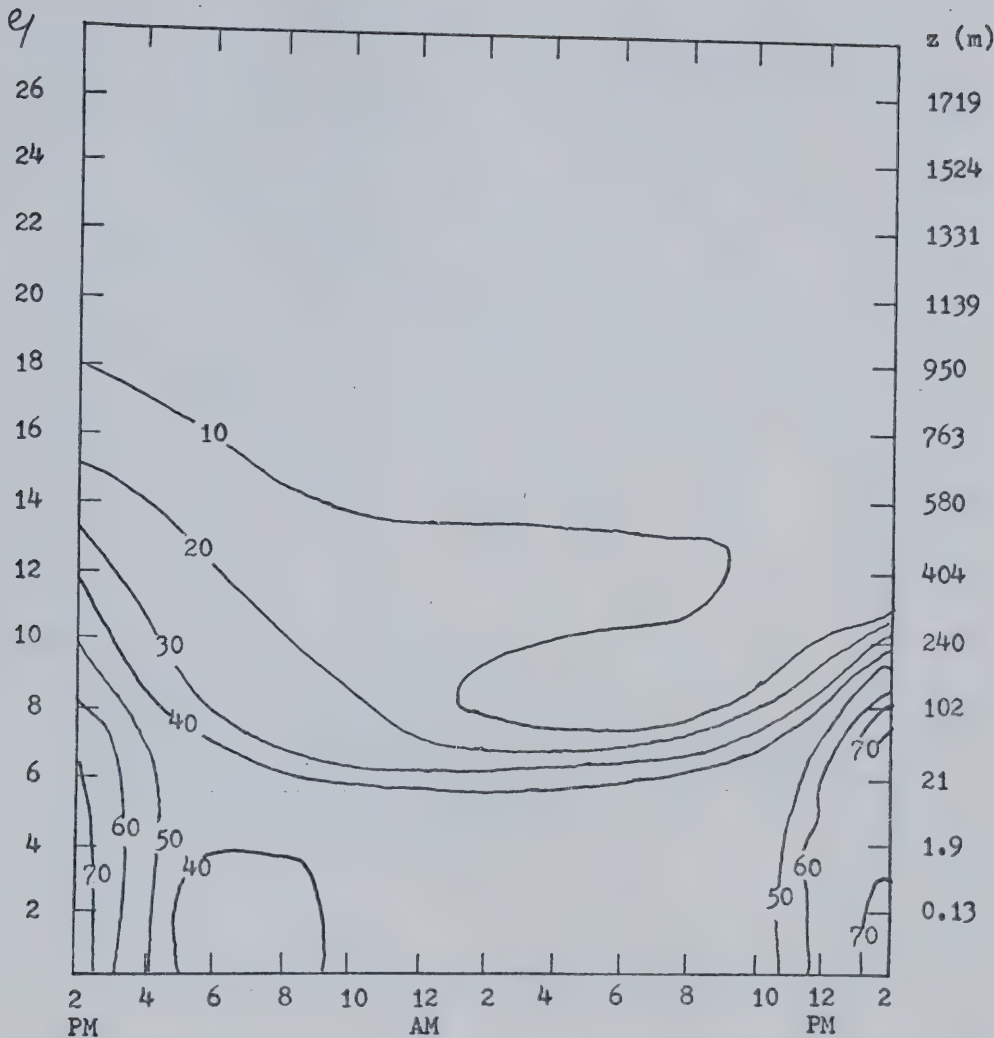


Figure 34. Diurnal cycle of the vertical profile of  $e$  for the case  $z_0 = 1 \text{ cm}$ ,  $V_g = 10 \text{ m/sec}$  and low thermal soil conductivity. The units are  $[\text{cm}^2/\text{sec}^2]$ .



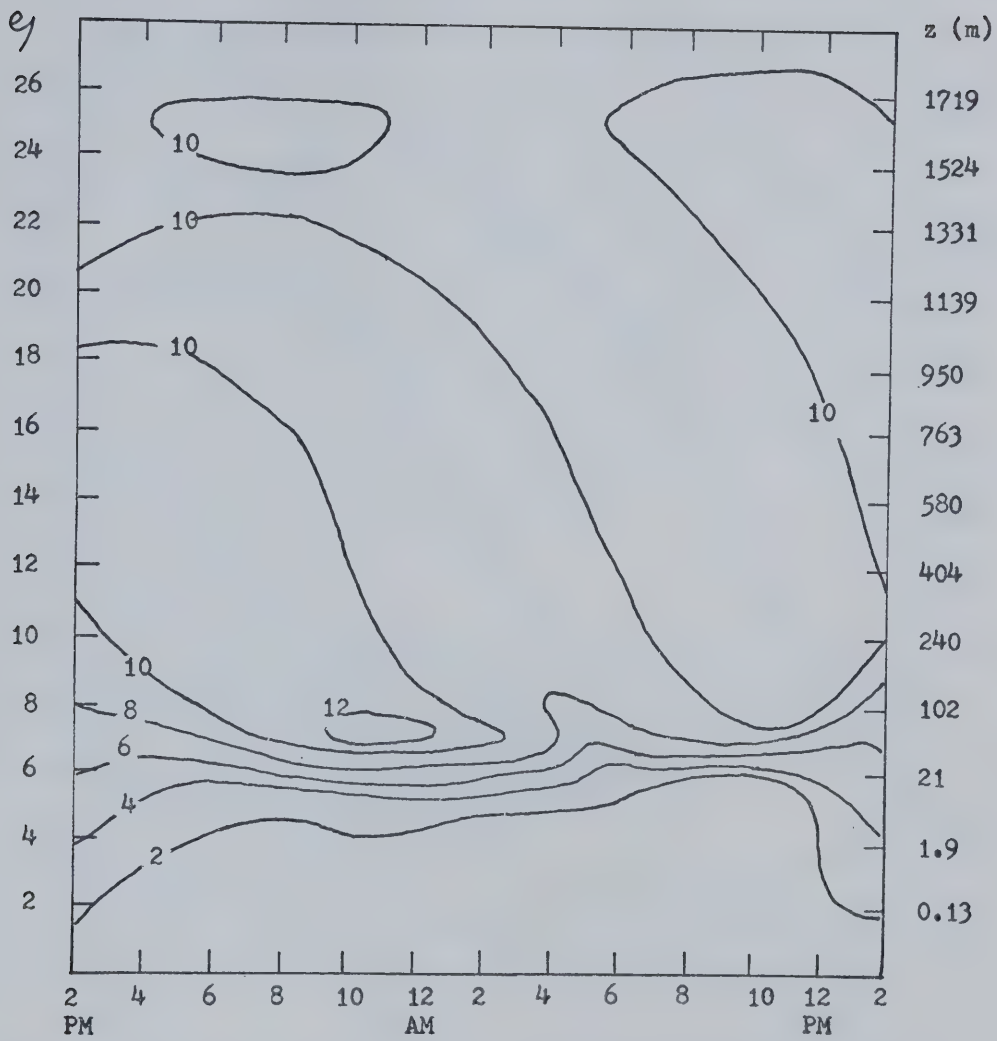


Figure 35. Diurnal cycle of the vertical profile of  $U$  for the case  $z_0 = 1 \text{ cm}$ ,  $V_g = 10 \text{ m/sec}$  and low soil conductivity. The units are [ $\text{m/sec}$ ].



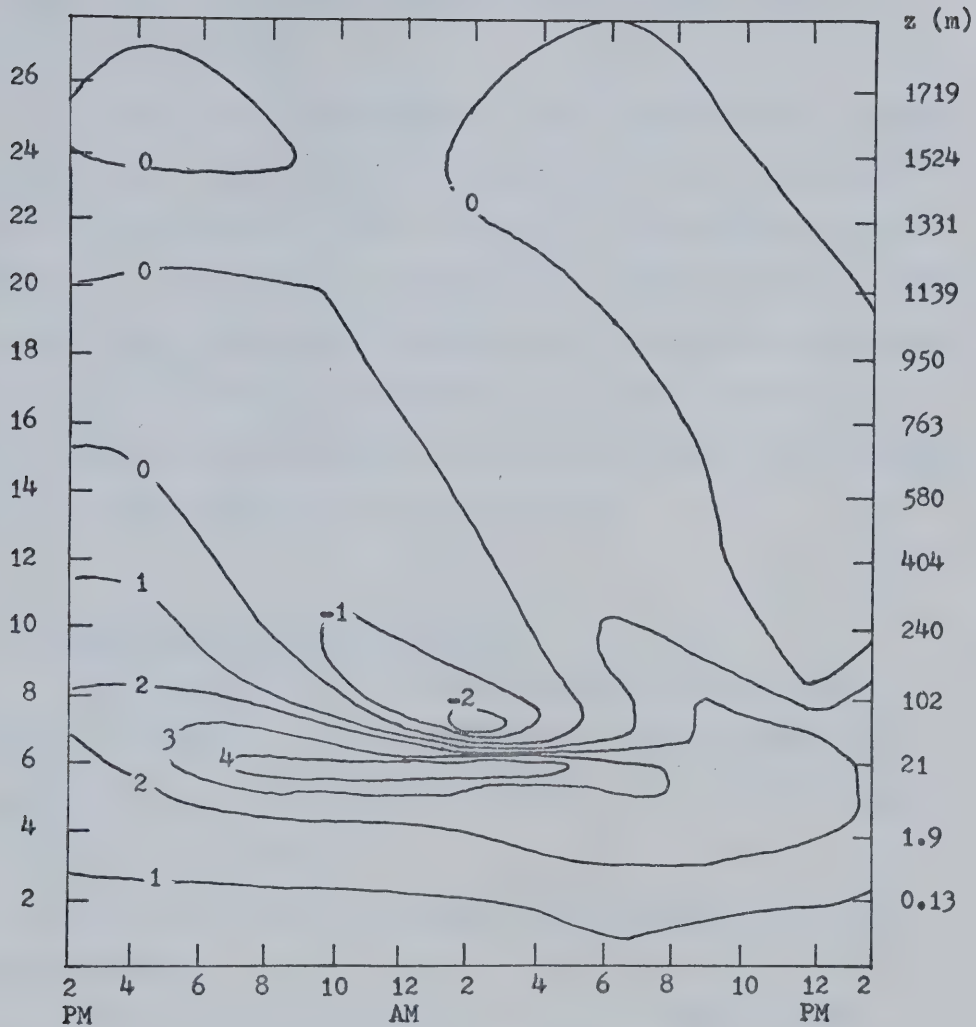


Figure 36. Diurnal variation of the vertical profile of  $V$  for the case  $z_0 = 1$  cm,  $V_g = 10$  m/sec and low soil conductivity. The units are [m/sec].



minimum near 6 PM is 15% lower over a poorly-conductive soil. However,  $\epsilon$  recovers after 12 AM and has almost the same profile as over soil with a high conductivity.

Figs. 35 and 36 represent the U and V profiles over a poorly-conductive soil. These are similar to the profiles over a good-conductive soil as represented in Figs. 18 and 21. The overnight minimum in U within the surface layer is reduced by about 20% over a poorly-conductive soil. Above the region of maximum wind gradient, the double-wind-maxima cycle is still observed but with an amplified amplitude. As shown in Fig. 11, the variations in  $\alpha$  are amplified over a poorly-conductive soil, with higher maxima and lower minima.

#### 6.2.4 Examination of the Other Variables.

We will examine very briefly the behavior of the other atmospheric variables. Only one specific case will be studied:  $z_0 = 1$  cm,  $V_g = 20$  m/sec and high soil conductivity. This case was chosen for the following reasons:

- the profiles of most of the variables are smoother with strong geostrophic winds.
- The overnight gradients in  $\Theta$ , U, V and  $\epsilon$  are spread out over a few more grid points.
- $K_t$  becomes negative at fewer grid points.

The diurnal variation of  $\ell$  is fairly regular as shown in Fig. 37. The diurnal variation is negligible close to  $z_0$ , reaches 8% of the mean value at 21 m and exceeds 50% of the mean value near the top of the boundary layer. Due to its definition,  $\ell$  is always increas-



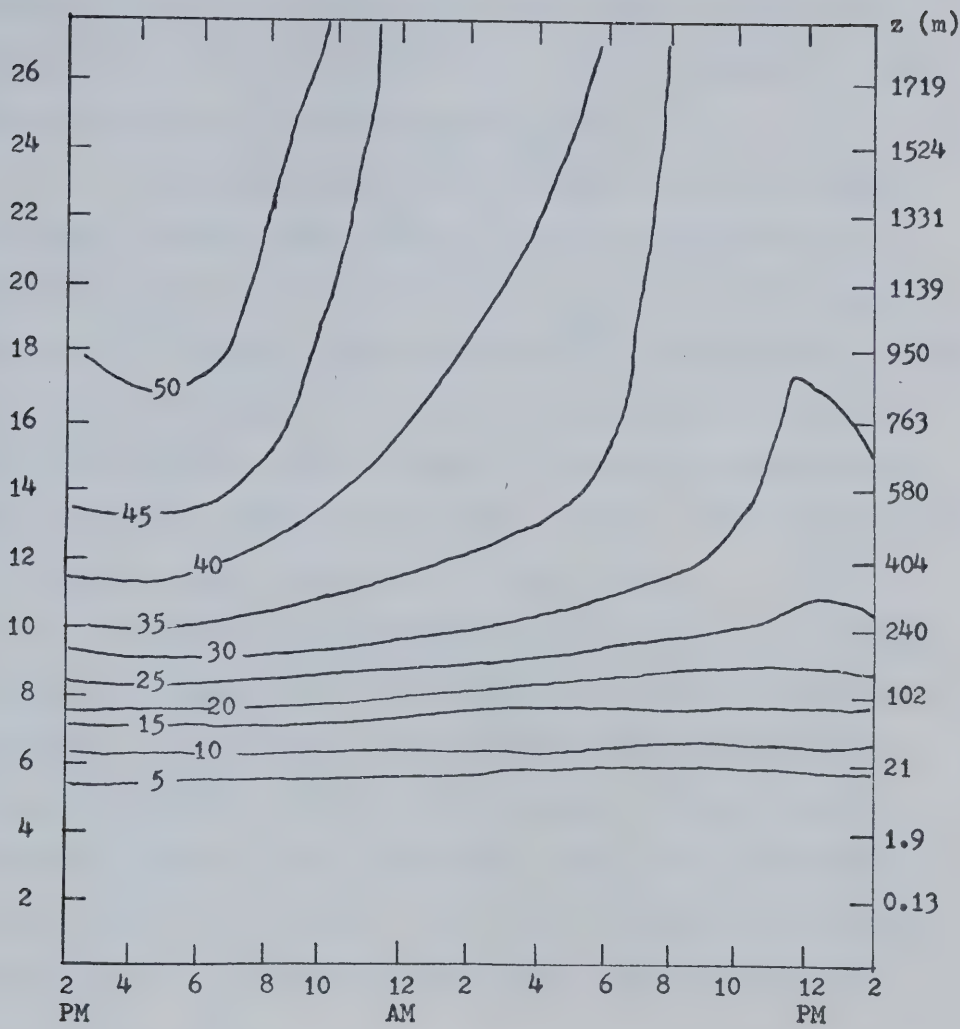


Figure 37. Diurnal variation of the vertical profile of  $\lambda$  for the case  $z_0 = 1$  cm,  $V_g = 20$  m/sec and high soil conductivity. The units are [m].



sing upwards. The delay of 6 to 8 hours between the time of change in stability in the lower boundary layer and the time of minimum for  $\lambda$  indicates clearly that the formula which computes  $\lambda$  depends to a large degree on the value of  $e$  in the uppermost levels.

As illustrated in Fig. 38,  $\overline{\theta^2}$  reaches an overnight maximum in the lower boundary layer just after the time of maximum cooling rate and decreases until the air becomes unstable near 6 AM. Between 8 AM and 12 PM there is a rapid increase in  $\overline{\theta^2}$  which corresponds to the increase in the warming rate. Under unstable conditions the maximum value of  $\overline{\theta^2}$  is always near the surface. However, the temperature gradient accumulates overnight between 20 m and 100 m. This is reflected in the large overnight maximum in  $\overline{\theta^2}$  in that region.

The diurnal cycles of  $\overline{u\theta}$  and  $\overline{v\theta}$  are shown in Figs. 39 and 40. Equations (2.195) and (2.196) indicate that these variables are proportional to the product of the appropriate wind gradient by the temperature gradient. Therefore, under stable conditions, these variables are positive if the wind increases with height and negative if the wind decreases with height. As the wind and temperature gradients accumulate overnight between 20 m and 100 m, the maximum value is reached in that region.

Figs. 41 and 42 illustrate the stress in the x and y directions. In the lower boundary layer,  $\overline{u w}$  has a large negative value during daytime and a smaller negative value during nighttime. This is another illustration of the effect of the decreasing turbulence overnight.  $\overline{v w}$  decreases between 2 PM and 6 PM but increases after 6 PM. Therefore, the overnight increase in roughness angle is accompanied by an increase in the stress in the y direction. These va-



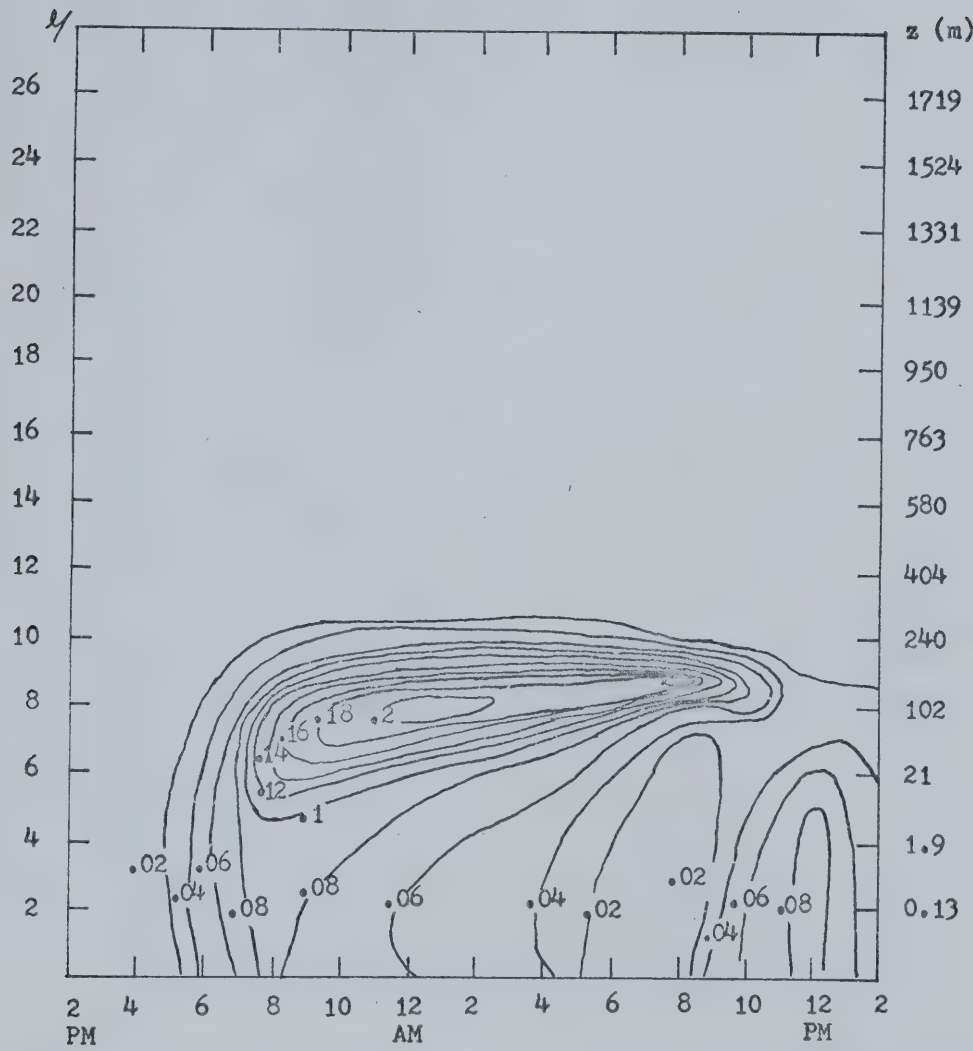


Figure 38. Diurnal variation of the vertical profile of  $\overline{\theta^2}$  for the case  $z_0 = 1$  cm,  $V_g = 20$  m/sec and high soil conductivity. The units are  $[^{\circ}\text{C}^2]$ .



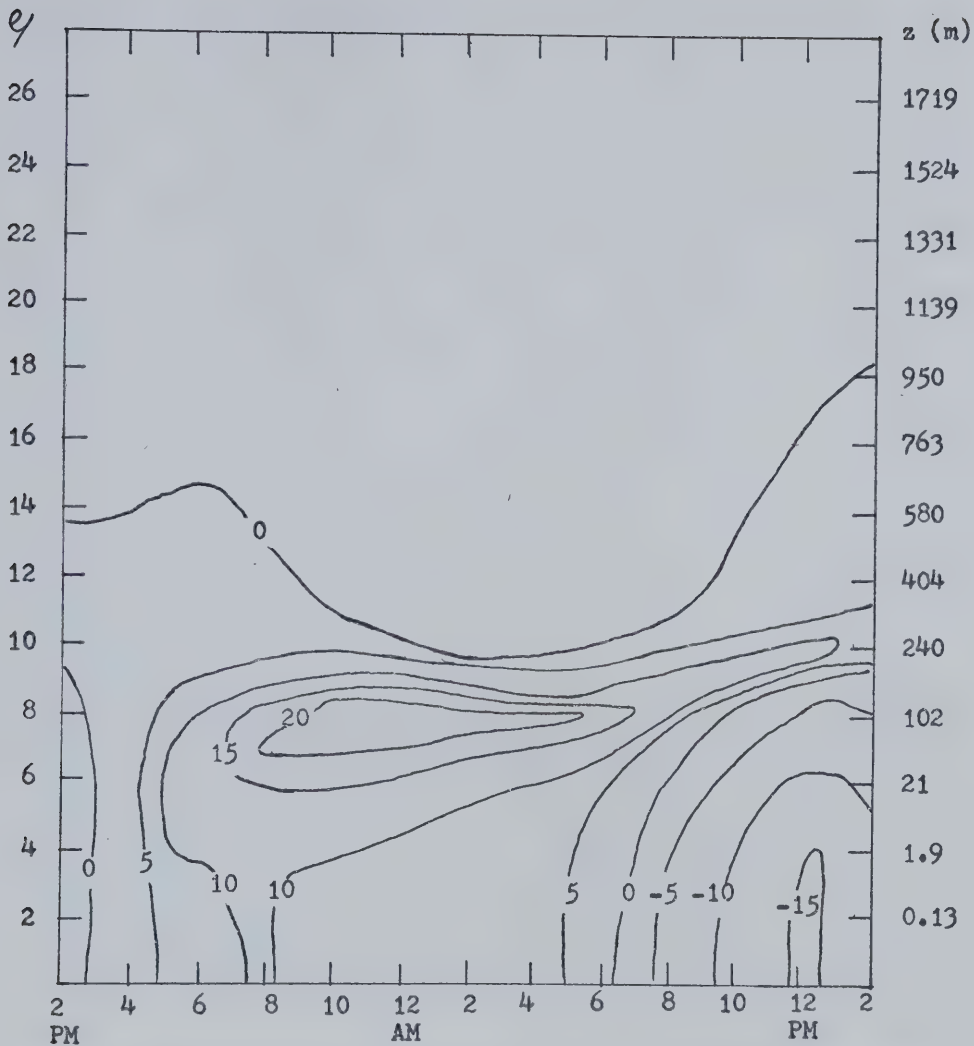


Figure 39. Diurnal cycle of the vertical profile of  $\bar{u}\theta$  for the case  $z_o = 1 \text{ cm}$ ,  $V_g = 20 \text{ m/sec}$  and high soil conductivity. The units are  $[\text{cm}^{-1}\text{C/sec}]$ .



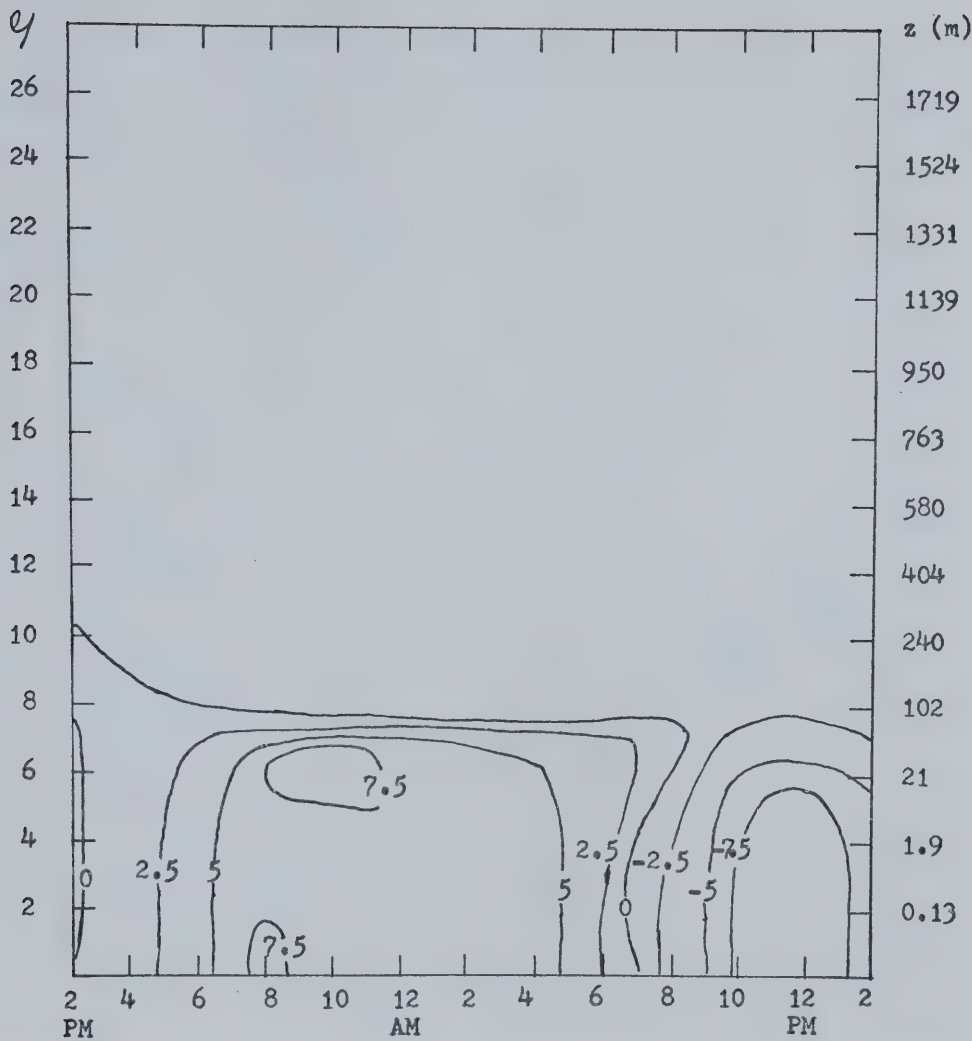


Figure 40. Diurnal cycle of the vertical profile of  $\bar{v}\theta$  for the case  $z_0 = 1$  cm,  $V_g = 20$  m/sec and high soil conductivity. The units are [cm- $^{\circ}$ C/sec].



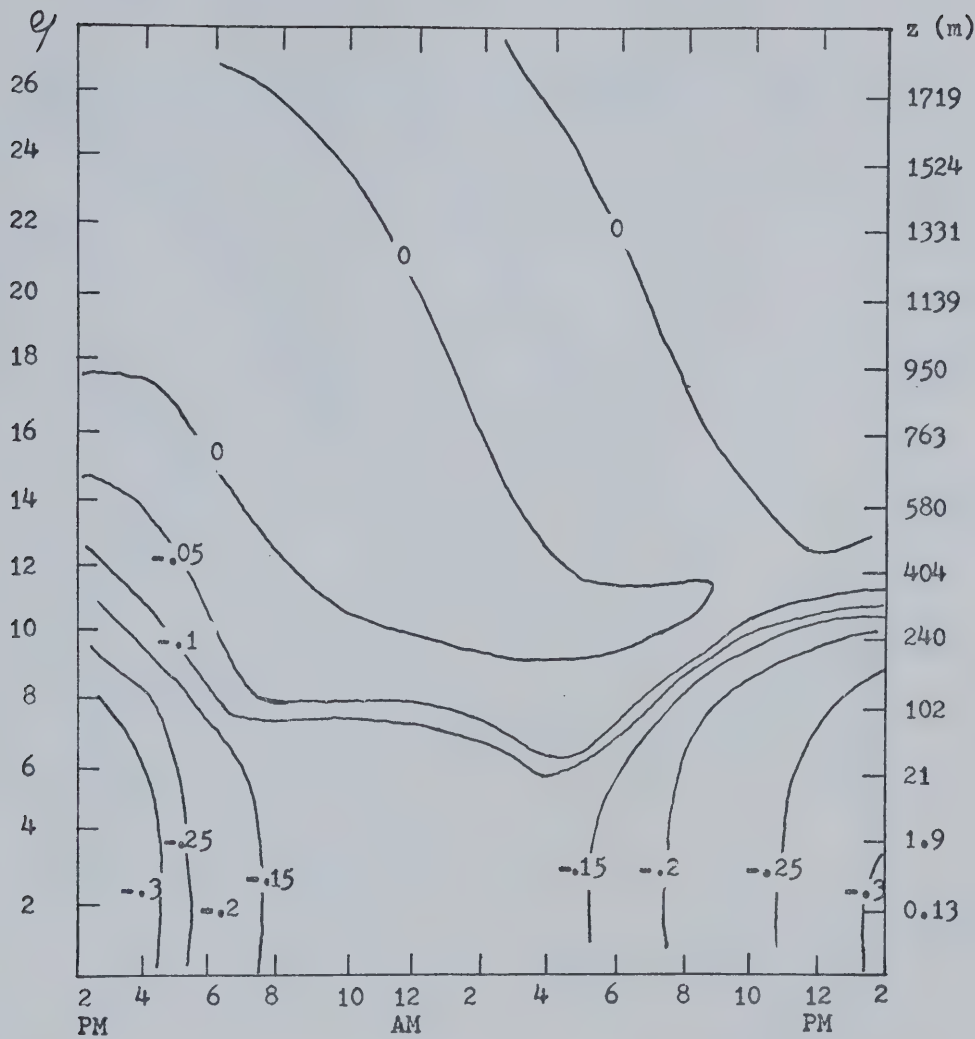


Figure 41. Diurnal variation of the vertical profile of  $\bar{u} w$  for the case  $z_0 = 1$  cm,  $V_g = 20$  m/sec and high soil conductivity. The units are  $[m^2/sec^2]$ .



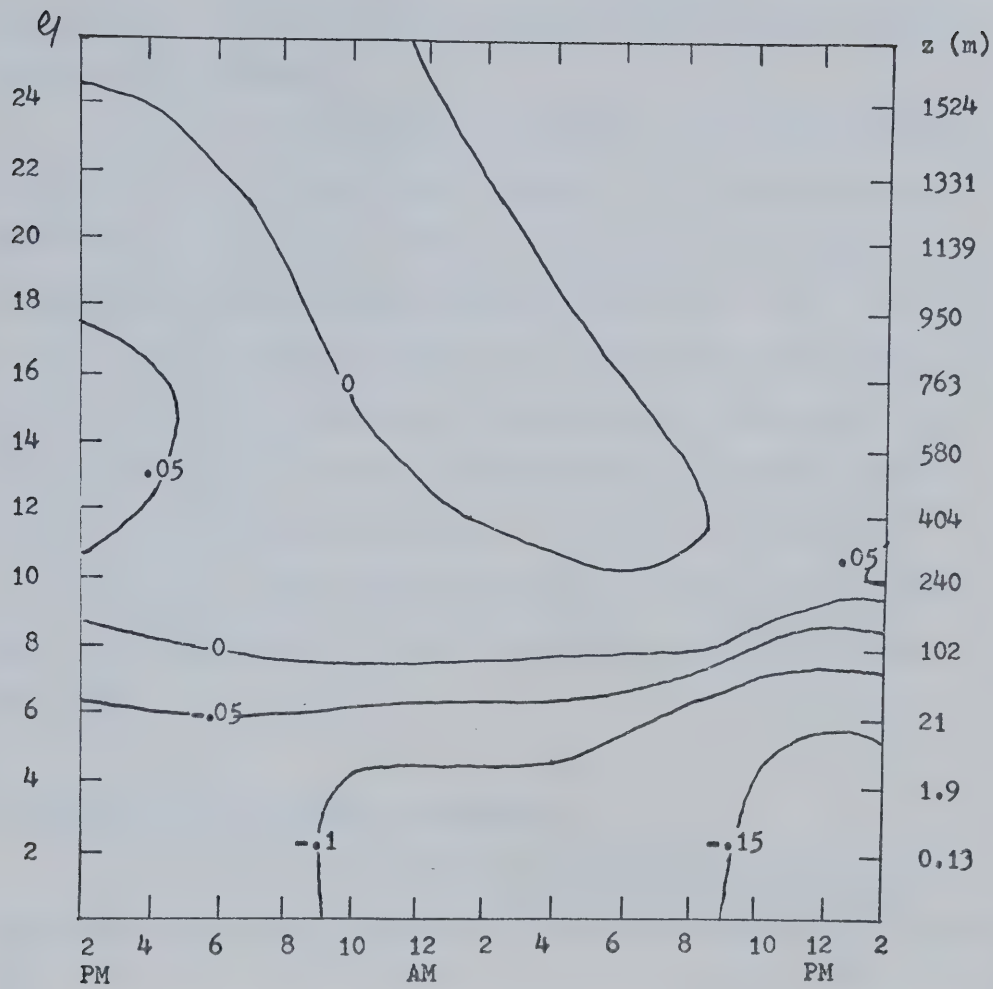


Figure 42. Diurnal cycle of the vertical profile of  $\bar{v} \bar{w}$  for the case  $z_0 = 1 \text{ cm}$ ,  $V_g = 20 \text{ m/sec}$  and high soil conductivity. The units are  $[\text{m}^2/\text{sec}^2]$ .



riables depend on the vertical gradient of the mean wind components.

Fig. 43 illustrates the behavior of  $K_m$  which has lower daytime values than  $K_t$ . However,  $K_m$  has a smaller tendency than  $K_t$  to develop negative values overnight.

Figs. 44 to 46 illustrate the behavior of  $\bar{u}^2$ ,  $\bar{v}^2$  and  $\bar{w}^2$  whose sum is simply  $e^2$ . Therefore, their behavior is very similar to the behavior of  $e$ . They reach a maximum during daytime and a minimum overnight. The approximate daytime contributions of  $\bar{u}^2$ ,  $\bar{v}^2$  and  $\bar{w}^2$  to  $e^2$  are, respectively, 45%, 32% and 23%. Fig. 47 represents the behavior of  $\bar{u} \bar{v}$ . Near the surface, the minimum is reached just after the time of maximum cooling rate and the maximum is obtained just after the time of maximum warming rate. This variable is proportional to the product of the gradients of U and V which explains the positive sign in the lowest 50 m and the negative sign in the region above 100 m.

### 6.3 Comparison of the Soil Temperatures.

Figs. 48 to 51 represent the diurnal variation of the soil temperature for the four simulations. The features common to all graphs are:

- 1- There is a time lag between the upper and lower levels in the time at which they respectively reach their maximum and minimum temperatures.
- 2- The temperature variation below 0.5 m is very small. This indicates that the soil depth of 1 m is appropriate for the numerical simulations for the periods of the order of one day.
- 3- The temperatures near the bottom increase almost continuously because the surface minimum temperature is too warm. The other levels



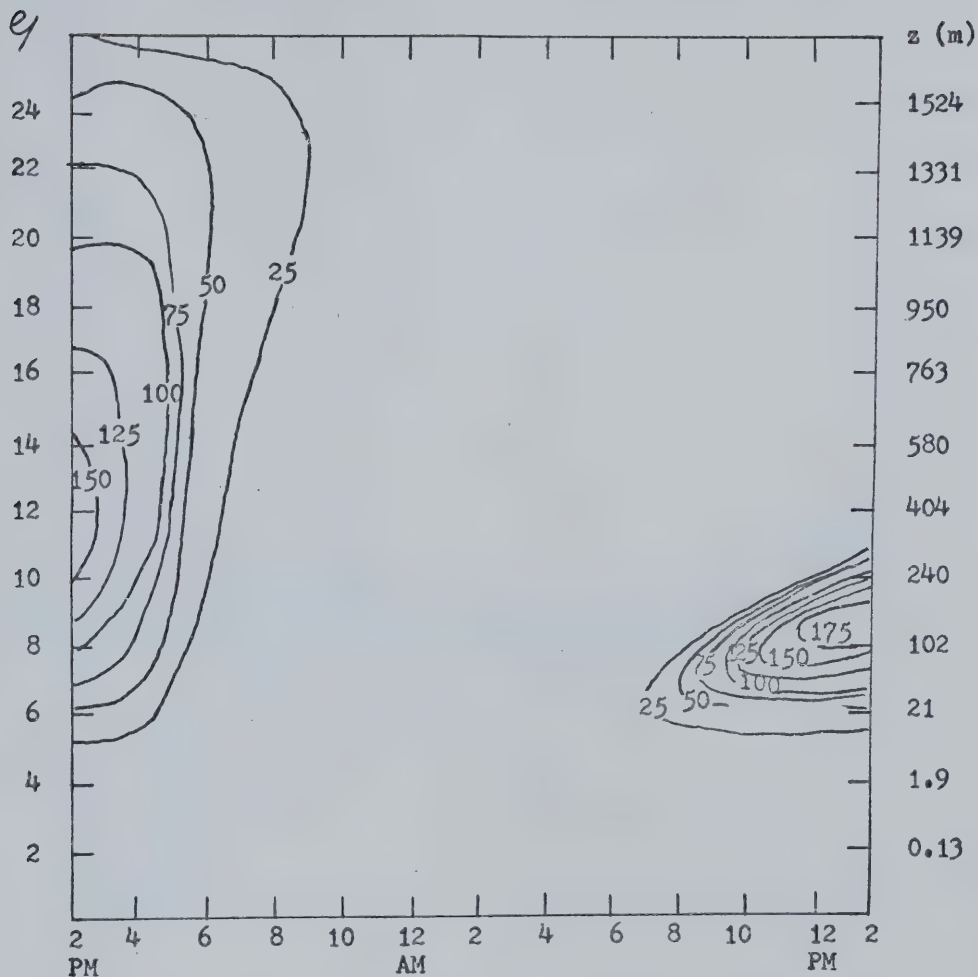


Figure 43. Diurnal cycle of the vertical variation of  $K_m$  for the case  $z_0 = 1$  cm,  $V_g = 20$  m/sec and high soil conductivity. The units are  $[10^3 \text{ cm}^2/\text{sec}]$ .



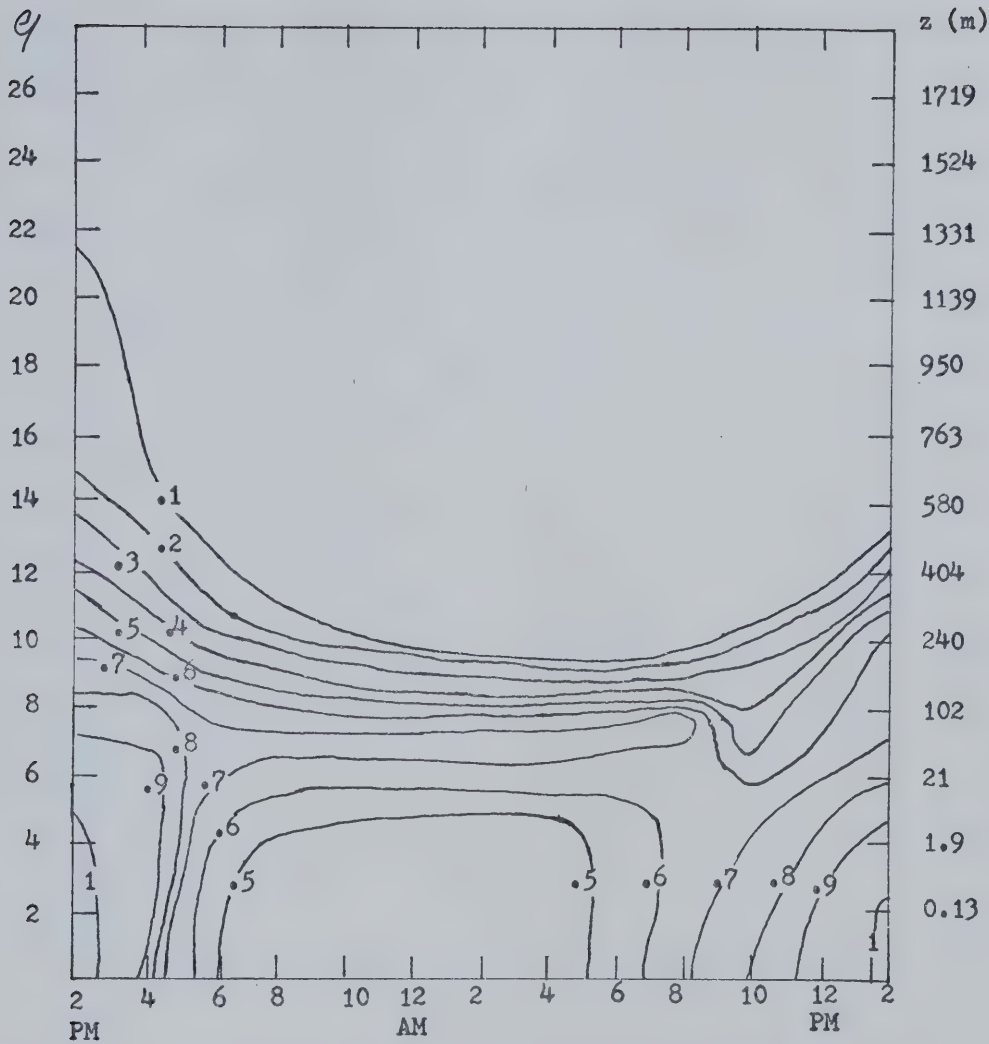


Figure 44. Diurnal variation of the vertical profile of  $\overline{u^2}$  for the case  $z_0 = 1 \text{ cm}$ ,  $V_g = 20 \text{ m/sec}$  and high soil conductivity. The units are  $[\text{m}^2/\text{sec}^2]$ .



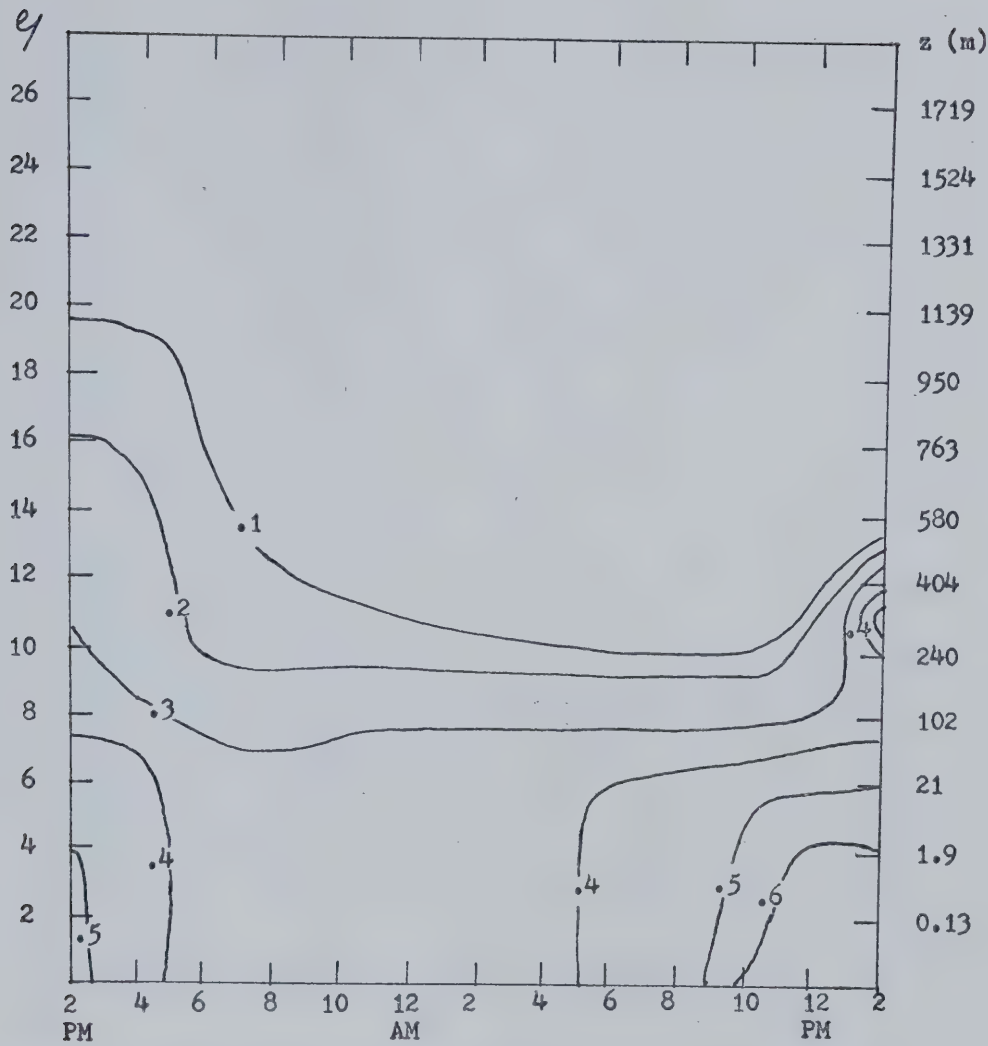


Figure 45. Diurnal variation of the vertical profile of  $\bar{v}^2$  for the case  $z_0 = 1$  cm,  $V_g = 20$  m/sec and high soil conductivity. The units are [ $m^2/sec^2$ ].



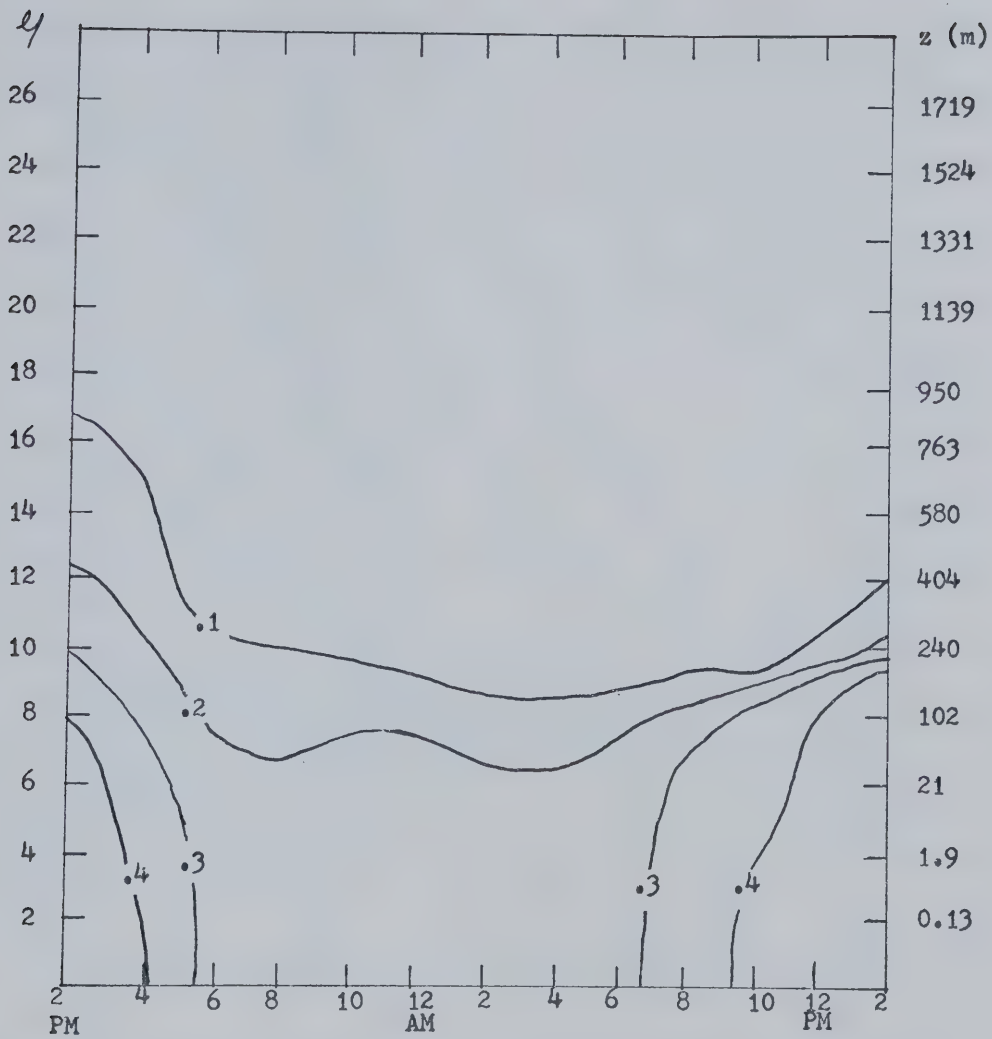


Figure 46. Diurnal variation of the vertical profile of  $\bar{w}^2$  for the case  $z_0 = 1$  cm,  $V_g = 20$  m/sec and high soil conductivity. The units are [ $m^2/sec^2$ ].



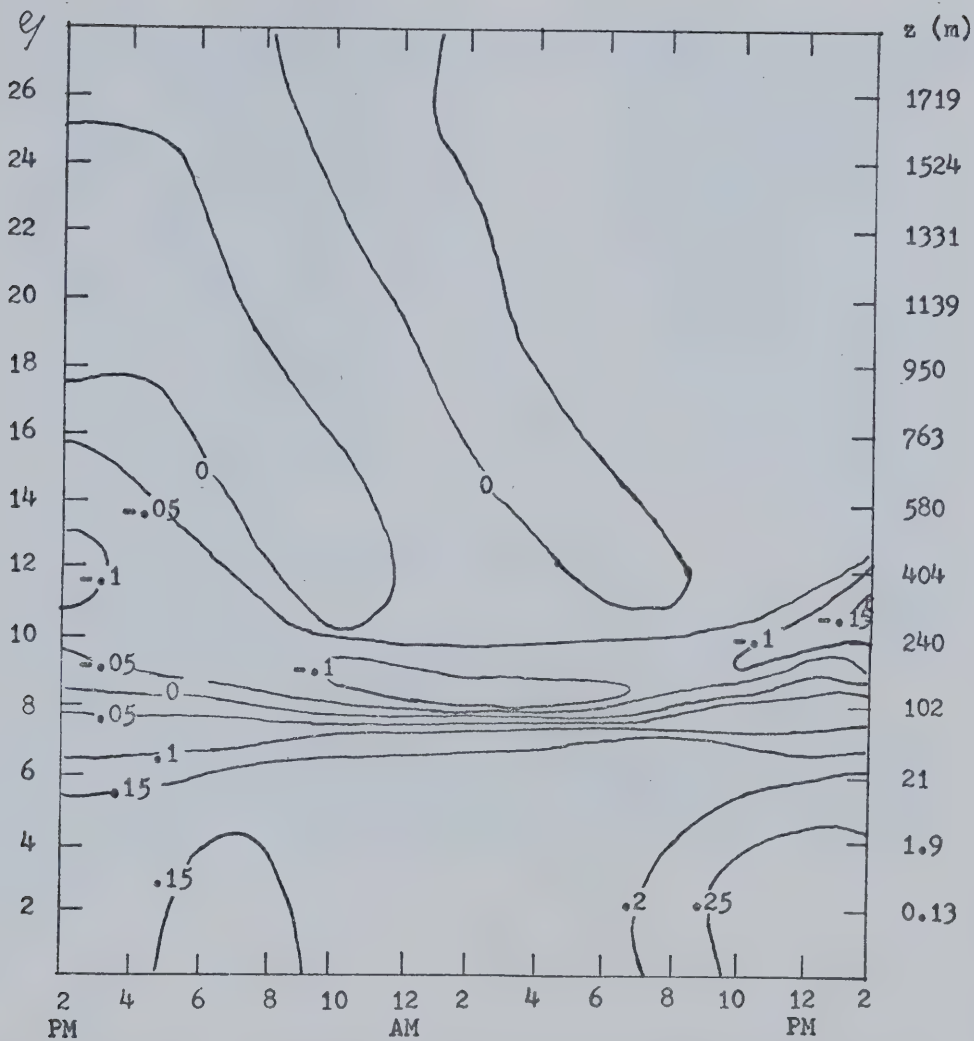


Figure 47. Diurnal variation of the vertical profile of  $\bar{u} \bar{v}$  for the case  $z_0 = 1$  cm,  $V_g = 20$  m/sec and high soil conductivity. The units are [ $m^2/sec^2$ ].



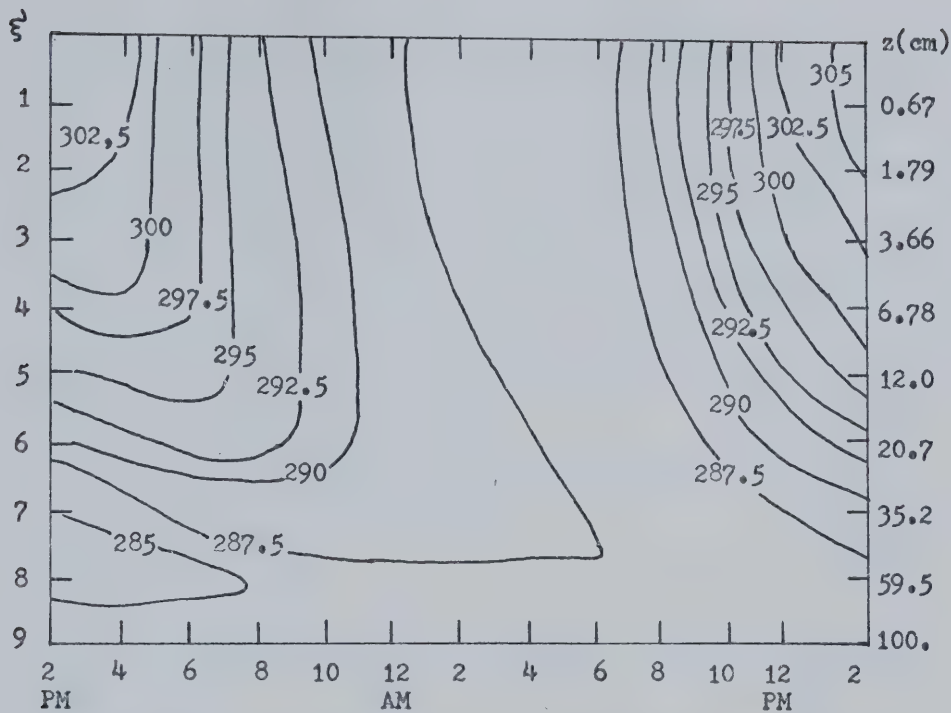


Figure 48. Diurnal variation of the soil temperature profile for the case  $z_0 = 1$  cm,  $V_g = 10$  m/sec and high soil conductivity. The units are [ $^{\circ}$ K].



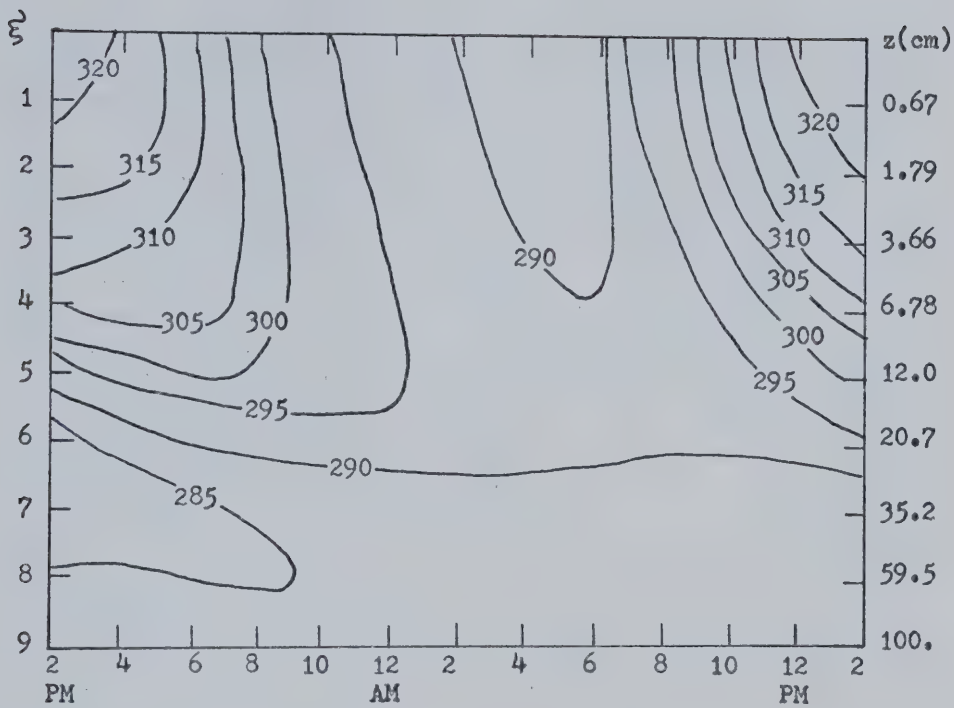


Figure 49. Diurnal variation of the soil temperature profile for the case  $z_0 = 1$  cm,  $V_g = 10$  m/sec and low soil conductivity. The units are [ $^{\circ}$ K].



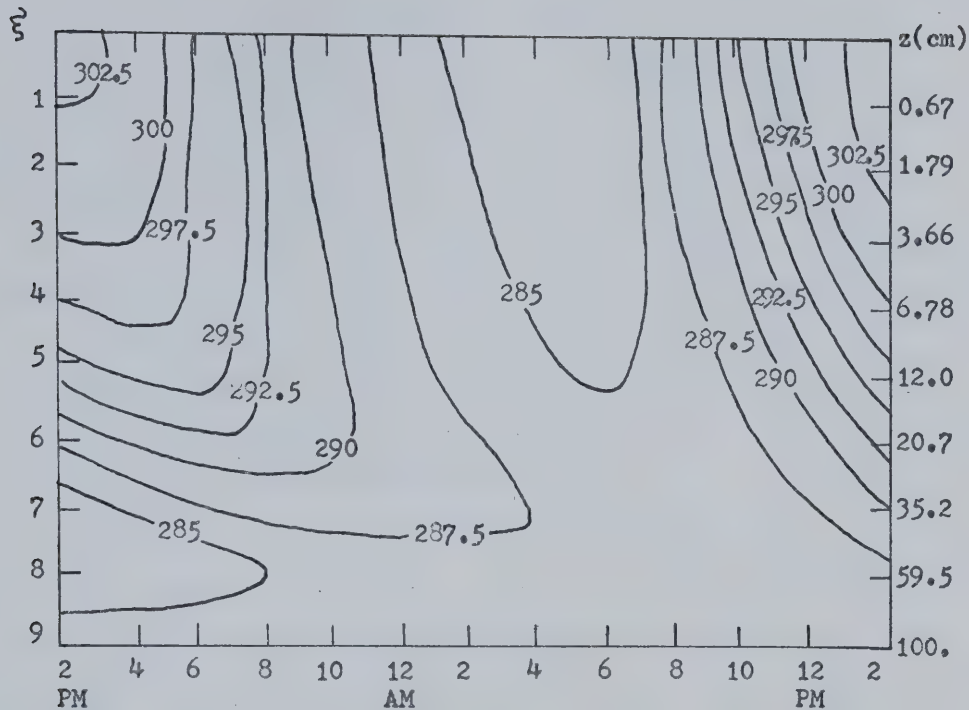


Figure 50. Diurnal variation of the soil temperature profile for the case  $z_0 = 100$  cm,  $V_g = 10$  m/sec and high soil conductivity. The units are [ $^{\circ}\text{K}$ ].



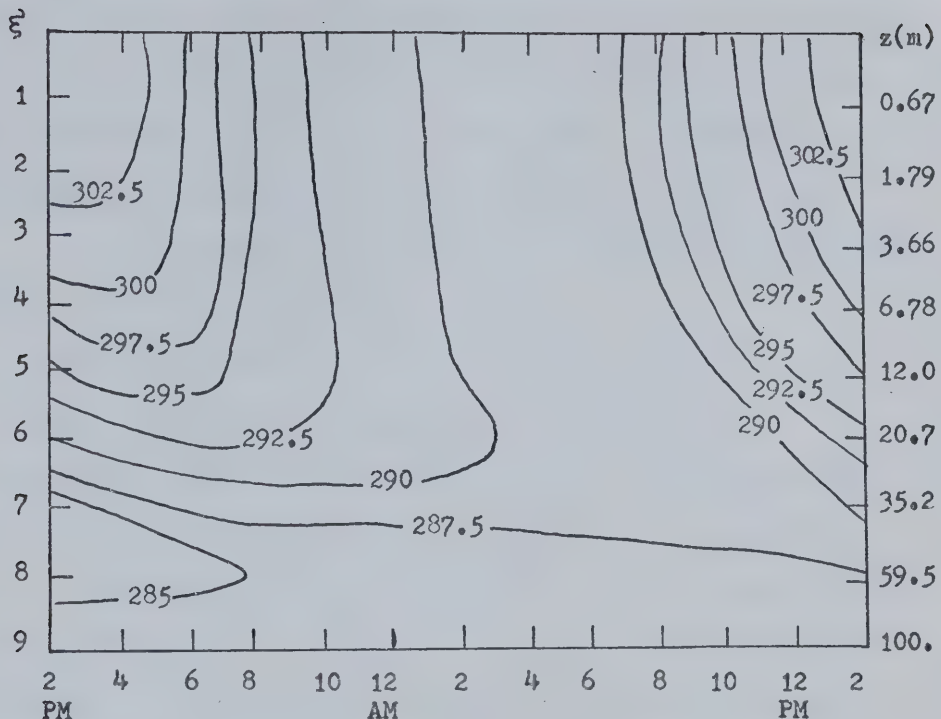


Figure 51. Diurnal variation of the soil temperature profile for the case  $z_0 = 1$  cm,  $V_g = 20$  m/sec and high soil conductivity. The units are [ $^{\circ}$ K].



are not perfectly cyclical. The second-day maximum is higher than that of the first day due to the decreased soil heat flux from one day to the other. The surface temperature could be lowered by modifying either the transmissivity factor or the albedo. In this way we could obtain more cyclical diurnal variations within the soil layer.

We now compare a poorly-conductive soil with a good-conductive one. The poorly-conductive soil has:

- 1- a larger temperature variation in the upper layers.
- 2- A smaller temperature variation in the lower layers.
- 3- The time lag between the maximum or minimum temperature in the upper levels and the lower levels is considerably increased.

All these differences are expected because we expect that the temperature wave will not penetrate a poorly-conductive soil as deeply as it would a good-conductive soil. This tends to concentrate the temperature gradients very close to the surface in the case of a poorly-conductive soil.

There is almost no difference between the soil temperature profiles due to a change in roughness height. The temperatures are slightly warmer in the case of  $z_0 = 1$  cm. A detailed calculation of the soil heat flux during the period 8 PM to 2 AM shows that the heat flux from the soil is about 10% higher with  $z_0 = 100$  cm. Therefore, the atmospheric heat flux and the soil heat flux are both larger overnight in the case of  $z_0 = 100$  cm, which should give a warmer surface temperature in this case. The number of iterations taken by the model with  $z_0 = 100$  cm was approximatively 2 to 3 times the number of iterations required by the model with  $z_0 = 1$  cm. This seems to have caused a significant difference in the convergence



Table 5. Comparison of the surface potential temperature between the four simulations of the urban heat island.

parameter \ model #	1	2	3	4
minimum $\bar{H}(z_0)$	289.5911	292.5137	287.9182	292.5120
maximum $\bar{H}(z_0)$	311.9797	310.2654	309.2634	330.2451
time of minimum	4 <sup>40</sup> AM	4 <sup>40</sup> AM	4 <sup>50</sup> AM	4 <sup>40</sup> AM
time of maximum	2 <sup>20</sup> PM	2 <sup>30</sup> PM	2 <sup>50</sup> PM	2 <sup>20</sup> PM
minimum $\bar{w\theta}(z_0)$	-3.54	-8.27	-5.49	-4.38
maximum $\bar{w\theta}(z_0)$	5.50	11.3	6.97	5.80
time of minimum	8 PM	7 <sup>40</sup> PM	7 <sup>40</sup> PM	8 PM
time of maximum	11 <sup>20</sup> AM	12 <sup>20</sup> PM	12 <sup>40</sup> PM	11 <sup>40</sup> PM
time of $\bar{w\theta}(z_0) = 0$	6 AM 4 <sup>10</sup> PM	7 AM 4 <sup>20</sup> PM	6 AM 3 <sup>50</sup> PM	5 <sup>35</sup> AM 3 <sup>40</sup> PM
Surface warming rate:				
minimum	-3.3	-2.9	-3.2	-6.0
maximum	4.0	2.9	3.7	6.4
time of minimum	6 <sup>50</sup> PM	6 <sup>50</sup> PM	7 <sup>10</sup> PM	6 <sup>20</sup> PM
time of maximum	8 <sup>50</sup> AM	9 <sup>30</sup> AM	9 <sup>30</sup> AM	9 <sup>30</sup> AM
$z_0$ [cm]	1	1	100	1
$v_g$ [m/sec]	10	20	10	10
soil conductivity	high	high	high	low



of the surface temperature for both simulations. The model usually converged without any oscillation when we used OMEGA = 0.7, which increases the probability of a build-up of systematic errors as is the case here.

#### 6.4 Assessment of the Urban Heat Island Effect.

We compare the quantities related to the behavior of the surface temperature for the four simulations in Table 5. Usually the city has a larger roughness height than the surrounding countryside. The city has also a higher soil thermal conductivity because of the abundance of concrete in the city and also because of the fact that clay, a poor thermal conductor, is often present in the countryside. Therefore, we expect a smaller diurnal amplitude over the city because of the increases in roughness height and soil thermal conductivity. The results seem to indicate that the countryside would be warmer than the city during daytime. However, another major factor counteracts the strong effect of the soil thermal conductivity: evaporation. There is generally a very important decline in evaporation over the city. This permits a large part of the solar energy to go into latent heat over the countryside. The difference in evaporation between the city and the countryside needed in order to obtain a warmer city depends mainly on the differences in the soil properties.

When the effects of evaporation and soil thermal properties nearly balance each other, the influence of other factors may become important in a specific case when we wish to determine which of the city or the countryside will become warmer during the daytime. The 99 cm



increase in roughness height cools down the city by 2 °C during daytime. The influence of an increase in the geostrophic wind is to reduce the amplitude of the diurnal temperature cycle and consequently to reduce the urban heat island effect in absolute value.

There is no significant difference in the times of maximum and minimum temperatures for all four simulations. However, the time of change in stability in the lower atmosphere is retarded by strong winds and by high soil conductivity.



## CONCLUSION

A numerical model using a more sophisticated approach to turbulence modelling than the ordinary K-theory has been applied with some success to the problem of the urban heat island. The unidimensional model basically describes the interaction between a soil layer and an atmospheric layer. Three factors were examined: roughness height, soil conductivity and wind speed. The model has demonstrated that the soil conductivity was an extremely important factor in determining the amplitude of the diurnal temperature cycle. The maximum temperature was considerably increased over a poorly conductive soil, which is often found in the countryside. Increased roughness height also reduced the amplitude of the diurnal temperature wave by a small amount. When we associate a high roughness height and a high soil conductivity with a city, we are led to the conclusion that the city is considerably cooler than the countryside during the daytime. The counterbalancing effect which was not studied is the difference in evaporation between the city and the countryside. If we suppose a dry city and a moist countryside, we expect that the daytime rural temperature will be cooler.

Many problems are associated with the numerical solution of the equations. An implicit finite-difference scheme was used in order to provide numerical stability and to permit a time step of 10 minutes. The equations have to be written very carefully in finite-difference form in order to reduce the round-off errors to which the temperature computations are very sensitive in the upper boundary layer. Double



precision had to be used for the mean quantities in order to obtain reasonable profiles above 1000 m. In some cases systematic errors have built up due to insufficient accuracy in the iterative procedure within each time step. The accuracy which we need in order to obtain good results must be determined by trial and error. The disadvantage of requiring more accuracy is the increase in computing time.

The most obvious improvement to the model is to include the moisture computations which present a few supplementary problems. We need a balance equation between the soil and atmospheric moisture. There is also the problem of water vapor build-up in the atmosphere. The main source of water vapor in the boundary layer is the evaporation at the surface which is enhanced during daytime. The water vapor is also transported fairly high in the atmosphere under unstable lapse rates. However, the main sink of water vapor is not the overnight condensation at the surface which involve only a shallow layer close to the ground under stable conditions. The main sink is the formation of clouds and precipitation. Therefore, we would need to incorporate some cloud physics into the model or we could remove artificially any excess water. If we include condensation in the atmosphere, we have to introduce a source term in the equation of temperature due to the release of latent heat. This would imply also a modification of the solar energy received at the surface of the earth due to reflection by the clouds and to absorption within the cloud. The infrared balance would also be affected.

Other improvements may include an albedo model which permits



a diurnal variation of the albedo with the solar angle. Radiative flux divergence could be important in the lowest 100 m over a city. The disadvantage of the roughness height concept over a city is that the value associated with very dense and tall buildings is of the order of a few meters. Therefore, we do not model the lowest meters over the city although often this is the layer in which we are interested. We could use two- and three-dimensional models in which some care has to be exercised in order to model properly the change in roughness height. As pointed out earlier, the forced-convection parameterization of some of the turbulent quantities gives a different result than the one predicted in the free-convection limit. Therefore, we must reconcile the two points of view. We would also like to model more complex soil layers in which the amount of water influences greatly the soil conductivity. Also, we could investigate the effects of two or more types of soil layers superposed one upon another.



## REFERENCES

- Angle, R.P., 1973: Airflow Modification due to a Change in Surface Roughness. M. Sc. thesis, University of Alberta, 130 pp.
- Atwater, M.A., 1966: Comparison of numerical methods for computing radiative temperature changes in the atmospheric boundary layer. *J. Appl. Meteor.*, 5, 824-831.
- Bornstein, R.D., 1968: Observations of the urban heat island effect in New York City. *J. Appl. Meteor.*, 7, 575-582.
- Brooks, D.L., 1950: A tabular method for the computation of temperature change by infrared radiation in the free atmosphere. *J. Meteor.*, 7, 313-321.
- Businger, J.A., 1972: The atmospheric boundary layer. Chapter 6, *Remote Sensing of the Troposphere*, U.S. Dept. of Commerce (Superintendent of Documents, Govt. Printing Office).
- Businger, J.A., J.C. Wyngaard, Y. Izumi and E.F. Bradley, 1971: Flux profile relationships in the atmospheric surface layer. *J. Atmos. Sci.*, 28, 181-189.
- Craig, C. and W. Lowry, 1972: Reflections on the urban albedo. Preprint of the Conference on Urban Environment and Second Conference on Biometeorology, 77-82.
- Deardorff, J.W., 1973: Three-dimensional numerical modeling of the planetary boundary layer. Workshop on Micrometeorology, A.M.S., 271-311
- Donaldson, C. duP., 1973: Construction of a dynamic model of the production of the atmospheric turbulence and the dispersal of atmospheric pollutants. Workshop on Micrometeorology. A.M.S., 313-390.
- Duckworth, F.S. and J.S. Sandberg, 1954: The effects of cities upon horizontal and vertical temperature gradients. *Bull. Amer. Meteor. Soc.*, 35, No. 5, 198-207.
- Dufort, E.C. and S.P. Frankel, 1953: Stability conditions in the numerical treatment of parabolic differential equations. Math. Tables Aids Comput., 7, 135-152.
- Elliot, W.P. and D.W. Stevens, 1961: A numerical method for computing radiative temperature changes near the earth's surface. GRD Research Notes, No. 69, L.G. Hanscom Field, Bedford, Mass., 21 pp.



- Eskinazi, S. and F.F. Erian, 1969: Energy reversal in turbulent flows. *Phys. Fluids*, 12, 1988-1998.
- Estoque, M.A., 1973: Numerical modeling of the planetary boundary layer. Workshop on Micrometeorology. A.M.S., 217-269.
- Godson, W.L., 1958: Atmospheric Thermodynamics. Research and Training Division, Meteor. Branch, D.O.T., Toronto, 117 pp.
- Hales, J.V., W. Zdunkowski and D. Henderson, 1963: A study of the physical thermodynamical and dynamical causes of low ceilings and visibilities. Final Rpt, Contract AF19(604)-7333 (DDC NO AD423535), Inter-Mountain Weather Inc., Salt Lake City, 77 pp.
- Haltiner, G.J., and F.L. Martin, 1957: Dynamical and Physical Meteorology. New York, McGraw-Hill, 74-156.
- Hanjalic, K. and B.E. Launder, 1972: Fully developed asymmetric flow in a plane channel. *J. Fluid Mech.*, 52, 609-638.
- Hage, K.D., 1972: Nocturnal temperatures in Edmonton, Alberta. *J. Appl. Meteor.*, 11, 123-129.
- Hage, K.D., 1975: Urban-rural humidity differences. *J. Appl. Meteor.*, 14, 1277-1283.
- Howard, L., 1833: The Climate of London Deduced from Meteorological Observations Made in the Metropolis and at Various Places Around it. 2nd ed., 3 vols. London, J. and A. Arch.
- Kolmogoroff, A.N., 1942: The equations of turbulent motion in an incompressible fluid. *Izv. Akad. Nauk. SSSR, Ser. Fiz.*, 6, No 1,2, 56-58.
- Kuo, H.L., 1968: The thermal interaction between the atmosphere and earth and the propagation of diurnal temperature waves. *J. Atmos. Sci.*, 25, 682-702.
- Landsberg, H.E., 1956: The Climate of Towns. Man's Role in Changing the Face of the Earth, University of Chicago Press, 1193 pp.
- Lilly, D.K., 1967: The representation of small-scale turbulence in numerical simulation experiments. *Proc. IBM Sci. Comput. Symp. Environmental Sci.*, IBM Form No. 320-1951, 195-210.
- McElroy, J.L., 1972: Effects of alternate land-use strategies on the structure of the nocturnal urban boundary layer. Preprint of the Conference on Urban Environment and Second Conference on Biometeorology, 185-190.



- Mellor, G.L., 1972: The large Reynolds number asymptotic theory of turbulent boundary layers. *Intern. J. Eng. Sci.*, 11, 851-873.
- Mellor, G.L., 1973: Analytic prediction of the properties of stratified planetary surface layers. *J. Atmos. Sci.*, 30, 1061-1069.
- Mellor, G.L. and H.J. Herring, 1968: Two methods of calculating turbulent boundary layer behavior based on numerical solutions of the equations of motion. Proc. AFOSR-IFF Stanford Conference, Vol. 1, 331-345.
- Mellor, G.L. and H.J. Herring, 1973: A survey of mean turbulent field closure models. *AIAA J.*, 11, 590-599.
- Mellor, G.L. and T. Yamada, 1974: A hierarchy of turbulence closure models for planetary boundary layers. *J. Atmos. Sci.*, 31, 1791-1806.
- Meroney, R.N., 1974: Buoyancy effects on a turbulent shear flow. Symposium on Atmospheric Diffusion and Air Pollution.
- Miller, E.L., R.E. Johnson and W.P. Lowry, 1972: The case of the muddled metromodel. Preprint of the Conference on Urban Environment and Second Conference on Biometeorology, 77-82.
- Mitchell, J.M., 1961: The temperature of cities. *Weatherwise*, 14, 224-229.
- Monin, A.S. and A.M. Yaglom, 1971: Statistical Fluid Mechanics: Mechanics of Turbulence. The MIT Press, 769 pp.
- Myrup, L.O., 1969: A numerical model of the urban heat island. *J. Appl. Meteor.*, 8, 908-918.
- Nappo, C.J., 1972: A numerical study of the urban heat island. Preprint of the Conference on Urban Environment and Second Conference on Biometeorology, 1-4.
- Ohmstede, W.P., 1966: Numerical solution of the transport and energy equations in the planetary boundary layer. Tech. Rpt ECOM-6020, U.S. dept of Commerce.
- Oke, T.R. and G.B. Maxwell, 1975: Urban heat island dynamics in Montreal and Vancouver. Atmos. Envir., 9, 191-200.
- Roden, G.I., 1966: A Modern statistical analysis and documentation of historical temperature records in California, Oregon and Washington, 1821-1964. *J. Appl. Meteor.*, 4, 3-24.



- Rotta, J.C., 1951: Statistische Theorie nichthomogener Turbulenz.  
Z. Phys., 129, 547-572; 131, 51-77.
- Sundborg, A., 1951: Climatological studies in Uppsala, with special  
regard to temperature conditions in the urban area.  
Geographica, No. 27, Universitet Geografiska Institutet,  
Uppsala, 111 pp.
- Taylor, P.A. and Y. De Lage, 1972: A note on finite-difference  
schemes for the surface and planetary boundary layers.  
Bound. Layer Meteor., 2, 108-121.
- Taulbee, D., 1973: private communication to Deardorff (1973).



## APPENDIX A

### LOG-LINEAR ATMOSPHERIC GRID

As explained in Chapter III the best transformation of coordinates in the lower boundary layer is,

$$\gamma = AC \left\{ \ln \left[ (z+z_0)/z_0 \right] / k_0 + z / l_0 \right\} \quad (A.1)$$

where,  $\gamma$  = log-linear coordinate

$z$  = ordinary vertical coordinate (cm) with origin at  $z_0$

$z_0$  = roughness height

$k_0$  = von Karman's constant

$l_0$  = length fixing the maximum size of the eddies

$AC$  = constant chosen for our convenience.

The grid is defined by the following statements,

- The maximum number of  $\gamma$  levels is 40
- $\gamma$  and  $z$  are zero at  $z_0$
- the top of the boundary layer is at 3000 m and correspond to  $\gamma = 39$
- the number of grid-points is fixed at 40 and the index  $k$  representing the height of the grid-point is related to  $k = \gamma + 1$ .

The constant  $AC$  is determined when we assign a value to  $z_0$  and  $l_0$ .

$$AC = \left[ \frac{39}{\frac{1}{k_0} \ln \left( \frac{300000+z_0}{z_0} \right) + \frac{300000}{l_0}} \right] \quad (A.2)$$

During the transformation of coordinates various derivatives of  $\gamma$  with respect to  $z$  appear; these derivatives can be derived exactly from equation (A.1).



$$\frac{\partial \psi}{\partial z} = AC \left[ \frac{1}{k_o(z+z_o)} + \frac{1}{l_o} \right] \quad (A.3)$$

$$\frac{\partial^2 \psi}{\partial z^2} = - \frac{1}{k_o(z+z_o)^2} \quad (A.4)$$

Therefore we only have to solve the equation for  $z$  at each  $\psi$  level. There are three iterative ways of solving (A.1) for  $z$ .

Method 1. Near  $z_o$  the grid is almost logarithmic because of the small contribution from the linear term in that region. The most rapidly converging formula is obtained by isolating the term inside the logarithm,

$$z = z_o \left\{ \exp \left[ k_o (\psi / AC - z / l_o) \right] - 1 \right\} \quad (A.5)$$

Method 2. Near the top of the boundary layer the grid is almost linear because the logarithmic term has a small influence there. Therefore we isolate the linear term,

$$z = l_o \left\{ \psi / AC - \ln \left[ (z+z_o) / z_o \right] / k_o \right\} \quad (A.6)$$

Method 3. If formulas (A.5) and (A.6) do not give reasonable results we can use formula (A.1) and do the iteration on  $\psi$  instead of on  $z$ . In this case we readjust the value of  $z$  until we get close enough to the integral value for a given level.

#### A.1 Determination of IKM.

Firstly we replace  $\psi$  by  $k = \psi + 1$  because most computing systems do not accept an index 0. The level IKM is the level representing the upper limit of the applicability of (A.5). Close to the roughness height the initial guess will be purely exponential,

$$z_i = z_o \left\{ \exp \left[ (k_o - 1) / AC \right] - 1 \right\} \quad (A.7)$$

where,  $z_i$  = initial guess for  $z$ .



The initial guess is always greater than the true value for  $z$  because we have neglected a negative number in the exponential, namely  $-z_i/\lambda_0$ . At some level the initial value of  $z$  will be large enough to cause the term inside the exponential in (A.5) to become negative; that level can be considered as the first one where the exponential initialization is inappropriate. Therefore, IKM is the level immediately below the first level where,

$$(k-1)/AC - z_i/\lambda_0 < 0 \quad (A.8)$$

#### A.2 Initialization of the Other Levels.

We use the assumption of a linear spacing to initialize all the other levels,

$$z_i = \gamma * (\text{top of the B.L.}) / (\text{maximum } \gamma) = (k-1) * 300000 / 39 \quad (A.9)$$

That initial guess is very good for the top levels where the spacing is indeed almost linear but there is a critical region where neither the exponential spacing nor the linear spacing are expected to be good. One way of determining that region is to input  $z_i$  into (A.6) in order to get a second guess  $z'$ ,

$$z' = \lambda_0 \left\{ \gamma / AC - \ln \left[ (z_i + z_0) / z_0 \right] / k_0 \right\} \quad (A.10)$$

The overestimation in  $z_i$  in the lower levels can cause  $z'$  to become negative which would stop the iterative procedure because the next guess would require the estimation of a logarithm of a negative number. Therefore, each time that  $z'$  is negative we readjust  $z_i$  to a smaller number

$$z'_i = z_i / B \quad (A.11)$$

where  $B$  is a positive constant greater than 1.



### A.3 Accelerated Gauss-Seidel Process.

We use the accelerated Gauss-Seidel process which consists in refining our initial guess by giving a weight both to the last approximation and to the new computed value. For example, we call,

$Z$  = last value of  $z$

$\text{TEMP}$  = computed value for  $z$

$\text{TP} = \text{TEMP} - Z$  = difference between two successive iterative values of  $z$

$Z' = Z + \text{TP} \text{ OMEGA}$  = new approximation to  $z$

$\text{OMEGA}$  is an acceleration factor which gives a weight both to  $Z$  and  $\text{TEMP}$ . It can vary from 0 to 2 and,

$\text{OMEGA} = 1$  implies that the computed value of  $z$  is  $\text{TEMP}$ .

$\text{OMEGA} > 1$  implies acceleration, appropriate for the cases in which

$Z'$  approaches a value steadily without oscillations.

$\text{OMEGA} < 1$  implies deceleration, appropriate for the cases where

$Z'$  oscillates around the real value of  $z$ .

Unfortunately it does not seem possible to devise a general formula for the optimum value of  $\text{OMEGA}$  in our problem. Some of the difficulties are,

- (a) close to  $z_0$ ,  $\text{OMEGA} = 1$  is fairly appropriate because the oscillations around the real value are damped very rapidly.
- (b) Near IKM large oscillations prevail due to the fact that the initial guess is poor in that region and also that neither (A.5) nor (A.6) are really appropriate there.
- (c) The level IKM is dependent on the roughness height  $z_0$  and to a lesser extent on  $\lambda_0$ .
- (d) Above IKM the iterative formula changes and most of the diffi-



culties arise near IKM where OMEGA < 1 is needed for convergence. Near the top of the boundary layer the convergence is rather rapid with OMEGA=1.

#### A.4 Detailed Analysis of OMEGA in a Specific Case.

With OMEGA = 1 two successive iterations will always give one value above and the other one below the actual value of z. This phenomenon is due to the form of the equations. When the formulas are applied in their appropriate regions the oscillations are damped very rapidly. It would be difficult to determine the best OMEGA a priori for all the grid points. However, after the solution has been obtained we can compute what the best OMEGA should have been. The best OMEGA is defined by

$$\text{OMEGA}' = (Z' - Z) / (\text{TEMP} - Z)$$

where,       $Z'$  = actual height of the grid point

$Z$  = last iterative value for  $z$ .

The best OMEGA is therefore defined as the one which would give the true value in only one iteration. We will study OMEGA in the special case where  $z_0 = 1$  cm and  $\lambda_0 = 2700$  cm. In this case we find that  $AC = 0.2650463308$ . In Tables 6 and 8 we list the computed values of the grid-point heights at various stages of iteration. In Tables 7 and 9 we have tabulated the computed best OMEGA at all stages of iteration.

##### A.4.1 Analysis of the Iterative Process Below IKM.

We note that the initialization is extremely good close to the ground and worsens considerably near IKM where the initial value



Table 6 . Computed values for the grid-point heights  $z(k)$  at various stages of iteration. The first entries in each columns are the initial values for which formula (A.7) was used. The successive values are computed from (A.5). The levels are in terms of  $k = y + 1$ .

$z(2)$	$z(3)$	$z(4)$	$z(5)$	$z(6)$
2.745382866	13.02789281	51.53982937	195.78177670	736.0339460
2.744050185	13.00422248	51.18997609	190.08504693	662.9963432
2.744050832	13.00426545	51.19234303	190.09731477	674.8039290
2.744050831	13.00426538	51.19232702 51.19232713	190.09700948 190.09701708 190.09701689	674.2916315 674.3364784 674.3325524 674.3328961 674.3328660 674.3328686 674.3328684

$z(7)$	$z(8)$	$z(9)$
2760.433670	10337.88097	38723.06763
1929.065229	2705.932184	255.8352926
2148.690295	7279.085837	37258.92336
2088.351785	4023.201229	300.3897878
2104.758060	6136.303980	37243.19405
2101.284420	4665.759005	308.9370814
2101.230814	5645.811378	37201.95099
2101.245422	4972.118966	310.5985422
2101.241441	5425.952268	37193.93929
2101.242526	5115.893194	310.9235327
2101.242311	5325.744693	37192.37819
2101.242289	5182.995555	310.9854507
2101.242295	5279.748775	37192.07383
2101.242293	5213.794914 5258.570325 5228.131046 5248.805082	310.9977602 37192.01448 311.0001605 37192.00291
	.	311.0007420
	:	37192.00009
	5240.437109	



Table 7. Best OMEGA corresponding to the computed values of the grid points at various stages of iteration.

$z(2)$	$z(3)$	$z(4)$	$z(5)$	$z(6)$
0.99390	0.9981	0.99327	0.9978	0.9198
0.99845	0.9983	0.99328	0.9957	0.91948
0.999			0.9957	0.91951
				0.91991
$z(6)$	$z(7)$	$z(9)$		
0.792898	0.6679	.		
0.783962	0.5542	.		
0.78635	0.6261	.		
0.785745	0.5760	0.2695		
0.78819	0.6092	0.7305		
0.7737	0.58637	0.2695		
0.83	0.60172	0.7305		
0.72	0.59122	.		
	0.59822	.		
	0.5934	.		
	0.5967			



Table 8. Computed values of the grid-point heights  $z(k)$  at various stages of iteration. We have used formula (A.10) for the initial values (first entry in each column) and formula (A.6) for the other values.

$z(10)$	$z(11)$	$z(12)$	$z(13)$	$z(14)$	$z(15)$
75000.0000	82500.0000	90000.0000	97500.0000	105000.000	112500.000
5087.24000	14538.9041	24054.5795	33624.0000	43239.2259	52893.8983
25843.0580	27930.2370	34233.2230	41836.5800	50083.3298	58715.5240
13306.2064	22893.9750	31511.1692	40150.8100	48949.8161	57910.0400
18426.7500	24427.7900	32150.3100	40468.0000	49098.6320	58016.6000
15915.3529	23927.5590	31995.4144	40407.3700	49102.9959	58002.4190
17045.5800	24087.1600	32032.6700	40418.9500	49102.3103	58004.3050
16516.3606	24035.8800	32025.6900	40416.7400	49102.4180	58004.0544
16759.6509	24052.3200	32025.8500	40417.1640	49102.4011	58004.0877
16646.8531	24047.0400	32025.3300		49102.4037	58004.0833
16698.9450	24048.7400	32025.4599		49102.4033	58004.0839
16674.8443	24048.1970	32025.4291		49102.4034	
16685.9853	24048.3718				
16680.0833	24048.3160				
.	24048.3339				
.	24048.3281				
.	24048.3303				
16682.5					

Table 9. Best OMEGA corresponding to the computed grid-point heights at some of the iteration steps.

$z(10)$	$z(11)$	$z(12)$	$z(13)$	$z(14)$	$z(15)$
0.8340	0.8600	0.879	0.8930	0.865	0.882
0.5586	0.7100	0.783	0.8270		
0.7306	0.7700	0.811	0.8421		
0.6590	0.7526		0.8419		
0.6945	0.7585				
0.6780					
0.6860					



is too large by a factor of 3. The number of iterations rises from 3 at the second grid point to 10 at the sixth grid point, jumps to 60 at the eighth grid point and would never converge at IKM = 9 because there is an oscillation between two stable values at this grid point. Examining the values of OMEGA at various stages of iteration, we observe that a different value for OMEGA is needed depending on whether we start from below the actual value or from above. This phenomenon peaks at IKM where the iteration process breaks down if we used OMEGA = 1. At IKM it converges to one value above the actual value for z and to another value below the actual value for z. This points out that there is no guarantee of an unique answer with this iteration process. In fact there are three solutions to the equation for  $\gamma$ : one using the lowest value for z in the linear term and the highest one in the logarithmic term, another one using the lowest value for z in the logarithmic term and the highest one in the linear term, and finally one using the actual value for z in both terms. Obviously we are interested only in the last solution. The only iteration process which would give an unique answer all the time is the one on  $\gamma$ , but this is generally a fairly slow process and difficult to implement. Now we will try to derive an analytical function which will give the best OMEGA at all levels below IKM. The matching can be done with the help of the following rules,

- (a) exact match of OMEGA = 1 at k = 1.
- (b) Match the lowest value for OMEGA at IKM, i.e. OMEGA = 0.2695.
- (c) Assume an exponential variation of OMEGA in terms of k.

Therefore, we will use an expression like,

$$\text{OMEGA}(k) = 1 + A \left\{ 1 - \exp \left[ (k-1)/(IKM-1) \right]^n \right\} \quad (\text{A.12})$$



where A and n are constants to be determined by fitting the actual values found for OMEGA at various grid points. Good values for these constants were found to be,

$$A = 0.425 \quad (A.13)$$

$$n = 3 \quad (A.14)$$

It is obvious that this formula will not be perfect for all roughness heights because of the arbitrariness in the choice of IKM and the discreteness of the levels which affect the efficiency of (A.5) at IKM. However, it is clear that an uniform value for OMEGA at all levels is not acceptable. A value of 1 would not give convergence to the desired value at IKM, whereas a value of 0.3 would increase considerably the number of iterations required at the grid points where convergence is rapid with OMEGA = 1. Formula (A.12) seems a fair compromise between simplicity, generality and speed of convergence.

#### A.4.2 Analysis of the Iterative Process Near and Above IKM.

It takes many more iterations near IKM than much above that level. We also note that the initialization improves as the level of the grid point increases. In this case the best OMEGA varies more gently above IKM than below it. Therefore, we try to fit an analytical expression of the form,

$$\text{OMEGA}(k) = 1 - B (NS-k)/(NS-IKP)^x \quad (A.15)$$

where, NS = top of the boundary layer = 40

IKP = IKM + 1

x = exponent determined to be about 5

B = constant determined to be about 0.32.



### A.5 Iteration Process on $\gamma$ .

In the cases where (A.5) nor (A.6) have not converged within the specified number of iterations, we can complete the process by the iteration on  $\gamma$  which uses (A.1) in the form,

$$\gamma' = AC \left\{ \ln \left[ (z' + z_0) / z_0 \right] / k_0 + z' / l_0 \right\} \quad (\text{A.16})$$

If we define  $\text{DIFF} = \gamma' - \gamma$ . Then, when DIFF is positive, the implication is that  $z'$  is too high and similarly, when DIFF is negative,  $z'$  is too low. Therefore, the next guess will be,

$$z'' = z' - f(\text{DIFF}) \quad (\text{A.18})$$

where  $f(\text{DIFF})$  is a positive function involving DIFF. This function has to be determined empirically and will probably vary from grid point to grid point.



## APPENDIX B

### STEADY-STATE ATMOSPHERIC EQUATIONS

#### B.1 Equations: First Form.

The basic equations in log-linear coordinates are given in Section 3.3.1 and simplify to,

$$-\frac{\partial^2 U}{\partial y^2} K_m \left( \frac{\partial U}{\partial z} \right)^2 - \frac{\partial U}{\partial y} \left( \frac{\partial K_m}{\partial y} \left( \frac{\partial U}{\partial z} \right)^2 + K_m \frac{\partial^2 U}{\partial z^2} \right) = f(V - V_g) \quad (B.1)$$

$$-\frac{\partial^2 V}{\partial y^2} K_m \left( \frac{\partial U}{\partial z} \right)^2 - \frac{\partial V}{\partial y} \left( \frac{\partial K_m}{\partial y} \left( \frac{\partial U}{\partial z} \right)^2 + K_m \frac{\partial^2 U}{\partial z^2} \right) = f(U_g - U) \quad (B.2)$$

$$-\frac{1.15}{3} \left( (\epsilon l \left( \frac{\partial U}{\partial z} \right)^2) \frac{\partial^2 \epsilon^2}{\partial y^2} + \left( \frac{\partial \epsilon l}{\partial y} \left( \frac{\partial U}{\partial z} \right)^2 + \epsilon l \frac{\partial^2 U}{\partial z^2} \right) \frac{\partial \epsilon^2}{\partial y} \right) = 2 \left( K_m \left| \frac{\partial \vec{V}}{\partial y} \right|^2 \left( \frac{\partial U}{\partial z} \right)^2 - \frac{\epsilon^3}{B_1 l} \right) \quad (B.3)$$

The diffusion operator  $\mathcal{D}(\cdot)$  is defined in (3.30) and used in the equation for  $K_m$ ,

$$K_m = \frac{A_1 l ((1-3C_1)\epsilon^3 + 0.23x^4 A_1 l \mathcal{D}(\epsilon^2))}{\epsilon^2 + 6 A_1^2 l^2 \left| \frac{\partial \vec{V}}{\partial y} \right|^2 \left( \frac{\partial U}{\partial z} \right)^2} \quad (B.4)$$

The other coefficients of diffusivity are not used in the computations but can be evaluated diagnostically,

$$K_t = K_w = \frac{A_1 l (\epsilon^3 + 4x0.23 A_1 l \mathcal{D}(\epsilon^2) - 6 A_1 l K_m \left| \frac{\partial \vec{V}}{\partial y} \right|^2 \left( \frac{\partial U}{\partial z} \right)^2)}{\epsilon^2} \quad (B.5)$$

The other turbulent moments involving  $\theta$  or  $q$  vanish,

$$\overline{\theta^2} = \overline{\theta q} = \overline{q^2} = 0 \quad (B.6)$$

The mean mixing ratio and the mean potential temperature are assumed constant throughout the boundary layer and their actual values



are determined by their values at the surface of the earth.

### B.2 Mixing Length.

The formula for the mixing length is,

$$\ell = \frac{k_o(z+z_o)}{1 + \frac{k_o(z+z_o)}{\ell_o}} \quad (B.7)$$

where  $\ell_o$  is defined by,

$$\ell_o = 0.1 \int_0^{\infty} \frac{z e dz}{e dz} \quad (B.8)$$

These integrals are transformed into finite summations by,

$$\int_0^{\infty} z e dz = \int_0^{\infty} z e \frac{dz}{dy} dy = \sum_{k=1}^n z(k) e(k) / DELZ(k) \quad (B.9)$$

$$\int_0^{\infty} z dz = \int_0^{\infty} z \frac{dz}{dy} dy = \sum_{k=1}^n z(k) / DELZ(k) \quad (B.10)$$

Now we look at the vertical derivative of  $\ell$ . In the surface layer  $\ell$  varies exponentially in  $y$ -coordinates. A simple centered finite-difference approximation like,

$$\left. \frac{\partial \ell}{\partial y} \right|_k = \frac{\ell(k+1) - \ell(k-1)}{2}$$

would have a large truncation error. Therefore, we will use a more exact formulation obtained by taking the derivative of (B.7) with respect to  $y$ ,

$$\left. \frac{\partial \ell}{\partial y} \right|_k = DELZZ(k) / \ell^2(k) \quad (B.11)$$

where

$$DELZZ(k) = - \left. \frac{\partial^2 y / \partial z^2}{AC \partial y / \partial z} \right|_k \quad (B.12)$$



### B.3. Vertical Derivative of $K_m$ .

As we know, in the surface layer  $K_m$  behaves like,

$$K_m = u_\infty k_o(z+z_o) \quad (\text{B.13})$$

The grid is predominantly logarithmic in that region, which implies,

$$\gamma \propto \ln[(z+z_o)/z_o] \quad (\text{B.14})$$

Therefore,

$$K_m \propto \exp(\gamma) \text{ and} \quad (\text{B.15})$$

$$\frac{\partial K_m}{\partial \gamma} \propto \exp(\gamma) \quad (\text{B.16})$$

Therefore, a simple finite-difference approximation to the vertical derivative of  $K_m$ ,

$$\frac{\partial K_m}{\partial \gamma} = \frac{K_m(k+1) - K_m(k-1)}{2} \quad (\text{B.17})$$

will be greatly in error in the lower boundary layer. The following transformation corrects the problem:

$$\frac{\partial K_m}{\partial \gamma} = K_m \frac{\partial \ln K_m}{\partial \gamma} \quad (\text{B.18})$$

This is better in the surface layer because

$$\ln K_m \propto \gamma \text{ and} \quad (\text{B.19})$$

$$\frac{\partial \ln K_m}{\partial \gamma} \propto \text{constant} \quad (\text{B.20})$$

The finite-difference approximation in the lower boundary layer should be

$$\frac{\partial K_m}{\partial \gamma} = \frac{K_m(k)}{2} \ln \left[ \frac{(K_m(k+1))}{(K_m(k-1))} \right] \quad (\text{B.20})$$



## B.4 Finite-Difference Equations.

### B.4.1 Mean Wind U.

The appropriate equation for U is (B.1) in which the various terms are approximated by,

$$2 \frac{\partial K_m}{\partial y} \Big|_k = DLNK = \begin{cases} K_m(k+1) - K_m(k-1) & \text{above the constant-flux layer} \\ K_m(k) \ln \left[ \frac{K_m(k+1)}{K_m(k-1)} \right] & \text{in the constant-flux layer} \end{cases} \quad (B.21)$$

$$A(2) = \frac{\partial K_m}{\partial y} \left( \frac{\partial y}{\partial z} \right)^2 + K_m \frac{\partial^2 y}{\partial z^2} = DLNK \frac{DELZ2(k)}{2} + K_m(k) DELZ2(k) \quad (B.22)$$

$$A(3) = K_m \left( \frac{\partial y}{\partial z} \right)^2 = K_m(k) DELZ2(k) \quad (B.23)$$

$$A(4) = \frac{\partial U}{\partial y} = [U(k+1) - U(k-1)]/2 \quad (B.24)$$

$$\frac{\partial^2 U}{\partial y^2} = U(k+1) - 2U(k) + U(k-1) \quad (B.25)$$

We group all the terms different from U(k),

$$DU = [U(k+1) + U(k-1)] A(3) + A(4) A(2) + F (V(k) - V_g) \quad (B.26)$$

Finally,

$$U(k) = DU / [2 A(3)] \quad (B.27)$$

### B.4.2 Equation for the Mean Wind V.

The terms A(2) and A(3) will be used also in the equation for V. The other terms are

$$A(5) = \frac{\partial V}{\partial y} = [V(k+1) - V(k-1)]/2 \quad (B.28)$$

$$\frac{\partial^2 V}{\partial y^2} = V(k+1) - 2V(k) + V(k-1) \quad (B.29)$$

All the terms except V(k) are grouped into,

$$DV = [V(k+1) + V(k-1)] A(3) + A(5) A(2) - F [U(k) - U_g] \quad (B.30)$$



Therefore,

$$V(k) = DV/[2 A(3)] \quad (B.31)$$

### B.4.3 Equation for e.

The equation for  $e$  is (B.3) in which we have to evaluate the vertical derivative of  $(e\ell)$ :

$$\frac{\partial e\ell}{\partial y} = e \frac{\partial \ell}{\partial y} + \ell \frac{\partial e}{\partial y} \quad (B.32)$$

We will use a simple centered finite-difference approximation to the vertical derivative of  $e$  such that

$$\frac{\partial e}{\partial y} = [e(k+1) - e(k-1)]/2 \quad (B.33)$$

The vertical derivative of  $\ell$  is given by (B.11) and will be called  $DL(k)$ . Therefore, (B.32) can be written as

$$DEL = e(k) DL(k) + \ell(k) [e(k+1) - e(k-1)]/2 \quad (B.34)$$

The coefficient of  $2 \frac{\partial e^2}{\partial y^2}$  becomes

$$A(14) = (DEL DELZ2(k) + e(k) \ell(k) DELZ2(k)) 0.23/2 \quad (B.35)$$

The coefficient of  $\frac{\partial^2 e^2}{\partial y^2}$  is

$$A(13) = e(k) \ell(k) DELZ2(k) 0.23 \quad (B.36)$$

We call

$$A(8) = \left| \frac{\partial \vec{V}}{\partial z} \right|^2 = \left[ \left( \frac{\partial U}{\partial z} \right)^2 + \left( \frac{\partial V}{\partial z} \right)^2 \right] = [A(4) A(4) + A(5) A(5)] DELZ2(k) \quad (B.37)$$

We isolate the terms in  $e^2(k+1)$  and those in  $e^2(k-1)$  and call AA and AB their respective coefficients,

$$AA = A(13) + A(14) \quad (B.38)$$

$$AB = A(13) - A(14) \quad (B.39)$$

Gathering all the terms except  $e^2(k)$ , we have



$$A(16) = e^2(k+1) AA + e^2(k-1) AB + 1.2 K_m(k) A(8) \quad (B.39)$$

Finally we obtain

$$e^2(k) = A(16)/A(15) \quad (B.40)$$

$$e(k) = \text{SQRT}[e^2(k)] \quad (B.41)$$

#### B.4.4 Equation for $K_m$ .

The array B contains most of the commonly-used variables which do not need to be computed each time that the program is run. In this case we have

$$B(28) = (1-3C_1) \quad (B.42)$$

$$B(61) = 3 A_1^2 \quad (B.43)$$

$$B(5) = A_1 \quad (B.44)$$

The diffusion operator applied to  $e^2$  is called A(9) where  
 $A(9) = 4 A_1 \mathcal{D}_1(e^2) = B(31) \mathcal{D}(k) [AA e^2(k+1) + AB e^2(k-1) - 2 A(13) e^2(k)] \quad (B.45)$

A(10) will represent  $e^3(k)$  so that

$$A(10) = e^2(k) e(k) \quad (B.46)$$

The denominator becomes

$$A(12) = e^2(k) + 2 B(61) \mathcal{D}^2(k) A(8) \quad (B.47)$$

$$A(11) = A(10) B(28) + A(9) \quad (B.48)$$

Therefore,  $K_m(k)$  is expressed as

$$K_m(k) = B(5) \mathcal{D}(k) A(11)/A(12) \quad (B.49)$$

#### B.4.5 Iteration scheme.

The accelerated Gauss-Seidel iteration process is used for  $U$ ,  $V$ ,  $K_m$  and  $e$ . The basic scheme has been described in detail in



Section 3.5. Some refinements were needed in order to prevent divergence which can occur very easily in the uppermost levels. Most of the problems occur when  $K_m$  drops to a very small value which causes the wind to become very large. Therefore, a minimum value much larger than the molecular diffusivity has to be specified near the top of the boundary layer. This can be done by specifying a reasonable value for  $K_m$  at the top of the boundary layer, say of the order of  $100 \text{ cm}^2/\text{sec}$ , and devising an analytical function for the minimum value of  $K_m$  at the uppermost grid points. In the lower boundary layer the molecular value (about  $0.15 \text{ cm}^2/\text{sec}$ ) can be used as the minimum value for  $K_m$ . When the top of the boundary layer is fixed at 2 or 3 km it is necessary generally to compute U and V in double precision in order to get a good value for  $K_m$ . However,  $K_m$ ,  $e$  and  $\ell$  have enough accuracy in single precision.

The next problem is to determine when the iteration procedure has been completed. This is done by comparing two successive iterative values of  $K_m$ . We could use a criteria expressing the minimum percentage that the difference between two successive iterative values must meet in order to have convergence. In our case this is not desirable because we are more likely to obtain much greater accuracy in the lower boundary layer than near the top of the boundary layer. If we used a percentage we would have to choose between either a fairly large percentage with a reasonable number of iterations or a small percentage and an unnecessarily large number of iterations. Therefore, it is better to use an absolute number of the order of 1 to  $10 \text{ cm}^2/\text{sec}$  as a criterion which would insure high accuracy in the region where it is desired, that is, in the lower and middle



boundary layer. We will probably have less accuracy in  $K_m$  near the top of the boundary layer but this has only a very small influence on the wind profile.

### B.5 Finite-Difference Equation for $K_t$ and $K_w$ .

As  $K_t$  and  $K_w$  are required in the time-dependent model they will be computed diagnostically from (B.5) which is transformed into

$$K_t(k) = K_w(k) = \left\{ B(5) \lambda(k) [A(10) + A(9)] \right\} / e^2(k) \quad (B.50)$$

### B.6 Finite-Difference Equations: Second Form.

The diffusion terms in the equations for U and V can be written in two forms. The first form uses (3.26) and (3.27) and has been discussed in the previous sections. The second form uses (3.26') and (3.27'), and it has the advantage of giving a reasonable profile of not only the mean wind but also of the stress. The second form should be used if the set (3.26') to (3.29') is used in the time-dependent model. The finite-difference expressions are much more stable near the top of the boundary layer when we use the second form. This permits a greater OMEGA near the top of the boundary layer and insures a faster convergence.

#### B.6.1 Equation for U.

The diffusion term in (3.26') can be expanded as,

$$\left[ \frac{\partial}{\partial y} \left( K_m \frac{\partial U}{\partial y} \frac{\partial y}{\partial z} \right) \right] \frac{\partial y}{\partial z} = \left[ \left( K_m \frac{\partial U}{\partial y} \frac{\partial y}{\partial z} \right) \Big|_{k+\frac{1}{2}} - \left( K_m \frac{\partial U}{\partial y} \frac{\partial y}{\partial z} \right) \Big|_{k-\frac{1}{2}} \right] \frac{\partial y}{\partial z} \quad (B.51)$$

In order to evaluate the stress at  $k+\frac{1}{2}$ , we recall that in



the surface layer

$$K_m \frac{\partial Y}{\partial z} \propto (\ell u_*) / (AC \ell) = \text{constant} \quad (\text{B.52})$$

Therefore, it seems justified to assume the following arithmetic average

$$XKMP = (K_m \frac{\partial Y}{\partial z}) \Big|_{k+\frac{1}{2}} = \frac{1}{2} [K_m(k+1) DELZ(k+1) + K_m(k) DELZ(k)] \quad (\text{B.53})$$

The vertical derivative of U is approximated by a finite-difference equation centered at  $k+\frac{1}{2}$

$$\frac{\partial U}{\partial Y} \Big|_{k+\frac{1}{2}} = U(k+1) - U(k) \quad (\text{B.54})$$

The stress is evaluated at  $k-\frac{1}{2}$  by the same procedure,

$$XKMM = (K_m \frac{\partial Y}{\partial z}) \Big|_{k-\frac{1}{2}} = \frac{1}{2} [K_m(k-1) DELZ(k-1) + K_m(k) DELZ(k)] \quad (\text{B.55})$$

$$\frac{\partial U}{\partial Y} \Big|_{k-\frac{1}{2}} = U(k) - U(k-1) \quad (\text{B.56})$$

The coefficient of  $U(k)$  is

$$A(3) = XKMP + XKMM \quad (\text{B.57})$$

We group all the terms except  $U(k)$  in

$$DU = XKMP U(k+1) + XKMM U(k-1) + F (V(k) - V_g) \quad (\text{B.58})$$

Finally,

$$U(k) = DU/A(3) \quad (\text{B.59})$$

### B.6.2 Equation for V.

The diffusion term in (3.27') is similar to the one in (3.26') with U being replaced by V. Therefore, it is sufficient to mention the resulting terms. All the terms except  $V(k)$  are grouped in

$$DV = XKMP V(k+1) + XKMM V(k-1) + F (U_g - U(k)) \quad (\text{B.60})$$



Finally,

$$V(k) = DV/A(3) \quad (B.61)$$



## APPENDIX C

### TIME-DEPENDENT ATMOSPHERIC EQUATIONS

#### C.1 Equations.

The basic equations for the time-dependent model in  $\gamma$ -coordinates are given in Section 3.3.1 and will not be repeated here. The equation for the mixing length  $\lambda$  and for its derivative with respect to  $\gamma$  have been derived in Section B.2. The discussion in Section B.3 about the vertical derivative of  $K_m$  in the steady-state model is also valid for the time-dependent model. However, in this case the thickness of the surface layer will vary according to the diurnal cycle and may be fairly small during the nocturnal inversion. Therefore, we should use (B.20) only up to the level expected to represent the top of the nearly-constant-stress layer during the nighttime.

#### C.2 Notation.

In our implicit finite-difference scheme all of the variables in the equations which are not differentiated with respect to time have to be evaluated at the two time steps  $t_o$  and  $t_o + \Delta t$ . This would imply repeating two nearly identical terms differing only in their time index. In our discussion we will outline how the calculations are done and write out these terms with a general time index  $t$ . The following arrays are frequently used:

A = expressions involving the atmospheric variables,

B = various constants,

C = expressions related to the computation of the surface tem-



perature,

D = expressions involving the atmospheric variables at the past time step  $t_0$ .

The variables starting with the letter D and containing at least three letters indicate a finite-difference approximation to a derivative. Termination with 1 implies the first derivative and termination with 2 implies the second derivative. For example,

$DU1$  = first derivative of U

$DT2$  = second derivative of  $\Theta$ .

The name of the variable being differentiated is found between D and 1 or 2. As the symbol  $\Theta$  is not generally available in FORTRAN, T has been substituted for it.

As pointed out in Section 3.3.2, the diffusion term can be expressed in two forms in  $\gamma$ -coordinates. Equations (3.26) to (3.29) involve differentiation of the coefficient of eddy diffusivity and the first and second derivatives of the mean quantities. This form leads to computational problems which are described in Section C.5. Equations (3.26') to (3.29') involve differentiation of the flux of the mean quantity with respect to  $\gamma$ . This second form gives a realistic variation of the flux in the vertical and is computationally more stable. Section C.3 uses the first form whereas Section C.4 uses the second form.

### C.3 Finite-Difference Equations: First Form.

#### C.3.1 Equation for U.

The basic equation is (3.26). The vertical derivative of  $K_m$  is evaluated as,



$$\frac{\partial K_m}{\partial \zeta} \Big|_t = DKM1 \Big|_t = \begin{cases} \frac{1}{2}(K_m(k+1,t) - K_m(k-1,t)) & \text{above the constant-flux layer} \\ \frac{K_m(k,t)}{2} \ln\left(\frac{K_m(k+1,t)}{K_m(k-1,t)}\right) & \text{in the constant-flux layer} \end{cases} \quad (C.1)$$

Other terms involved in the diffusion term are,

$$A(2) \Big|_t = \frac{1}{2} \left( \frac{\partial K_m}{\partial \zeta} \left( \frac{\partial \zeta}{\partial z} \right)^2 + K_m \frac{\partial^2 \zeta}{\partial z^2} \right) \Big|_t = \frac{1}{2} (DKM1 \Big|_t \text{DELZ2}(k) + K_m(k,t) \text{DELZ2}(k)) \quad (C.2)$$

$$A(1) \Big|_t = K_m \left( \frac{\partial \zeta}{\partial z} \right)^2 = K_m(k,t) \text{DELZ2}(k) \quad (C.3)$$

The ratio of these two coefficients is,

$$AA \Big|_t = A(2)/A(1) \Big|_t \quad (C.4)$$

The geostrophic and Coriolis terms become,

$$FAC = f(V - V_g) = \frac{1}{2}f(V(k, t_o) + V(k, t_o + \Delta t) - 2V_g) \quad (C.5)$$

The first and second derivative terms are,

$$DU1 \Big|_t = 2 \frac{\partial U}{\partial \zeta} = U(k+1,t) - U(k-1,t) \quad (C.6)$$

$$DU2 \Big|_t = \frac{\partial^2 U}{\partial \zeta^2} = U(k+1,t) - U(k,t) + U(k-1,t) - U(k,t) \quad (C.7)$$

The diffusion term at  $t_o$  is evaluated as,

$$D(k,1) = (DU2 \Big|_{t_o} + AA \Big|_{t_o} DU1 \Big|_{t_o}) \quad (C.8)$$

If we exclude  $U(k, t_o + \Delta t)$  in the diffusion term at  $t_o + \Delta t$ ,

we are left with,

$$DU \Big|_{t_o + \Delta t} = (U(k+1, t_o + \Delta t) + U(k-1, t_o + \Delta t) + (AA \text{ DU1}) \Big|_{t_o + \Delta t}) \quad (C.9)$$

The coefficient of  $U(k, t_o + \Delta t)$  is,

$$CST = 1/\Delta t + A(1) \quad (C.10)$$

Therefore, the expression for  $U(k, t_o + \Delta t)$  is,

$$U(k, t_o + \Delta t) = \left\{ U(k, t_o) / \Delta t + FAC + A(1) \left[ \frac{DU + D(k,1)}{2} \right] \right\} / CST \quad (C.11)$$



### C.3.2 Equation for V.

The equation for  $V$  is very similar to the one for  $U$ . Therefore, the coefficients of the diffusion term involved in (3.26) are the same ones as those involved in (3.25). The first and second derivative terms are:

$$DV_1 \Big|_t = 2 \frac{\partial V}{\partial y} = V(k+1,t) - V(k-1,t) \quad (C.12)$$

$$DV_2 \Big|_t = \frac{\partial^2 V}{\partial y^2} = V(k+1,t) - V(k,t) + V(k-1,t) - V(k,t) \quad (C.13)$$

The diffusion term at  $t_o$  becomes,

$$D(k,2) = (DV_2 \Big|_{t_o} + AA \Big|_{t_o} DV_1 \Big|_{t_o}) \quad (C.14)$$

A part of the diffusion term at  $t_o + \Delta t$  is,

$$DV \Big|_{t_o + \Delta t} = (V(k+1,t_o + \Delta t) + V(k-1,t_o + \Delta t) + (AA \cdot DV_1) \Big|_{t_o + \Delta t}) \quad (C.15)$$

The geostrophic and Coriolis terms are written as,

$$FAC = f(U_g - U) = \frac{1}{2}f \left\{ 2V_g - [V(k,t_o) + V(k,t_o + \Delta t)] \right\} \quad (C.16)$$

Finally,

$$V(k,t_o + \Delta t) = \left\{ V(k,t_o) / \Delta t + FAC + A(1) \left\{ [DV + D(k,2)] / 2 \right\} \right\} / CST \quad (C.17)$$

### C.3.3 Equation for $\Theta$ .

The derivative of  $K_t$  with respect to  $y$  is,

$$\frac{\partial K_t}{\partial y} \Big|_t = DKT_1 \Big|_t = \begin{cases} \frac{1}{2}(K_t(k+1,t) - K_t(k-1,t)) & \text{above the constant-flux layer} \\ \frac{K_t(k,t)}{2} \ln\left(\frac{K_t(k+1,t)}{K_t(k-1,t)}\right) & \text{in the constant-flux layer} \end{cases} \quad (C.18)$$

The coefficients involved in the diffusion term at  $t_o$  are,

$$A(6) \Big|_t = \frac{1}{2} \left( \frac{\partial K_t}{\partial y} \left( \frac{\partial \psi}{\partial z} \right)^2 + K_t \frac{\partial^2 \psi}{\partial z^2} \right) \Big|_t =$$

$$\frac{1}{2} (DKT_1 \Big|_t DELZ2(k) + K_t(k,t) DEL2Z(k)) \quad (C.19)$$



$$A(5) \Big|_t = K_t (\frac{\partial \psi}{\partial z})^2 = K_t(k,t) \text{DELZ2}(k) \quad (C.20)$$

The first and second derivatives of  $\psi$  with respect to  $z$  are,

$$DT1 \Big|_t = 2 \frac{\partial \psi}{\partial z} = \psi(k+1,t) - \psi(k-1,t) \quad (C.21)$$

$$DT2 \Big|_t = \frac{\partial^2 \psi}{\partial z^2} = \psi(k+1,t) - 2\psi(k,t) + \psi(k-1,t) \quad (C.22)$$

The diffusion term evaluated at  $t_o$  is,

$$D(k,3) = (DT2 \Big|_{t_o} + A(6)/A(5)DT1) \Big|_{t_o} \quad (C.23)$$

Part of the diffusion term at  $t_o + \Delta t$  can be written as,

$$DDT \Big|_{t_o + \Delta t} = \psi(k+1,t_o + \Delta t) + \psi(k-1,t_o + \Delta t) + [A(6)/A(5)DT1] \Big|_{t_o + \Delta t} \quad (C.24)$$

The coefficient of  $\psi(k,t_o + \Delta t)$  is,

$$CST2 = 1/\Delta t + A(5) \quad (C.25)$$

Therefore,

$$\psi(k,t_o + \Delta t) = \left\{ \psi(k,t_o)/\Delta t + A(5) [[DDT + D(k,3)]/2] \right\} / CST2 \quad (C.26)$$

#### C.3.4 Equation for Q.

The basic equation is (3.29). The vertical derivative of  $K_w$  is,

$$\frac{\partial K_w}{\partial z} \Big|_t = DKW1 \Big|_t = \begin{cases} \frac{1}{2}(K_w(k+1,t) - K_w(k-1,t)) & \text{above the constant-flux layer} \\ \frac{K_w(k,t)}{2} \ln(\frac{K_w(k+1,t)}{K_w(k-1,t)}) & \text{in the constant-flux layer} \end{cases} \quad (C.27)$$

The coefficients of the diffusion terms are,

$$A(9) \Big|_t = \frac{1}{2} \left( \frac{\partial K_w}{\partial z} (\frac{\partial \psi}{\partial z})^2 + K_w \frac{\partial^2 \psi}{\partial z^2} \right) \Big|_t = \frac{1}{2} (DKW1 \Big|_t \text{DELZ2}(k) + K_w(k,t) \text{DEL2Z}(k)) \quad (C.28)$$

$$A(8) = K_w (\frac{\partial \psi}{\partial z})^2 = K_w(k,t) \text{DELZ2}(k) \quad (C.29)$$

The first and second derivative terms become,



$$DQ1 \Big|_t = 2 \frac{\partial Q}{\partial \theta} = Q(k+1,t) - Q(k-1,t) \quad (C.30)$$

$$DQ2 \Big|_t = \frac{\partial^2 Q}{\partial \theta^2} = Q(k+1,t) - Q(k,t) + Q(k-1,t) - Q(k,t) \quad (C.31)$$

The diffusion term at  $t_o$  is,

$$D(k,4) = (DQ2 \Big|_{t_o} + (A(9)/A(8)) DQ1 \Big|_{t_o}) \quad (C.32)$$

The diffusion term at  $t_o + \Delta t$  can be written as follows when we exclude  $Q(k,t_o + \Delta t)$ ,

$$DDQ \Big|_{t_o + \Delta t} = Q(k+1,t_o + \Delta t) + Q(k-1,t_o + \Delta t) + (A(9)/A(8)) DQ1 \Big|_{t_o + \Delta t} \quad (C.33)$$

The coefficient of  $Q(k,t_o + \Delta t)$  is,

$$CST3 = 1/\Delta t + A(8) \quad (C.34)$$

Finally,

$$Q(k,t_o + \Delta t) = \left\{ Q(k,t_o) / \Delta t + A(8) \left[ [DDQ + D(k,4)] / 2 \right] \right\} / CST3 \quad (C.35)$$

### C.3.5 Equation for $e$ .

Equation (3.31) is the equation for  $e^2$ . We define some of the terms which are frequently used in the equations. The various derivatives of the mean quantities are called,

$$A(11) \Big|_t = 2 \left| \frac{\partial \bar{V}}{\partial z} \right|^2 = 2 \left( \left( \frac{\partial \bar{U}}{\partial z} \right)^2 + \left( \frac{\partial \bar{V}}{\partial z} \right)^2 \right) = \frac{1}{2} ((DU1)^2 + (DV1)^2) \Big|_t \quad DELZ2(k) \quad (C.36)$$

$$DTA \Big|_t = 2 \frac{\partial \bar{H}}{\partial z} = 2 DT1 \Big|_t \quad DELZ(k) \quad (C.37)$$

$$DQA \Big|_t = 2 \frac{\partial \bar{Q}}{\partial z} = 2 DQ1 \Big|_t \quad DELZ(k) \quad (C.38)$$

The covariances representing the heat flux and the flux of water vapor are, respectively,

$$WT \Big|_t = 2 \bar{w}\bar{e} = - K_t(k,t) DTA \quad (C.39)$$

$$WQ \Big|_t = 2 \bar{w}\bar{q} = - K_w(k,t) DQA \quad (C.40)$$



These two covariances can be combined through the concept of virtual temperature,

$$A(12) \Big|_t = 2 \frac{g}{T_o} \overline{w \theta_v} = B(21) WT + B(20) WQ \quad (C.41)$$

where,

$$B(21) = g/T_o \quad (C.42)$$

$$B(20) = 0.6078 \text{ g} \quad (C.43)$$

We define,

$$AF \Big|_t = e \lambda \Big|_t = e(k,t) \lambda(k,t) \quad (C.44)$$

The coefficients of the diffusion terms are,

$$A(13) \Big|_t = \frac{5x0.23}{3} e \lambda \left( \frac{\partial \gamma}{\partial z} \right)^2 = B(22) AF \Big|_t \text{ DELZ2}(k) \quad (C.45)$$

$$A(14) \Big|_t = \frac{1}{2} \left( e \lambda \Big|_t \frac{\partial^2 \gamma}{\partial z^2} + \frac{\partial e \lambda}{\partial \gamma} \left( \frac{\partial \gamma}{\partial z} \right)^2 \right) = \quad (C.46)$$

$$\frac{1}{2} \left\{ AF \text{ DELZ2}(k) + [ \lambda(k,t) DE \Big|_t + e(k,t) DL(k) ] \text{ DELZ2}(k) \right\}$$

where,  $DE \Big|_t = \frac{\partial e}{\partial \gamma} = \frac{1}{2}(e(k+1,t) - e(k-1,t)) \quad (C.47)$

$$DL(k) = \frac{\partial \lambda}{\partial \gamma} = \text{DELZZ}(k) / \lambda^2(k,t) \quad (C.48)$$

$$B(22) = \frac{5x0.23}{3} \quad (C.49)$$

The terms evaluated at  $t_o$  are grouped in,

$$D(k,5) = \left( \frac{\partial}{\partial z} (e \lambda \frac{\partial e}{\partial z}) + K_m \left| \frac{\partial \vec{V}}{\partial z} \right|^2 + \frac{g}{T_o} \overline{w \theta_v} + e^2 \left( 2/\Delta t - \frac{2e^3}{B_1 \lambda} \right) \right) \Big|_{t_o} = \\ (A(13) \text{ DE2} + A(14) \text{ DE1} + A(12)) \Big|_{t_o} + K_m(k,t_o) A(11) \Big|_{t_o} + e^2(k,t_o) (2/\Delta t \\ - B(24) e(k,t_o) / \lambda(k,t_o)) \quad (C.50)$$

The terms which are different from  $e^2(k,t_o + \Delta t)$  and which are evaluated at  $t_o + \Delta t$ , are,

$$A(16) = \left( \frac{5x0.23}{3} \left[ \frac{\partial}{\partial z} (e \lambda \frac{\partial e}{\partial z}) \right] + 2(K_m \left| \frac{\partial \vec{V}}{\partial z} \right|^2 + \frac{g}{T_o} \overline{w \theta_v}) \right) \Big|_{t_o + \Delta t} =$$

$$B(22) (A(13) \text{ DE2} + A(14) \text{ DE1}) + K_m(k,t) A(11) + A(12) \quad (C.51)$$



Finally,

$$E2T = e^2(k, t_o + \Delta t) = (D(k, 5) + A(16)) / [2(1/\Delta t + A(13)) \Big|_{t_o + \Delta t} + B(24) \\ e(k, t_o + \Delta t) / l(k, t_o + \Delta t)] \quad (C.52)$$

$$e(k, t_o + \Delta t) = (e^2(k, t_o + \Delta t))^{\frac{1}{2}} = \text{SQRT}(E2T) \quad (C.53)$$

### C.3.6 Computation of $\bar{\theta}^2$ .

Equation (3.32) is used. The coefficients of the diffusion term are similar to A(13) and A(14) which were derived for  $e^2$ . The only difference is that the constant B(22) has been replaced by 0.23. Therefore,

$$A'(13) \Big|_{\bar{\theta}^2} = 0.6 A(13) \Big|_{e^2} \quad (C.54)$$

$$A'(14) \Big|_{\bar{\theta}^2} = 0.6 A(14) \Big|_{e^2} \quad (C.55)$$

The first and second derivatives are respectively,

$$DT21 \Big|_t = 2 \left( \frac{\partial \bar{\theta}^2}{\partial y} \right) = \bar{\theta}^2(k+1, t) - \bar{\theta}^2(k-1, t) \quad (C.56)$$

$$DT22 \Big|_t = \left( \frac{\partial^2 \bar{\theta}^2}{\partial y^2} \right) = \bar{\theta}^2(k+1, t) - 2\bar{\theta}^2(k, t) + \bar{\theta}^2(k-1, t) - \bar{\theta}^2(k, t) \quad (C.57)$$

A term which is encountered in  $\bar{\theta}^2$ ,  $\bar{\theta}q$  and  $\bar{q}^2$ , is,

$$A(21) \Big|_{t_o} = 2(1/\Delta t - e/(l B_2)) \Big|_{t_o} = 2/\Delta t - B(26) e(k, t_o) / l(k, t_o) \quad (C.58)$$

where,

$$B(26) = 2/B_2 \quad (C.59)$$

The terms evaluated at the past time step  $t_o$  are,

$$D(k, 6) = (A'(13) DT22 + A'(14) DT21 - WT DQA/2) \Big|_{t_o} + \bar{\theta}^2(k, t_o) A(21) \Big|_{t_o} \quad (C.60)$$

The coefficient of  $\bar{\theta}^2(k, t_o + \Delta t)$  is,

$$A(18) = 2(1/\Delta t + A(13)) + B(26) e(k, t_o + \Delta t) / l(k, t_o + \Delta t) \quad (C.61)$$

The terms different from  $\bar{\theta}^2(k, t_o + \Delta t)$  at  $t_o + \Delta t$ , are,



$$A(19) = [A'(13) DT22 + A'(14) DT21 - WT DQA/2] \Big|_{t_0 + \Delta t} \quad (C.62)$$

Finally,

$$\bar{q^2}(k, t_0 + \Delta t) = (A(19) + D(k, 7)) / A(18) \quad (C.63)$$

### C.3.7 Computation of $\bar{q^2}$ .

The reference equation is (3.33) whose formulation is similar to (3.32). Therefore, the coefficients  $A'(13)$ ,  $A'(14)$ ,  $A(18)$  and  $A(21)$  remain unchanged. The first and second derivative terms are,

$$DQ21 \Big|_t = 2 \frac{\partial \bar{q^2}}{\partial y} = \bar{q^2}(k+1, t) - \bar{q^2}(k-1, t) \quad (C.64)$$

$$DQ22 \Big|_t = \frac{\partial^2 \bar{q^2}}{\partial y^2} = \bar{q^2}(k+1, t) - \bar{q^2}(k, t) + \bar{q^2}(k-1, t) - \bar{q^2}(k, t) \quad (C.65)$$

The terms which are evaluated at the past time step, are,  
 $D(k, 7) = (A'(13) DQ22 + A'(14) DQ21 - WQ DQA/2) \Big|_{t_0} + \bar{q^2}(k, t_0) A(21)$

(C.66)

We group together all the terms evaluated at  $t_0 + \Delta t$ , except  $\bar{q^2}(k, t_0 + \Delta t)$ .

$$A(22) = A'(13) DQ22 + A'(14) DQ21 - WQ DQA/2 \quad (C.67)$$

Therefore,

$$\bar{q^2}(k, t) = (A(22) + D(k, 7)) / A(18) \quad (C.68)$$

### C.3.8 Equation for $\bar{\theta q}$ .

Equation (3.34) is used for  $\bar{\theta q}$ . Again, the coefficients  $A'(13)$ ,  $A'(14)$ ,  $A(18)$  and  $A(21)$  are the same ones as derived for  $\bar{q^2}$ . The first and second derivatives are,



$$\text{DTQ1} \Big|_t = 2 \frac{\partial \overline{\theta q}}{\partial y} = \overline{\theta q}(k+1,t) - \overline{\theta q}(k-1,t) \quad (\text{C.69})$$

$$\text{DTQ2} \Big|_t = \frac{\partial^2 \overline{\theta q}}{\partial y^2} = \overline{\theta q}(k+1,t) - \overline{\theta q}(k,t) + \overline{\theta q}(k-1,t) - \overline{\theta q}(k,t) \quad (\text{C.70})$$

The terms evaluated at  $t_o$  are,

$$D(k,8) = (A'(13) \text{ DTQ2} + A'(14) \text{ DTQ1} - (WQ \text{ DTA} + WT \text{ DQA})/4) \Big|_{t_o} + \overline{\theta q}(k,t_o) A(21) \Big|_{t_o} \quad (\text{C.71})$$

The term at  $t_o + \Delta t$  which is equivalent to  $D(k,8)$ , is,

$$A(22) = (A'(13) \text{ DTQ2} + A'(14) \text{ DTQ1} - (WQ \text{ DTA} + WT \text{ DQA})/4) \Big|_{t_o + \Delta t} \quad (\text{C.72})$$

The final result is that,

$$\overline{\theta q}(k,t_o) = (A(22) + D(k,8))/A(18) \quad (\text{C.73})$$

### C.3.9 Equation for $K_m$ .

Equation (3.35) is the equation for  $K_m$ . We will drop the time index for the next three sections because the coefficients of diffusivity  $K_m$ ,  $K_t$  and  $K_w$  are evaluated diagnostically at the time step  $t_o + \Delta t$ . Some terms are common to all three coefficients of eddy diffusivity and are,

$$AG = e^3 = e^2(k) e(k) \quad (\text{C.74})$$

$$A(23) = 4 A_1 \int \frac{\partial}{\partial z} (e \int \frac{\partial e^2}{\partial z}) \quad (\text{C.75})$$

When we use the results which we have obtained in the previous sections, we can rewrite (C.75) as,

$$A(23) = B(31) (A'(13) DE2 - 2 e^2(k) + A'(14) DE1) \int(k) \quad (\text{C.76})$$

where,  $B(31) = 4 A_1 \quad (\text{C.77})$



Also,

$$AR = B(5) \lambda(k) \quad (C.78)$$

where,

$$B(5) = A_1 \quad (C.79)$$

The numerator in (3.35) is expanded as,

$$A(24) = AR (B(28) AG + A(23) + (B(43) WT + B(45) WQ)) \lambda(k) \quad (C.80)$$

where,

$$B(28) = 1 - 3C_1 \quad (C.81)$$

$$B(43) = \frac{21}{2} \frac{A_1}{T_0} g \quad (C.82)$$

$$B(45) = \frac{21}{2} A_1 0.6078 g \quad (C.83)$$

The denominator is,

$$A(25) = e^2(k,t) + B(47) (A(11) + 1.5 (B(21) DTA + B(20) DQA)) \lambda^2(k) \quad (C.84)$$

where,

$$B(47) = 3 A_1^2 \quad (C.85)$$

Finally,

$$K_m(k) = A(24)/A(25) \quad (C.86)$$

### C.3.10 Equation for $K_t$ .

Equation (3.36) is appropriate for  $K_t$ . A term common to both  $K_t$  and  $K_w$  is,

$$\begin{aligned} AX &= e^3 + 4 A_1 0.23 \lambda \frac{\partial}{\partial z} (e \lambda \frac{\partial e^2}{\partial z}) - 6 A_1 \lambda K_m \left| \frac{\partial V}{\partial z} \right|^2 \\ &= AG + A(23) - B(36) \lambda(k) K_m(k) A(11) \end{aligned} \quad (C.87)$$

where,

$$B(36) = 3 A_1 \quad (C.88)$$

The numerator in (3.36) is,

$$A(26) AR = AR (AX + B(46) WQ \lambda(k) - 6 \lambda(k) (B(21) \bar{\theta}^2(k) + B(20) \bar{\theta} q(k))) / DTA \quad (C.89)$$

where,

$$B(46) = 6 A_1 0.6078 g \quad (C.90)$$



The denominator becomes,

$$A(27) = e^2(k) + B(58) DTA \lambda^2(k) \quad (C.91)$$

where,

$$B(58) = 6A_1^2 g/T_0 \quad (C.92)$$

Therefore,

$$K_t(k) = AR A(26)/A(27) \quad (C.93)$$

### C.3.11 Equation for $K_w$ .

Equation (3.37) is used for  $K_w$ . The numerator can be expressed as,

$$A(28) AR = AR \left\{ AX + B(63) \lambda(k) WT - 6 e(k) [B(21) \overline{\theta q}(k) + B(20) \overline{q^2}(k)] / DQA \right\} \quad (C.94)$$

where,

$$B(63) = 6 A_1 g/T_0 \quad (C.95)$$

The denominator is,

$$A(29) = e^2(k) + B(33) \lambda^2(k) DQA \quad (C.96)$$

Finally,

$$K_w(k) = AR A(28)/A(29)$$



#### C.4 Finite-Difference Equations: Second Form.

##### C.4.1 Equation for U.

The diffusion term in (3.26') is expanded as,

$$\frac{\partial}{\partial y} \left( K_m \frac{\partial U}{\partial y} \frac{\partial U}{\partial z} \right) \frac{\partial U}{\partial z} = \left[ \left( K_m \frac{\partial U}{\partial y} \frac{\partial U}{\partial z} \right) \Big|_{k+\frac{1}{2}} - \left( K_m \frac{\partial U}{\partial y} \frac{\partial U}{\partial z} \right) \Big|_{k-\frac{1}{2}} \right] \frac{\partial U}{\partial z} \quad (\text{C.97})$$

In order to evaluate the stress at  $k + \frac{1}{2}$ , we recall that in the surface layer,

$$K_m \frac{\partial U}{\partial z} \propto (\ell u_s) / (AC\ell) = \text{constant} \quad (\text{C.98})$$

Therefore, it seems justified to assume the following arithmetic average,

$$2 XKMP \Big|_t = \left( K_m \frac{\partial U}{\partial z} \right) \Big|_{k+\frac{1}{2}, t} = \frac{1}{2} [K_m(k+1, t) DELZ(k+1) + K_m(k, t) DELZ(k)] \quad (\text{C.99})$$

The vertical derivative of U is approximated by a finite-difference equation centered at  $k + \frac{1}{2}$ ,

$$\frac{\partial U}{\partial y} \Big|_{k+\frac{1}{2}, t} = U(k+1, t) - U(k, t) \quad (\text{C.100})$$

The stress is evaluated at  $k - \frac{1}{2}$  by the same procedure,

$$2 XKMM \Big|_t = \left( K_m \frac{\partial U}{\partial z} \right) \Big|_{k-\frac{1}{2}, t} = \frac{1}{2} [K_m(k-1, t) DELZ(k-1) + K_m(k, t) DELZ(k)] \quad (\text{C.101})$$

$$\frac{\partial U}{\partial y} \Big|_{k-\frac{1}{2}, t} = U(k, t) - U(k-1, t) \quad (\text{C.102})$$

We group all the results and obtain,

$$\frac{1}{2} \frac{\partial}{\partial z} \left( K_m \frac{\partial U}{\partial z} \right) \Big|_t = DELZ(k) [U(k+1, t) XKMP - U(k, t)(XKMM + XKMP) + U(k-1, t) XKMM] \quad (\text{C.103})$$

We will use the same finite-difference scheme as described in Section 3.4.2. As a result, we group the expressions evaluated at



the past time step in  $D(k,1)$ ,

$$D(k,1) = \text{DELZ}(k) \left\{ [U(k+1, t_o) - U(k, t_o)] \text{XKMP} \Big|_{t_o} + [U(k-1, t_o) - U(k, t_o)] \text{XKMM} \Big|_{t_o} + F[V(k, t_o)/2 - V_g] \right\} \quad (\text{C.104})$$

The coefficient of  $U(k, t_o + \Delta t)$  is,

$$\text{CST} = 1/\Delta t + (\text{XKMP} + \text{XKMM}) \Big|_{t_o + \Delta t} \text{DELZ}(k) \quad (\text{C.105})$$

Finally,

$$U(k, t_o + \Delta t) = \left\{ [\text{XKMP} \Big|_{t_o + \Delta t} U(k+1, t_o + \Delta t) + \text{XKMM} \Big|_{t_o + \Delta t} U(k-1, t_o + \Delta t)] \text{DELZ}(k) + D(k, 1) - F[V(k, t_o + \Delta t)/2 + U(k, t_o)/\Delta t] \right\} / \text{CST} \quad (\text{C.106})$$

The mathematical expressions could have been condensed but the condensed expressions would not minimize the round-off errors as well as the expanded version of the equations. In Section C.6 we will discuss in some detail the problem of round-off errors in the determination of the profile of the mean quantities.

#### C.4.2 Equation for V.

The diffusion term in (3.27') is similar to the one in (3.26') with  $U$  being replaced by  $V$ . Therefore, it is sufficient to mention the resulting terms. The expressions evaluated at  $t_o$  are,

$$D(k,2) = \text{DELZ}(k) \left\{ [V(k+1, t_o) - V(k, t_o)] \text{XKMP} \Big|_{t_o} + [V(k-1, t_o) - V(k, t_o)] \text{XKMM} \Big|_{t_o} + F[U_g - U(k, t_o)/2] \right\} \quad (\text{C.107})$$

Consequently,

$$V(k, t_o + \Delta t) = \left\{ [\text{XKMP} \Big|_{t_o + \Delta t} V(k+1, t_o + \Delta t) + \text{XKMM} \Big|_{t_o + \Delta t} V(k-1, t_o + \Delta t)] \text{DELZ}(k) + D(k, 2) - F[U(k, t_o + \Delta t)/2 + V(k, t_o)/\Delta t] \right\} / \text{CST} \quad (\text{C.108})$$



### C.4.3 Equation for $\Theta$ .

The diffusion term involved in (3.28') is similar to the one in (3.26') if we replace  $U$  by  $\Theta$ , and  $K_m$  by  $K_t$ . Therefore, parts of the heat-flux terms are,

$$2 \cdot XKTM|_t = (K_t \frac{\partial \Theta}{\partial z})|_{k-\frac{1}{2}, t} = \frac{1}{2} [K_t(k-1, t) \text{DELZ}(k-1) + K_t(k, t) \text{DELZ}(k)] \quad (\text{C.109})$$

$$2 \cdot XKTP|_t = (K_t \frac{\partial \Theta}{\partial z})|_{k+\frac{1}{2}, t} = \frac{1}{2} [K_t(k+1, t) \text{DELZ}(k+1) + K_t(k, t) \text{DELZ}(k)] \quad (\text{C.110})$$

When we use the centered finite-difference approximation to the  $\ell_y$ -derivative of  $\Theta$ , we obtain,

$$\frac{1}{2} \left( \frac{\partial}{\partial z} K_t \frac{\partial \Theta}{\partial z} \right)|_t = \text{DELZ}(k) [\Theta(k+1, t) \cdot XKTP|_t - \Theta(k, t) (XKTP + XKTM)|_t + \Theta(k-1, t) \cdot XKTM|_t] \quad (\text{C.111})$$

The expressions computed at the past time step are grouped into,

$$D(k, 3) = \text{DELZ}(k) \left\{ [\Theta(k+1, t_o) - \Theta(k, t_o)] \cdot XKTP|_{t_o} + [\Theta(k-1, t_o) - \Theta(k, t_o)] \cdot XKTM|_{t_o} \right\} \quad (\text{C.112})$$

The coefficient of  $\Theta(k, t_o + \Delta t)$  is,

$$\text{CST2} = 1 / \Delta t + (XKTM + XKTP)|_{t_o + \Delta t} \text{DELZ}(k) \quad (\text{C.113})$$

Finally,

$$\Theta(k, t_o + \Delta t) = \Theta(k, t_o) \left\{ \left[ (XKTP|_{t_o + \Delta t} (\Theta(k+1, t_o + \Delta t) / \Theta(k, t_o)) + XKTM|_{t_o + \Delta t} (\Theta(k-1, t_o + \Delta t) / \Theta(k, t_o))) \right] \text{DELZ}(k) \right\} / \text{CST2} \quad (\text{C.114})$$

### C.4.4 Equation for $Q$ .

Equation (3.29') is similar to (3.28') if we replace  $K_t$  by  $K_w$ , and  $\Theta$  by  $Q$ . Therefore, parts of the water-vapor-flux terms are,



$$2 \text{ XKWP} \Big|_t = (K_w \frac{\partial Q}{\partial z}) \Big|_{k+\frac{1}{2}, t} = \frac{1}{2} [K_w(k+1, t) \text{ DELZ}(k+1) + K_w(k, t) \text{ DELZ}(k)] \quad (\text{C.115})$$

$$2 \text{ XKWM} \Big|_t = (K_w \frac{\partial Q}{\partial z}) \Big|_{k-\frac{1}{2}, t} = \frac{1}{2} [K_w(k-1, t) \text{ DELZ}(k-1) + K_w(k, t) \text{ DELZ}(k)] \quad (\text{C.116})$$

The diffusion term can be expressed as,

$$\frac{1}{2} \left( \frac{\partial}{\partial z} K_w \frac{\partial Q}{\partial z} \right) \Big|_t = \text{DELZ}(k) [Q(k+1, t) \text{ XKWP} \Big|_t - Q(k, t)(\text{XKWP} + \text{XKWM}) \Big|_t \\ + Q(k-1, t) \text{ XKWM} \Big|_t] \quad (\text{C.117})$$

in which the centered finite-difference approximation has been used to evaluate the  $\gamma$ -derivative of  $Q$ . The expressions computed at  $t_o$  are,

$$D(k, 4) = \text{DELZ}(k) \left\{ [Q(k+1, t_o) - Q(k, t_o)] \text{ XKWP} \Big|_{t_o} + [Q(k-1, t_o) - Q(k, t_o)] \text{ XKWM} \Big|_{t_o} \right\} \quad (\text{C.118})$$

The coefficient of  $Q(t_o + \Delta t)$  is,

$$\text{CST3} = 1/\Delta t + (\text{XKWP} + \text{XKWM}) \Big|_{t_o} \text{ DELZ}(k) \quad (\text{C.119})$$

Finally,

$$Q(k, t_o + \Delta t) = \left[ [\text{XKWP} \Big|_{t_o + \Delta t} Q(k+1, t_o + \Delta t) + \text{XKWM} \Big|_{t_o + \Delta t} Q(k-1, t_o + \Delta t)] \text{ DELZ}(k) + D(k, 4) + Q(k, t_o)/\Delta t \right] / \text{CST3} \quad (\text{C.120})$$

#### C.4.5 Other Equations.

The other equations are left unchanged and can be found from Section C.3.5 to Section C.3.11.



### C.5 Computational Problems.

In this section we will deal with the computational problems associated with the first form of the diffusion term. We will discuss only the problems encountered with (3.28) for the following reasons:

- 1) The computation of the temperature profile is the most sensitive to these problems.
- 2) The equation for  $\Theta$  is simpler to analyse than the ones for  $U$  and  $V$  because it does not involve Coriolis or pressure-gradient forces.
- 3) The derived conclusions from the analysis of  $\Theta$  are applicable to the other 3 main quantities because of the similitude of the equations.

Therefore, it is sufficient to analyse the behavior of the equation for  $\Theta$ . Another simplifying assumption in the analysis is the use of the forward-in-time finite-difference approximation to (3.28) instead of the finite-difference approximation used in our equations and described in section 3.4.2. Therefore,

$$\frac{\partial A}{\partial t} = f \quad (\text{C.121})$$

will be approximated in our discussion by,

$$A(t_0 + \Delta t) = A(t_0) + \Delta t f(t_0 + \Delta t) \quad (\text{C.122})$$

The reasons for that simplification are:

- 1) The finite-difference equation becomes simpler as it involves roughly only half the number of terms required by the other time-finite-difference approximation.
- 2) The conclusions which will be drawn from our discussions are almost immediately applicable to the actual finite-difference equations used in the program if we look into the effect caused by two consecutive



time steps.

#### C.5.1. Formation of Artificial Inversions: Case of no Real Inversion.

The inversion can be generated only by the earth's surface in our model because the temperature at the top of the boundary layer is kept fixed at all times. The top of the inversion will be carried upward with the help of turbulent diffusion. The diurnal temperature cycle has only one maximum and one minimum per day because we neglect advection and cloud formation. The model is started from neutral stability at the time of maximum temperature. Therefore, the earth's surface will cool down for the first few hours creating a stable layer throughout the atmosphere without any inversion. If the model develops any inversion, this will be caused by numerical problems. The model ran smoothly until we obtained a region where  $K_t$  was varying rapidly due to the increasing stability, and this caused the formation of an unstable layer on top of the surface-based stable layer. This behavior caused a deterioration of the model and ultimately caused divergence of the results. The finite-difference version of (3.28) becomes, when we neglect the time-derivative term,

$$\Theta(k) = \frac{(A(1) + A(2))\Theta(k+1) + (A(1) - A(2))\Theta(k-1)}{2 A(1)} \quad (\text{C.123})$$

where,  $A(1) = K_t(k) \text{ DELZ2}(k)$ , associated with the second derivative,

and  $A(2) = K_t \frac{\partial^2 \psi}{\partial z^2} + \frac{\partial K_t}{\partial \psi} \left( \frac{\partial \psi}{\partial z} \right)^2$ , associated with the first derivative of  $\Theta$  with respect to  $\psi$ .

If we restrict  $K_t$  to non-negative values, then  $A(1)$  is always positive. However,  $A(2)$  can be of either sign depending on the sign of the  $\psi$ -derivative of  $K_t$ . Some possibilities are,



Case 1:  $A(2) = A(1)$

In this case we have:  $\Theta(k) = \Theta(k+1)$

Case 2:  $A(2) = 0$

Now, we obtain:  $\Theta(k) = \frac{\Theta(k+1) + \Theta(k-1)}{2}$

Case 3:  $A(2) = -A(1)$

This implies:  $\Theta(k) = \Theta(k-1)$

Therefore, for

$$A(2) \in [-A(1), A(1)]$$

we have,  $\Theta(k) \in [\Theta(k-1), \Theta(k+1)]$

where  $\in$  signifies that the term on the left-hand side is within the range defined by the terms inside the brackets on the right-hand side.

Conversely if  $A(2)$  is not in the above-defined range, then  $\Theta(k)$  is computed outside the range  $[\Theta(k-1), \Theta(k+1)]$ . This means that the diffusion term which normally tends to smooth out any temperature gradient, would increase the temperature gradient if certain conditions are met. We will derive the conditions under which such nonphysical results are obtained from the finite-difference scheme. Mathematically,  $A(2) > |A(1)|$  implies that,

$$\frac{\partial \ln K_t}{\partial y} \geq \left| 2 - \frac{\partial^2 y / \partial z^2}{\frac{\partial y}{\partial z}} \right|^2 \quad (\text{C.124})$$

Equation (C.124) can be put into a finite-difference formula and, for the grid usually used in our simulations, requires a variation in  $K_t$  of an order of magnitude between two successive grid points. Excessive cooling or warming will be computed whenever condition (C.124) is met. This problem can be partly cured by imposing that  $A(2) \leq |A(1)|$  at all time steps. But this is an arbitrary assumption



which interferes with the computational scheme. The inclusion of the time derivative term adds very little, and the condition  $A(2) < |A(1)|$  insures now that,

$$\Theta(k, t_0 + \Delta t) \in [\Theta(k, t_0), \Theta(k-1, t_0 + \Delta t), \Theta(k+1, t_0 + \Delta t)] \quad (C.125)$$

#### C.5.2. Blocking of the Height of the Daytime Inversion.

Another problem related to the use of (3.28) appears a few hours after sunrise when the inversion height, after rising relatively well, suddenly refuses to move higher than about 50 m. This produces a very unstable surface layer capped by a very stable layer. The causes for that behavior are a complex interaction between  $K_t$ ,  $\overline{\theta^2}$  and  $\Theta$ .

1.  $K_t$  depends strongly on the sign of the temperature gradient. A small value of  $K_t$  is obtained in stable cases and a large one in unstable cases. The difference in sign of the temperature gradient means usually a few orders of magnitude difference in the computed value of  $K_t$ .

2.  $\overline{\theta^2}$  should nearly vanish whenever the temperature gradient decreases to a very small value. Below the inversion, in the unstable region,  $\overline{\theta^2}$  is relatively large. In the stable region above the inversion,  $\overline{\theta^2}$  is again important where the temperature gradient is large. Therefore, we expect a minimum in  $\overline{\theta^2}$  at the inversion. However, the value of this minimum becomes dominated by the diffusion term and the time-dependent terms in (3.32) and no longer by the temperature gradient term. That means that  $\overline{\theta^2}$  does not vanish in the limit of a very small temperature gradient.



3. The equation for  $\bar{H}$  is not solved in terms of the vertical variation of the heat flux. Consequently, the computed temperature profile cannot force alone the lifting of the inversion height, but permits very often the existence of a very unstable layer capped off by a very stable layer.

In the equation for  $K_t$  the product  $\bar{\theta}^2 \frac{\partial \bar{H}}{\partial z}$  appears. Near the inversion,  $\bar{\theta}^2$  is larger than expected from the limit  $\Delta \bar{H} \rightarrow 0$  and  $\frac{\partial \bar{H}}{\partial z}$  is positive. This gives a very small value to  $K_t$ , which in turns prevents the lifting of the inversion height. In order to lift the inversion height we would need  $\Delta \bar{H} < 0$ , which causes large values for  $\bar{\theta}^2$  and  $K_t$ . This would maintain the inversion height at a relatively high position. The computational scheme seems to be able to lift the inversion height under some conditions which are not always met. One way of curing the problem is to neglect the time-dependent and the diffusion terms in (3.32) near the inversion height. This allows a smaller value for  $\bar{\theta}^2 \frac{\partial \bar{H}}{\partial z}$  near the inversion height, which permits a larger value for  $K_t$  and which ultimately will lead to the lifting of the inversion height. However, this method of solving the problem can initiate some oscillations caused by the variations in  $\bar{\theta}^2$  because we are using two different formulas to compute  $\bar{\theta}^2$ . Therefore, convergence is not readily insured at each time step.



## C.6 Refinements to the Finite-Difference Equations.

### C.6.1 Double Precision.

Near the top of the boundary layer, the mean atmospheric variables vary slowly both in the vertical and in time. However, the coefficients of eddy diffusivity and the other turbulent quantities vary appreciably in that region and their exact value depend to a great extent on the gradient of the mean atmospheric variables. Therefore, in order to get a good estimate of the turbulent quantities we need a fairly accurate evaluation of the mean variables. This implies that double precision is generally needed for  $U$ ,  $V$ ,  $H$  and  $Q$  whereas single precision is probably always sufficient for all of the other atmospheric variables. The great inconvenience of double precision is that it requires 2 to 4 times the computing time of single precision. Consider a specific example in which we assign 7 decimal digits to single precision and 14 decimal digits to double precision. We define an elementary operation as the operation between two digits. We will compare the number of elementary operations required for addition and multiplication in single precision with the number of similar operations in double precision. We consider two numbers  $A$  and  $B$  which consist of  $n$  digits each,

$$A = x_1 x_2 \cdots x_n \quad (C.126)$$

$$B = y_1 y_2 \cdots y_n \quad (C.127)$$

The addition  $A+B$  involves  $n$  elementary addition of the type  $x_i+y_i$ . If  $x_n+y_n > 10$  we add 1 to  $x_{n-1}$ . There is on the average a 50% probability that this additional operation has to be done. Therefore, an addition requires  $3 n/2$  elementary operations.



Table 10. Average number of elementary operations for addition and multiplication in single and double precision when we use the decimal system.

precision operation	single 7 digits	double 14 digits
addition	10	21
multiplication	126	509

Table 11. Average number of elementary operations for addition and multiplication in single and double precision when we use the binary system.

precision operation	single 7 digits	double 14 digits
addition	9	18
multiplication	102	399



By similar reasoning we can estimate that an average multiplication will require about  $[(n-1)^2 + n^2]3/2$  elementary operations. Table 10 compares the number of elementary operations required in single precision and in double precision for the operations of addition and the operations of multiplication in the decimal system. Table 11 does the same comparison in the binary system. The most important conclusion which can be drawn is that addition requires only about twice as much computing in double precision with respect to single precision, whereas multiplication in double precision needs at least 4 times the computing time of a single precision multiplication. Therefore, if we want to save computing time, we should try to reduce the number of multiplications which are done in double precision. For example the temperature difference  $\Theta(k+1) - \Theta(k-1)$  is computed in double precision and the resulting value is put in a single precision variable DT1. This temperature difference is needed, for example, in the computation of some of the turbulent variables. By using DT1 we do not lose any significant information and we gain by reducing the number of computations performed in double precision.

#### C.6.2 Minimization of Round-Off Errors.

The round-off errors can be very important near the top of the boundary layer. During some numerical experiments these have been observed to add up consistently. This effect was most visible on the temperature profile which showed an increasingly large temperature gradient between the top two grid points. When the computations were done in single precision this was enough to prevent the convergence of the model. In double precision the problem is somewhat



reduced but problems can arise if the model is run long enough. Therefore, it seems important to devise a finite-difference scheme which reduces the possible round-off errors. This is achieved mostly by being careful in choosing the order of the operations inside an expression. We will take the example of a constant isentropic atmosphere, for which a round-off error will mean a deviation from the constant value. Ordinarily the computer transforms the decimal numbers into hexadecimal numbers. There are a few operations in real number arithmetics which should not give any round-off errors. These are

- 1- The hexadecimal representation of a small real decimal number without any decimal part is exact. For example 3. would have an exact hexadecimal representation whereas  $0.3 \times 10^1$  would not.
- 2- The difference  $A - A = 0.$  exactly.
- 3- The division  $A/A = 1.$  exactly.
- 4- The sum  $A + 0. = A$  exactly.
- 5- The operations  $A \times 1 = A$  and  $A \div 1 = A$  exactly.
- 6- The addition or subtraction of two small real numbers without any decimal part is exact.

There are other operations which may give round-off errors:

- 1- The multiplication between two real numbers A and B, followed by the division by B, gives A with a round-off error.  $(A \times B)/B = A + \text{round-off error.}$  This round-off error could be prevented by changing the order of the operations:  $A \times (B/B) = A \times (1) = A$  without round-off error.
- 2- The operation  $(A + A)/A$  gives 2 with a round-off error. This can be cured by  $(A/A + A/A) = 1. + 1. = 2.$  exactly.



We go back to (C.26) in which  $D(k,3)$  is identically zero for a constant-temperature profile because  $DT1|_{t_0}$  and  $DT2|_{t_0}$  are exactly zero according to operation 2 which is the difference between two equal numbers. We note that  $DT1|_{t_0 + \Delta t}$  is also identically zero for the same reason. We are left with

$$\textcircled{H}(k, t_0 + \Delta t) = \left[ \textcircled{H}(k, t_0) / \Delta t + A(5) \left\{ \frac{1}{2} [\textcircled{H}(k+1, t_0 + \Delta t) + \textcircled{H}(k-1, t_0 + \Delta t)] \right\} \right] / [1 / \Delta t + A(5)]$$

The operation  $\frac{1}{2}[\textcircled{H}(k+1, t_0 + \Delta t) + \textcircled{H}(k-1, t_0 + \Delta t)]$  may or may not give a round-off error in the case of an isentropic atmosphere. For example, we suppose a four-digit accuracy and  $\textcircled{H} = 501.3$ . The real sum is 1002.6 which is transformed in four-digit accuracy into 1003. with a round-off error of 0.4. The subsequent division by 2 yields 501.5 with a round-off error of 0.2. However if  $\textcircled{H} = 301.3$ , the sum is 602.6 and the divison by 2 gives back 301.3 with no round-off errors. Therefore, we suppose temporarily that there is no round-off errors for that operation. We have the ratio

$$\textcircled{H} = \frac{\textcircled{H}/\Delta t + A(5) \textcircled{H}}{1/\Delta t + A(5)}$$

The operation  $\textcircled{H}/\Delta t$  and  $A(5)\textcircled{H}$  are very likely to have round-off errors as well as the subsequent addition. Therefore, that formulation is very likely to give rise to round-off errors. However, if we rearrange the terms as,

$$\textcircled{H} = \textcircled{H} \left[ \frac{1/\Delta t + A(5)}{1/\Delta t + A(5)} \right]$$

The factor  $1/\Delta t + A(5)$  is common to both the denominator and the numerator and will give some answer B with round-off errors with respect to the true solution. This is not important as  $B/B = 1$  without any round-off error, and  $\textcircled{H}$  is computed without any round-off



error. Therefore, the best finite-difference equation isolates and factor A(5). Equation (C.26) is rewritten as

$$\begin{aligned} \textcircled{H}(k, t_0 + \Delta t) = & \textcircled{H}(k, t_0) \left\{ (1/\Delta t + A(5)) \left[ \frac{\text{DDT}/\textcircled{H}(k, t_0) + D(k, 3)/\textcircled{H}(k, t_0)}{2} \right] \right. \\ & \left. / (1/\Delta t + A(5)) \right\} \end{aligned}$$

We have noted that in actual numerical tests  $\text{DDT}/\textcircled{H}(k, t_0)$  gave exactly 2. with no round-off errors. This implies that there is no need to extend the division inside DDT. The rearrangement of the terms is effected for all the other finite-difference equations for the mean quantities.

#### C.6.3 Higher-Order Approximation to the Derivatives.

In Section 3.4 we have devised finite-difference approximations to the first and second derivatives which were more exact by an order of approximation in the Taylor Series. As pointed out previously there is no need for the improved and time-consuming second-order approximation to the derivatives in the regions where the atmospheric variables are varying gently, namely in the surface layer and in the upper boundary layer. The higher-order approximation is optional in the time-dependent model and is used in the region determined by the range  $[m(4), m(3)]$ , where  $m$  is an integer variable used in the program.

#### C.6.4 Restriction on the Temperature Profile.

As noted in Section C.5, (3.28) has a tendency to create many stable-unstable transitions. We can devise limits to the temperature at each grid point based on the principle that there is no internal energy source term and that warming and cooling can only



come from the other levels. In the program we have called

$$D(k_o, 10) = \Theta(k_o+1, t_o) - \Theta(k_o, t_o)$$

which represents the stability at the past time step above the grid point  $k_o$ . At the actual time step, the stability around  $k_o$  is defined by

$$\text{SIGN} = \Theta(k_o+1, t_o + \Delta t) - \Theta(k_o-1, t_o + \Delta t)$$

From the knowledge of these two variables we want to impose a restriction on  $\Theta(k_o, t_o + \Delta t)$ . As an example, we suppose that  $D(k_o, 10)$  is positive, which implies stability above the grid point  $k_o$  at the past time step. If SIGN is also positive, that implies that the layer around  $k_o$  at the actual time step is also stable. The restriction to  $\Theta(k_o, t_o + \Delta t)$  is to impose the condition that it must be smaller than  $\Theta(k_o+1, t_o + \Delta t)$ . Only when  $\Theta(k_o-1, t_o)$  is greater than  $\Theta(k_o, t_o)$  is it possible to expect that the restriction interferes with a real change in stability. But this case is certainly rare as it would require very rapid changes in the surface temperature. We tabulate all the possible combinations of  $D(k_o, 10)$  with SIGN and the restriction imposed on  $\Theta(k_o, t_o + \Delta t)$  in Table 12. This restriction on the temperature is optional in the time-dependent model. It can be imposed for any layer that we wish, it can be done during the computations at each grid point or after a complete iteration has been completed. Whenever the restriction is imposed, we reset  $\Theta(k_o, t_o + \Delta t)$  within the range  $[\Theta(k_o+1, t_o + \Delta t), \Theta(k_o-1, t_o + \Delta t)]$ .



Table 12. Restriction on  $\mathbb{H}(k_o, t_o + \Delta t)$ . We define:

$$D(k_o, 10) = \mathbb{H}(k_o + 1, t_o) - \mathbb{H}(k_o, t_o)$$

and

$$\text{SIGN} = \mathbb{H}(k_o + 1, t_o + \Delta t) - \mathbb{H}(k_o - 1, t_o + \Delta t)$$

$D(k_o, 10)$ SIGN	positive	negative
positive	$< \mathbb{H}(k_o + 1, t_o + \Delta t)$	$> \mathbb{H}(k_o - 1, t_o + \Delta t)$
negative	$< \mathbb{H}(k_o - 1, t_o + \Delta t)$	$> \mathbb{H}(k_o + 1, t_o + \Delta t)$



## APPENDIX D

### INFRARED FLUX DUE TO WATER VAPOR

#### D.1 Hypotheses.

The following hypotheses are made in order to simplify the computational task:

Hypothesis 1: the pressure at the roughness height is constant at all times. This implies that the pressure at the top of the boundary layer will vary.

Hypothesis 2: we neglect the infrared flux emitted by the layer between  $z_0$  and the ground. This layer is fairly thin and the infrared flux received at the earth's surface is not modified sensibly by neglecting the contribution from that layer.

Hypothesis 3: the layer above the boundary layer is not modelled and we neglect the infrared flux coming from that layer. That assumption is justified by the relatively rapid decrease in the mixing ratio with height and by the fact that most of the infrared flux emitted by water vapor and received at the ground is emitted in the lowest 100 meters of the boundary layer.

Hypothesis 4: only the mean infrared flux will be considered and consequently we will use only the mean atmospheric variables in our computations.

Hypothesis 5: the hydrostatic equation will be used to compute the mean pressure.



### D.2 Computation of Temperature.

In the computation of the infrared radiation we need the temperature which can be obtained from the definition of potential temperature. In index form we have

$$T(k) = \Theta(k) \left[ \frac{P(k)}{P_0} \right]^K \quad (D.1)$$

where  $K = R/C_p$  and  $P_0$  = reference pressure = 1000 mb.

### D.3 Computation of Pressure.

We use the hydrostatic approximation

$$\frac{\partial P}{\partial z} = - \rho g \quad (D.2)$$

The perfect gas law is

$$P = \rho R T_v \quad (D.3)$$

The virtual temperature  $T_v$  is related to the temperature  $T$  and to the mixing ratio  $Q$  by the approximate expression

$$T_v = T (1 + 0.6078 Q) \quad (D.4)$$

Combining these equations with (D.1) we obtain

$$P^{K-1} \frac{\partial P}{\partial z} = - \frac{g P_0}{R \Theta (1+0.6078 Q)} \quad (D.5)$$

$$\frac{1}{K} \frac{\partial P^K}{\partial z} = - \frac{g P_0}{R \Theta (1+0.6078 Q)} \quad (D.6)$$

Equation (D.6) has isolated the pressure and will be used in a finite-difference form

$$P(k+1) = P(k) \left[ 1 - \frac{2 g (P_0)^K / \text{DELZ}(k+\frac{1}{2})}{C_p P(k)^K [\Theta(k+1) + \Theta(k)] \{1 + 0.3039 [Q(k+1) + Q(k)]\}} \right]^{1/K} \quad (D.7)$$



#### D.4 Equation for the Infrared Flux.

The basic equations for the infrared flux are (5.9) and (5.10) which we recall here,

$$F_w(0) = \sum_{k=1}^n (\bar{\sigma} T_k^4) \Big|_k \left( \frac{\partial \epsilon}{\partial u} \right) \Delta u \quad (D.8)$$

$$\Delta u = \bar{P} \bar{Q} \frac{\Delta P}{g} \quad (D.9)$$

where  $F_w(0)$  = infrared flux received at  $z_0$  due to water vapor

$n$  = index of the top level considered

$\epsilon$  = emissivity of water vapor

$\bar{P}$  = average pressure of the layer [mb]

$\bar{Q}$  = average mixing ratio in the layer (g/g)

$g$  = gravity = 980 cm/sec<sup>2</sup>

$T_k$  = average temperature of the layer (°K)

$\Delta u$  = path length in a given layer (cm)

$\sigma$  = Stefan-Boltzmann constant.

We will consider the layers between grid points. An average quantity in the layer will be taken as the arithmetic mean of the value of that quantity at the upper grid point and of its value at the lower grid point. For example, the average pressure is,

$$\bar{P} = [P(k+1) + P(k)]/2$$

Therefore, (D.9) is written in finite-difference form as,

$$\Delta u = [P(k+1) + P(k)][P(k+1) - P(k)][Q(k+1) + Q(k)]/(4 g) \quad (D.10)$$

The total path length  $w$  is defined as the sum of all the path lengths contained in the layers between  $z_0$  and the top of the layer under consideration,



$$w = \sum_{(z_0)}^{(\text{top})} \Delta u \quad (\text{D.11})$$

The slope of the emissivity curve can be derived from Table 2,

$$\frac{\partial \varepsilon}{\partial u} = \frac{0.1579}{1+4275 w} \quad \text{for } 0 < w < 10^{-4} \quad (\text{D.12})$$

$$\frac{\partial \varepsilon}{\partial u} = \frac{0.0396}{w} \quad \text{for } 10^{-4} < w < 10^{-3} \quad (\text{D.13})$$

$$\frac{\partial \varepsilon}{\partial u} = \frac{0.0565}{w} \quad \text{for } 10^{-3} < w < 10^{-2} \quad (\text{D.14})$$

$$\frac{\partial \varepsilon}{\partial u} = \frac{0.0653}{w} \quad \text{for } 10^{-2} < w < 10^{-1} \quad (\text{D.15})$$

$$\frac{\partial \varepsilon}{\partial u} = \frac{0.0778}{w} \quad \text{for } 10^{-1} < w \quad (\text{D.16})$$

The finite-difference equation corresponding to (D.8) is,

$$F_w(0) = \sum_{k=1}^n \sigma (T^4(k+1) + T^4(k)) \left( \frac{\partial \varepsilon}{\partial u} \right)_k (\Delta u)_k / 2 \quad (\text{D.17})$$

## D.5 Computation of the Infrared Flux.

All the quantities can now be computed and the successive steps in the computation of the infrared flux are,

### D.5.1 For the Lower Boundary:

Step 1: Compute from (D.1) the temperature at  $z_0$ .

### D.5.2 For the Other Levels.

Step 2: the pressure at the grid point  $k+1$  is computed from (D.7).

Step 3: the temperature at the grid point  $k+1$  is computed from (D.5).

Step 4:  $\Delta u$  is computed from (D.10).

Step 5: the total path length  $w$  is computed from (D.11).

Step 6: the contribution to the infrared radiation from each layer is



computed from (D.12)

D.5.3. Integrated Result.

Step 7: finally the contribution from each layer to the infrared flux is added up to give the total infrared flux received at the ground.



## APPENDIX E

### SOLUTION OF THE SURFACE TEMPERATURE EQUATION

We will use the results obtained in Chapter V and transform the equations into a finite-difference form. Equation (5.20) becomes,

$$E = KW(2)*(Q(3)-Q(1))*DELZ(2)/2 \quad (E.1)$$

where  $KW(k)$  = coefficient of eddy diffusivity for water vapor at

grid point  $k = \gamma + 1$

$DELZ(k)$  = the derivative of  $\gamma$  with respect to  $z$  at grid-point  $k$

$Q(k)$  = mixing ratio at grid-point  $k$

Equation (5.19) is transformed into

$$S = KS(2) (TS(3)-TS(1)) DDZ(2)/2 \quad (E.2)$$

where  $KS(l)$  = molecular coefficient of diffusivity in the soil

at grid-point  $l = \xi + 1$

$TS(l)$  = soil temperature at grid-point  $l$

$DDZ(l)$  = first derivative of  $\xi$  with respect to  $z_s$  at grid-point  $l$ .

The equation for the atmospheric-sensible-heat flux involves the potential temperature whereas all the other terms in (5.1) contain the temperature. This is why we transform (5.10) into a form compatible with the other terms. The equation for the potential temperature is

$$\left(\frac{\mathbb{H}}{T}\right) = \left(\frac{1000}{P}\right)^K \quad (E.3)$$



where

$$K = R/C_p = 2/7$$

Taking the derivative of the logarithm of (E.3), we have

$$\frac{\partial \ln(\bar{H})}{\partial z} = \frac{\partial \ln T}{\partial z} - K \frac{\partial \ln p}{\partial z} \quad (E.4)$$

We use the hydrostatic approximation in (E.4) so that

$$\frac{\partial \bar{H}}{\partial z} = \frac{\bar{H}}{T} \left( \frac{\partial T}{\partial z} + \frac{g}{C_p} \right) \quad (E.5)$$

Equation (E.5) becomes, in a finite-difference form,

$$\Delta \bar{H} = (\Delta T + \Delta z g/C_p) \bar{H}/T \quad (E.6)$$

The integral form of (5.13) is

$$\Delta \bar{H} = \frac{H}{k_o u_*} P_{rt} \ln \left( \frac{z+z_o}{z_o} \right) \quad (E.7)$$

We combine the last two equations and obtain

$$H = \frac{k_o u_*}{P_{rt} \ln(z+z_o)/z_o} \frac{[\bar{H}(2) - \bar{H}(1)]}{[T(2) - T(1)]} [\bar{H}(2) + \bar{H}(1)] + \frac{g}{C_p} z(2) \quad (E.8)$$

In the last expression we have evaluated the finite-difference equation between  $z_o$  and the first grid point. We combine the outgoing terrestrial infrared radiation with the sky infrared radiation due to  $\text{CO}_2$ ,

$$R\uparrow = \epsilon \sigma T^4(0) \quad (E.9)$$

where  $\epsilon = (1 - 0.18)\epsilon_1$  = effective emissivity of the ground.

The infrared radiation from water vapor ( $F_w$ ) has been computed in Appendix D, and the incoming solar radiation ( $I_a$ ) has been defined in Chapter V. Therefore, the following equation results if we group all the results,

$$T^4(0) + C(2) T(0) + C(1) = 0 \quad (E.10)$$



where,

$$C(2) = \frac{\rho_s c_s K_s DDZ(2)/2 + BB}{\varepsilon \sigma}$$

$$BB = \rho C_p \frac{k_o u_*}{P_{rt} (\ln(z+z_o)/z_o)} \left[ \frac{H(2) + H(1)}{T(2) + T(1)} \right]$$

$$C(1) = - \frac{[I_a + F_w + L K_w(2) Q(3) - Q(1) DELZ(2)/2 + BB T(2) + \frac{g_z(2)}{C_p}]}{\varepsilon \sigma}$$

Equation (E.10) can be solved exactly. We will follow the steps outlined in the 14th Edition of the CRC Abridged Mathematical Tables (1967), pp. 291-293. This requires that we solve first a resolvent cubic equation, whose solution gives the desired solution to the quartic equation after a few manipulations. The procedure will be simplified by making use of the fact that  $C(1)$  is always negative and that  $C(2)$  is always a real number.

### E.1 Solution of the Resolvent Cubic Equation.

The quartic equation to be solved is of the type

$$x^4 + a x^3 + b x^2 + c x + d = 0 \quad (E.11)$$

where

$$a = b = 0$$

$$c = C(2) \gg 0$$

$$d = C(1) \ll 0$$

The resolvent cubic equation is

$$y^3 + e y + f = 0 \quad (E.12)$$

where

$$e = -4d = -4C(1) \geq 0$$

$$f = -c^2 = -[C(2)]^2 \leq 0$$

Now we let

$$A = \left( -\frac{f}{2} + \left( \frac{f^2}{4} + \frac{e^3}{27} \right)^{\frac{1}{2}} \right)^{\frac{1}{3}} \quad (E.13)$$



$$B = \left( -\frac{f}{2} + \left( \frac{f^2}{4} + \frac{e^3}{27} \right)^{\frac{1}{2}} \right)^{\frac{1}{3}} \quad (\text{E.14})$$

The three solutions are

$$y_1 = A + B \quad (\text{E.15})$$

$$y_2 = -\frac{1}{2}[(A+B)-(A-B)(-3)^{\frac{1}{2}}] \quad (\text{E.16})$$

$$y_3 = -\frac{1}{2}[(A+B)-(A-B)(-3)^{\frac{1}{2}}] \quad (\text{E.17})$$

If the discriminant  $(\frac{f^2}{4} + \frac{e^3}{27})$  is

$> 0$  we have one real root and two imaginary roots,

$= 0$  we have three real roots of which at least two are equal,

$< 0$  we have three unequal real roots.

In our case

$e^3 > 0$  because  $e$  is always positive, and

$f^2 > 0$  because  $f$  is real.

Therefore, the discriminant is always positive and the only real root is  $y_1$ . We define the following variables:

$$C(3) = -\frac{1}{2}f = C(2) C(2)/2 \quad (\text{E.18})$$

$$C(4) = f^2/4 = C(3) C(3) \quad (\text{E.19})$$

$$C(5) = e^3/27 = -[C(1)]^{1/3} 64/27 \quad (\text{E.20})$$

The discriminant is

$$\text{DIS} = C(4) + C(5) \quad (\text{E.21})$$

The constants  $A$  and  $B$  are, therefore,

$$C(7) = A = [C(3) + \text{SQRT}(\text{DIS})]^{1/3} \quad (\text{E.22})$$

$$C(8) = B = [C(3) - \text{SQRT}(\text{DIS})]^{1/3} \quad (\text{E.23})$$

where  $\text{SQRT}$  = square root of the function inside the parenthesis.

Therefore, the solution of the resolvent cubic equation is

$$Y_1 = C(7) + C(9) \quad (\text{E.24})$$



We note that B is always negative but smaller in absolute value than A, so that Y<sub>1</sub> is always positive.

### E.2 Solution of the Quartic Equation.

We define R as

$$R = \left( a^2/4 - b + Y_1 \right)^{\frac{1}{2}} = \text{SQRT}(Y_1) \quad (\text{E.25})$$

Therefore, R will always be real and positive. In this case we define D and E as

$$D = (-R^2 - 2 c/R)^{\frac{1}{2}} \quad (\text{E.26})$$

$$E = (-R^2 + 2 c/R)^{\frac{1}{2}} \quad (\text{E.27})$$

We must eliminate all of the non-physical roots. c = C(2) is always positive which implies that D is an imaginary number and is rejected for that reason. E is the only real root for which the following inequality must be satisfied:

$$-R^2 + 2 c/R \geq 0 \quad (\text{E.28})$$

The two possible solutions are

$$x = \frac{1}{2} \left( -R \pm \sqrt{E} \right) \quad (\text{E.29})$$

As R and E are both positive, the only positive real solution of the quartic equation is

$$x = \frac{1}{2} \left( -R + \sqrt{E} \right)$$



## APPENDIX F

### LIST OF SYMBOLS

- $\alpha$  kinematic coefficient of viscosity for heat  
also roughness angle; angle between the lower boundary layer wind and the geostrophic wind
- $\gamma$  ratio of the heat capacity at constant pressure over the heat capacity at constant volume for air
- $\delta$  Kronecker's delta  
also solar declination
- $\Delta$  finite difference operator  
partial derivative operator
- $\epsilon$  alternating tensor  
also ratio of the gas constant for dry air over the one for water vapor  
also effective emissivity of the earth's surface
- $\epsilon_1$  emissivity of the earth's surface
- $\phi$  latitude
- $K$  ratio of the gas constant over the heat capacity at constant pressure for the air
- $\lambda, \Lambda$  various length scales
- $\mu, \mu_*$  first and second coefficients of viscosity
- $\mu^r$  molecular coefficient of diffusion for heat
- $\nu$  kinematic coefficient of viscosity
- $\rho, \rho_s$  density of the air and density of the soil



- $\sigma$  rate of strain  
 also frequency in the Fourier analysis  
 also Stefan-Boltzmann's constant
- $\tau$  stress
- $(\bar{H}), \theta$  mean and fluctuating potential temperature
- $\xi$  soil logarithmic coordinates
- $\gamma$  atmospheric log-linear coordinates
- $\psi$  zenith angle
- $\Omega$  earth's angular velocity
- a albedo  
 also constant between  $\frac{1}{2}$  and 1 used in the expression for the path length for water vapor  
 also departure from isotropy in the ordering of terms
- A,B various constants
- $B_\nu$  blackbody radiance
- $C_p, C_v$  heat capacities of dry air at constant pressure and at constant volume
- $C_{p_v}$  heat capacity of water vapor at constant pressure
- C set of constants used in the computations of the surface temperature
- $c_s$  soil heat capacity
- CST coefficient of  $U(k, t_o + \Delta t)$  and  $V(k, t_o + \Delta t)$
- CST2 coefficient of  $(\bar{H})(k, t_o + \Delta t)$
- CST3 coefficient of  $Q(k, t_o + \Delta t)$
- d total derivative operator  
 also half the soil depth in Myrup's (1969) model
- D amplitude of the Fourier modes



DDZ	derivative of $\xi$ with respect to the soil linear coordinate
DD2Z	second derivative of $\xi$ with respect to $z_s$
DDZ2	square of DDZ
DELZ	first derivative of $\ell$ with respect to $z$
DELZZ	ratio of the $\ell$ -derivative of $\ell$ over $\ell^2$
DEL2Z	second derivative of $\ell$ with respect to $z$
DELZ2	square of DELZ
DIFF	constant used in various expressions
DL	first derivative of $\ell$ with respect to $\gamma$
DEL	first derivative of $e \ell$ with respect to $\gamma$
$\Delta$	diffusion operator
e	$\overline{u_1 u_1}$ also partial pressure of water vapor
	also coefficient in the resolvent cubic equation used to find the surface temperature
E	latent heat flux also part of the solution of the quartic equation
f	Coriolis parameter also used to represent any function also one of the coefficients in the resolvent cubic equation
$F_{comp}$	computed value of a function F
$F_{past}$	last iterative value of a function F
$F_{new}$	new iterative value of F
F	flux
$F_w$	total infrared sky radiation received at the earth's surface
H	sensible heat flux from the atmosphere



i	$\sqrt{-1}$
	also an index
$I_a$	net solar radiation
$I_\nu$	intensity of radiation at frequency $\nu$
IKM	level at which the iterative formula computing the grid point height changes
IKP	IKM + 1
j	a general index
$\vec{k}$	wavenumber vector
k	grid point
$k_o$	von Karman's constant
	also a specific grid point
$K_m$	coefficient of eddy diffusivity for momentum
$K_s$	molecular soil thermal conductivity
$K_t$	coefficient of eddy diffusivity for heat
$K_w$	coefficient of eddy diffusivity for water vapor
k	absorption coefficient of water vapor in a thin layer
$K_{ijkl}$	fourth-order tensor relating $G_{ij}$ to the gradient of the mean wind
l	wavenumber
	also a general index
$\ell$	mixing length
$\ell_o$	maximum size of the eddies
L	latent heat of vaporization
m	number of increments in Taylor's series
n	represents various exponents



NS	top of the boundary layer in terms of $k = \gamma + 1$
OMEGA	acceleration factor in the Gauss-Seidel iteration scheme
p	pressure
$P_o$	reference pressure = 1000 mb
$P_{rt}$	turbulent Prandtl number
$q, Q$	fluctuating and mean mixing ratio for water vapor
R	gas constant of the dry atmosphere
$R_w$	gas constant of the water vapor
$R\downarrow$	infrared sky radiation
$R\uparrow$	terrestrial outgoing infrared radiation
$R_o$	solar constant
$R_n$	net radiation at the surface of the earth
S	entropy
$S_a$	entropy of dry air
$S_v$	entropy of the water vapor
S	soil heat flux
t	time
T	absolute temperature
$T_v$	virtual temperature
$T_r$	transmissivity of the cloudless atmosphere
$T_{runc}$	truncation error
$u, U$	fluctuating and mean winds along the x direction
$u_*$	friction velocity
$v, V$	fluctuating and mean winds in the y direction
$V_g$	geostrophic wind



w,W	fluctuating and mean winds in the z direction
w	path length in water vapor
x	the first Cartesian coordinate in the horizontal
y	the second Cartesian coordinate in the horizontal also solution of the resolvent cubic equation
z	vertical Cartesian coordinate
Z	zenith solar angle
$z_s$	roughness height
zs	proportion at each grid point of the total temperature difference between the surface and the bottom of the soil layer
$z_o$	roughness height
$z_1$	canopy height in Myrup's (1969) model
$z_2$	top of the boundary layer in Myrup's model









B30155